# REACTIVITIES LEADING TO POTENTIAL CHEMICAL REPAIR OF SUNLIGHT-INDUCED DNA DAMAGE: MECHANISTIC STUDIES OF CYCLOBUTANE PYRIMIDINE DIMER (CPD) LESIONS UNDER ALKALINE CONDITIONS
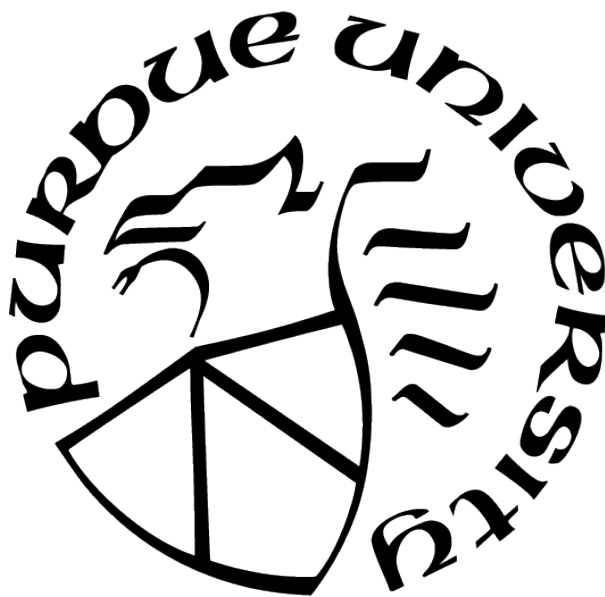
by

**Ritu Chaturvedi**

**A Dissertation**

*Submitted to the Faculty of Purdue University*

*In Partial Fulfillment of the Requirements for the degree of*

**Doctor of Philosophy**

Department of Chemistry and Chemical Biology

Indianapolis, Indiana

December 2020

# THE PURDUE UNIVERSITY GRADUATE SCHOOL
## STATEMENT OF COMMITTEE APPROVAL

**Dr. Eric C. Long, Chair**

Department of Chemistry & Chemical Biology

**Dr. Michael J. McLeish**

Department of Chemistry & Chemical Biology

**Dr. Jingzhi Pu**

Department of Chemistry & Chemical Biology

**Dr. Ian K. Webb**

Department of Chemistry & Chemical Biology

**Approved by:**

Dr. Eric C. Long

Dedicated to my father

# ACKNOWLEDGMENTS

I am immensely thankful to the faculty, staff and students of the Department of Chemistry & Chemical Biology, IUPUI, whose support has been pivotal in the completion of this dissertation. A special thanks to our Graduate Program Administrator, Ms. Kitty A. O'Doherty, who I accidentally contacted during my application process to Purdue University, WL. Kitty not only encouraged me to apply to IUPUI but also guided me every step of the way. Her support is as crucial to my Ph.D. journey as any of my professors.

I am thankful to the students at IUPUI, especially Christine, Greta, Thakshila, Kapil, Mark, Sara, Brienna, Sheridan, Melanie, Veronica and Rebecca, who started as peers but gradually became important friends, which I will cherish forever. A special shout-out to the postdocs in the department, especially Surya and Makafui *aka* Mark, who provided valuable discussions and greatly helped me to execute the organic syntheses part of my research with ease.

A special token of thanks to my family back in India for their continued support throughout this journey. A special shout-out to my little brother Ritesh, who sponsored my first air ticket to the U.S. A huge shout-out to my husband and my best friend, Dr. Avanish Bharati, for his continued support throughout this journey; more importantly, for helping me out with the Latex template that I used while writing this document and taking care of all the technical bugs so that I could focus on my scientific writing.

I am thankful to all my Ph.D. committee members; Dr. McLeish, who provided valuable lessons in scientific writing; Dr. Webb for helping with the discussions and experiments related to all the aspects of mass spectrometry described in this dissertation, and Dr. Pu for the stimulating discussions related to computer modelling of the molecules mentioned in this dissertation. I am immensely thankful to our department chair, Dr. Basu whose support has been crucial every step of the way, even when it was most required and least expected. Last and most important token of thanks to my Ph.D. advisor and mentor, Dr. Long, whose role has been extremely crucial to my overall journey as a scientific researcher and without whose support none of this would be possible. His support and guidance will

remain with me throughout my research career and will forever reflect in my approach to scientific problems, writing and most importantly, while mentoring my own students.

# TABLE OF CONTENTS

# LIST OF TABLES

# LIST OF FIGURES

16

18

# ABSTRACT

Cyclobutane pyrimidine dimers (CPD) are the predominant DNA lesions formed upon exposure of this biopolymer to sunlight. Given the potentially dire biological consequences of DNA lesions [1]–[4], there is a need to fully characterize their behaviour, with an eye towards understanding their complete reactivity and as a possible means to detect and quantify their presence in the genome. The work described in this dissertation describes studies of the alkaline reactivity of CPD lesions generated within dinucleotide & polynucleotide strands. It was found that CPD-TpT is generally inert under alkaline conditions at room temperature, which is in agreement with earlier studies on alkaline hydrolysis of CPD-thymine and CPD-thymidine [5]. However, a re-evaluation of the same reaction in the presence of $^{18}$O labelled water demonstrated that, similar to other UV-induced DNA lesions containing a saturated pyrimidine ring, CPD undergoes a water addition at the C4=O group of the nucleobase leading to the formation of a hemiaminal intermediate [6]. This intermediate, however, does not lead to hydrolysis products and completely reverts to starting material under those same conditions. Moreover, the two C4=O groups present on 3′ and 5′-thymines in a CPD molecule show different chemical reactivities, with the 3′ C4=O group having greater affinity towards water addition as compared to the one on 5′ end, a fact reflected in different rates of exchange with the incoming nucleophile leading to the hemiaminal intermediate. The $^{18}$O labelling reaction was also investigated in CPD lesions generated within oligonucleotides to probe the cause of asymmetry between the 3′ *vs* 5′ C4=O groups; ultimately, it was determined that the asymmetric reactivity observed to occur between the two C4=O groups was an intrinsic property of the CPD molecule and did not arise as a result of asymmetry in a dinucleotide setting.

In addition to the above studies, during the course of the investigation of the nucleophilic reactivity of CPD, a chemical reaction was observed leading to what appeared to be the rapid and total chemical reversal of CPD lesions to the original TpT (thymine-thymine dinucleotide)! This "repair" reaction occured when CPD reacted with hydrazine, and appears facilitated by an inert atmosphere under which it rapidly proceeds to completion at room temperature.

# 1. INTRODUCTION

## 1.1 DNA structure, damage and repair

The intention of this section is to acquaint the reader with the details of DNA structure important to understanding the formation, outcome and repair of cyclobutane pyrimidine dimer (CPD) lesions.

### 1.1.1 B-form DNA structure

The primary structure of DNA consists of phosphodiester-linked nucleotide units that contain a $2'$-deoxy-D-ribose sugar ring and an aromatic nucleobase (Figure 1.1). The nucleobases found in DNA include the purines adenine (A) and guanine (G) and the pyrimidines cytosine (C) and thymine (T). The primary structure of DNA has a consistent $5' \longrightarrow 3'$ polarity with both a negatively charged sugar-phosphate backbone and an array of relatively hydrophobic nucleobases, amphiphilic features which ultimately drive the assembly and maintenance of secondary and tertiary nucleic acid structures.

While DNA is known to exist in several polymorphs (A-form, B-form and Z-form), the predominant DNA structure found under physiological conditions is referred to as the B-form. This conformation of DNA contains two antiparallel strands of nucleic acid connected by stacked Watson-Crick $A \cdot T$ and $G \cdot C$ base pairs that spiral around a central polymer axis in a right-handed helical sense (Figure 1.2). The specific nature of Watson-Crick base pairing results in a duplex composed of single strands that are self-complementary; thus, knowledge of the nucleobase order in one strand is sufficient to define the primary sequence of the other, a feature that facilitates the replication and repair of DNA.

.

The right-handed helical structure of B-form DNA (Figure 1.2) contains a hydrophobic interior of Watson-Crick base pairs stacked nearly perpendicular to the central polymer axis at 3.4 Å intervals [7], [8]. The π-π stacking interactions that occur between these aromatic planes provide a substantial stabilizing force that helps to maintain the duplex nature of DNA [9]. Further, each base-pair plane of B-form DNA is rotated approximately 36° relative to the one preceding it, resulting in a complete right-handed helical turn for
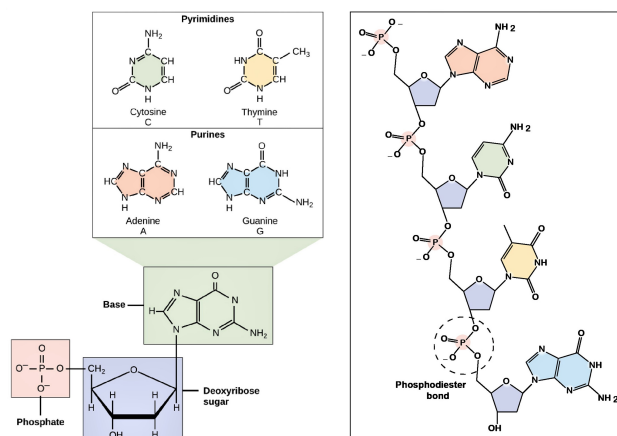
**Figure 1.1.** The primary structure of DNA. Figure credits: left panel, figure adapted from "Nucleic Acids: Figure 1," by OpenStax College, Biology (CC BY 3.0). Right panel, figure adapted from "DNA Chemical Structure," by Madeleine Price Ball (CC0/public domain).
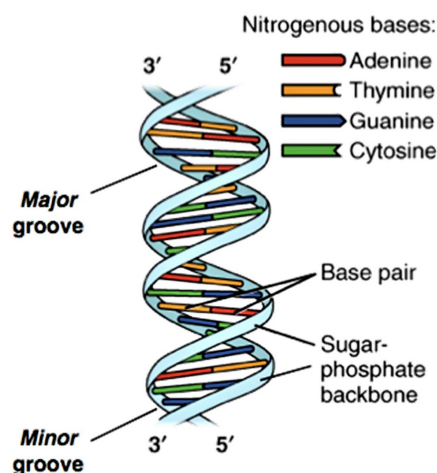


**Figure 1.2.** Double-helical structure of DNA. Figure modified from "DNA Structure and Sequencing: Figure 3," by OpenStax College, Biology (CC BY 3.0).

every 10 contiguous base pairs and thus a helical pitch of 34 Å (3.4 Å/repeat unit X 10 base pairs/helical turn). With the Watson-Crick base pairs inside, the anionic sugar-phosphate backbone spirals around the outside of the helix, creating a hydrophilic exterior with a net charge of -2 for each base pair repeat unit. The high density of negative charge associated with this biopolymer also dictates to some extent the character of agents which associate with it: agents that bind most efficiently to DNA often possess a net overall positive charge. Two

other important structural details of the sugar-phosphate backbone include the deoxyribose ring conformation and the $N$-glycosidic bond angles: in B-form DNA the deoxyribose ring adopts a C2′-*endo* conformation, while the $N$-glycosidic bond angle is in an anti-configuration (Figures 1.3, 1.4)



**Figure 1.3.** Deoxyribose sugar pucker conformations. Figure adapted from [10]



**Figure 1.4.** The $N$-glycosidic bond angles found in DNA structures. Figure adapted from [11]

The overall 3-D structure of B-form DNA creates two distinct helical grooves, the minor and the major, which spiral around the exterior surface of the double strand (Figure 1.2). In B-form DNA, the minor groove is narrow, while the major groove is wide, with both grooves possessing a moderate, nearly equivalent depth. Importantly, these two grooves create unique microenvironments for the binding and recognition of ligands (*i.e.*, proteins or small molecules). The floors of the major and minor grooves are defined by the opposite sides of the stacked Watson-Crick base-pair planes which create patterns of hydrogen-bond

donor and acceptor sites within the plane of the base pair (Figure 1.5) [12]. Thus, the floors of the grooves of the DNA helix would differ for individual base-pair sequences with respect to their patterns of H-bond donors, H-bond acceptors, and sites available for hydrophobic interactions (*e.g.*, the C5 methyl group of thymidine). These differences form the basis, in part, for the sequence-selective binding of certain ligands [13].
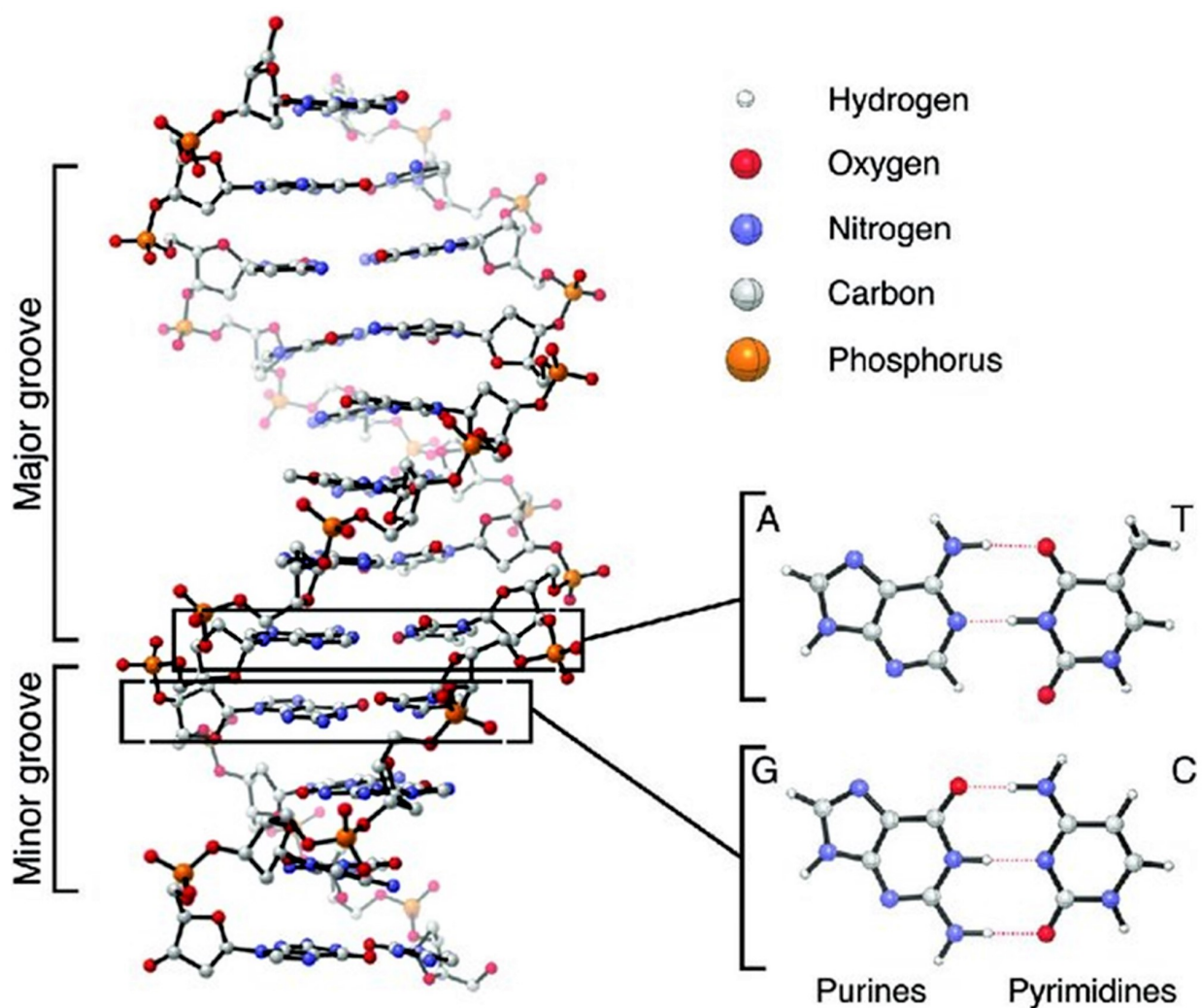


**Figure 1.5.** Structures of B-DNA and Watson–Crick base pairs. Hydrogen atoms on the B-DNA helix have been removed for clarity. Figure adapted from [14]

Table 1.1 shows the base stacking free energy values for adjacent nucleobases, which are indicative of the contribution of individual nucleobase steps to the overall stability of duplex DNA [15]. As tabulated, the parameter values are scattered from -0.19 kcal/mol for the TpA step to -2.17 kcal/mol for the GpC step. This range is generally consistent with parameter values for coaxial stacking. Based on these values, GpC is the most stable contact, TpA is the least stable contact and a tendency towards more efficient stacking for mixed dinucleotides is in the order TpG<ApG<GpA<GpT. When similar nucleobases are stacked next to each other, the stacking energy seems indifferent to the identity of the base. This is evident by the similar values of stacking free energies for ApA, TpT, GpG and CpC steps ranging between -1.11 kcal/mol and -1.44 kcal/mol. In general, GpG and CpC steps (both with energy values of -1.44 kcal/mol) appear to be more stable than ApA and TpT steps, both of which have a stacking free energy value as -1.11 kcal/mol.

**Table 1.1.** Stacking free energy parameters for adjacent pairs of nucleobases in a duplex DNA strand (the reported values of $\Delta$G are in kcal/mol) [15]

| KL | A | T | G | C |
|----|-------|-------|-------|-------|
| A | -1.11 | -1.34 | -1.06 | -1.81 |
| T | -0.19 | -1.11 | -0.55 | -1.43 |
| G | -1.43 | -1.81 | -1.44 | -2.17 |
| C | -0.55 | -1.06 | -0.91 | -1.44 |

From Table 1.1, it is also evident that the stabilizing effect of two stacked thymine residues is higher than it would be if thymine was stacked next to an adenine or a guanine nucleobase. In terms of structure, the two thymines in a TpT step do not lie in the same plane. Rather, the two nucleobases display a "propeller twist" arrangement in which they rotate counter relative to one another along the long axis of the base pair, giving the base pair a propeller-like geometry (Figure 1.6). The C4=O groups on adjacent thymine nucleobases in a TpT step are hydrogen-bonded with the amine hydrogens from the adenine nucleobases on the complementary strand, as highlighted in Figure 1.6.

Along with the B-form, A-form DNA is another relatively well-studied polymorph of DNA. A-form DNA is not naturally abundant in living cells; however, B-form DNA transforms into an A-form helix as the relative humidity of its environment decreases to 75% and

C4=O groups
in a TpT step
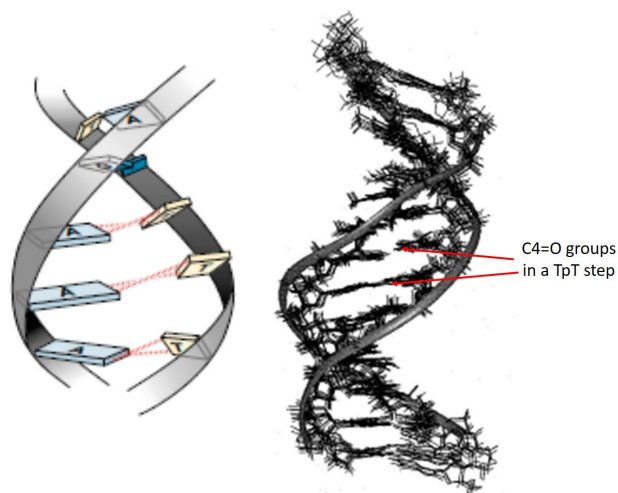
**Figure 1.6.** Section of a DNA double helix showing a thymine-thymine step. Figure modified from [16]

the NaCl concentration drops below 10%. Interestingly, of relevance here, UV irradiation of A-Form DNA found in "packaged" DNA of bacterial endospores leads to the formation of spore photoproduct (SP) lesions. A comparison of the helix structural parameters from crystallized examples of the two forms of DNA is shown in Figure 1.7 [7].
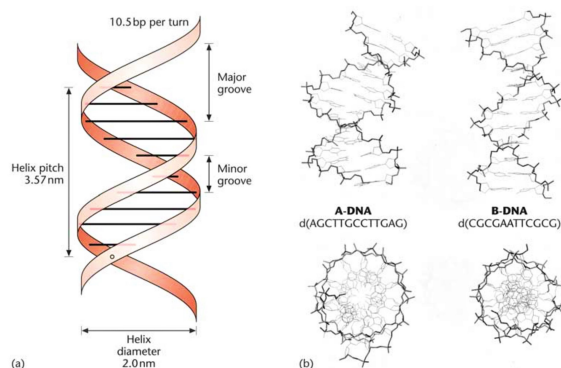


**Figure 1.7.** Different conformations of the DNA double helix. (a) The structure of B-DNA as proposed by Watson and Crick in 1953, based on fibre diffraction studies. Modified from Sinden *et al.* (1998) [17]. (b) A- and B-DNA, as seen from the side of the helix (above), and looking down the helix axis (below). The structures were drawn from the crystal structures, using the Cn3D programme, available from the NCBI home page.

### 1.1.2 UV-Induced DNA damage

DNA is vulnerable to chemical and physical damage [18]. As a result, DNA lesions are generated under the constant stress of agents like sunlight, oxygen and oxidizing radicals, *etc.* [19]–[21]. Ultraviolet light harms cells by directly interacting with, and altering chemically, the nucleobases of DNA, leading to UV-induced DNA photoproducts. Of the three categories of solar ultraviolet radiation, only UV-A and UV-B are capable of penetrating the earth's atmosphere [22]. Thus, these two categories of solar radiation pose the maximum danger to humans, especially as depletion of the ozone layer allows higher levels of ultraviolet radiation to reach the surface of the earth (Figure 1.8) [23]–[26]. It has been demonstrated that the ability of UV light to damage a given nucleobase in DNA is determined by two factors: (1) the sequence of the DNA in the immediate vicinity of the photoproduct (refer to Table 1.1 summarizing the relative stabilities of various dinucleotide steps) [15], and (2) the flexibility of the DNA at the site of the photoproduct (pyrimidine-rich sequences generally account for relatively flexible regions of the DNA) [27]. For pyrimidines, the predominant photoreaction in double-stranded DNA involves covalent dimerization between adjacent pyrimidine residues, leading to the formation of various kinds of pyrimidine dimers [28]–[30]. In contrast to adjacent pyrimidines, non-adjacent, pyrimidines (pyrimidines flanked on either side by a purine) do not readily form UV photoproducts in double-stranded DNA. This is attributed to torsional constraints imposed by the double helix which make it difficult for non-adjacent pyrimidines to adopt a geometry necessary for photoreaction (Table 1.1)[15]. In contrast to that, adjacent pyrimidines have the required geometry optimal for dimer formation (refer to "propeller geometry" explained in Figure 1.6) [16]. Dimerization is also much easier in melted DNA because the geometrical changes required for adjacent pyrimidine residues to dimerize are easier to adopt in single-stranded DNA [27]. Although purines are believed to be resistant to UV damage relative to pyrimidines, it has been shown that at moderate UV dosages, purines flanked on their 5′ side by two or more contiguous pyrimidines readily form UV photoproducts in double-stranded DNA. In this case, flanking pyrimidines appear to activate purine photoreactions by transferring triplet excitation energy to the purine. In support of this notion, melting of the DNA helix greatly inhibits the ability of flanking

pyrimidines to activate purine photoreactions, presumably by disrupting intimate orbital overlap required for triplet transfer [27].
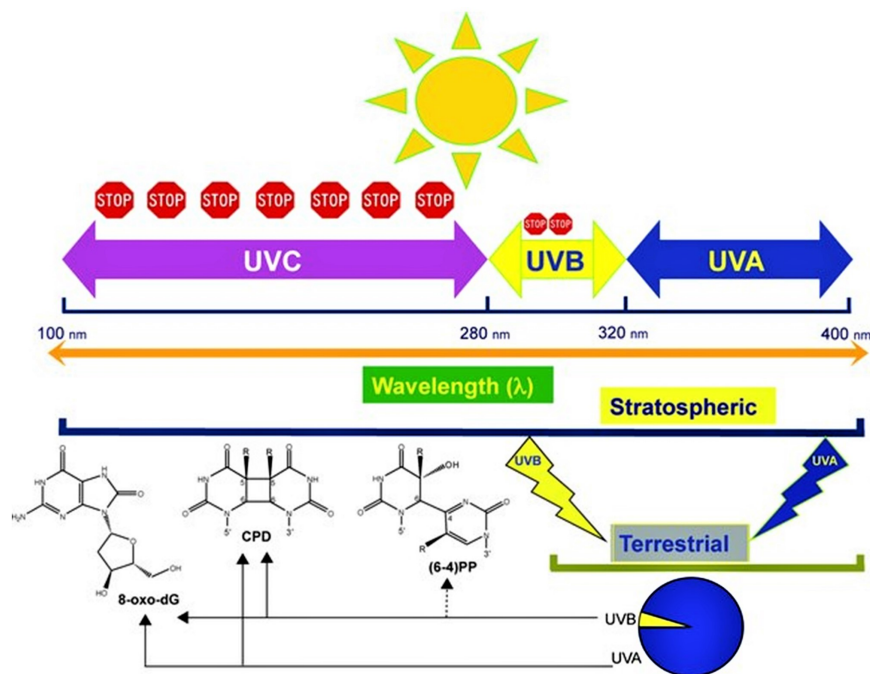


**Figure 1.8.** Overview of UV induced DNA damage showing the parts of UV radiation reaching the earth's surface and the lesions that result from UV-B exposure. Figure adapted from [31]

As noted earlier, direct DNA damage occurs when a photon of UV light is absorbed by a DNA pyrimidine. Photon absorption leads to two classes of pyrimidine dimers in most living cells: (1) cyclobutane pyrimidine dimers (CPDs) [3], [32], [33] and (2) pyrimidine (6-4) pyrimidone photoproducts (6-4PPs) [34], [35]. Another lesion, spore photoproduct (SP) is formed upon UV-irradiation of bacterial endospores where conditions of low hydration force the DNA into an uncommon A-form [36], [37]. This unique DNA conformation, coupled with the presence of small acid soluble proteins (SASPs) in spore genomic DNA alters the outcome of the thymine photoreaction, making SP the dominant photoproduct. Figure 1.9 illustrates the three classes of naturally occurring UV lesions: CPD, 6-4PP and SP. Included here also is 5,6-dihydro-2′-deoxyuridine (dHdU) which is formed when cytosine is exposed to ionizing radiation under anoxic conditions (and is considered a general structural model for lesions containing a saturated pyrimidine ring) [38].
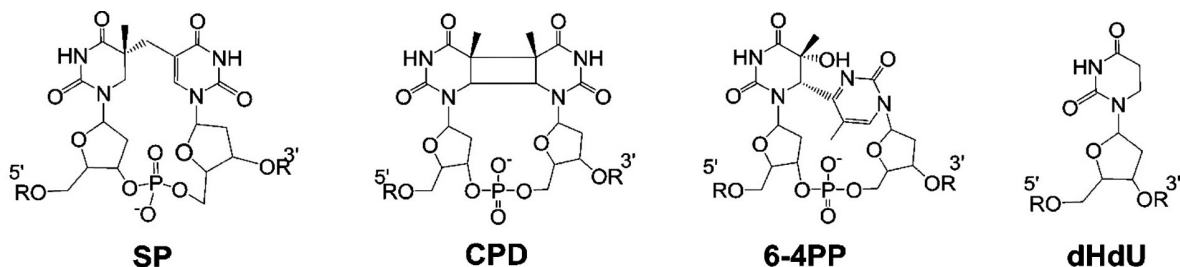
**Figure 1.9.** Naturally occurring thymine dimers and dHdU that possess a saturated pyrimidine ring. Figure adapted from [6]

*Why do these lesions form?* DNA is a very large molecule that absorbs the energy it gains on interaction with a photon of UV light and then quickly releases that energy as heat. During the time after the DNA absorbs the energy and before it dissipates the heat, it is in a higher energy state and is more reactive; the shorter this reactive time is, the less likely it is that the DNA will undergo a harmful reaction. It turns out that DNA is extremely effective at dissipating the extra energy quickly, so it becomes damaged less than 0.1% of the time it absorbs UV light. In cases where damage does occur, there are different ways excited DNA can react; however the cross-linking of two base pairs is the most common. If two pyrimidine base pairs (thymine or cytosine) are stacked upon each other, the two rings can fuse together via a pericyclic reaction to form a cyclobutane pyrimidine dimer (Figure 1.10). The pericyclic reaction is possible because of the close proximity of the rings and how their symmetries align (Figure 1.6). This leads to a four-carbon cyclobutane "bridge" between adjacent pyrimidine residues. Importantly, dimerization between the pyrimidines makes it difficult for DNA replication enzymes to determine what base pairs should be across from the fused pyrimidines, leading to errors. Such errors can change the DNA sequence of a daughter strand and ultimately how it encodes a protein, resulting in a mutant protein product. If the mutation occurs in an area which codes DNA repair enzymes or tumour suppressing proteins, such mutations can lead to cancer.

Cyclobutane thymine dimers, which account for more than 90% of all lesions formed in the human genome upon UV-B irradiation, block replicative and transcriptional polymerases [20], [39], [40], resulting in bypass replication by error-prone Y-polymerases like pol$\eta$ in the former case, and transcription-coupled repair in the latter. In the absence of efficient repair,
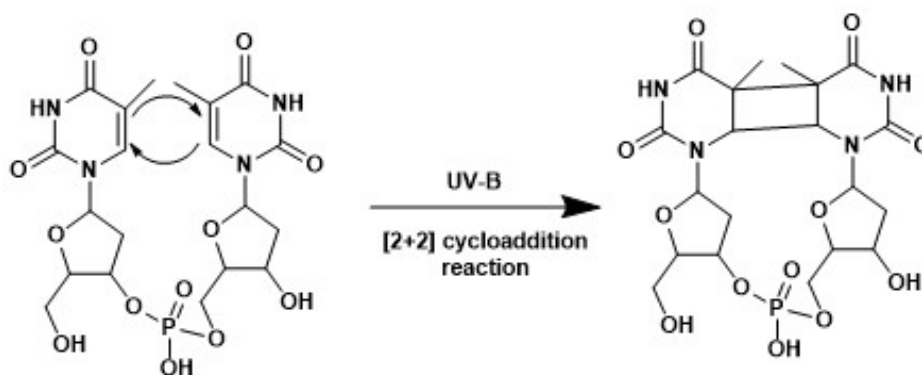
**Figure 1.10.** Dimerization of adjacent pyrimidine nucleobases on UV irradiation

these lesions can result in mutations, cancer and cell death. To avoid mutagenesis and carcinogenesis by the CPD lesion, this damage is repaired by the well-studied nucleotide excision repair (NER) pathway in cells.

### 1.1.3 DNA repair mechanisms and human disease

DNA damage repair occurs in both prokaryotic and eukaryotic organisms, and many of the proteins involved are highly conserved throughout evolution. In fact, cells in both forms of life have evolved a number of mechanisms to detect and repair various kinds of DNA damage, irrespective of the cause of the damage. Since DNA plays a vital role in the process of cell division, DNA repair is closely tied to regulation of the cell cycle. In brief, cell division occurs through a process involving the G1, S, G2 and M phases of the cell cycle, with DNA replication occurring in the S-phase and mitosis occurring in M phase. During the course of the cell cycle, active checkpoint mechanisms ensure that the DNA of a cell is intact before allowing replication and cell division to occur. Errors in these checkpoint mechanisms can result in an accumulation of DNA damage, which, in turn, can lead to mutations.

Underscoring the importance of proper DNA repair, genetic defects in the DNA repair machinery underlie a number of diseases in humans, but generally share common traits. Most notably, defects in DNA repair can translate into diseaases and a predisposition towards cancer. These disorders include ataxia-telangiectasia (AT), a degenerative motor condition that is caused by a failure to repair oxidative DNA repair in the cerebellum, and xeroderma

pigmentosum (XP), a condition characterized by an increased sensitivity to sunlight and linked to a defect in an important ultraviolet damage repair mechanism (Table 1.2) [41]–[44]. In addition, a number of genes that have been implicated in carcinogenesis, *e.g.*, like the RAD group, have also been indicated to encode proteins actively associated with DNA damage repair. *In the next sections, the main concepts associated with DNA repair mechanisms relevant to this research will be reviewed.*

**Table 1.2.** Some human hereditary diseases and cancers associated with DNA-repair defects

| Syndrome | Affected Repair Pathway | Defective Protein | Type of Genomic Defect | Cancer |
|---|---|---|---|---|
| Xeroderma pigmentosum (XP) | Nucleotide excision repair | XP, CS | Point mutations | Skin cancer |
| Ataxia telanglectasia (AT) | DNA DSB response | ATM | Chromosome aberrations | Lymphomas |
| AT-like disorder | DNA DSB response | MRE11 | Chromosome aberrations | Lymphomas |
| Nijmegan breakage syndrome (NBS) | DNA DSB response | NBS1 | Chromosome aberrations | Lymphomas |
| BRCA1/BRCA2 | Homologous recombination | BRCA1, BRCA2 | Chromosome aberrations | Breast cancer |
| Werner syndrome | Homologous recombination | WRN helicase | Chromosome aberrations | Various |
| Bloom syndrome | Homologous recombination | BLM helicase | Chromosome aberrations | Leukemia |
| Hereditary nonpolyposis colorectal cancer (HNPCC) | Mismatch repair | MLH1, MSH2 | Microsatellite instabilty | Colorectal |
| Fanconi anemia | DNA crosslink repair | FANC-D2 | Chromosome aberrations | Leukemia |
| Li Fraumeni | DNA DSB response | p53, others? | Cell-cycle checkpoints | Many |
| Riddle | DNA DSB response | RNF168 | Cell-cycle checkpoints | Unknown |

**Nucleotide Excision Repair (NER) in eukaryotes and prokaryotes: Enzymatic repair**

When direct DNA damage fuses two nucleobases together, the DNA obtains a distinct bulge in its normal double helical shape (Figure 1.11). Several enzymes actively screen the DNA within living cells looking for such structural abnormalities [45]. When a bulge is detected, repair proteins are activated that cut out the damaged part of the DNA and put in the correct base pairs [46]–[52]. This process is called nucleotide excision repair (NER). Both CPD and 6-4PP lesions are repaired through NER. In eukaryotic organisms, NER utilizes the products of several genes. Defects in some of these genes are linked to the human disease XP, as well as other conditions that are characterized by an increased susceptibility to skin cancer that is elevated about a thousand-fold over normal [41]–[44].

The NER process in eukaryotes is carried out by at least 18 protein complexes via four discrete steps, namely: (1) detection of damage; (2) excision of the DNA segment surrounding
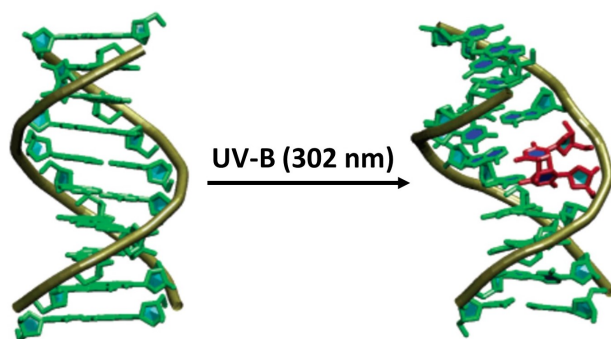
**Figure 1.11.** Stereoview representations of the crystal structures of B-form DNA decamer before and after the dimerization of adjacent pyrimidine nucleobases to form a CPD lesion. The thymidines making up the dimer are drawn in red. The view shows part of the major groove of the molecule. In CPD-containing DNA, the phosphodeoxyribose backbone shows a sharply kinked (30°) structure. Figure modified from [3]

and including the damaged site; (3) filling in the resulting gap using DNA polymerase; and (4) sealing the nick between newly incorporated DNA and older DNA using DNA ligase (Figure 1.12). In bacteria the process of NER is carried out by three proteins, called UvrA, UvrB and UvrC [42], [53]–[55].
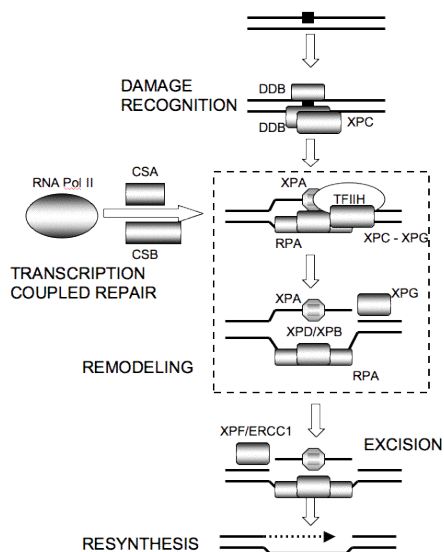


**Figure 1.12.** Schematic representation of the nucleotide excision repair pathway

33

**'Photoreactivation' as a repair pathway**

Along with enzymatic means of DNA lesion repair, bacteria, along with several other organisms, possess a mechanism of DNA damage repair known as photoreactivation that is carried out by a class of enzymes called 'photolyases'. Photolyases are monomeric proteins with molecular weights ranging between 50-60 kDa that possess stoichiometric amounts of two chromophores/cofactors. One of these cofactors is FADH, and the second chromophore is either methenyltetrahydrofolate (MTHF) or 8-hydroxy-5-deazariboavin (8-HDF) (Figure 1.13). The photolyase repair process is often referred to as 'light repair' since it requires light energy. In contrast, NER and other repair mechanisms are called 'dark repair' mechanisms, as they are not dependent on light as an energy source.

During photoreactivation, photolyases cause the DNA helix to extrude a pyrimidine dimer, if present, and then bind to it. Upon lesion recognition, an enzyme-bound chromophore (MTHF or 8-HDF) absorbs a photon of light to initiate the reaction. The overall enzymatic process results in a direct reversal of damaged DNA to its undamaged form (Figures 1.14 and 1.15) [43], [56]–[59]. Photolyases are known to occur in numerous organisms including fungi, plants, invertebrates (fruit flies) and vertebrates including frogs [20], [43]. However, photolyases do not appear to exist in humans [58], [60], [61].
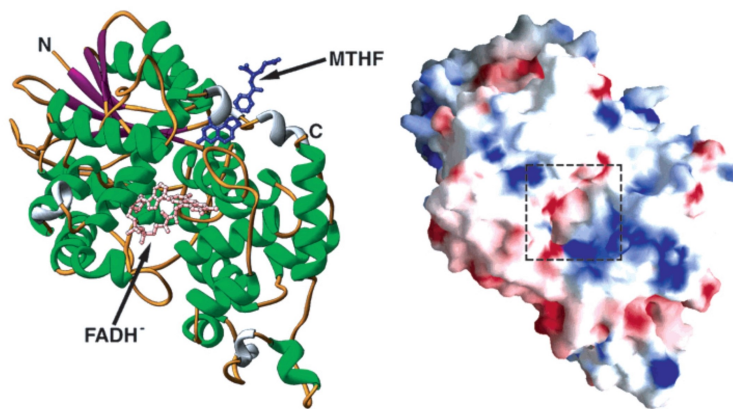


**Figure 1.13.** Crystal structure of *E. coli* photolyase: (A) Ribbon diagram representation showing the N-terminal $\alpha/\beta$ domain, the C-terminal $\alpha$-helical domain, and the positions of the two cofactors; (B) surface potential representation showing the solvent-exposed residues. Key: blue, basic groups; red, acidic groups; white, hydrophobic groups. The square marks the hole leading to FAD in the core of the R-helical domain [62]
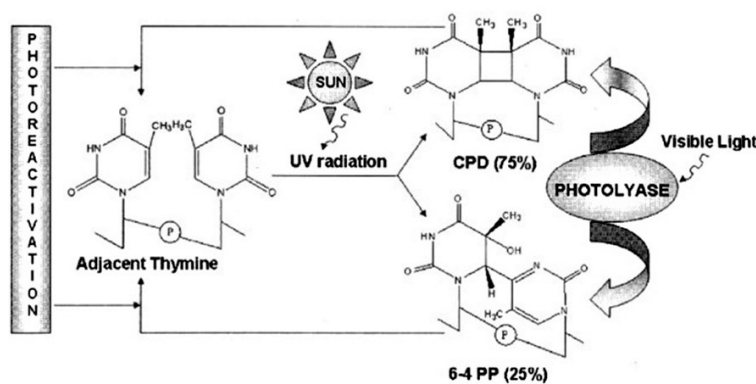
**Figure 1.14.** (A) cyclobutane pyrimidine dimer (CPD) and (B) pyrimidine (6-4) pyrimidone photoproduct (6-4PP), both formed after the dimerization of adjacent thymidine residues and their photoreactivation by the enzyme photolyase in the presence of light. Figure adapted from [63]
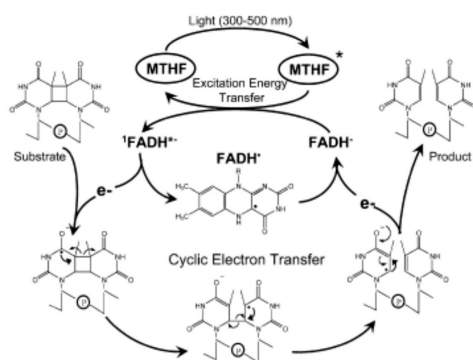


**Figure 1.15.** An illustration of the key molecular events in the photoreactivation of a CPD molecule. MTHF absorbs a 300-500 nm photon and transfers the excitation energy to FADH- by FRET. The $^1$(FADH-)$^*$ transfers an electron to CPD, which undergoes [2 + 2] cycloreversion to generate a Pyr and a Pyr$^{\circ-}$; back electron transfer to FADH$^{\circ}$ restores the catalytic cofactor to the active reduced form, and the dimer is converted to canonical bases. Figure adapted from [64]

## 1.2 Alkaline Reactivity of UV-Induced DNA Lesions

As noted earlier, the two prominent DNA lesions induced by UV light are the *cis-syn* cyclobutane pyrimidine dimer (CPD) and the pyrimidine (6-4) pyrimidone photoproduct (6-4PP), both formed as a result of dimerization between adjacent stacked pyrimidine bases in DNA. Importantly, the generation of these lesions can not only lead to genetic mutations, but can also alter the chemical stability and reactivity of genomic DNA [4]. For example,

undamaged DNA is known to withstand acids and bases; however, DNA containing UV-induced damage is very sensitive to alkali. In fact, the 6-4PP lesion was originally identified as a UV-induced alkali-sensitive DNA lesion. DNA strand cleavage occurs at the site of this lesion when UV-irradiated DNA is subject to hot alkali treatment (Figure 1.16) [65], [66]. Indeed, this procedure has been used to identify (and quantify) the 6-4PP lesion in short, well-defined DNA sequences at single nucleotide resolution. Alkaline lability has also been employed in DNA foot-printing experiments to monitor DNA-protein interactions *in vivo*. Thus, if the altered reactivity of lesion-containing DNA is fully understood, the knowledge obtained might be exploited for the detection/quantification of these lesions along with revealing their fundamental reactivities.
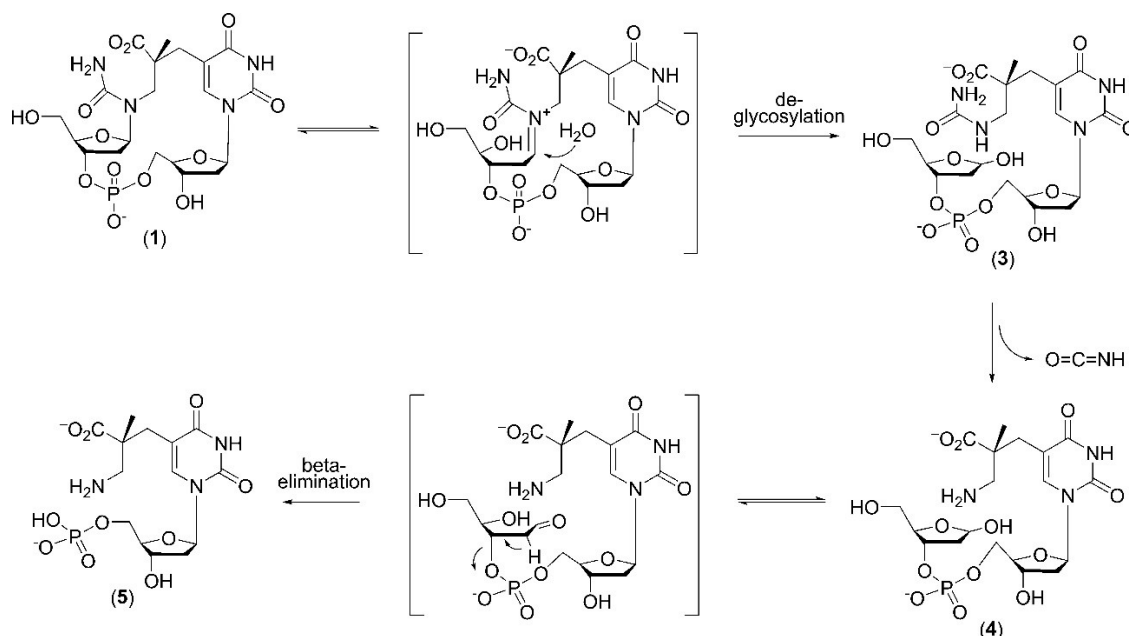


**Figure 1.16.** General scheme for SP-induced strand cleavage reaction in the presence of 0.2 M KOH at 90°C for 0.5 hours. By extension, this reaction is also valid for strand cleavage caused by other DNA lesions containing a saturated pyrimidine ring *e.g.* 6 4-PP and dHdU, since alkali-induced N3-C4 bond cleavage has been shown as a common feature in all these lesions. Figure adapted from [6]

While the chemical reactivity of the 6-4PP lesion has been studied in detail, the reactivity of the most commonly found DNA UV-induced lesion, *i.e.*, cyclobutane pyrimidine dimer (CPD) still remains obscure. *In the following sections the chemistries of the pyrimidine (6-4)*

*pyrimidone photoproduct (6-4PP), 5-pyrimidinyl-5,6-dihydropyrimidine (spore photoproduct, SP) and 5,6-dihydo-2'-deoxyuridine (dHdU) lesions under alkaline conditions will be reviewed for later comparison to our work on the alkaline reactivity of the CPD lesion.*

### 1.2.1 Alkaline hydrolysis of pyrimidine (6-4) pyrimidone photoproduct (6-4PP) lesions leading to DNA strand scission

Pyrimidine (6-4) pyrimidone photoproduct (6-4PP) is a common DNA photo-damage product formed upon exposure to the UV component of sunlight. Upon forming, this lesion leads to a sharp kink in the DNA double-helical structure, thereby distorting it significantly [67]. NMR and X-ray diffraction studies have revealed that presence of a 6-4PP lesions causes a distortion of around 44° in the double helical structure (Figure 1.17(b)) [68], [69]. In contrast, the cyclobutane pyrimidine dimer (CPD) causes relatively minor structural distortion, *i.e.*, a 36° helical bend towards the major groove (Figures 1.17(a) and 1.18) [1]–[3]. In comparison to CPD, 6-4PP is much more mutagenic [70]–[72]; it arrests the replicative fork of general replicative DNA polymerases. *Underscoring the importance of this lesion, when it is bypassed by the human Y-polymerase polη, there is a 7-fold higher tendency for the insertion of a G instead of an A opposite to the 3′-T of the 6-4PP lesion.* [73], [74] Due to the drastic DNA structural distortion caused by this lesion, it is believed to be readily recognized by the DNA repair machinery leading to its quick removal in living cells (half-life of 6-4PP = 2.3h) [75]. 6-4PP lesions that elude the repair pathway are suggested to be the primary cause of UV-B induced cell apoptosis especially in NER-deficient cells [76], [77].

Given the above, it was thus significant to understand the physical and chemical properties of 6-4PP. 6-4PP is alkali labile, inducing DNA strand scission upon hot alkaline treatment [66], [80], [81]: *alkaline treatment initiates a nucleophilic attack on the C4=O group on 5′-thymine of 6-4PP, forming a hemiaminal intermediate, that can lead to the rupture of the N3-C4 bond to yield a hydrolysis product* (Figure 1.19)[82]. The above is followed by a deglycosylation reaction at the 3′- thymine, ultimately leading to DNA strand scission (Figure 1.16) [83].

A re-examination of the 6-4PP alkaline hydrolysis reaction under more detailed conditions suggested that the resulting water adduct is not as stable as previously suggested. Also,
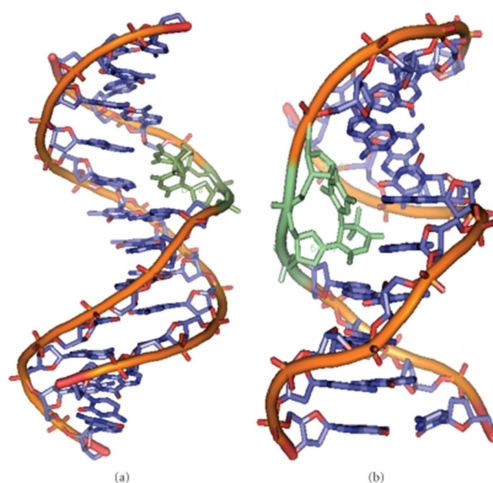
**Figure 1.17.** Structures of DNA duplexes showing the presence of (a) CPD and (b) 6-4PP lesion (in green). Hydrogen atoms are not shown, prepared from PDB entries 1TTD [78] and 1CFL [79] using PyMOL. (version 1.1r1)
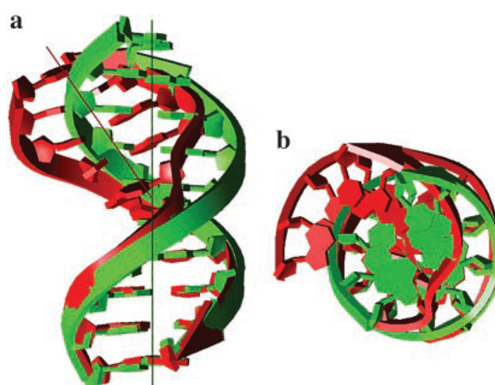


**Figure 1.18.** Schematic diagram illustrating CPD-induced kink of the DNA helix. Regular B-DNA and CPD-containing DNA are depicted in green and red, respectively. (a) Side view with a helical axis. (b) Top view. Figure adapted from [3]

it was found that the hydrolysis product undergoes an additional deamination reaction to yield 2-oxazolidinone (5-4) pyrimidone, eliminating the N3 as a molecule of ammonia (Figure 1.20)[72].

### 1.2.2 Alkaline hydrolysis of spore photoproduct (SP) and DNA strand scission

SP is formed as a result of a unique environment found exclusively within endospores. Endospores possess a low hydration environment and the presence of specialized DNA-binding
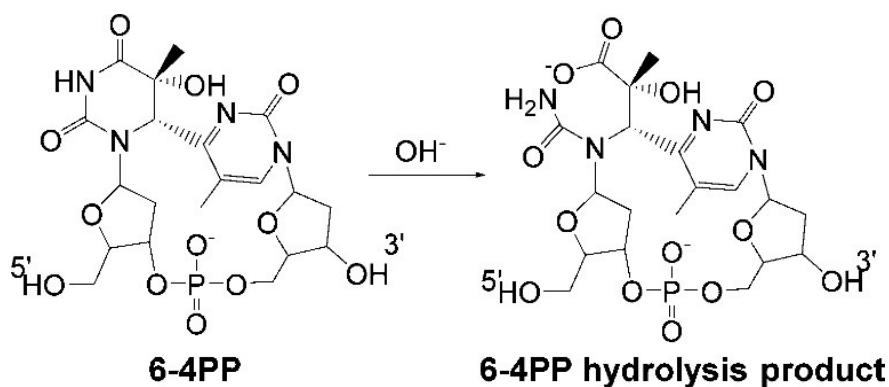
**Figure 1.19.** Alkaline hydrolysis reaction in 6-4PP as described by Higurashi *et al.* [82]. Figure adapted from [72]
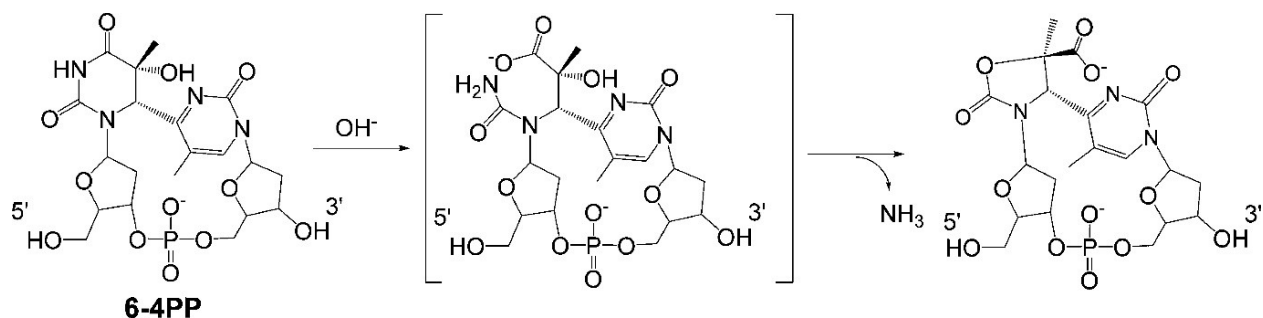


**Figure 1.20.** Modified hydrolysis reaction of 6-4PP

proteins called Small Acid Soluble Proteins (SASPs). Under these conditions, DNA transforms from a more commonly found B-form to an A-form, leading to a change in the proximity of nucleobase pyrimidines to one another [84], [85]. UV irradiation of this A-form of DNA results in SP as the dominant (>95% yield) photo-lesion [36], [86].

To investigate the chemical reactivity of SP, the behaviour of this lesion was studied at and above physiological pH values [6]. *These studies showed that the loss of aromaticity in the thymine residue on the 5′-side of the SP dimer, activates the C4 position in this nucleobase, making it susceptible to water addition and formation of a hemiaminal intermediate at or above neutral pH. Under basic conditions, this hemiaminal species undergoes a rupture of the N3-C4 bond leading to a hydrolysis product that readily triggers a cascade of elimination reactions that can, eventually, lead to DNA strand scission* (Figures 1.16 and 1.21).

The formation of hemiaminal intermediates in SP occurs at pH 7.4, and is facilitated by basic conditions. Once formed, the fate of the hemiaminal intermediate is dependent on the
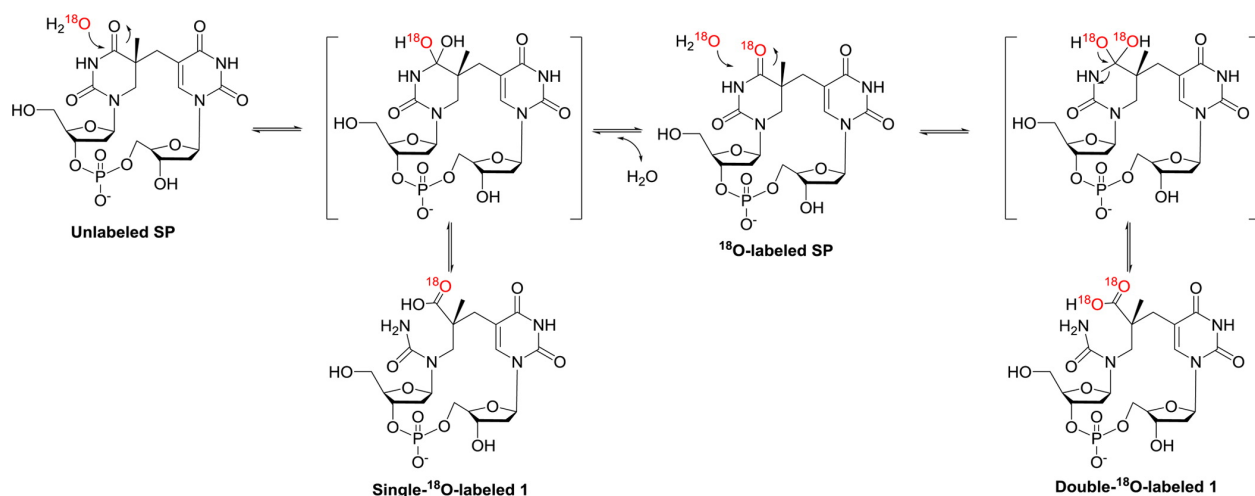
**Figure 1.21.** General scheme for $^{18}$O incorporation into SP TpT. Figure adapted from [6]

pH of the surrounding medium. A high hydroxide concentration (such as that found at pH 13 and above) forces a vast majority of the hemiaminal intermediate to decompose via N3-C4 bond rupture, resulting in the SP hydrolysis product. A low hydroxide concentration, however, favours hydroxide elimination from the hemiaminal intermediate, thus reverting to SP. This observation is supported by the rates of $^{18}$O exchange in SP, during which the vast majority of SP hemiaminal intermediates decay back to SP, as indicated by the negligible yield of SP hydrolysis product at pH 11 and the mere 70% yield under conditions of concentrated base.

The fate of the SP hydrolysis product also depends on the pH of solution. In a neutral medium, the hydrolysis product is unstable leading to a cascade of elimination reactions and, ultimately, strand scission. Under strong alkaline conditions, however, the major decay pathway of the hydrolysis product is to eliminate water and revert to SP (again via the hemiaminal intermediate).

### 1.2.3 Complete decay of dHdU hemiaminal intermediates to elimination products at alkaline pH

5,6-dihydro-2′-deoxyuridine (dHdU) pyrimidine lesions result from ionizing damage to cytosine under anoxic conditions [38]. It has been demonstrated that treatment of dHdU with concentrated base for 30 minutes resulted in its complete conversion to the hydrolysis

product dHdU-H$_2$O [6]. This is in contrast to the slower and incomplete conversion of SP to its hydrolysis product SP-H$_2$O under the same conditions. These results suggest that relative to SP, the N3-C4 bond in dHdU is more prone to base hydrolysis (Figure 1.22).
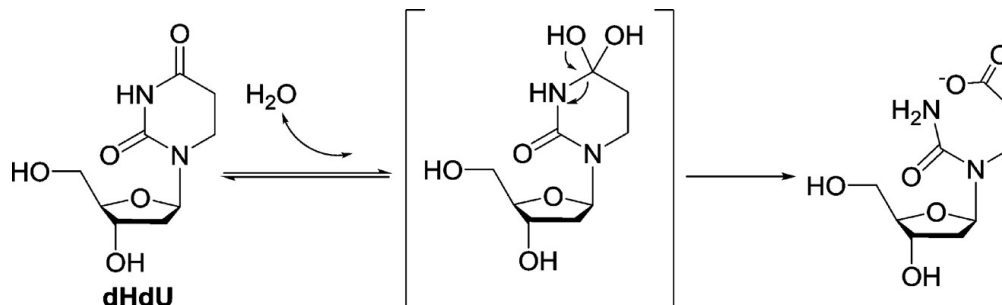


**Figure 1.22.** General scheme for alkaline hydrolysis in dHdU photolesion. Figure adapted from [6]

$^{18}$O incorporation experiments in dHdU (under conditions of concentrated base) indicated the presence of a double $^{18}$O labeled dHdU-H$_2$O adduct, suggesting that the single $^{18}$O labeled dHdU-H$_2$O must be formed, similar to that observed in SP. However, the unchanged ratio of single to double $^{18}$O labeled dHdU-H$_2$O over an extended period of time indicated that the dHdU hydrolysis product is not prone to reversal in contrast to the reversible formation of SP hydrolysis product at alkaline pH. Further analysis of dHdU under weak basic conditions (pH 11.0) suggested that the formation of an hemiaminal intermediate is reversible (similar to that observed in SP), but the formation of hydrolysis products from the decomposition of hemiaminal species is not [6].

### 1.2.4 Hemiaminal intermediate formation during deamination of damaged cytosine (C) and 5-methylcytosine (5mC) at neutral pH

It is worth mentioning that there is evidence for the formation of hemiaminal species in the chemistry of cytosine residues as well as thymine and uracil. The C4-NH$_2$ moieties in damaged cytosine (C) and 5-methylcytosine (5mC) are known to be prone to deamination reactions at neutral pH [32], [87], which are also suggested to be mediated by a hemiaminal intermediate [88], [89]. Similarly, hemiaminal species are also known to occur during

the deamination reactions of cytidine and adenosine catalyzed by cytidine and adenosine deaminase enzymes respectively [90], [91].

*These results suggest that N3-C4 bond cleavage is probably a common feature possessed by saturated pyrimidine residues.*[6] **Collectively, it appears that in a saturated pyrimidine residue, the C4 position becomes a "hot spot" for subsequent water addition-elimination reactions via a tetrahedral intermediate in living cells, the decay route of which appears to be influenced by the chemical environment of the ring (based on different reaction outcomes observed in case of different lesions under similar reaction conditions) (Figure 1.23)**. The crystal structure of SP and NMR study of dHdU suggest alterations in the structure of a saturated pyrimidine ring that further support this hypothesis. In the case of SP, the crystal structure of the lesion revealed clearly that the 5′- thymine ring is distorted from a planar structure, with the C6 and the methyl moiety located 0.5 Å above the plane defined by the other five atoms (Figure 1.24) [88], [89]. Even in dHdU, loss of aromaticity results in a similar outcome, as shown by a NMR spectroscopic study [38]. Although the C4 amide moiety undergoes little structural alteration due to resonance interactions among the carbonyl moieties and the lone pairs of the two N atoms still intact, in all these instances, **loss of aromaticity and the ring distortion likely activate the C4 position in these saturated nucleobases, promoting the generation of a hemiaminal intermediate.** The formation of a hemiaminal intermediate also suggests the presence of a labile oxygen at C4 position of the molecule that is exchangeable with the aqueous solution.
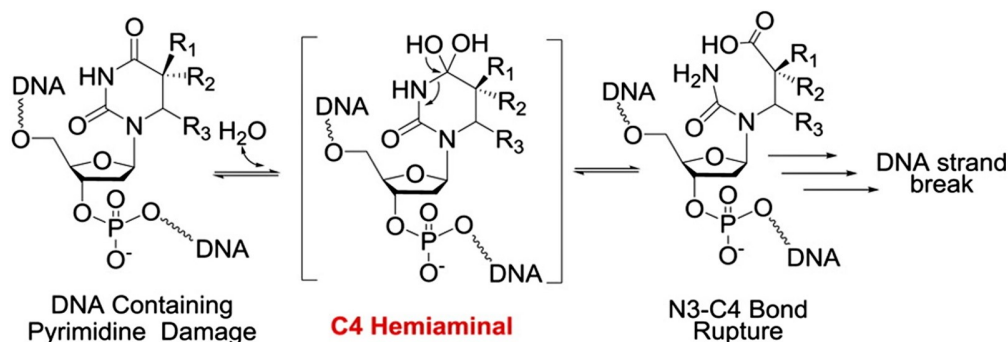


**Figure 1.23.** General scheme for alkaline hydrolysis of DNA containing pyrimidine damage. Figure adapted from [6]
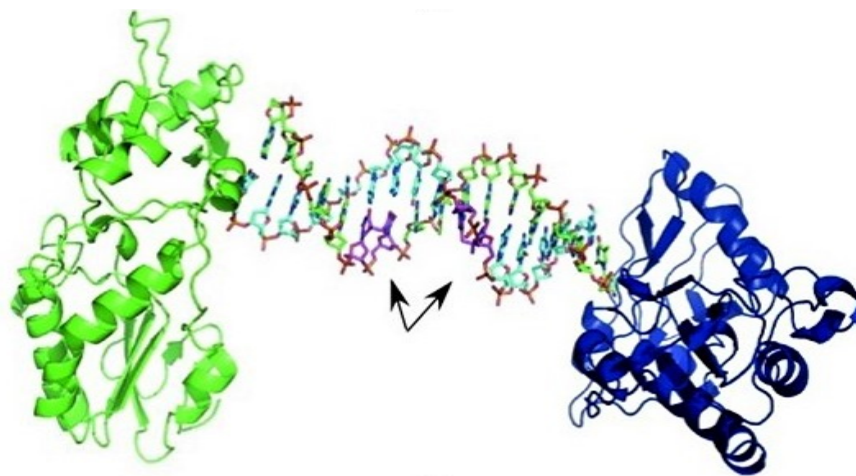
**Figure 1.24.** Crystal structure of the SP-containing duplex 16-mer oligonucleotide in a host–guest complex. Figure adapted from [88]

### 1.2.5 Summary: Alkaline hydrolysis of various DNA lesions and previous studies of the alkaline reactivity of CPD lesions

To date, the base-catalyzed addition-elimination reactivity of the pyrimidine lesions 6-4PP, SP, dHdU and CPD have been studied to various extents. Although it appears that the first step, *i.e.* formation of a gem-diol intermediate at C4=O followed by rupture of the N3-C4 bond probably occurs for all lesions [6], the ultimate fate of the resulting modified lesion varies significantly among pyrimidine dimer lesions. At one extreme, the N3-C4 bond rupture of the gem-diol intermediate in dHdU is *irreversible*; the hydrolysis product that results has few choices but to undergo the deglycosylation process eventually leading to DNA strand scission. In contrast, the hydrolysis reaction of SP is *reversible*, which lowers the yield of the hydrolysis product and reduces the DNA strand cleavage efficiency. Similar to dHdU, the hydrolysis product of 6-4PP is *unlikely to be reversible* after the formation of the gem-diol intermediate [4], [83]; the putative hydrolysis product is not stable and, thus, cannot be isolated. What can be isolated is the deaminated product, 2-oxazolidinone (5-4) pyrimidone [72]. Thus, even if there is a possibility of the hydrolysis reaction in 6-4PP to be reversible, deamination initiated by the 5′-OH group in the putative hydrolysis product effectively competes with the reverse reaction, leading to 2-oxazolidinone (5-4) pyrimidone as the final hydrolysis product.

In contrast to the reactivities of 6-4PP, SP and dHdU described in the previous sections, there are very few studies on the alkaline hydrolysis of cyclobutane pyrimidine dimer (CPD). While previous studies have explored the reactivity of CPD derived from two thymines (nucleobases) or two thymidines (nucleobase + sugar) moieties, these model studies fail to reflect DNA in living systems. Indeed, the study of the alkaline reactivity of CPD derived from thymine alone explored the reactivity of four isomers *i.e. cis-syn, cis-anti, trans-syn* and *trans-anti*, all of which are formed when a solution of free thymine is irradiated with UV radiation (Figure 1.25) [5], but unlikely to form in biologically-relevant DNA structure. The *cis-syn* and *trans-syn* isomers (labeled as isomers 1 and 3 in Figure 1.25) were found to be stable even in presence of concentrated alkaline solutions at room temperature (Figure 1.26). The *trans-anti* isomer (labeled as isomer 4 in Figure 1.25), however, underwent ring opening in presence of 0.01 M NaOH solution at room temperature to yield a cyclobutane dicarboxylic acid derivative (Figures 1.26 and 1.27). Under conditions of high temperature, however, even the *cis-syn* isomer that was refractory to hydrolysis at room temperature, underwent ring opening to yield the cyclobutane dicarboxylic acid derivative (Figure 1.28) [92], [93]. In all these experiments, no attempt was made to reveal the reversibility of the generated hydrolysis product. Moreover, no studies are known for the alkaline reactivity of CPD derived from nucleotides, the biologically relevant form of DNA.
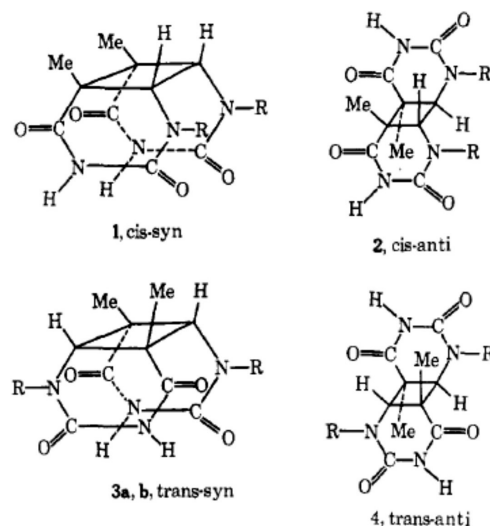


**Figure 1.25.** The four possible isomers of CPD-thymine (R=H) formed after UV-irradiation of a frozen solution of thymine. Figure adapted from [5]
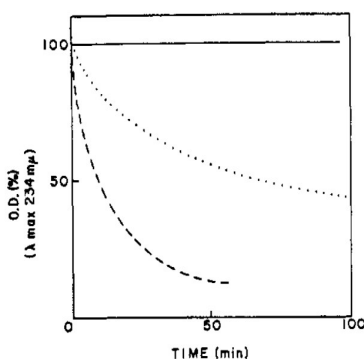
**Figure 1.26.** Stability of thymine dimers 1 and 3 to base (-) and easy alkaline ring opening of dimer 4 by 0.01 N NaOH (. . .) and 0.1 N NaOH (- - -) at room temperature (1.6 X $10^{-4}$ mol/l.). Figure adapted from [5]
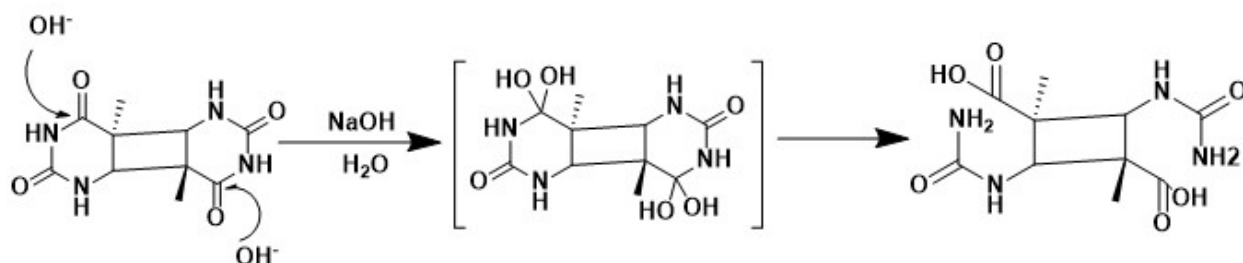


**Figure 1.27.** General scheme showing alkaline hydrolysis in *trans,anti* isomer of CPD-thymine at room temperature

Thus, the chemical structure of a given pyrimidine lesion influences the outcome of its reaction with alkali. Although dHdU and SP share similar chemical structures, the cross-link bond between the two thymine bases in SP likely places some degree of restriction on the 3D structure, which influences the reverse reaction, even though the negatively charged carboxyl moiety is a weak electrophile and the amide is a weak nucleophile. Given that the stacking interactions that occur between the two thymine residues are maintained in both SP and *cis-syn* CPD, as revealed by the dinucleotide as well as lesion-containing oligonucleotide structures, it is thus highly likely that the *cis-syn* CPD may also exhibit a similar reversible hydrolysis reaction.
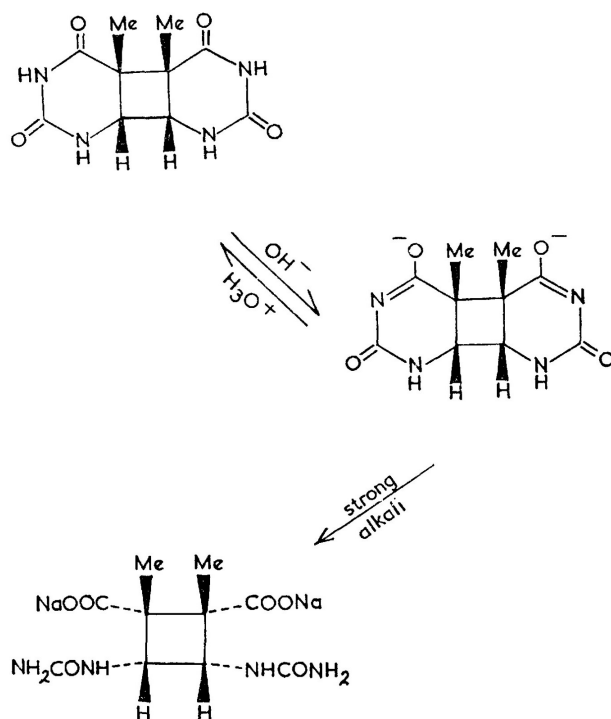
**Figure 1.28.** Alkaline hydrolysis of *cis-syn* CPD-Thymine in presence of 0.1M NaOH at 75°C for ≈ 24 hours. Figure adapted from [93]

### 1.2.6 Thesis statement

*In light of the above studies, it is hypothesized that the C4 position of a saturated pyrimidine residue becomes a "hot spot" for water addition-elimination reactions via a tetrahedral intermediate, the final outcome of which appears to be influenced by the chemical environment of the ring.*

The work described in Chapters 2 and 3 tests the above hypothesis in the most common DNA lesion encountered in living cells *i.e.*, the *cis-syn* isomer of cyclobutane pyrimidine dimer (CPD). As noted earlier, previous work on cyclobutane pyrimidine dimers formed from thymine and thymidine clearly show that *cis-syn* CPD is stable in teh presence of high concentration of alkali (1M) at room temperature (Figure 1.26). Since all other lesions with a saturated pyrimidine ring undergo ring-opening under much milder conditions than employed in the case of CPD, the inertness of CPD to alkaline hydrolysis indicates a possibly unique reactivity worthy of investigation.

As described in subsequent chapters, the results of our studies of cyclobutane pyrimidine dimers derived from dinucleotide TpT confirm the results found with CPD lesions derived from free thymines and thymidines. We found that CPD-TpT does not react even in presence of concentrated alkali (up to 1M concentration). Even more fascinating was the observation that CPD-TpT is refractory to hydrolysis even at higher temperatures (up to 90°C) (Figure 1.29). In comparison, CPD-thymine underwent ring opening in presence of concentrated alkali when the temperature was increased only to 75°C (Figure 1.28). This observation indicates the reduced lability of the N3-C4 bond in a dinucleotide environment *vs* the cyclization of free nucleobase (thymine).
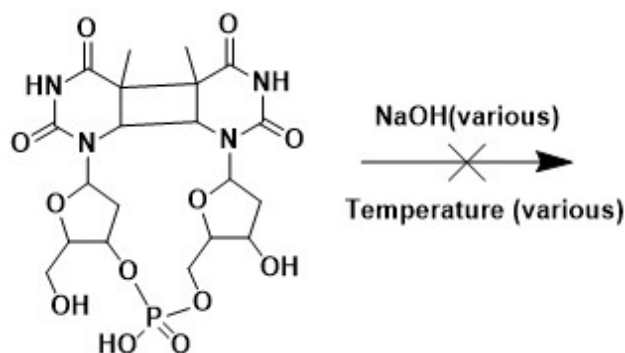


**Figure 1.29.** General overview of alkaline hydrolysis reaction of cyclobutane pyrimidine dimer from dinucleotide TpT (CPD-TpT)

However, our investigation of the same reaction in $^{18}$O labelled water indicates that, similar to other DNA lesions, CPD undergoes a water addition at the C4 carbonyl group leading to the formation of a hemiaminal intermediate. This intermediate, however, does not lead to hydrolysis products and completely reverts back to the starting material (Figure 1.30). Moreover, the two C4 carbonyl groups present on 3′ and 5′-thymines in a CPD molecule show different predispositions towards water attack, which is reflected by different rates of exchange with the incoming nucleophile leading to the hemiaminal intermediate. Along with studies involving dinucleotide models, the reactivities of these lesions were further explored in an oligonucleotide setting and in various structural variants of CPD-TpT, to prove that the observed differential reactivity observed between C4 carbonyl groups on 3′ and 5′-thymines

in CPD is an intrinsic property of the CPD lesion, and not simply an artifact of steric accessibility .
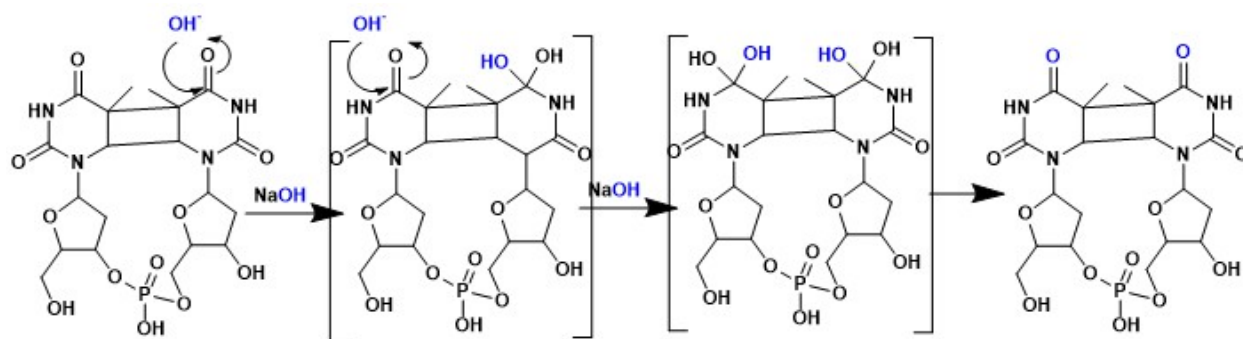


**Figure 1.30.** Nucleophilic addition to C4 carbonyl groups in a CPD molecule leading to the formation of a gem-diol intermediate

Hydrazine-induced CPD repair as a novel and efficient DNA repair pathway

During our investigation of the nucleophilic reactivity of the cyclobutane pyrimidine dimer (CPD) molecule, a chemical reaction leading to the rapid and total reversion and chemical repair of CPD lesion to TpT was discovered! This repair reaction occurs in the presence of hydrazine monohydrate, and is facilitated by an inert atmosphere under which the reversal of CPD to TpT is completed rapidly (in less than two hours). In the presence of oxygen, the rate of this reaction is significantly reduced (starting material not completely used up even after 24 hours, at elevated temperatures). As described in Chapter 4, this reaction was investigated using four orthogonal techniques: reverse-phase HPLC, UV-Visible spectroscopy, NMR spectroscopy and LC-MS, in an attempt to determine the reaction rate and to characterize the intermediate(s) and possible mechanisms involved.

# 2. DEFINING THE ALKALINE REACTIVITY OF DINUCLEOTIDE CYCLOBUTANE PYRIMIDINE DIMER (CPD) LESIONS

## 2.1 Introduction

This chapter reports the investigation of the alkaline reactivity of a dinucleotide model of the most common DNA photolesion encountered in living cells, the cyclobutane pyrimidine dimer (CPD) [3], [32], [33]. Photo-irradiation of living cells results primarily in the formation of the *cis-syn* isomer of CPD. As outlined in Chapter 1, earlier work on cyclobutane pyrimidine dimers resulting from free thymine nucleobases and thymidine nucleosides clearly show that *cis-syn* CPD is stable in the presence of a high concentration of alkali (1 M) at room temperature [5]. The results described in this chapter investigated cyclobutane pyrimidine dimers resulting from the dinucleotide TpT and are consistent (Figure 2.1); our additional investigation of the same reaction in $^{18}$O labeled water indicated that, similar to other DNA lesions, CPD undergoes a water addition at the C4 carbonyl group leading to the formation of a hemiaminal intermediate. This intermediate, however, does not lead to further hydrolysis products and completely reverts to the starting lesion (Figure 2.2). Moreover, these investigations determined that the two C4 carbonyl groups present on each of the 3′ and 5′ thymines in a CPD molecule show different chemical reactivities, which are reflected by different rates of exchange with the incoming nucleophile leading to the hemiaminal intermediate.
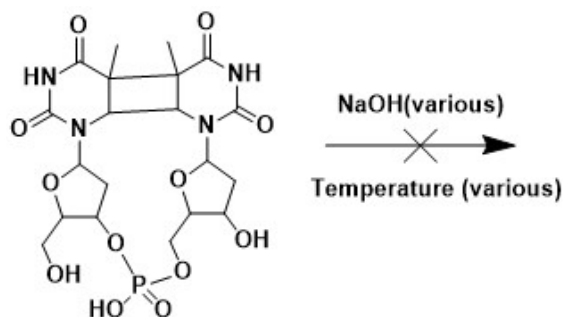


**Figure 2.1.** General overview of alkaline hydrolysis reaction of cyclobutane pyrimidine dimer from dinucleotide TpT (CPD-TpT)
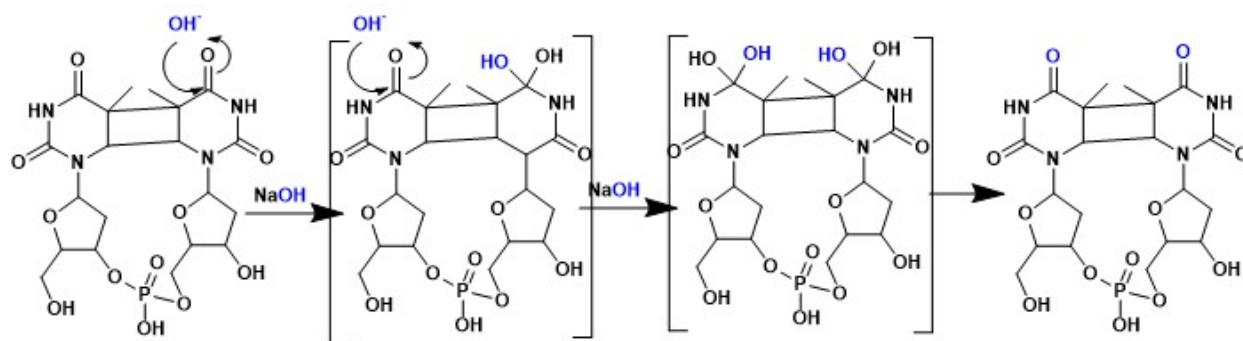
**Figure 2.2.** Nucleophilic addition to C4 carbonyl groups in a CPD molecule
leading to the formation of a gem-diol intermediate

As reviewed in Chapter 1, the alkali-catalyzed addition-elimination reactions of four kinds of pyrimidine lesions: 6-4PP, SP, dHdU and CPD, have been reviewed to varying extents [5], [6], [72], [82], [83], [92], [93]. *Although it appears that the first step, i.e., formation of gem-diol intermediate at C4=O followed by rupture of the N3-C4 bond probably occurs for all lesions, the fate of the resulting hydrolysis products varies significantly across various lesions.* The N3-C4 bond rupture from the gem-diol intermediate in dHdU is irreversible [6]. The hydrolysis product that results has fewer choices but to undergo the deglycosylation process eventually leading to strand scission. In contrast, the hydrolysis reaction in SP is reversible, which lowers the yield of the hydrolysis product and reduces the strand cleavage efficiency [6]. Similar to dHdU, the hydrolysis product in 6-4PP is not likely to be reversible [72]. The putative hydrolysis product of 6-4PP (formed after the cleavage of N3-C4 bond) is not stable and thus, cannot be isolated. It undergoes an additional deamination step to yield 2-oxazolidinone (5-4) pyrimidone, the final product of 6-4PP alkaline hydrolysis. Thus, even if there is a possibility of the hydrolysis reaction in 6-4PP to be reversible, deamination initiated by the 5-OH group in the putative hydrolysis product effectively competes with the reverse reaction, leading to 2-oxazolidinone (5-4) pyrimidone as the final hydrolysis product. Thus, the chemical structure of a given pyrimidine lesion determines the outcome of its reaction upon base treatment, *i.e.* its alkaline lability. For example, although dHdU and SP share similar chemical structures, the cross-link bond between the two thymine bases in SP likely places some degree of restriction on the 3D structure, which drives the occurrence of

the reverse recyclization reaction, even though the negatively charged carboxyl moiety is a weak electrophile and the amide is a weak nucleophile.

In comparison to 6-4PP, SP and dHdU, there are very few studies devoted to understanding the alkaline hydrolysis of cyclobutane pyrimidine dimer (CPD) [5], [92], [93]. Even the ones that are available, explore the reactivity of CPD lesion derived from thymine (nucleobase only) or thymidine (nucleoside) moieties, none of which reflect the true state of DNA in living systems. Indeed, the study on alkaline reactivity of CPD-thymine explored the reactivity of all four possible isomers which result on irradiation of thymine base with UV radiation [5]. The *trans,anti* isomer of CPD-thymine was readily hydrolyzed, resulting in a full-hydrolysis product with the two N3-C4 bonds cleaved. In contrast, *cis-syn* CPD-thymine was initially refractory to hydrolysis even in presence of concentrated alkali (Figures 1.26 and 1.27). A later study, however, found that a 24 hour treatment using 0.1 M sodium hydroxide solution at 75°C, resulted in a full-hydrolysis product (Figure 1.28) [92], [93]. However, no attempt was made to reveal the reversibility of the generated hydrolysis product. It should be noted that the stacking interactions between the two thymine residues are maintained in both SP and *cis-syn* CPD, as revealed by the dinucleotide as well as lesion-containing oligonucleotide structures. It is thus, highly likely that the *cis-syn* CPD may also exhibit a similar reversible hydrolysis reaction. Moreover, no studies have been reported for the alkaline reactivity of CPD derived from dinucleotides, a much closer model to true DNA relative to free nucleobases.

## 2.2  Results

### 2.2.1  ESI-MS analyses of the alkaline hydrolysis of CPD-TpT in $^{18}$O labelled water

Incubation of dinucleotide CPD-TpT with various amounts of NaOH (up to 1 M concentration for 1 mM CPD-TpT) at various temperatures (up to 90°C) failed to yield hydrolysis products. This result was different from the results obtained during alkaline hydrolysis of CPD-thymine at elevated temperatures that led to the cleavage of the N3-C4 bond and subsequent formation of a cyclobutane dicarboxylic acid derivative (Figure 1.28) [92], [93]. To investigate the formation of a hemiaminal intermediate during alkaline hydrolysis of a

51

CPD lesion, the same reaction was conducted in the presence of $^{18}O$ labelled water. For this reaction, CPD-TpT was suspended in 250 mM NaOH solution prepared in $^{18}O$ labelled water. The final concentration of CPD-TpT was 1 mM. After every 24 hours, $\approx 0.5$ $\mu$L of the reaction mixture was withdrawn and was rapidly quenched by mixing with $\approx 19.5$ $\mu$L of 1 M ammonium acetate buffer to arrest the progress of the reaction. The aliquot containing the quenched reaction mixture was stored at -20°C. Similar aliquots were obtained after every 24 hours for a period of 18 days. After each collection, the eppendorf tube containing the original reaction mixture was carefully sealed to avoid the interaction of NaOH solution in the reaction mixture with atmospheric carbon dioxide, that is known to reduce the alkalinity of NaOH due to the formation of sodium carbonate.

ESI LC-MS (negative ion mode) analyses of the reaction between 1 mM CPD-TpT and 250 mM NaOH in $^{18}O$ labelled water at room temperature (Figure 2.3) showed a rapid decrease in the intensity of the mass of CPD-TpT that reached a base value of approximately 4% in 5 days whereafter it became constant. The decrease in M peak was accompanied by an increase in the intensity of (M+2) (formed by the exchange of a single $^{16}O$ with $^{18}O$ atom) and (M+4) (formed by the exchange of two $^{16}O$ atoms) peaks. *This observation suggests the existence of two sites of nucleophilic attack in the CPD molecule and a differential reactivity of the two sites towards an incoming nucleophile (evidenced by the different rates of increase of the M+2 and M+4 peaks).*
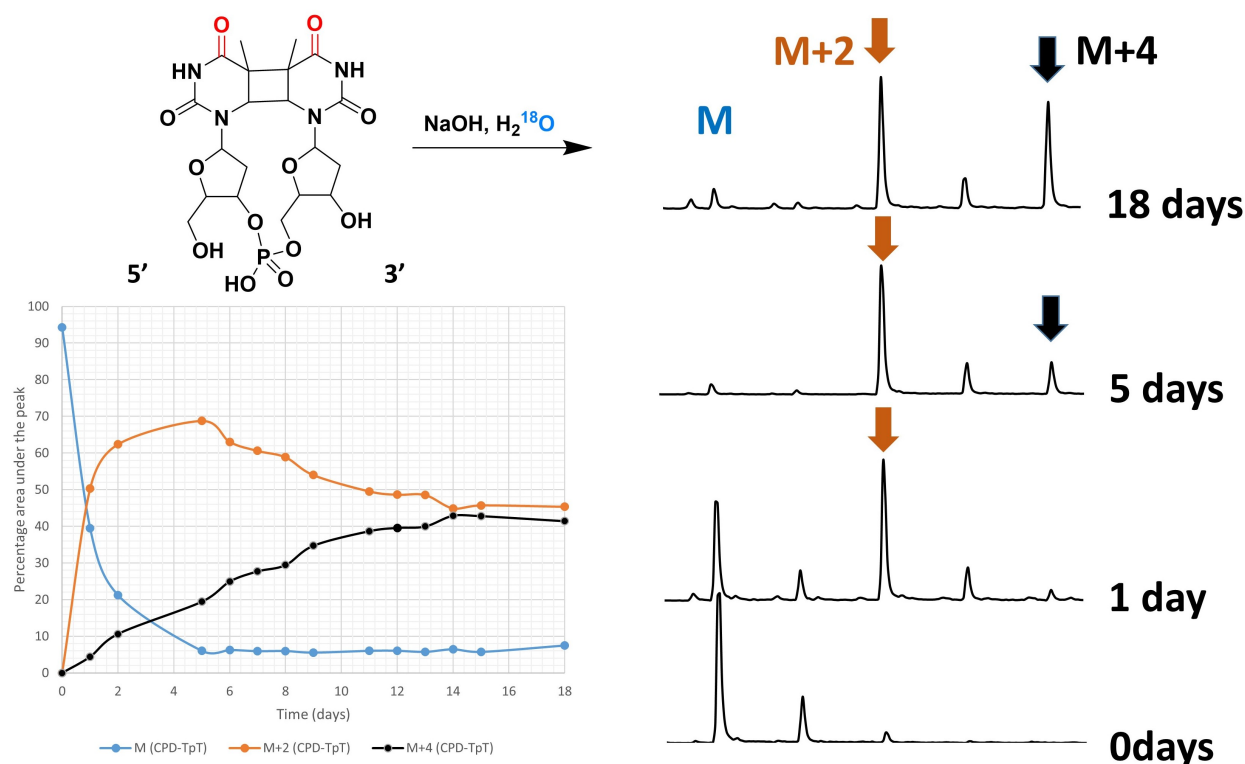
**Figure 2.3.** ESI-MS analysis of $^{18}$O exchange reaction in 1 mM CPD-TpT in presence of 250 mM NaOH solution in $^{18}$O labeled water at room temperature. Right panel: ESI-MS chromatograms showing $^{18}$O incorporation in CPD-TpT (increase in intensity of M+2 and M+4 peaks accompanying the decrease in M peak), Left panel: $^{18}$O exchange reaction kinetics in CPD-TpT monitored using ESI-MS over 18 days.

### 2.2.2 $^{13}$C NMR spectroscopic analyses of alkaline hydrolysis of CPD-TpT in $^{18}$O labelled water

In an attempt to clearly identify the site of $^{18}$O exchange in our CPD model (C2=O or C4=O), the same exchange reaction (CPD-TpT+NaOH in $^{18}$O labelled water) was again monitored using $^{13}$C NMR spectroscopy and ESI-MS. It should be noted that the carbonyl groups on C2 and C4 positions in a CPD molecule (C2=O and C4=O) have different chemical shift values on a $^{13}$C NMR spectrum (Figure 2.4). In fact, even the two C2=O groups on each of the 3′ and 5′ ends of the molecule (and the two C4=O groups) appear as distinct peaks on the $^{13}$C NMR spectrum of CPD-TpT. As shown in Figure 2.4, the two C2=O groups have chemical shift values of 153.6165 ppm and 154.1394 ppm, respectively while the two C4=O

groups appear at 172.4110 ppm and 173.3148 ppm respectively. Figure 2.5 shows the $^{13}$C NMR spectrum of TpT for reference. In a TpT molecule, the two C2=O groups appear at 151.4545 ppm and 151.6308 ppm respectively. In comparison, the two C4=O groups appear at 166.1712 ppm and 166.3362 ppm respectively. Thus, the process of dimerization between the two thymine rings has more effect on the electronic environment around the C4=O groups as compared to that of the C2=O groups. Figures 2.4 and 2.5 clearly show that the dimerization process leads to a downfield shift of approximately 6 ppm for the C4=O groups. For the C2=O groups, this shift is ≈2 ppm. Formation of the cyclobutane ring also leads to increased differentiation between the environments of the two C4=O groups (and the two C2=O groups). This is reflected by the difference in $^{13}$C chemical shift values; 0.9038 ppm in CPD-TpT versus 0.165 ppm in TpT for the C4=O groups and 0.5229 ppm vs 0.1763 ppm for the C2=O groups.
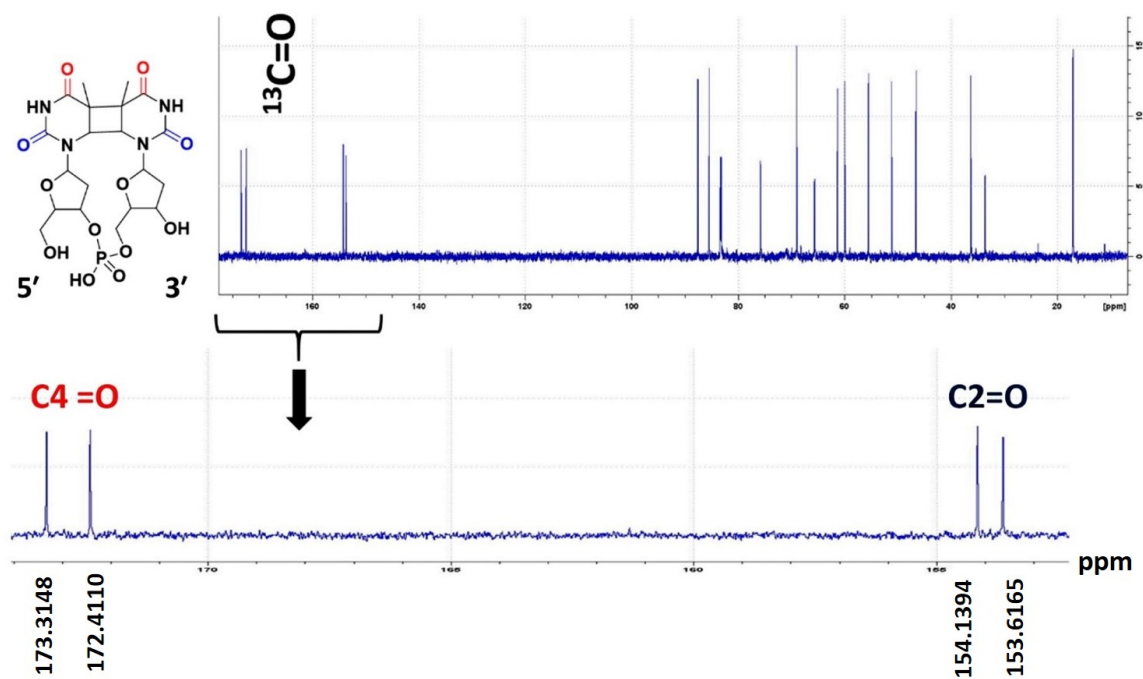


**Figure 2.4.** $^{13}$C NMR spectrum of dinucleotide CPD-TpT

54
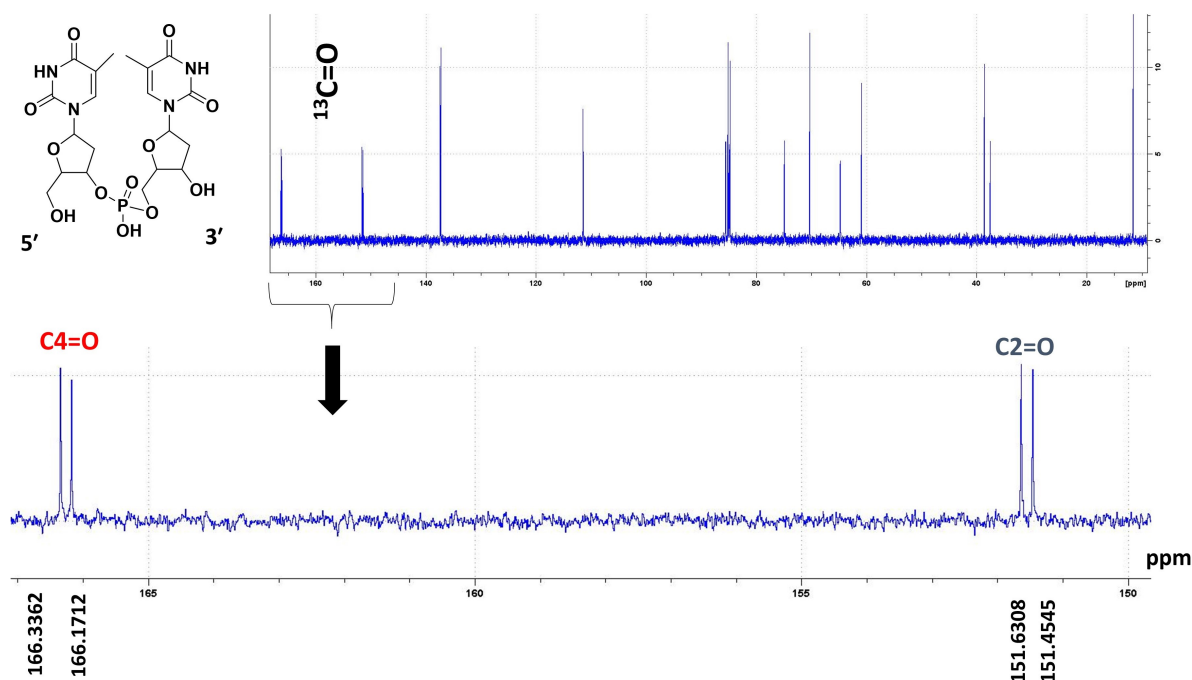
**Figure 2.5.** $^{13}$C NMR spectrum of dinucleotide TpT

The electronic influence of $^{16}$O is different than that of $^{18}$O on the carbon atom in a carbonyl group. As a result, an $^{18}$O atom directly attached to a $^{13}$C atom has been shown to cause a small (0.010-0.050 ppm) upfield shift in the $^{13}$C NMR resonance position as compared to that of the $^{16}$O isotopomer (Figure 2.6) [72], [94]–[97]. Keeping that in mind, an $^{18}$O-induced upfield shift in the $^{13}$C NMR resonance position of the carbonyl group undergoing the exchange reaction was expected. *It should be noted that the intensity of the original* $C{=}^{16}O$ *peak decreases as the new* $C{=}^{18}O$ *peak emerges out of it.*

The reaction was set up by suspending $\approx$ 132 mM CPD-TpT in 250 mM NaOH solution prepared in $^{18}$O labelled water. At each time point, the reaction progress was first screened using LC-MS to ensure the optimal formation of (M+2) and (M+4) species. After a quick check with LC-MS, the reaction mixture was neutralized using an equimolar solution of HCl (to avoid signal reduction in the NMR peak of $^{13}$C=O carbon atom caused by NaOH). The reaction mixture pH was monitored using litmus paper. The NaCl salt formed as a result of the neutralization process was removed from the reaction mixture using RP-HPLC. The resulting solution was evaporated to dryness and re-dissolved in $D_2O$ for NMR measurements.

The results of $^{13}$C NMR-based investigation of the exchange reaction are summarized in Figure 2.7 and Figure 2.8 shows the ESI-MS scans taken right before the $^{13}$C NMR spectra. *As shown in Figure 2.7, there was no detectable change in the intensity of the two C2=O groups. In contrast, there was a clear indication of an $^{18}O$-induced upfield shift in the $^{13}C$ NMR resonances of both C4=O groups; this observation supports the notion that the C4=O group is the site of nucleophilic attack in a CPD molecule.*

Among the two available C4=O groups (on 3′ and 5′ ends), the one appearing downfield on the $^{13}$C NMR spectrum appears to react faster than the other C4=O. It makes sense, since the carbonyl group that appears downfield is more deshielded, and is therefore, more electrophilic that the other one. Based on these results, the following structures were assigned for the (M+2) and (M+4) species (Figure 2.9). It can be seen that there is still ambiguity in the structure assignment of the (M+2) species, since the chemical shift(s) due to the two C4=O (and the two C2=O) remain to be assigned (Figure 2.10).
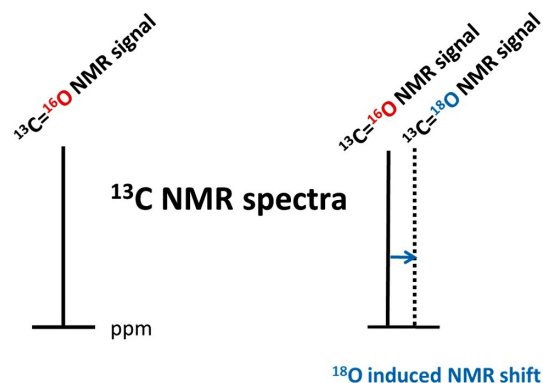


**Figure 2.6.** $^{18}$O-induced shift in $^{13}$C-NMR chemical shift
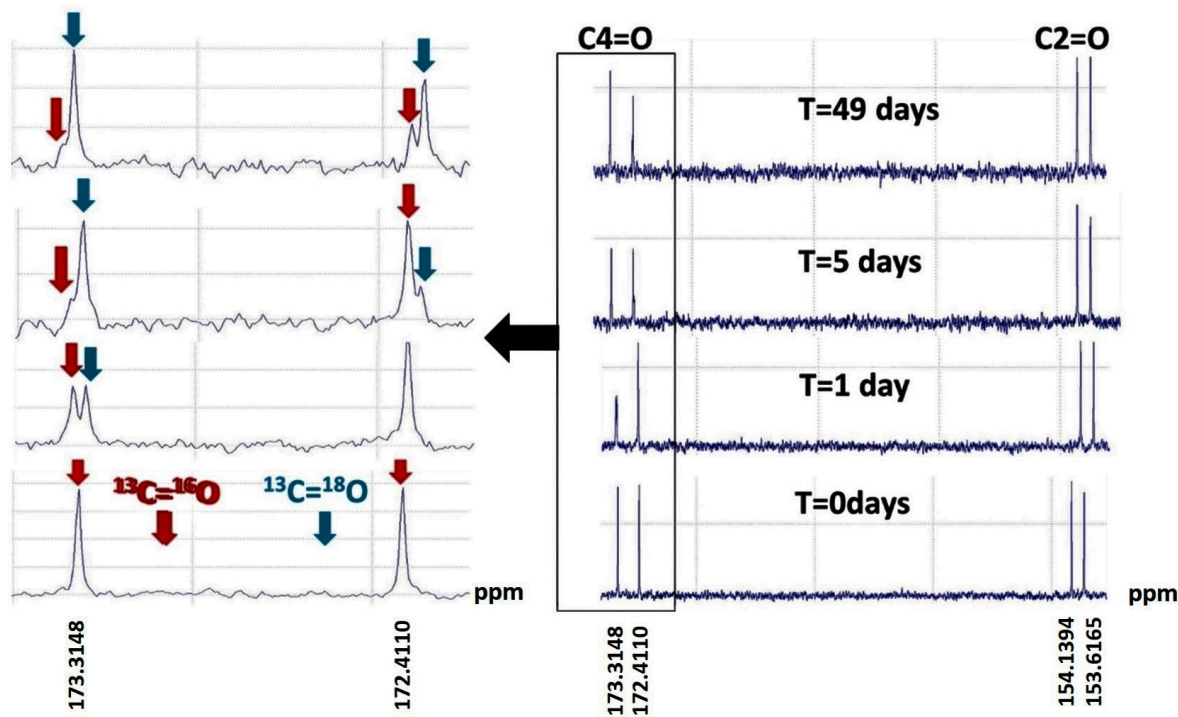
**Figure 2.7.** Selective $^{18}O$ incorporation into C4=O of CPD-TpT observed via $^{13}C$-NMR. Please refer to Figures 2.29, 2.30, 2.31 and 2.32 for the complete NMR spectrum at each of these time points.

### 2.2.3 Two-dimensional NMR (HMBC) analyses of CPD-TpT to determine the more electrophilic C4=O group

To distinguish between the two potential C4=O groups (and the two C2=O groups) on $3'$ or $5'$ termini of the CPD dinucleotide model, the molecule was analyzed using long-range heteronuclear correlation NMR spectroscopy (HMBC). ($H^1$, $^{13}C$)-HMBC provides correlations between protons and carbons that are two or three bonds apart from each other (though occasionally four-bond or even five-bond correlations may be observed). Thus, the carbon associated with the C4=O group was expected to undergo long-range heteronuclear coupling with the hydrogen(s) associated with the $-CH_3$ group and the $-CH_2$ group at C6 position (Figure 2.11). Since the $H^1$ NMR spectrum of CPD-TpT is well-characterized (Figure 2.12) [98], we could easily distinguish between the $-CH_3$ groups (and the $-CH_2$ groups) of the $3'$ and $5'$ ends. Thus, following the correlation of these peaks with the C=O group carbons, we could distinguish between the two C4=O carbonyl carbons (and the two C2=O carbons).
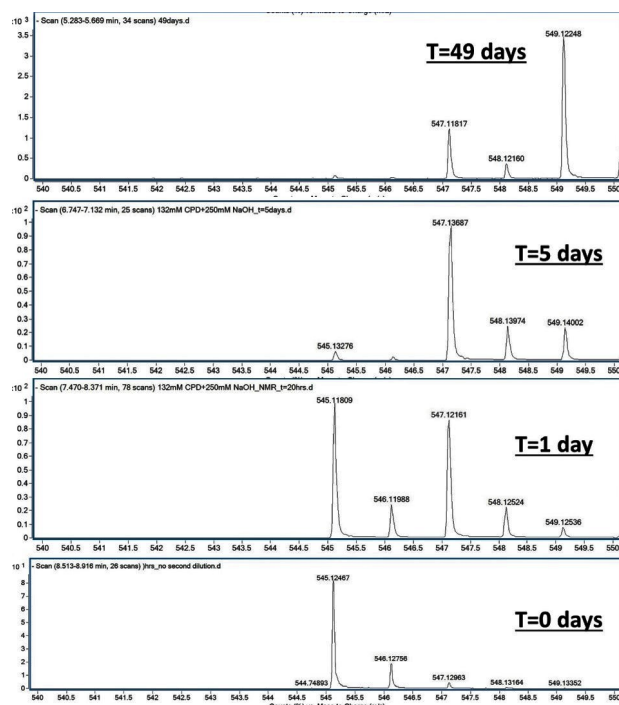
**Figure 2.8.** $^{18}O$ exchange reaction in CPD-TpT: ESI-MS scans recorded right before NMR analysis. The M peak ($m/z$=545) was rapidly replaced by a M+2 peak ($m/z$=547) at T=1 day. After 5 days, the M peak ($m/z$=545) was almost completely depleted and a M+4 peak ($m/z$=549) started showing up, that continued to grow throughout the course of the reaction.
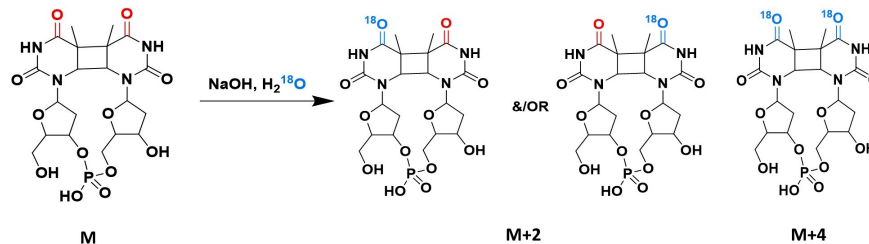


**Figure 2.9.** Possible structure(s) of the reaction products

Figure 2.13 shows the full HMBC spectrum for CPD-TpT with the cross-peaks between C4=O carbons and -CH$_2$ hydrogens highlighted. Based on known assignment of the H$^1$ NMR peaks [98], the -CH$_2$ hydrogen with the more downfield chemical shift (approximately 4.35 ppm) was assigned as the one from the 3′ terminus. *Consequently, since it showed a correlation with the downfield C4=O carbon (appearing at 173.3148 ppm), this C4=O carbon could be assigned as the one from 3′ end of the molecule.*
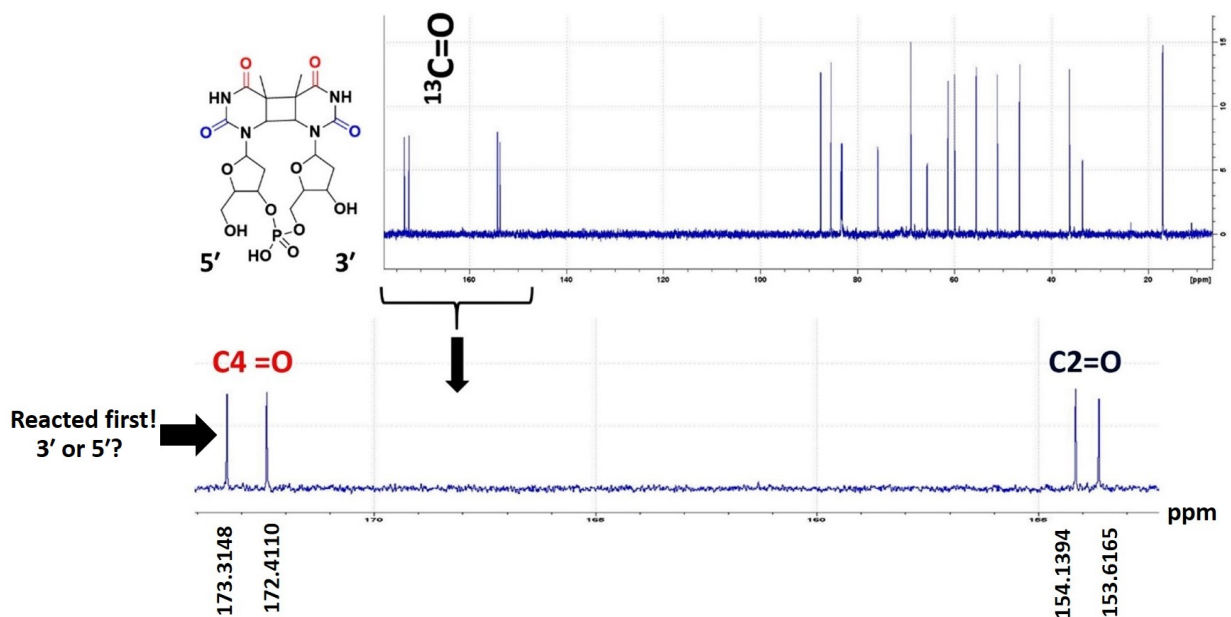
**Figure 2.10.** $^{13}$C NMR spectrum for CPD-TpT showing the more reactive C4=O moiety

To confirm this assignment, the cross-peaks between the C4=O carbon atoms and the –CH$_3$ group protons were examined as highlighted in Figure 2.14. Again, the –CH$_3$ proton appearing (relatively) upfield was identified as the one from the 3′ end. *Since it correlated with the downfield C4=O carbon, that carbon atom could surely be assigned as the one from 3′ end of the molecule, confirming our earlier assignment.* It should be noted that the C4=O carbon with relatively downfield resonance shift was the one that reacted first with the incoming nucleophile. *Thus, on the basis of our HMBC assignment, the C4=O carbon from 3′ side of the CPD molecule appears to be more reactive than the one from 5′ side.*
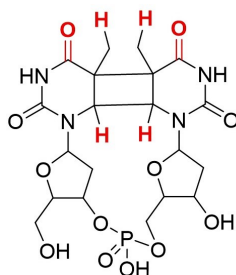


**Figure 2.11.** Structure of CPD-TpT with the highlighted hydrogen atoms (in red) undergoing long-range coupling with the C4=O groups

59

| Dideoxy-nucleoside | Residue | Chemical shift of | | | | | | | | |
|---|---|---|---|---|---|---|---|---|---|---|
| | | H1′ | H2′ | H2″ | H3′ | H4′ | H5′ | H5″ | CH$_3$/H5 | H6 |
| | | ppm | | | | | | | | |
| dCpdT | dCp- | 6.15 | 2.42 | 2.66 | 4.71 | 4.19 | 3.85 | 3.78 | 5.98 | 7.84 |
| | -pdT | 6.31 | 2.44 | 2.42 | 4.61 | 4.14 | 4.14 | 4.09 | 1.88 | 7.71 |
| t,s-dUpdT | dUp[ ]- | 5.27 | 3.29 | 2.57 | 4.72 | 4.12 | 3.70 | 3.66 | 3.75 | 4.59 |
| | -p[ ]dT | 5.72 | 2.15 | 2.03 | 4.53 | 3.89 | 4.15 | 4.21 | 1.48 | 4.32 |
| Δ1 | dYp- | 0.88 | −0.87 | 0.09 | −0.01 | 0.07 | − | − | 2.23 | 3.25 |
| | -pdY | 0.59 | 0.29 | 0.39 | 0.08 | 0.25 | − | − | 0.40 | 3.39 |
| c,s-dUpdT | dUp[ ]- | 5.62 | 2.70 | 2.32 | 4.66 | 4.20 | 3.73 | 3.68 | 3.50 | 4.44 |
| | -p[ ]dT | 6.02 | 2.34 | 2.20 | 4.26 | 3.95 | 3.95 | 4.10 | 1.63 | 4.40 |
| Δ2 | dYp- | 0.53 | −0.28 | 0.34 | 0.05 | −0.01 | − | − | 2.48 | 3.40 |
| | -pdY | 0.29 | 0.10 | 0.22 | 0.35 | 0.19 | − | − | 0.25 | 3.31 |
| dTpdC | dTp- | 6.22 | 2.35 | 2.52 | 4.76 | 4.16 | 3.82 | 3.77 | 1.88 | 7.68 |
| | -pdC | 6.29 | 2.32 | 2.43 | 4.56 | 4.18 | 4.15 | 4.07 | 6.10 | 7.97 |
| t,s-I-dTpdU | dTp[ ]- | 5.24 | 3.30 | 2.57 | 4.72 | 4.12 | 3.68 | 3.68 | 1.48 | 4.35 |
| | -p[ ]dU | 5.63 | 2.15 | 1.99 | 4.54 | 3.86 | 4.15 | 4.21 | 3.67 | 4.56 |
| Δ3 | dYp- | 0.98 | −0.95 | −0.05 | 0.04 | 0.04 | − | − | 0.40 | 3.33 |
| | -pdY | 0.66 | 0.17 | 0.44 | 0.02 | 0.32 | − | − | 2.43 | 3.41 |
| c,s-dTpdU | dTp[ ]- | 5.66 | 2.56 | 0.37 | 4.65 | 4.16 | 3.68 | 3.68 | 1.65 | 4.43 |
| | -p[ ]dU | 5.96 | 2.23 | 2.04 | 4.36 | 3.86 | 4.03 | 3.94 | 3.60 | 4.63 |
| Δ4 | dYp- | 0.56 | −0.21 | 0.15 | 0.11 | 0.00 | − | − | 0.23 | 3.25 |
| | -pdY | 0.33 | 0.09 | 0.39 | 0.20 | 0.32 | − | − | 2.50 | 3.34 |
| dTpdT | dTp- | 6.20 | 2.35 | 2.55 | 4.75 | 4.16 | 3.81 | 3.76 | 1.87 | 7.66 |
| | -pdT | 6.31 | 2.35 | 2.36 | 4.57 | 4.10 | 4.13 | 4.06 | 1.88 | 7.68 |
| t,s-dTpdT | dTp[ ]- | 5.24 | 3.27 | 2.57 | 4.74 | 4.17 | 3.70 | 3.66 | 1.46 | 4.26 |
| | -p[ ]dT | 5.69 | 2.18 | 2.00 | 4.52 | 3.87 | 4.10 | 4.11 | 1.48 | 4.35 |
| Δ5 | dTp- | 0.96 | −0.92 | −0.02 | 0.01 | −0.01 | − | − | 0.41 | 3.40 |
| | -pdT | 0.62 | 0.17 | 0.36 | 0.05 | 0.23 | − | − | 0.40 | 3.41 |
| c,s-dTpdT | dTp[ ]- | 5.65 | 2.61 | 2.38 | 4.65 | 4.16 | 3.72 | 3.67 | 1.52 | 4.25 |
| | -p[ ]dT | 5.98 | 2.31 | 2.10 | 4.32 | 3.93 | 4.10 | 3.99 | 1.47 | 4.33 |
| Δ6 | dTp- | 0.55 | −0.26 | 0.17 | 0.10 | 0.00 | − | − | 0.35 | 3.41 |
| | -pdT | 0.33 | 0.04 | 0.26 | 0.20 | 0.17 | − | − | 0.41 | 3.35 |

**Figure 2.12.** H$^1$ chemical shifts of the di-deoxy-nucleoside monophosphates dCpdT, dTpdC. dTpdT and their photoproducts at 300 K. Chemical shifts are in ppm relative to DSS. Adapted from [98]

### 2.2.4 Characterization of CPD-TpT with a selective $^{15}$N label on the 3′ side

To unambiguously verify the assignment of the C=O groups on the 3′ and 5′ ends of the CPD molecule, a CPD-TpT molecule with a selective $^{15}$N label on the 3′ end was synthesized. Since $^{15}$N is NMR active (I=1/2), it will selectively split the two carbonyl groups (both C2=O and C4=O) on the 3′ end leaving the 5′ carbonyls unperturbed (Figure 2.15).

Figure 2.16 shows the ESI-MS spectrum of 3′ $^{15}$N-CPD-TpT showing a $^{15}$N enrichment of around 73%. Figure 2.17 shows the $^{13}$C NMR spectrum of this same structure. This figure clearly shows the C4=O group with downfield chemical shift was split into a doublet. *These results establish that the peak with higher chemical shift value (more downfield) is located at the 3′ end of the molecule (the one that reacted first), which is in agreement with the results of our HMBC-based assignment.* It should be noted that $^{15}$N, that has a nuclear spin value of 1/2 (I=1/2) splits the C=O peak into a doublet (2I+1). The third peak seen in the $^{13}$C NMR resonance position of the C4=O (and C2=O) from 3′ end was the singlet
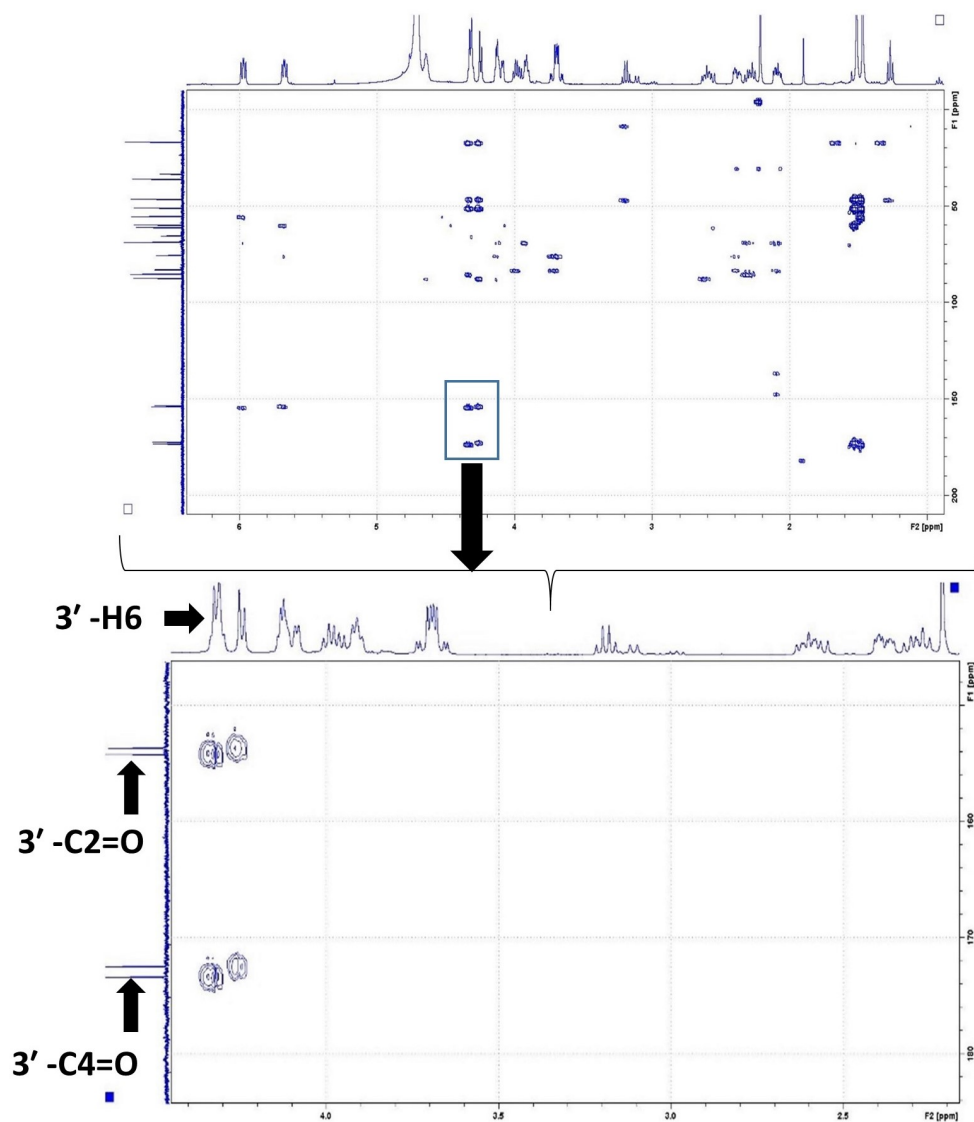
**Figure 2.13.** H$^1$-$^{13}$C HMBC spectrum showing the cross-peaks between -H6 hydrogens and C4=O groups

due to $\approx 27\%$ of the molecules that were without a $^{15}$N enrichment (Figure 2.18). Figure 2.19 shows a comparison of C=O group chemical shift values between $^{15}$N CPD-TpT and $^{15}$N TpT, both with an $^{15}$N label at the 3′ end. The figure clearly shows the effect of dimerization of the thymine rings on the environment around the C=O groups, with the C4=O group undergoing higher structural perturbation as compared to the C2=O group. The figure also shows a 'switch' between the chemical shift values of C4=O peaks from 3′ and 5′ ends, as
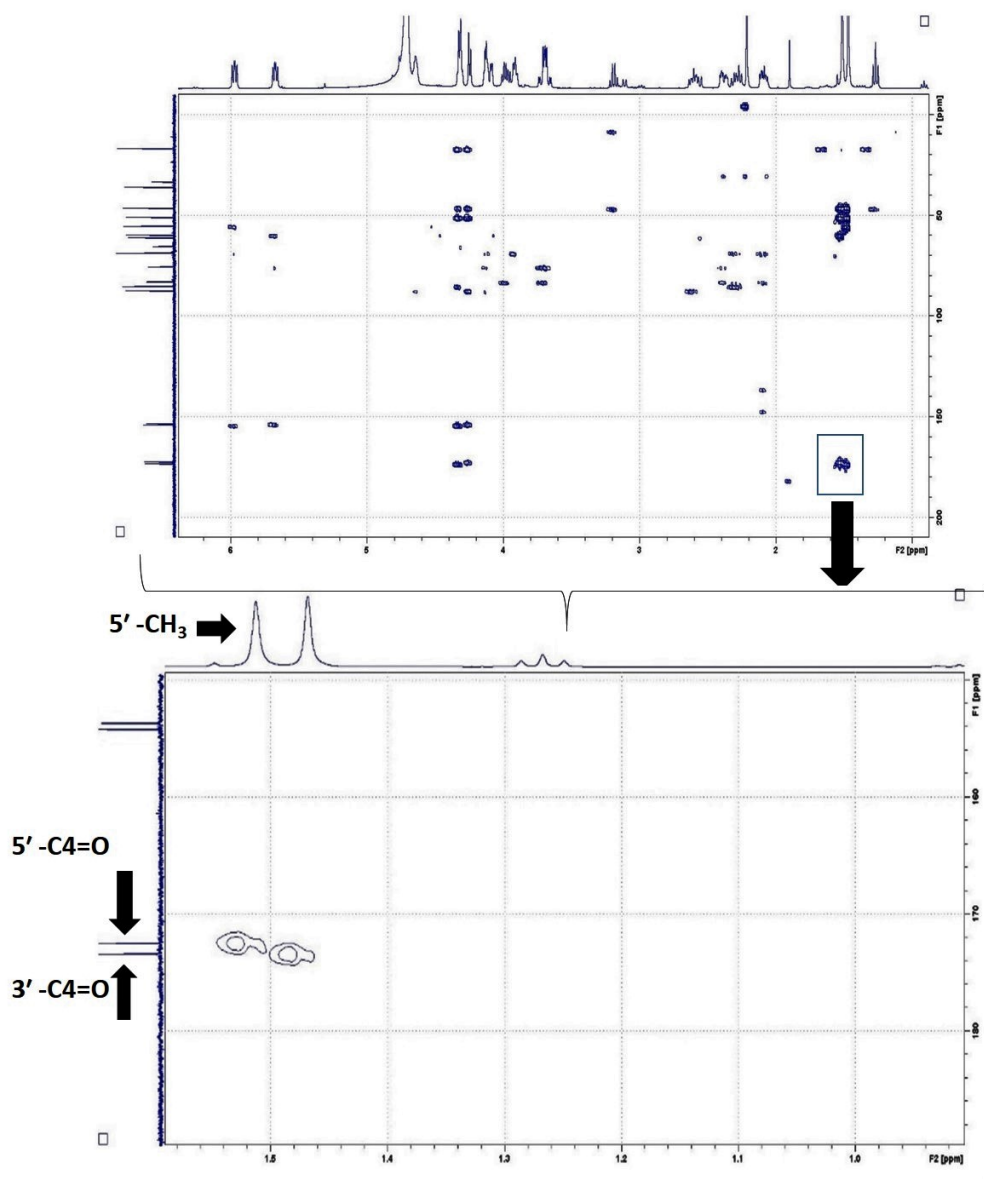
**Figure 2.14.** $H^1$-$^{13}$C HMBC spectrum showing the cross-peaks between -CH3 hydrogens and C4=O groups

a result of the dimerization process. *This 'switch' implies that the structural perturbation as result of dimerization is more pronounced in case of the C4=O group from 3′ side of the molecule as compared to the C4=O from 5′ side.* Based on the results of this HMBC-based assignment and the $^{13}$C NMR spectrum of $^{15}$N CPD-TpT, we assign a structure to the M+2 species observed during the $^{18}$O labeling experiment: Figure 2.20 shows the final products obtained after alkaline hydrolysis of CPD-TpT in $^{18}$O labeled water.

62
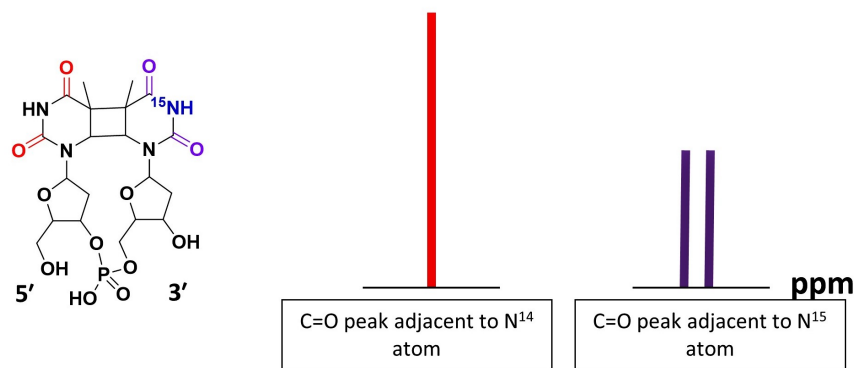
**Figure 2.15.** Schematic representation of $^{15}$N induced splitting in the $^{13}$C chemical shift of a C=O group
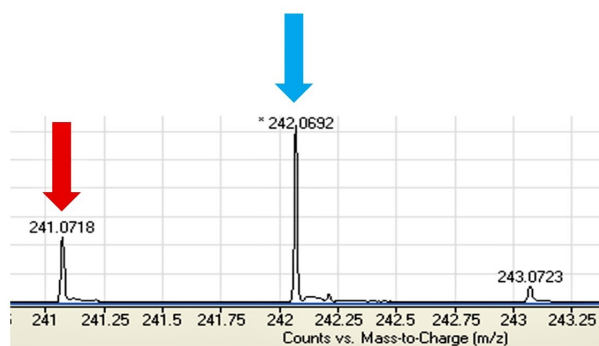


| Compound name | m/z=241 | m/z=242 |
|---|---|---|
| Batch2_N15 Thymidine | 26.81218488 | 73.18781512 |

**Figure 2.16.** ESI-MS chromatogram of CPD-TpT with selective $^{15}$N enrichment on the 3′ side

## 2.3 Discussion

The alkaline reactivity of the most common DNA lesion encountered in living cells *i.e.* cyclobutane pyrimidine dimer (CPD) was investigated using a unique dinucleotide model. Photo-irradiation of living cells results primarily in the formation of the *cis-syn* isomer of CPD. Earlier work on cyclobutane pyrimidine dimers resulting from thymine and thymidine clearly show that *cis-syn* CPD is stable in presence of high concentration of alkali (1 M) at room temperature (Figure 1.26) [5]

63
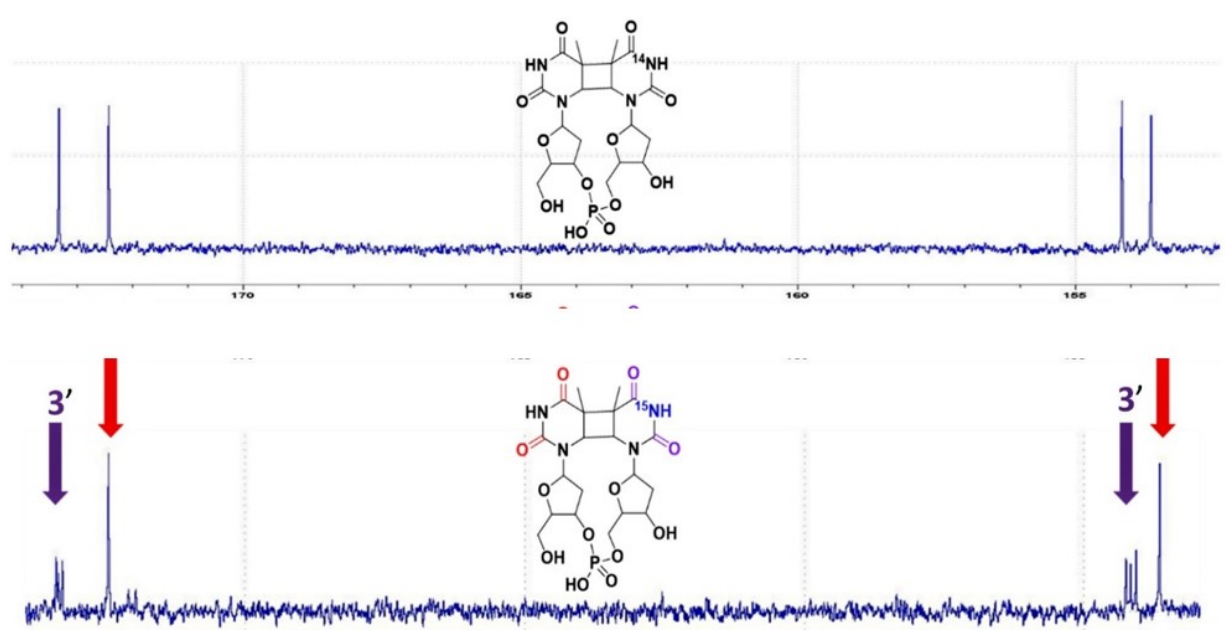
**Figure 2.17.** ^{13}C NMR spectrum of CPD-TpT with a selective ^{15}N label on 3′ side showing the C2=O and C4=O groups



**C4=O**

⬇ (blue) Doublet resulting from the interaction of C4=O with 73.2% of N[15]-labeled N3 (I=1/2 for N[15])

⬇ (red) Singlet resulting from the interaction of C4=O with 26.8% of unlabeled N3 (I=0 for N[14])
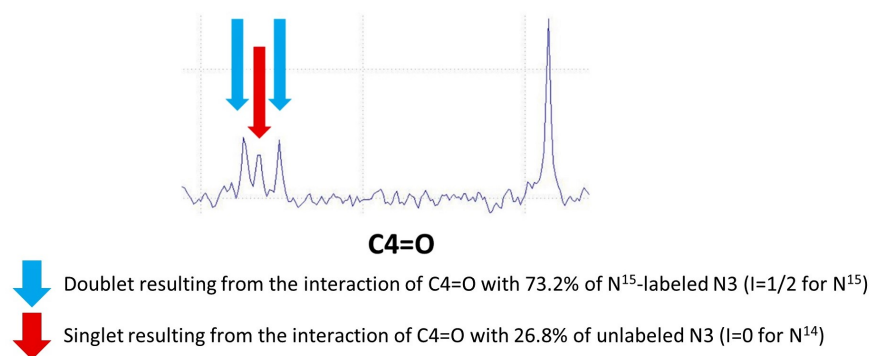
**Figure 2.18.** ^{13}C NMR spectrum of 3′ [15]N CPD-TpT showing the splitting induced by ^{15}N atom

Our results using dinucleotide CPD-TpT model confirm the same results. However, our investigation of the reaction in [18]O labeled water indicated that, CPD does indeed undergo a water addition at the C4=O group leading to the formation of a hemiaminal intermediate. These results are consistent with the results obtained during the investigation of chemical reactivities of other DNA lesions containing a saturated pyrimidine ring, *i.e.*, 6-4PP, SP and dHdU [6], [72], in all of which the C4=O group was the first site of nucleophilic attack

64
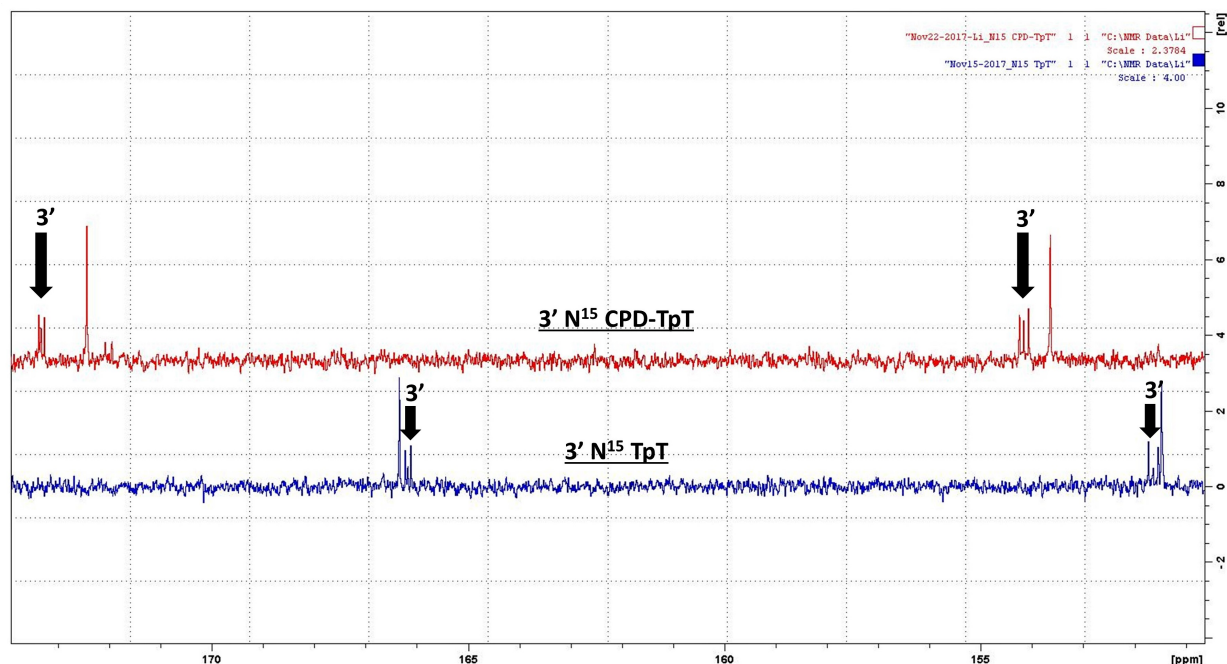
**Figure 2.19.** $^{13}$C NMR spectrum showing the "switch" in the position of 3′ C4=O as a result of dimerization between the two thymine rings
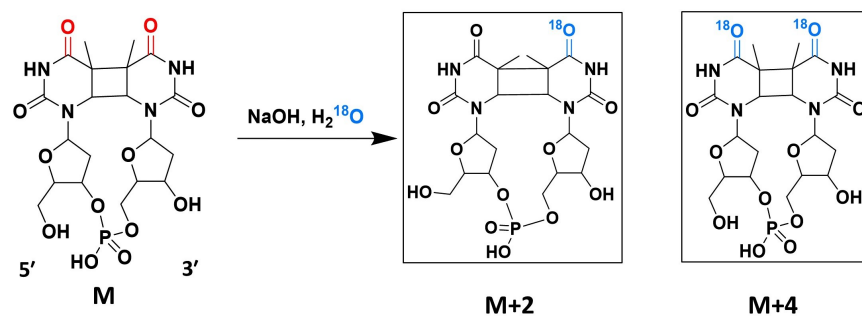


**Figure 2.20.** Products obtained after alkaline hydrolysis of CPD-TpT lesion in presence of $^{18}$O labeled water

and the C2=O remained unaffected. In case of CPD however, the hemiaminal intermediate completely reverts to the starting material (Figure 2.21). Moreover, the two C4 carbonyl groups present on 3′ and 5′-thymines in a CPD molecule show different chemical reactivities, the 3′ being more reactive, which is reflected by different rates of exchange with the incoming nucleophile leading to the hemiaminal intermediate.
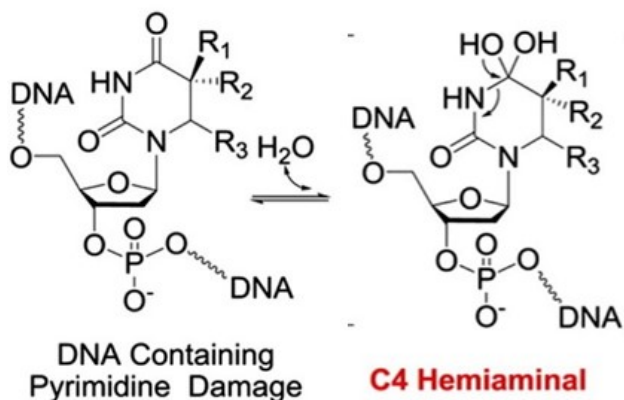
**Figure 2.21.** General scheme for alkaline hydrolysis of DNA lesions containing a saturated pyrimidine ring. All of these lesions are shown to undergo the formation of a hemiaminal/gem-diol intermediate as a result of nucleophilic attack on the C4=O group. The fate of the intermediate thus formed depends on the chemical environment of the ring. In case of 6-4PP, SP and dHdU, formation of the hemiaminal intermediate is followed by rupture of the N3-C4 bond, leading to a hydrolysis product. In case of CPD however, the hemiaminal intermediate eliminated a molecule of water and reverted to the starting material. Figure adapted from [6]

Based on our investigation of the alkaline reactivity of CPD using ESI-MS, $^{13}$C NMR spectroscopy and the synthesis of 3′ $^{15}$N-CPD-TpT, it was found that *the formation of a hemiaminal intermediate is indeed a common property of DNA lesions containing a saturated pyrimidine ring* [6]. Our investigation indicated that CPD, similar to other sunlight-induced DNA lesions containing a saturated pyrimidine ring, undergoes the formation of a hemiaminal intermediate upon interaction with alkali. However, in contrast to other lesions, the hemiaminal intermediate formed in the case of CPD does not lead to a subsequent cleavage of the N3-C4 bond and rather reverts to the starting material. Our experiments on the alkaline reactivity of CPD in $^{18}$O labelled water did establish the lability of the oxygen atom associated with the C4=O group.

In addition to the lability of C4=O oxygen, we also established the differential reactivity of the two C4=O groups contained within a CPD lesion on the 3′ and 5′ ends. It should be pointed out that earlier results, based on the crystal structure of a DNA duplex containing a CPD lesion, provide some evidence of structural asymmetry between the 3′ and 5′ thymines (based on the strength of hydrogen bonds between the C4=O groups in a CPD

lesion and the amine hydrogens on complementary adenine residues) [3]. However, there is no evidence/explanation of the cause of this asymmetry, neither is there any evidence for this kind of structural asymmetry in a single-stranded DNA strand. Furthermore, there is no known evidence of any asymmetry in reactivity between the two C4=O groups of a CPD lesion contained within a DNA strand.

### 2.3.1 Biological consequences

Similar to many other repair proteins, both the direct-photoreversal enzyme photolyase and the excision repair enzyme T4 endonuclease V employ base flipping to access the thymine dimer lesion. *The mechanistic cycle showing CPD repair by photolyase enzyme clearly show the C4=O group on 3' end as the first site of electron attack in a CPD molecule. However, there is no known evidence to prove that. Our results provide a firm and clear evidence to support this observation!* (Figure 2.22)
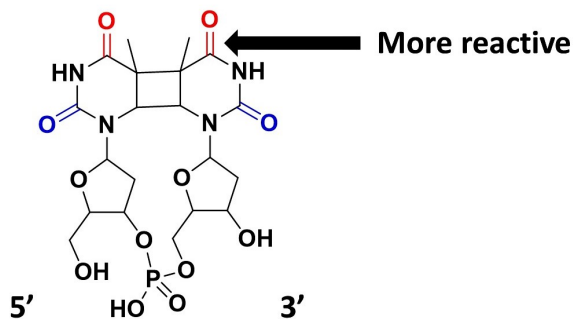


**Figure 2.22.** Schematic representation of the order of alkaline reactivity in CPD-TpT

## 2.4 Experimental

### 2.4.1 Materials and general methods

All reagents and chemicals were purchased from Sigma Aldrich, Fisher Scientific, Alfa Aesar and VWR Chemicals and used without further purification. All reactions were carried out using oven or flame-dried glassware in freshly distilled solvents. Purification of reaction products was carried out by flash chromatography using silica gel (Dynamic Adsorbents Inc, 32-63 $\mu$m). NMR spectra were obtained using a Bruker 400 MHz NMR Fourier transform spectrometer using deuterium oxide as a solvent and with residual water acting as an internal standard. The chemical shifts in NMR spectra were reported in parts per million (ppm).

### 2.4.2 HPLC product analyses

HPLC analyses were performed at room temperature using a Waters (Milford, MA) HPLC system coupled to a 2489 UV-Vis detector at 260 nm and 230 nm. A Waters $C^{18}$ RP column (2.5 $\mu$m particle size, 50 $\times$4.6 mm i.d.) was equilibrated in solvent A (10 mM ammonium acetate in water, pH 6.8), and compounds were eluted with an ascending gradient (0%-10%) of acetonitrile from 1min to 20 min at a flow rate of 1 mL/min. Semi-preparative HPLC analyses were performed at room temperature with the same Waters HPLC setup. An XBridge OST $C^{18}$ column (2.5 $\mu$m particle size, 50 $\times$10 mm i.d.) was equilibrated in solvent A (10 mM ammonium acetate in water, pH 6.8), and compounds were eluted with an ascending gradient (1-10%) of acetonitrile in 20 min at a flow rate of 4.73 mL/min.

### 2.4.3 LC/MS product analyses

LC/MS-based assays of $^{18}$O incorporation were conducted using Agilent 1200-6520 capillary LC-Q-TOF MS spectrometer using a Waters $C^{18}$-RP column (2.5 $\mu$m particle size, 50 x 4.6 mm i.d.). The column was equilibrated in solvent A (10 mM ammonium acetate in water) and acetonitrile (solvent B) in 20 min at a flow rate of 1 mL/min. The mass signals were monitored using negative ion mode. Data were acquired via "Agilent MassHunter

Workstation Data Acquisition (B.03.00)" software and analyzed via "Qualitative Analysis of MassHunter Acquisition Data (B.03.00)" software.

### 2.4.4  Synthesis and characterization of dinucleotide CPD-TpT

CPD-TpT was synthesized following the protocol developed by Bdour *et al.* (Figure 2.23) [99]. CPD-TpT formed after UV-B irradiation of TpT was purified using reverse-phase HPLC (Figure 2.24) and its concentration was determined using UV-Visible absorption spectroscopy ($\epsilon$=1500 M$^{-1}$ cm$^{-1}$) [100] [101]. Figures 2.25 and 2.26 show the $^{13}$C and $^{31}$P NMR spectra for TpT. Figures 2.27 and 2.28 show the $^{13}$C and $^{31}$P NMR spectrum for CPD-TpT.

### 2.4.5  Formation of CPD-TpT (M+2) and (M+4) species for ESI-MS and $^{13}$C NMR studies

Dinucleotide CPD-TpT was dissolved in 0.25 M NaOH to a final concentration of 1 mM for ESI-MS analysis and $\approx$ 132 mM for $^{13}$C NMR analysis. The resulting solution was maintained at room temperature (25°C) to allow the formation of (M+2) and (M+4) species as assessed by monitoring 0.5 $\mu$L aliquots of the reaction mixture by LC-MS. For NMR analyses, the reaction mixture was first monitored using LC-MS at various time points to ensure the optimal formation of (M+2) and (M+4) species. After a quick check with LC-MS, the reaction mixture was neutralized using an equimolar solution of HCl. After neutralization, the solution was evaporated to dryness and re-dissolved in D$_2$O for NMR measurements. Figures 2.29, 2.30, 2.31 and 2.32 represent the $^{13}$C NMR spectra showing $^{18}$O incorporation in CPD-TpT at T=0 day, T=1 day, T=5 days and T=49 days.

### 2.4.6  Synthesis of CPD-TpT variant with a selective $^{15}$N label at the 3′ side

$^{15}$N labelled thymidine used in this synthesis was synthesized using the protocol developed by Bdour *et al* [99]. TpT with a selective $^{15}$N label at the 3′ side was synthesized using the scheme developed by Bdour *et al*[99] after minor modifications. Since we wanted a label only at the 3′ side of the molecule, we used thymine phosphoramidite (without $^{15}$N enrichment) during the coupling step. CPD was obtained after irradiating an aqueous solution of TpT

(selectively $^{15}$N labelled at the 3′ side) with UV-B radiation for $\approx$ 4 hours. The reaction produced a mixture of *trans-syn* and *cis-syn* isomers of CPD. The *cis-syn* isomer that is the major product of the reaction (>86% yield) was purified using reverse phase HPLC, followed by desalting and lyophilisation. Concentration of CPD-TpT lesion was determined using UV-Visible absorption spectroscopy ($\epsilon$=1500 M$^{-1}$ cm$^{-1}$). Figure 2.33 shows the $^{13}$C NMR spectrum for dinuceotide TpT with the $^{15}$N label on 3′ side. Figure 2.34 shows the $^{13}$C NMR spectrum for the CPD lesion that results from it.
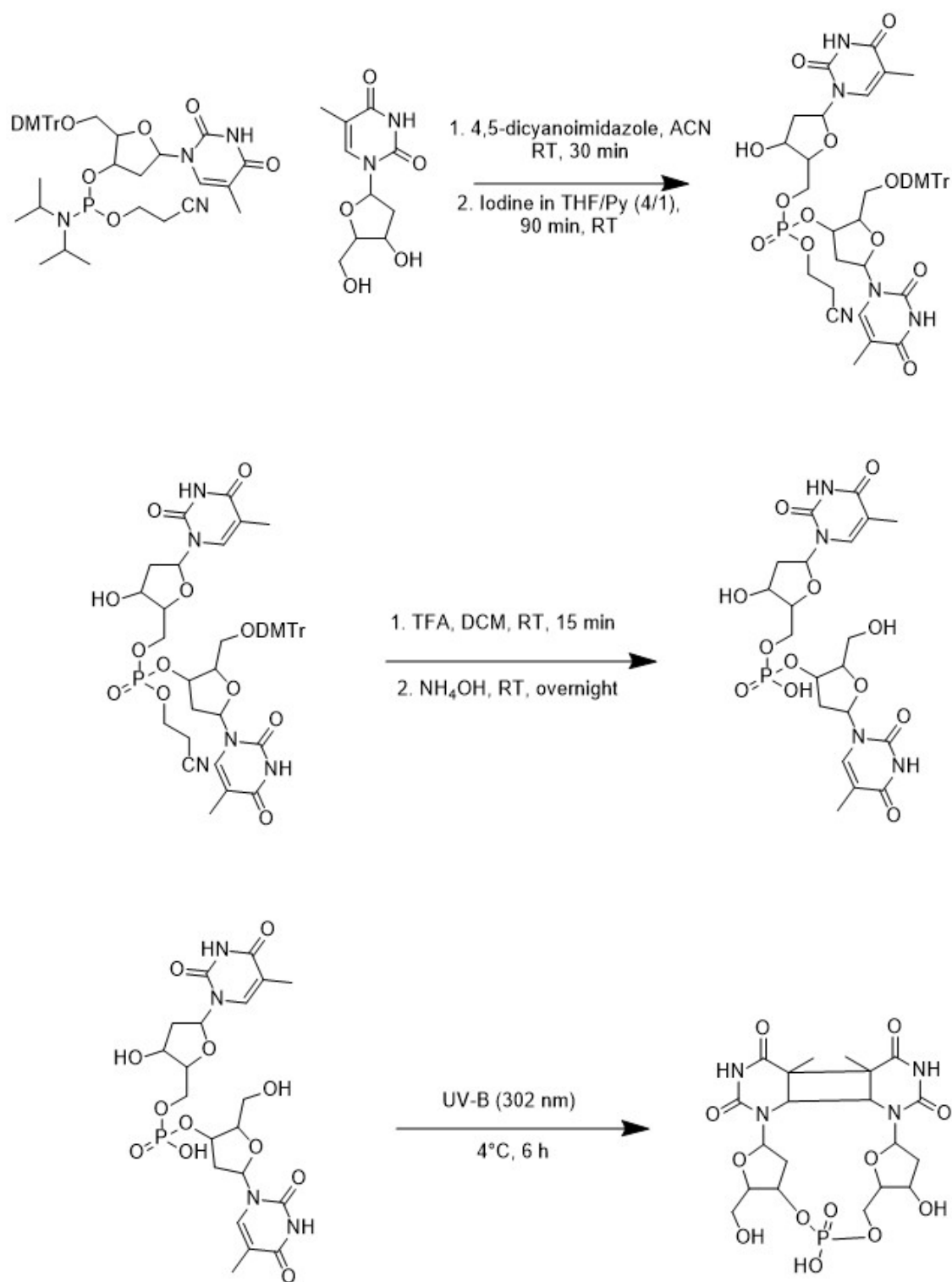
**Figure 2.23.** Reaction scheme for synthesis of CPD-TpT. Modified from [99]
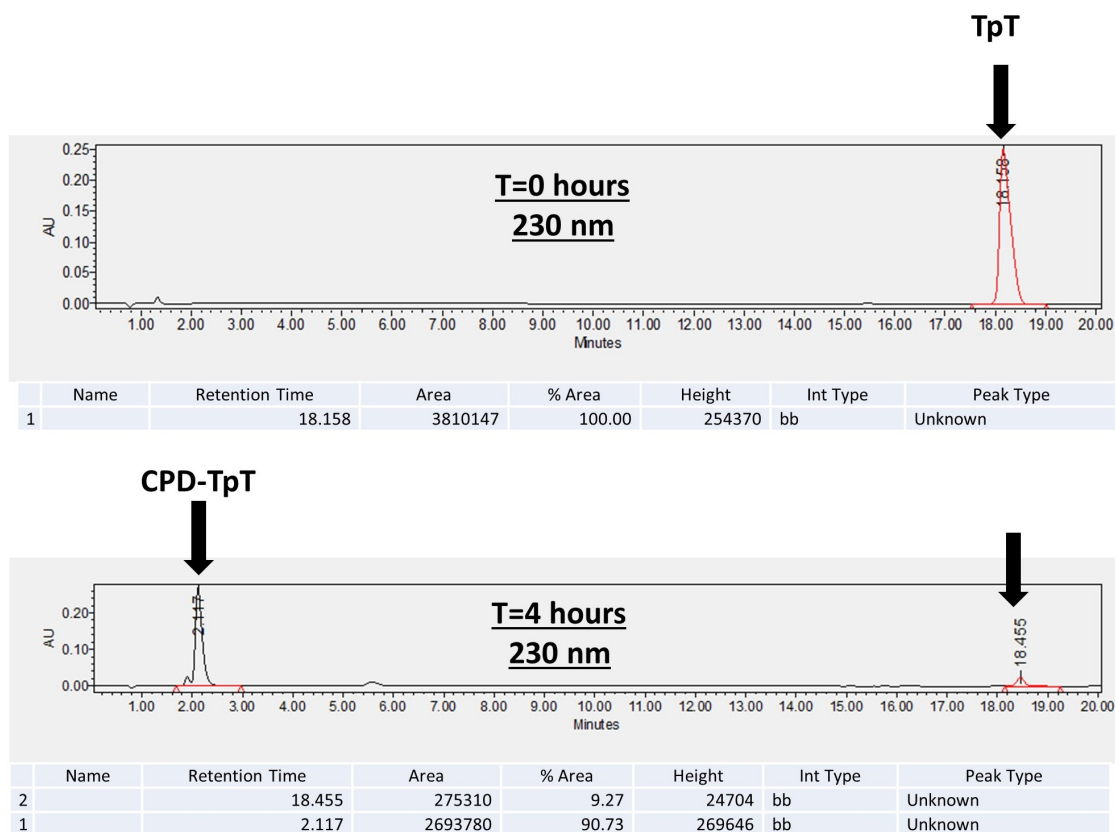
**Figure 2.24.** Reverse-phase HPLC chromatogram showing UV-B photo-irradiation of TpT

| | Name | Retention Time | Area | % Area | Height | Int Type | Peak Type |
|---|---|---|---|---|---|---|---|
| 1 | | 18.158 | 3810147 | 100.00 | 254370 | bb | Unknown |

| | Name | Retention Time | Area | % Area | Height | Int Type | Peak Type |
|---|---|---|---|---|---|---|---|
| 2 | | 18.455 | 275310 | 9.27 | 24704 | bb | Unknown |
| 1 | | 2.117 | 2693780 | 90.73 | 269646 | bb | Unknown |
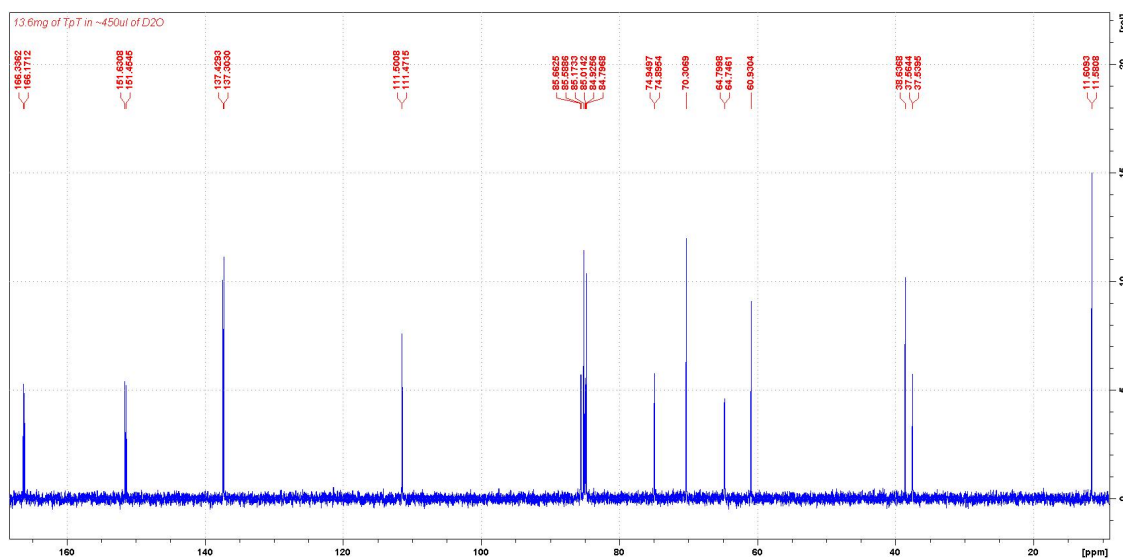


**Figure 2.25.** $^{13}$C NMR spectrum for TpT
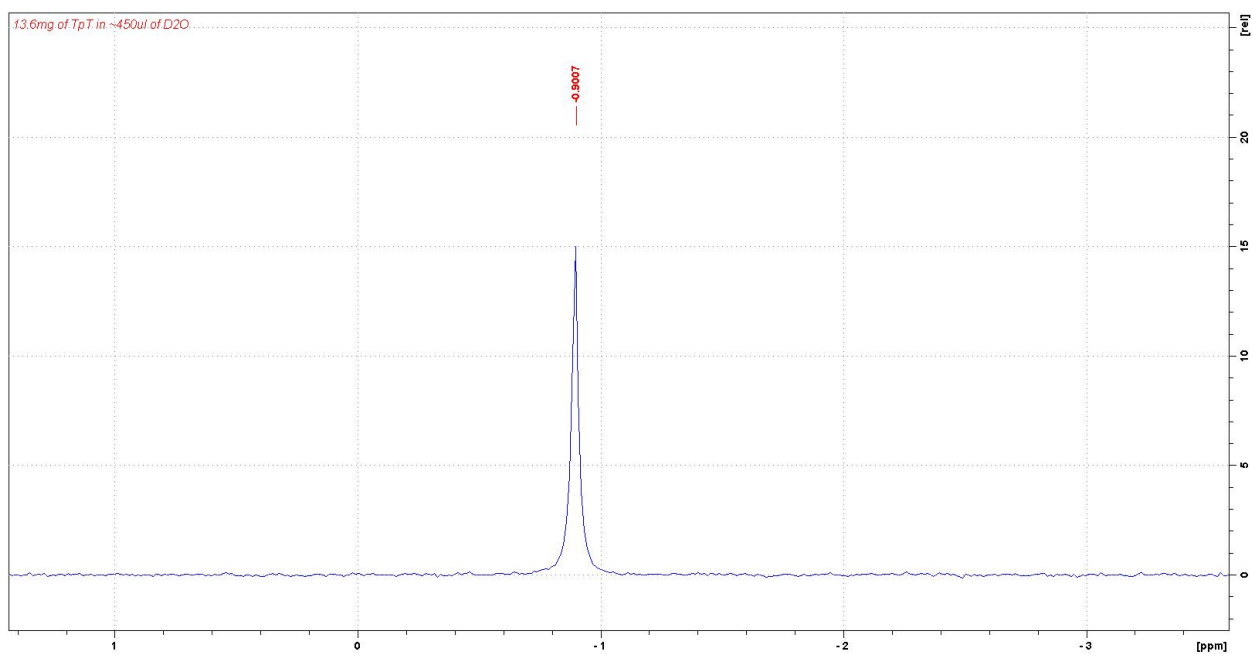
**Figure 2.26.** $^{31}$P NMR spectrum for TpT
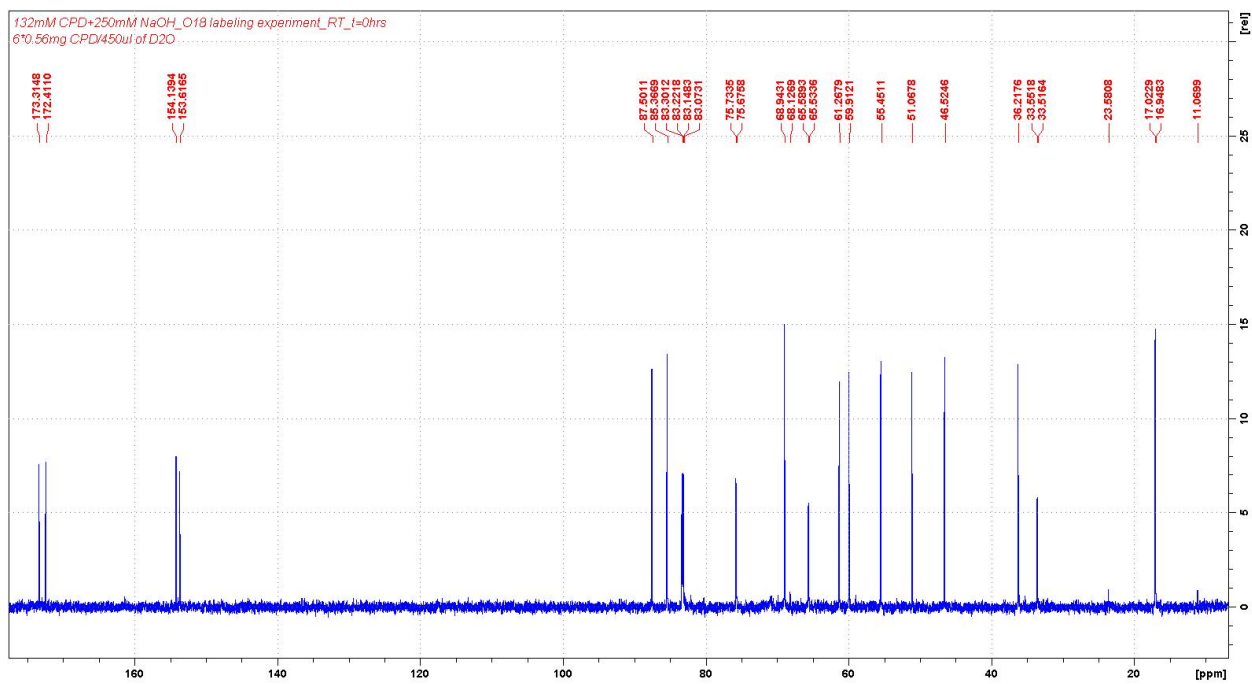


**Figure 2.27.** $^{13}$C NMR spectrum for CPD-TpT
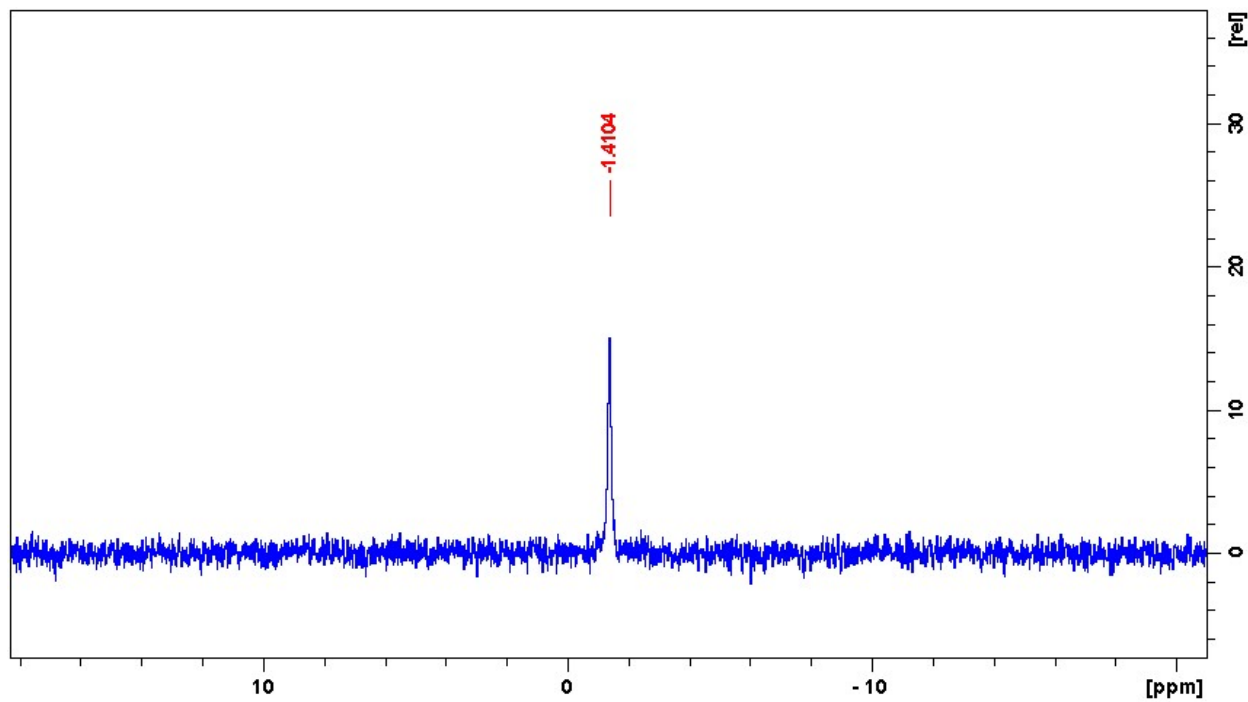
**Figure 2.28.** $^{31}$P NMR spectrum for CPD-TpT
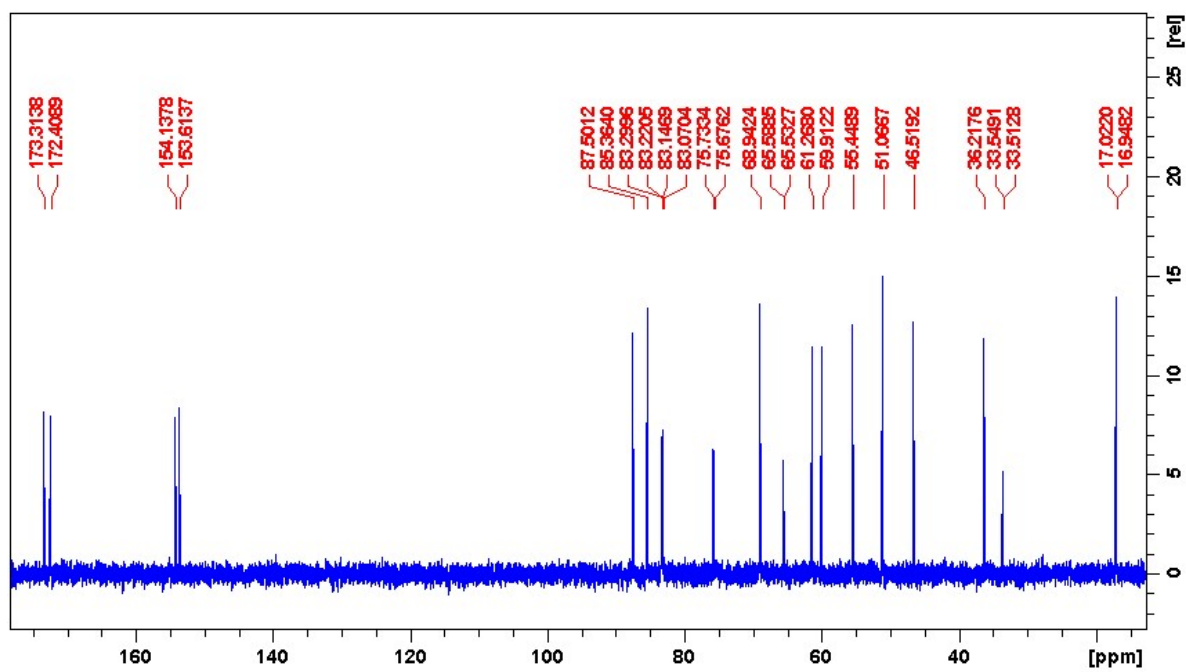


**Figure 2.29.** Full $^{13}$C NMR spectrum showing $^{18}$O incorporation in CPD-TpT at T=0 days
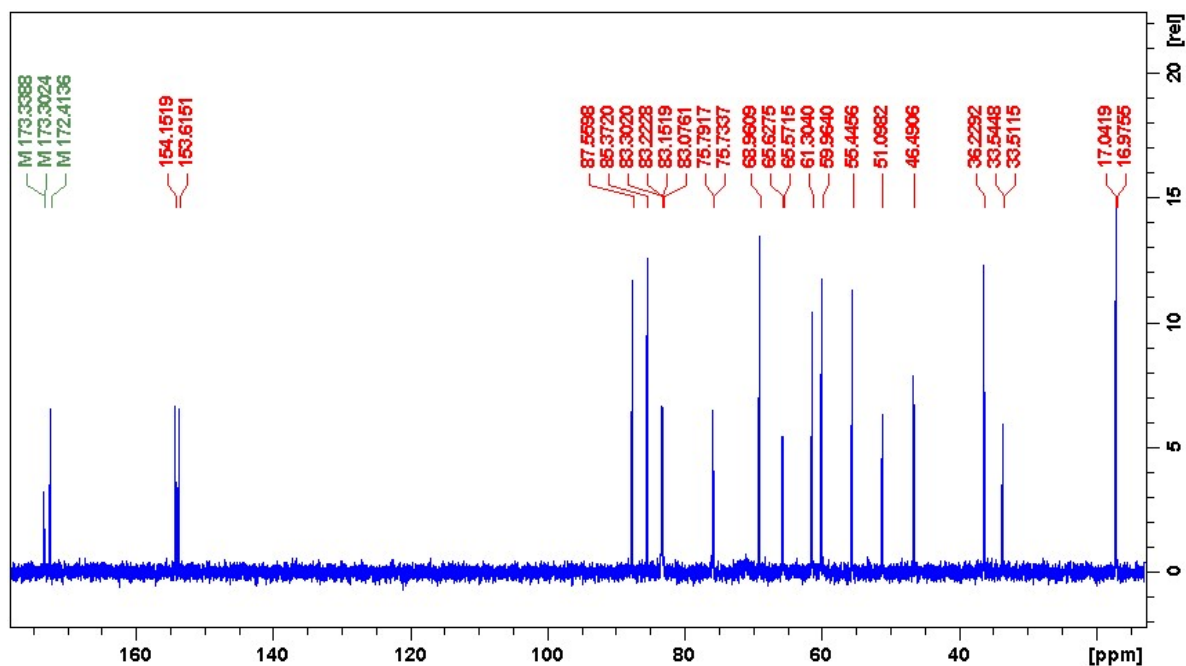
**Figure 2.30.** Full $^{13}$C NMR spectrum showing $^{18}$O incorporation in CPD-TpT at T=1 day
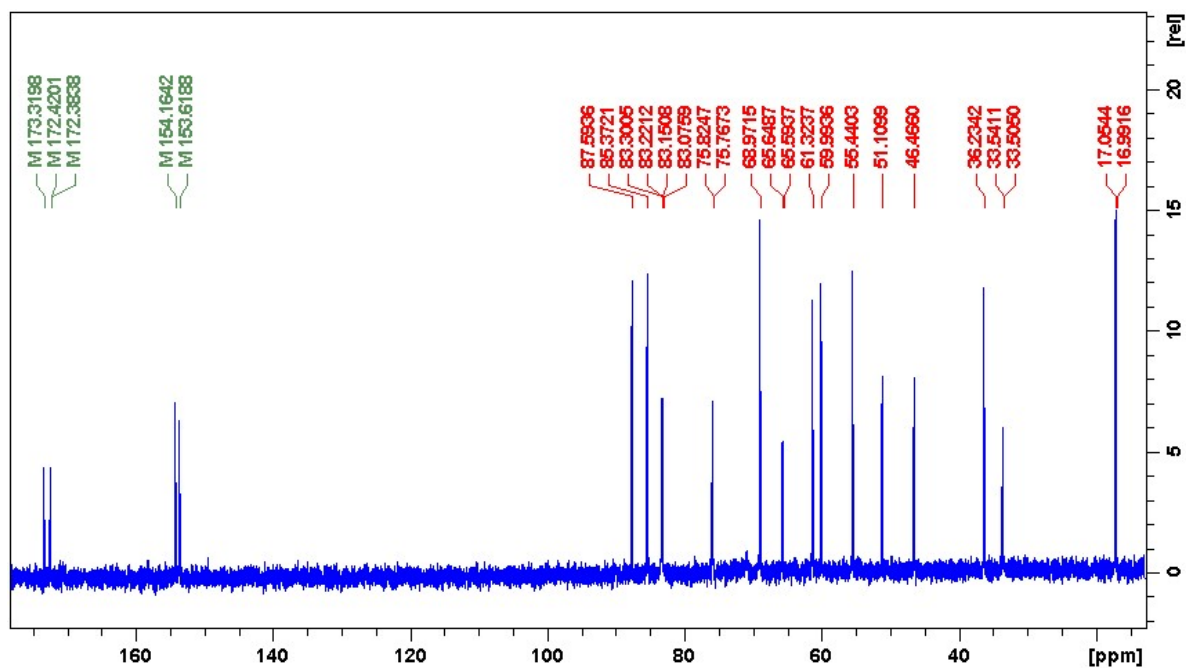


**Figure 2.31.** Full $^{13}$C NMR spectrum showing $^{18}$O incorporation in CPD-TpT at T=5 days
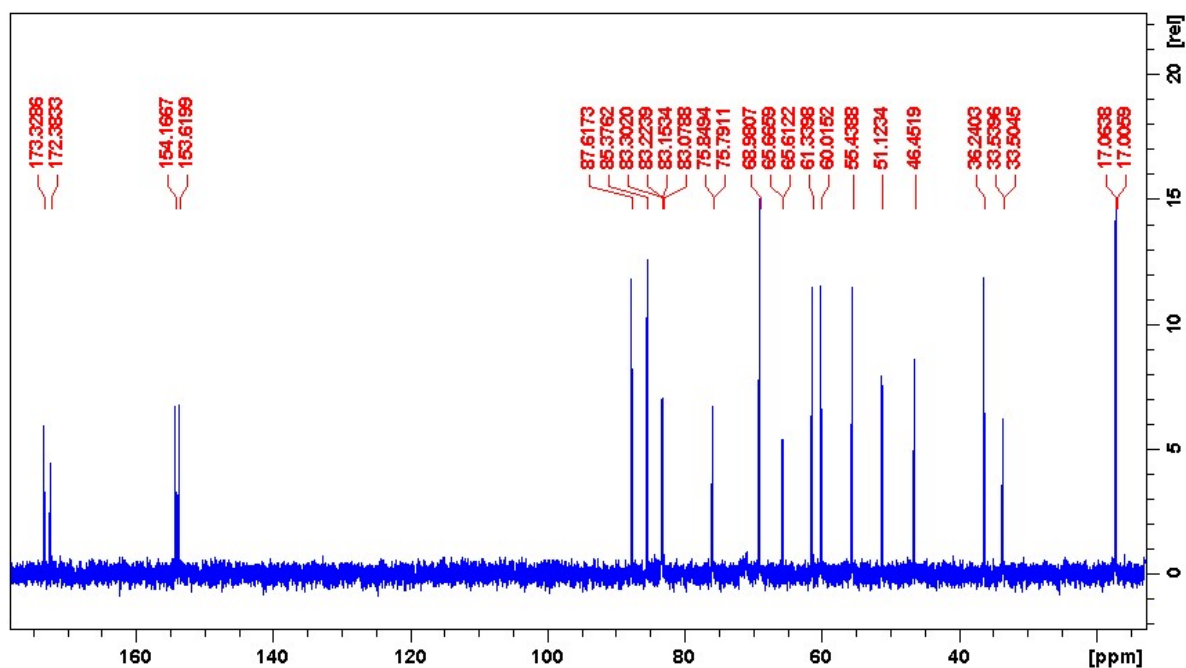
**Figure 2.32.** Full $^{13}C$ NMR spectrum showing $^{18}O$ incorporation in CPD-TpT at T=49 days
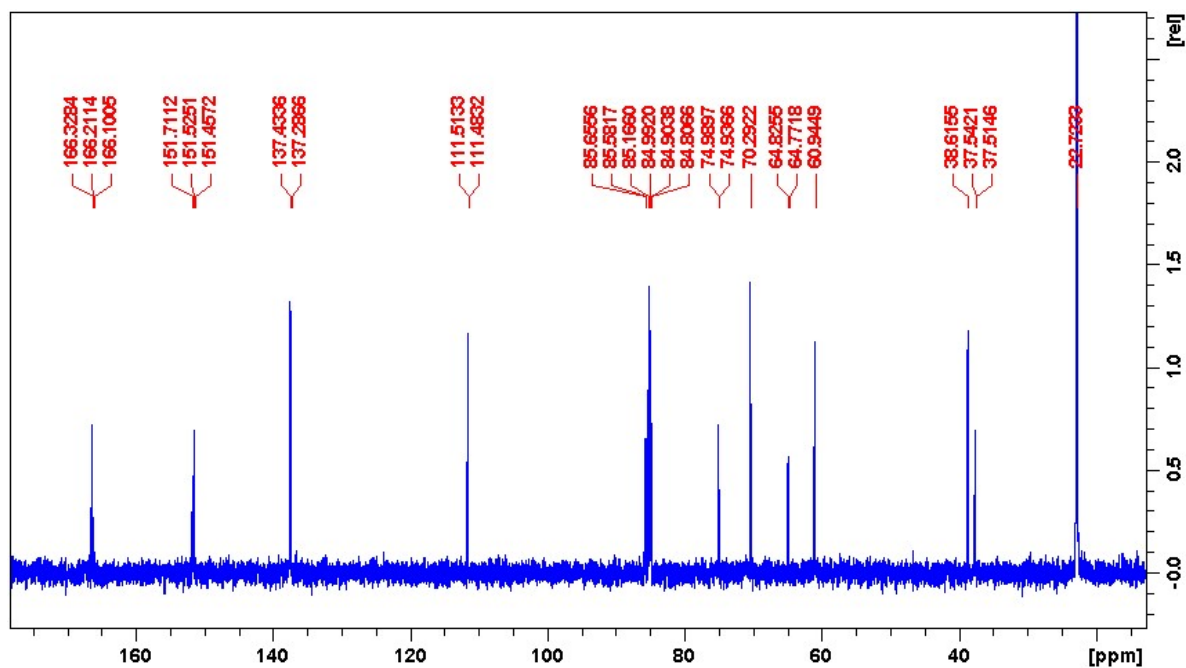


**Figure 2.33.** $^{13}C$ NMR spectrum for dinucleotide TpT with a selective $^{15}N$ label on the 3′ end
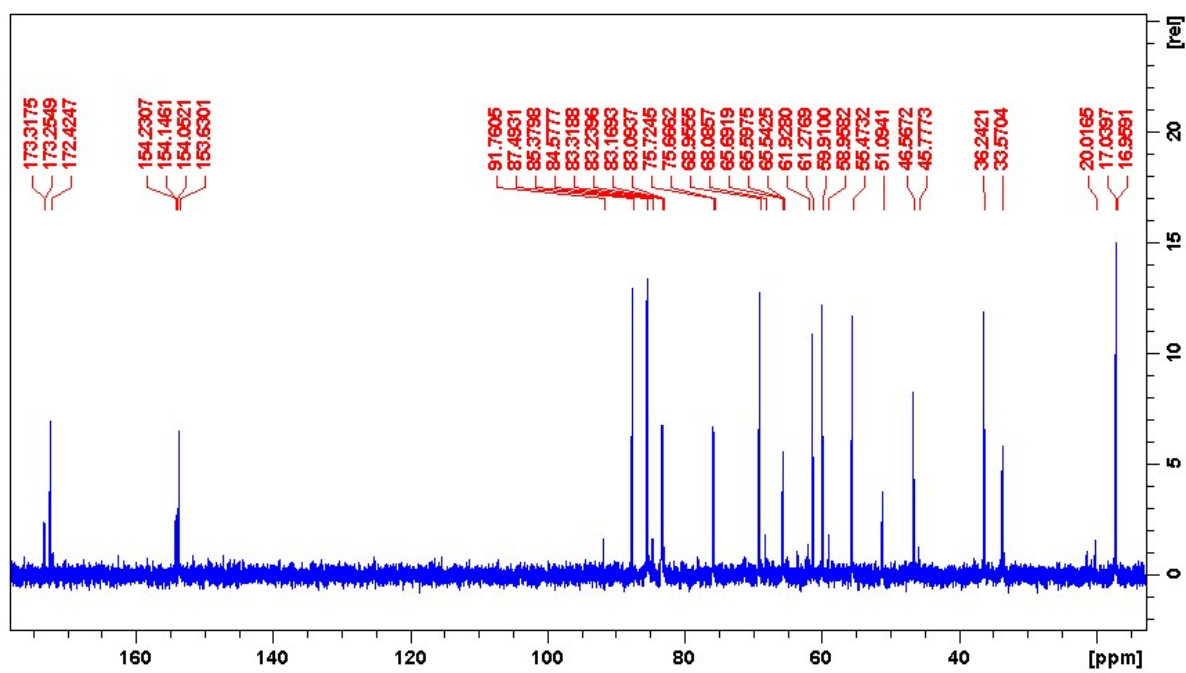
**Figure 2.34.** $^{13}$C NMR spectrum for CPD-TpT with a selective $^{15}$N label on the 3′ end of the molecule

# 3. DEFINING THE ALKALINE REACTIVITY OF CYCLOBUTANE PYRIMIDINE DIMER (CPD) LESIONS IN OLIGONUCLEOTIDES

## 3.1 Introduction

The work presented in Chapter 2 described the alkaline reactivity of cyclobutane pyrimidine dimer (CPD) lesions generated from dinucleotides. *These studies indicated that, similar to other DNA lesions, CPD undergoes a water addition at the C4 carbonyl group of the thymine residue leading to the formation of a hemiaminal intermediate. Further, as shown by the $^{18}O$ labeling studies with CPD-TpT, this intermediate does not lead to hydrolysis products and completely reverts back to the starting material under alkaline conditions. Together these results indicate that the two C4 carbonyl groups present on the 3′ and 5′ thymines in a CPD molecule show different chemical reactivities towards hydrolytic attack, with the C4=O group on 3′ thymine being more reactive (Figure 3.1).*
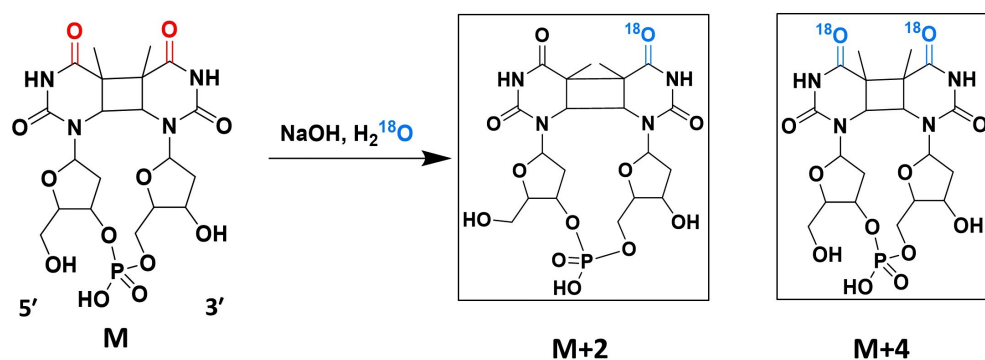


**Figure 3.1.** Products obtained after alkaline hydrolysis of CPD-TpT lesion in presence of $^{18}O$ labeled water

*What leads to the observed difference in the reactivities of the two possible C4=O groups in a CPD molecule? Is it an intrinsic property of the CPD molecule OR does it occurs due to the structural asymmetry in a CPD lesion?* To investigate these possibilities further, alkaline hydrolysis reaction were conducted on a CPD lesion contained within a DNA hexanucleotide AATTAA (AA$\hat{T}T$AA) and tetranucleotide ATTA (A$\hat{T}T$A). It should be noted that a CPD-TpT molecule ($\hat{T}T$) has some degree of structural asymmetry between the 3′ and 5′ ends; however once a $\hat{T}T$ lesion is flanked by adenine groups on both sides, it loses that asymmetry (Figure 3.2). Thus, if the differential reactivity between the two C4=O groups is an intrinsic property of a CPD molecule, a similar result should be observed in the reactivity of AA$\hat{T}T$AA and A$\hat{T}T$A. As outlined herein, it was determined that the observed asymmetry in alkaline reactivity, between the C4 carbonyl groups on the 3′ and 5′ thymines in CPD, is an intrinsic property of the CPD residue.
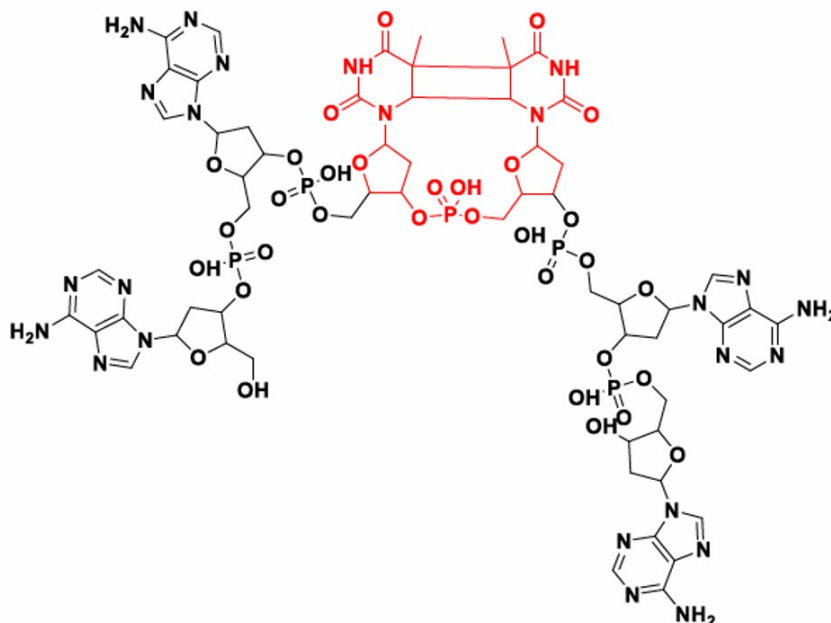


**Figure 3.2.** Structural representation of a CPD-AATTAA (AA$\hat{T}T$AA) molecule (the CPD-TpT or $\hat{T}T$ molecule is highlighted in red and the four adenosine groups are shown in black)

## 3.2 Results

### 3.2.1 Analyses of the alkaline hydrolysis of hexanucleotide AA$T\hat{T}$AA in $^{18}$O labelled water via ESI-MS

AA$T\hat{T}$AA was obtained by UV-B irradiation of an aqueous solution of AATTAA maintained at 4°C for $\approx$ 4 hours. The *cis-syn* isomer required for our experiments was purified from the UV-irradiated mixture using reverse-phase HPLC followed by desalting and lyophilisation (Figure 3.3). The concentration of AA$T\hat{T}$AA was determined using UV-visible absorption spectroscopy (Figure 3.4)( Molar extinction coefficient for AATTAA was obtained using the *oligoanalyzer tool* from IDT DNA technologies, $\epsilon$=69600 M$^{-1}$ cm$^{-1}$) [102]). The resulting powder (after lyophilisation) was suspended in 250 mM NaOH solution prepared in $^{18}$O labelled water to a final concentration of 1 mM. After every 24 hours, $\approx$ 0.5 $\mu$L of the reaction mixture was withdrawn and rapidly quenched by mixing with $\approx$ 19.5 $\mu$L of 1 M ammonium acetate buffer to arrest the progress of the reaction. The aliquot containing the quenched reaction mixture was stored at -20°C. Similar aliquots were obtained after every 24 hours for a period of 10 days. After each collection, the eppendorf tube containing the original reaction mixture was carefully sealed to avoid the interaction of NaOH solution in the reaction mixture with atmospheric carbon dioxide (known to reduce the alkalinity of NaOH due to the formation of sodium carbonate).

AA$T\hat{T}$AA (molar mass 1799.3 g/mole) being a hexanucleotide, contains five phosphate groups and thus potentially five different charged states. The spectra shown in Figure 3.5 correspond to -2 state ($m/z$ = 898.65), which is the most abundant charged state. For the -2 charged state, the M, M+2 and M+4 species appear at $m/z$ values of 898.18, 899.18 and 900.18 respectively. For comparison, Figure 3.6 shows the deconvoluted mass spectra for AA$T\hat{T}$AA for the same time points. It should be noted here that the normal isotopic distribution in a hexanucleotide molecule involves a higher ratio of M+2 and M+4 peaks as compared to that in a dinucleotide, because of the higher number of carbon atoms in this molecule (Refer to Figure 3.5 left panel, T=0 time point). Due to this, the relative ratios of M, M+2 and M+4 species are $\approx$ 70%, 25% and 5% at the first time point *i.e.* T=0 days.

ESI LC-MS (negative ion mode) analysis of the reaction between 1 mM AA$\hat{T}T$AA and 250 mM NaOH in $^{18}$O labelled water at room temperature showed a similar trend to that observed in dinucleotide CPD-TpT (or $\hat{T}T$). Once again, there was a rapid decrease in the intensity of M peak followed by an increase in the intensity of (M+2) and (M+4) peaks (Figure 3.5). *A similar reaction pattern in $AA\hat{T}TAA$ proves that the asymmetry in reactivity between the two C4=O groups is an intrinsic property of the CPD molecule and is NOT due to the asymmetry in structure in a dinucleotide.*



**AATTAA**

260nm

| | Name | Retention Time | Area | % Area | Height | Int Type | Peak Type |
|---|---|---|---|---|---|---|---|
| 1 | | 17.608 | 3557897 | 100.00 | 335098 | bb | Unknown |

**CPD-AATTAA**

**AATTAA**

260nm

| | Name | Retention Time | Area | % Area | Height | Int Type | Peak Type |
|---|---|---|---|---|---|---|---|
| 1 | | 14.364 | 27045554 | 64.85 | 1808044 | VV | Unknown |
| 2 | | 15.447 | 5179322 | 12.42 | 402845 | VV | Unknown |
| 3 | | 17.552 | 9482597 | 22.74 | 756591 | VV | Unknown |
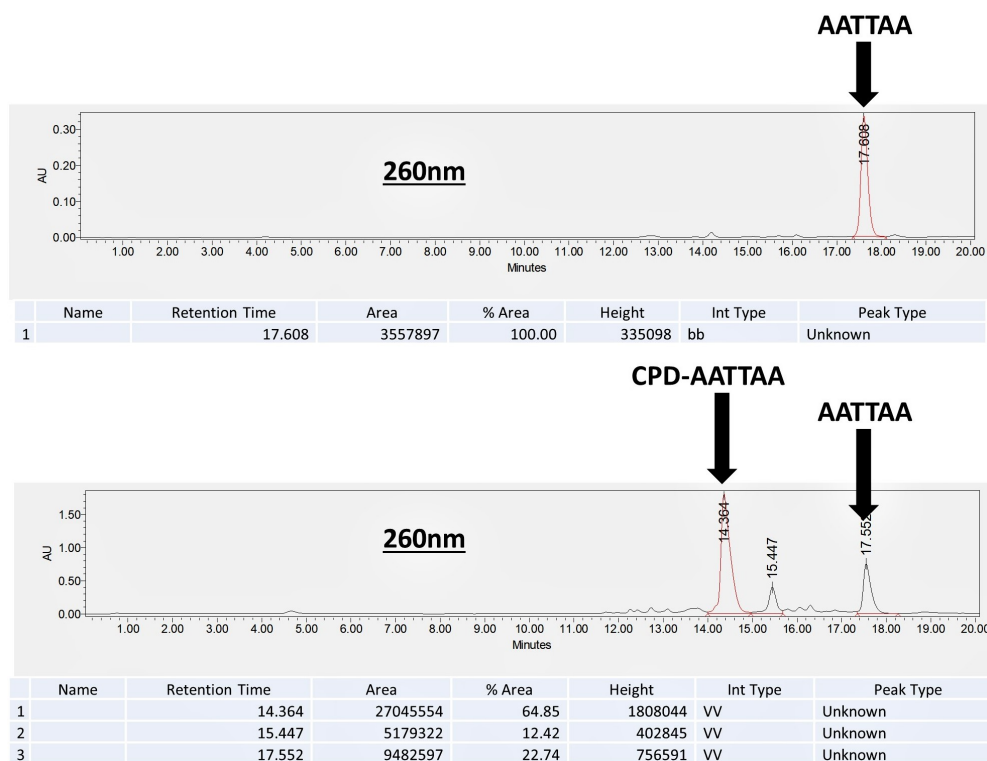
**Figure 3.3.** RP-HPLC chromatogram showing AA$\hat{T}T$AA and unreacted AATTAA after UV-B photo-irradiation
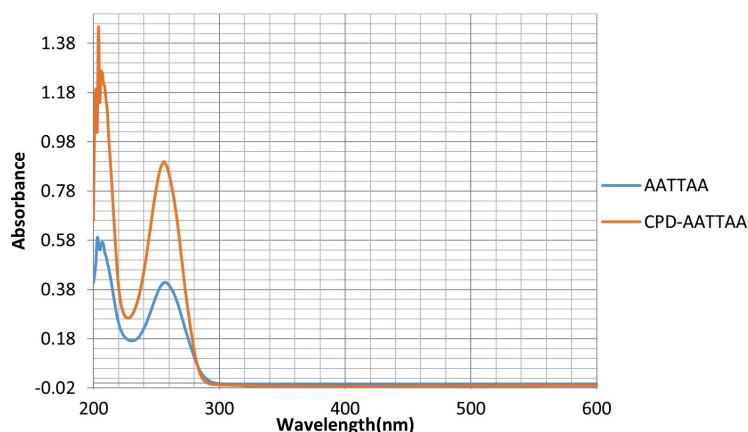
**Figure 3.4.** UV-Visible absorption spectrum for $AA\hat{T}TAA$

## 3.2.2 Analyses of alkaline hydrolysis of hexanucleotide $AA\hat{T}TAA$ in $^{18}O$ labelled water using $^{13}C$ NMR spectroscopy

To determine if $AA\hat{T}TAA$ followed the same reaction pattern as dinucleotide $\hat{T}T$, the alkaline hydrolysis of $AA\hat{T}TAA$ was studied using $^{13}C$ NMR spectroscopy. At each time point (Figure 3.7), the reaction progress was first screened using LC-MS to ensure the optimal formation of (M+2) and (M+4) species. After a quick screening with LC-MS, the reaction mixture was neutralized using an equimolar solution of HCl (to avoid signal reduction in the NMR peak of $^{13}C=O$ carbon atom caused by NaOH). pH of the reaction mixture was monitored using a litmus paper. The NaCl salt formed as a result of the neutralization process was removed from the reaction mixture using RP-HPLC. The resulting solution was evaporated to dryness and re-dissolved in $D_2O$ for NMR measurements. It is worth mentioning here that $AA\hat{T}TAA$, having a higher molar mass than $\hat{T}T$, has relatively slower NMR relaxation times. Unfortunately this results in peak broadening and further reduces the already poor resolution between $C=^{16}O$ and $C=^{18}O$ peaks. The $^{13}C$ NMR spectra at different time points are overlaid in Figure 3.7.

As with the dinucleotide substrate lesion, the C2=O groups showed no detectable $^{18}O$ exchange. *However, among the two C4=O groups, the one occuring upfield (with a lower chemical shift value) reacted first. This differed from what was observed in the case of dinucleotide $\hat{T}T$*and observation leads to the following two possibilities:
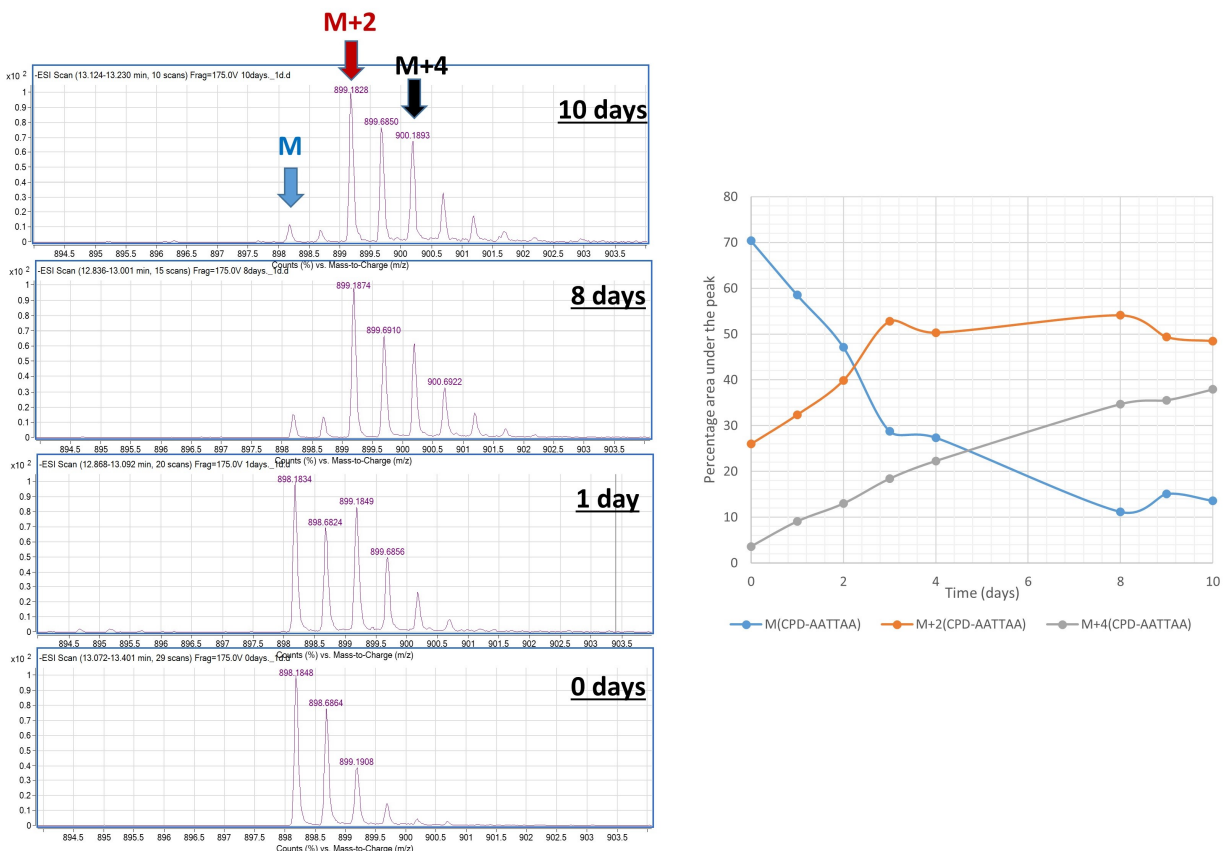
**Figure 3.5.** Left panel: ESI-MS chromatograms for -2 charged state of AA$T\hat{T}$AA showing $^{18}$O enrichment over a period of 10 days 2. $^{18}$O reaction kinetics in AA$T\hat{T}$AA monitored using ESI-MS

- The reaction pattern in AA$T\hat{T}$AA is reversed relative to dinucleotide $T\hat{T}$; with the 5$'$ C4=O group reacting first in this oligonucleotide environment.

- The reaction pattern in AA$T\hat{T}$AA remains the same as $T\hat{T}$. However, now the two C4=O groups have simply undergone a change in chemical shift values.

This issue was addressed by synthesizing an oligonucleotide with a selective $^{15}$N label (on 3$'$ or 5$'$ side) using solid-phase DNA synthesis to permit the selective NMR coupling between the $^{15}$N and C4=O group on 3$'$ side of the lesion. This experiment was carried out on a tetranucleotide molecule (A$T\hat{T}$A) rather than a hexanucleotide, since it was expected to show a similar trend in reactivity as hexanucleotide AA$T\hat{T}$AA and was relatively easier to
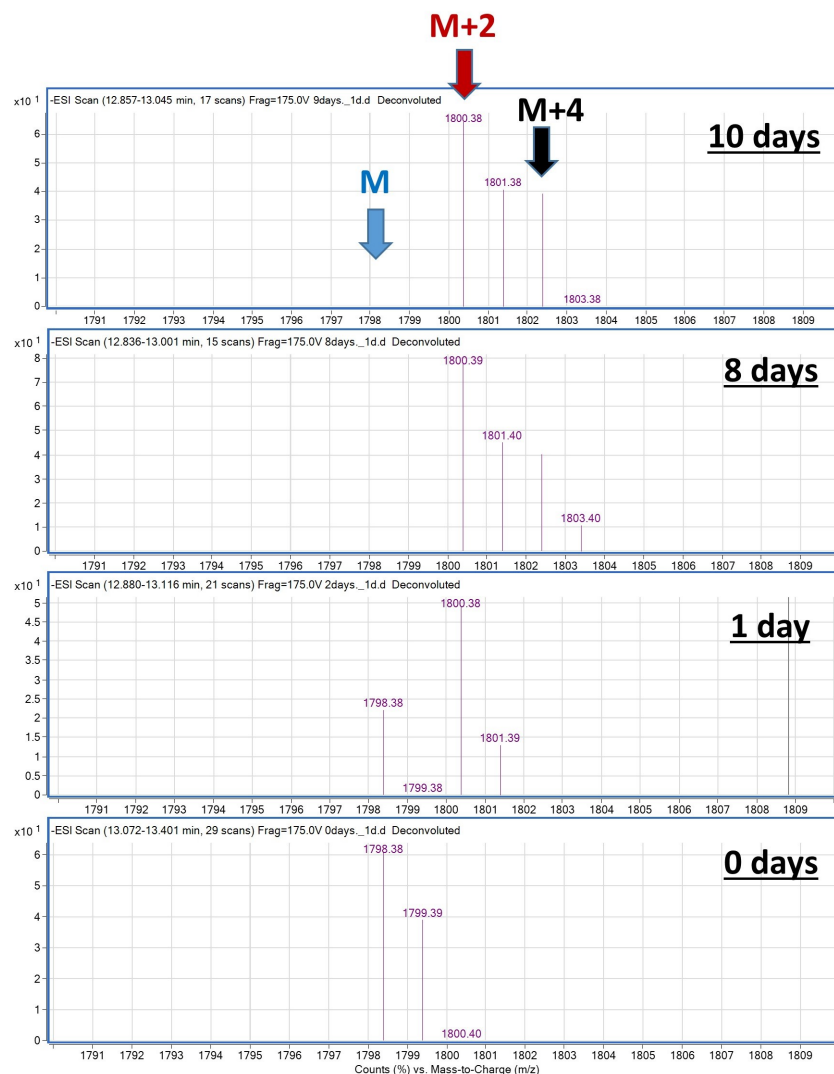
**Figure 3.6.** Deconvoluted ESI-MS chromatograms for $\text{AA}\hat{T}\text{TAA}$ showing $^{18}\text{O}$ enrichment over a period of 10 days

synthesize. The following results summarize the ESI-MS and $^{13}\text{C}$ NMR analyses of the $^{18}\text{O}$ labelling reactions in $\text{A}\hat{T}\text{TA}$.

### 3.2.3 Study of alkaline hydrolysis of $\text{A}\hat{T}\text{TA}$ in $^{18}\text{O}$ labelled water using ESI-MS

ATTA was synthesized using standard solid-phase DNA synthesis technique using controlled pore glass (CPG) beads [103]. $\text{A}\hat{T}\text{TA}$ was obtained after UV-B irradiation of an aqueous solution of ATTA maintained at 4°C for $\approx$ 4 hours. The *cis-syn* isomer was purified using reverse-phase HPLC after which it was desalted and lyophilized. The concentration of
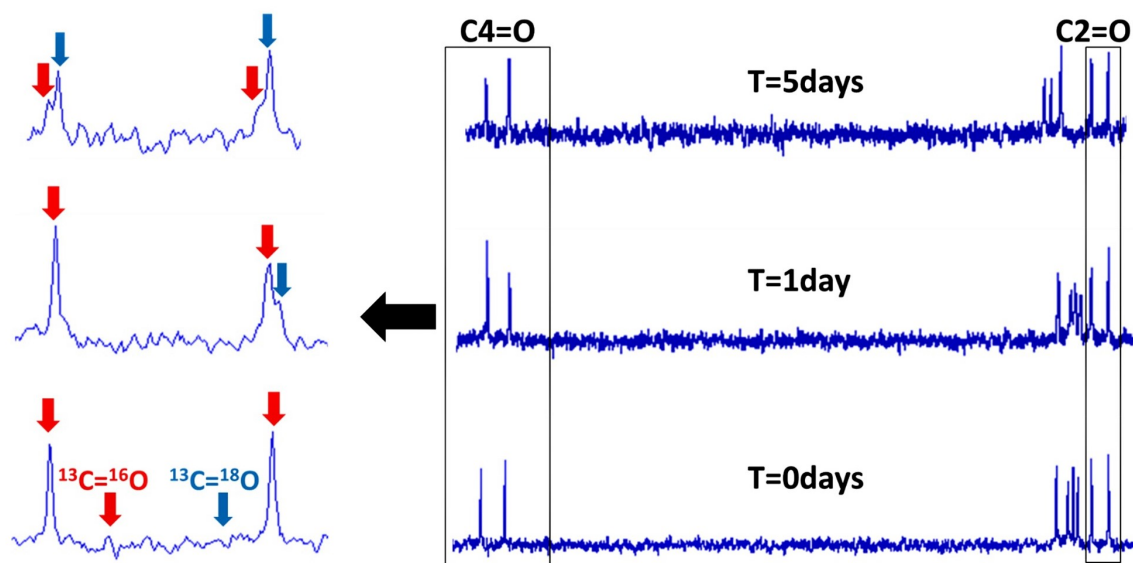
**Figure 3.7.** $^{13}$C NMR spectra showing $^{18}$O exchange in AAT̂TAA over time. Please refer to Figures 3.19, 3.21 and 3.22 for the complete spectrum at each time point.

AT̂TA in solution was determined using UV-visible absorption spectroscopy (Figure 3.8)( Molar extinction coefficient for ATTA was obtained using the *oligoanalyzer tool* from IDT DNA technologies, $\epsilon$=45600 M$^{-1}$ cm$^{-1}$) [102]. The powder obtained after lyophilisation was suspended in 250 mM NaOH solution prepared in $^{18}$O labelled water to a final concentration of 1 mM. Aliquots were collected after every 24 hours in the same way as described earlier in the case of T̂T and AAT̂TAA. Figure 3.9 shows the ESI-MS spectra obtained at various time points and the kinetic curve for the complete $^{18}$O exchange reaction for a 1 mM solution of AT̂TA in the presence of 250 mM NaOH. *As illustrated, AT̂TA exhibited a similar differential reactivity between the two available C4=O groups as was seen earlier in the case of T̂T and AAT̂TAA.* Figure 3.10 shows a comparison of the rates of $^{18}$O labelling in AT̂TA and T̂T in presence of 250 mM NaOH.
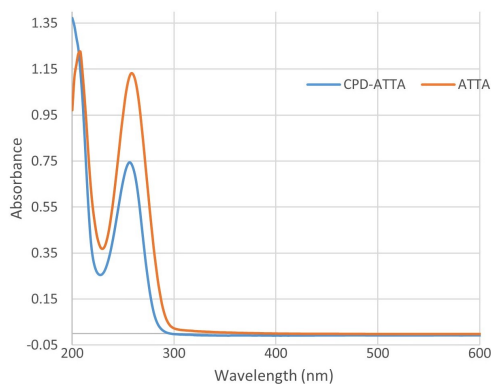
**Figure 3.8.** UV-Visible absorption spectrum for A$\hat{T}$TA and ATTA
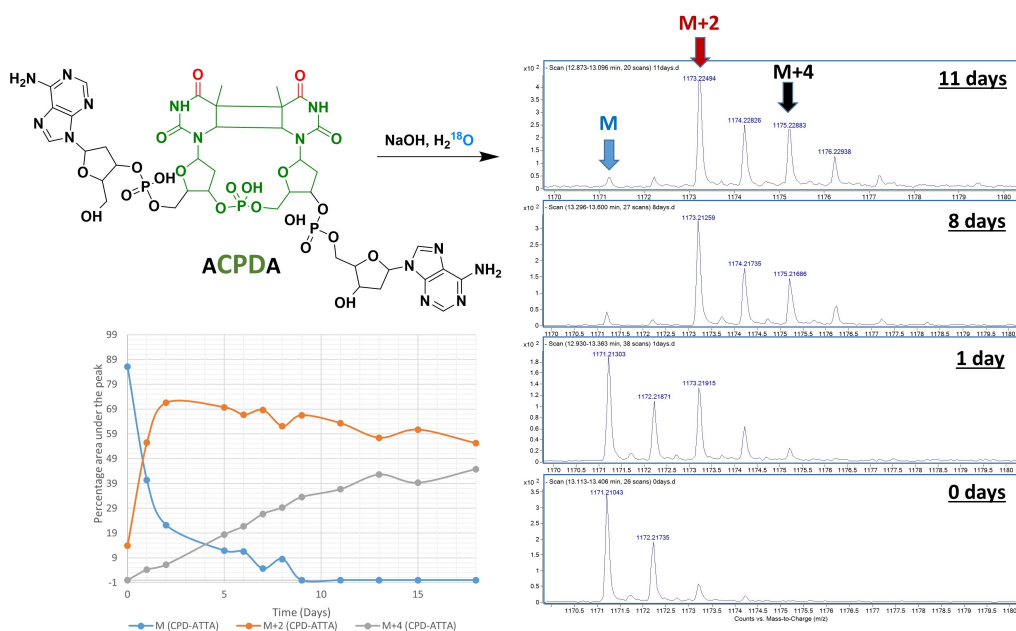


**Figure 3.9.** Right panel: ESI-MS chromatograms showing $^{18}$O enrichment in A$\hat{T}$TA over a period of 10 days Lest panel: $^{18}$O reaction kinetics in A$\hat{T}$TA monitored using ESI-MS

### 3.2.4 $^{13}$C NMR spectroscopic analyses of alkaline hydrolysis of A$\hat{T}$TA in $^{18}$O labelled water

To ascertain that the reaction pattern in A$\hat{T}$TA, the alkaline hydrolysis reaction was studied again using $^{13}$C NMR spectroscopy (each time point analysed simultaneously using ESI-MS for comparison. Once again, slower relaxation times of C=O groups in CPD-ATTA resulted in broader peaks and reduced resolution between C=$^{16}$O and C=$^{18}$O peaks relative
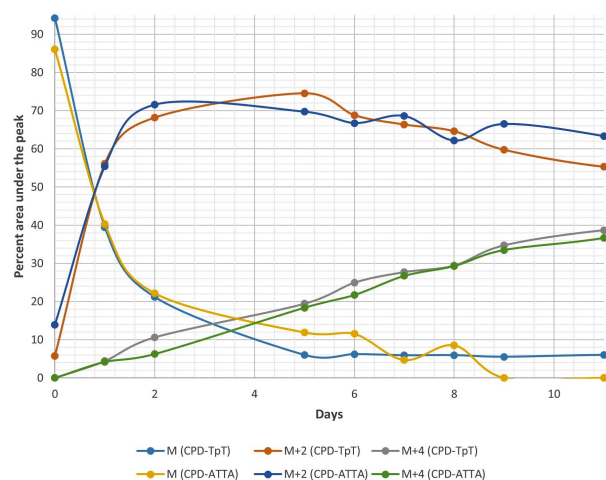
**Figure 3.10.** $^{18}$O labeling of A$\hat{T}$TA in 250 mM NaOH in presence of $\hat{T}T$ as internal standard measured using ESI-MS

to those in dinucleotide $\hat{T}T$. The results are summarized in Figure 3.11. A*s is apparent from the $^{13}C$ NMR spectra, the C4=O with relatively upfield chemical shift undergoes exchange first, similar to the trend observed in the case of AA$\hat{T}TAA$.* Thus, the NMR peak assignment from A$\hat{T}T$A can safely be applied to AA$\hat{T}T$AA.
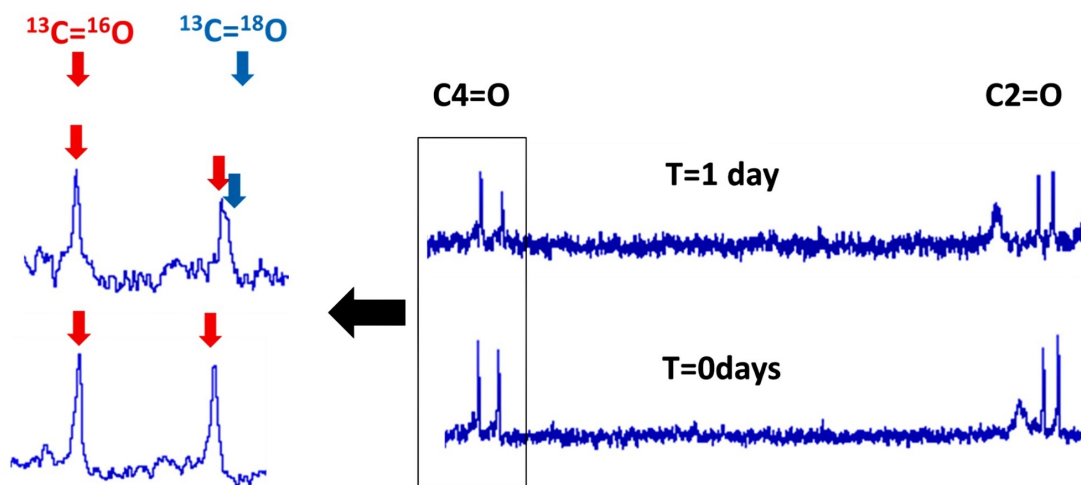


**Figure 3.11.** $^{13}$C NMR spectra showing $^{18}$O exchange in CPD-ATTA over time. Please refer to Figures 3.23 and 3.25 for the complete NMR spectrum at each of these time points.

### 3.2.5 Synthesis and characterization of AT̂TA with a selective $^{15}$N label at the 3′-thymine residue

To identify the initial site of nucleophilic attack in AT̂TA (by default also in AAT̂TAA), AT̂TA with a selective $^{15}$N label at the 3′ position was synthesized. $^{15}$N being NMR active (I=1/2) interacts with the C=O groups in its vicinity (both C2=O and C4=O groups on 3′ end of the molecule) and splits them into a doublet (2I+1). The C2=O and C4=O group peaks on the 5′ end of the lesion are left unaffected, and are thus differentiated from the ones at 3′ end of the molecule (Figure 3.12). Figure 3.13 shows the ESI-MS spectrum of 3′ $^{15}$N $^{15}$N , showing around 69% $^{15}$N incorporation. Figure 3.14 shows a section of $^{13}$C NMR spectrum for the compound highlighting the C2=O and C4=O groups. The complete $^{13}$C NMR spectrum, along with H$^1$, $^{15}$N and $^{31}$P NMR spectra for the compound, can be found in the Experimental section of this chapter. *As is evident from Figure 3.14, the C4=O with a relatively upfield chemical shift (the one that was shown to react first) remains at the 3′ end of the molecule. This establishes beyond reasonable doubt that in AT̂TA and in AAT̂TAA, the C4=O group on the 3′ end of the lesion reacts first followed by the 5′ C4=O group. There is no noticeable exchange seen on the C2=O groups during the time course of the reaction.*

*The above results indicate that the order of hydrolytic reactivity in a CPD molecule is unaffected by the presence of neighbouring groups around the CPD moiety or by a change in chain length. The final outcome of the exchange reaction is as depicted for dinucleotide T̂T in Figure 3.15.*



**ACPDA**
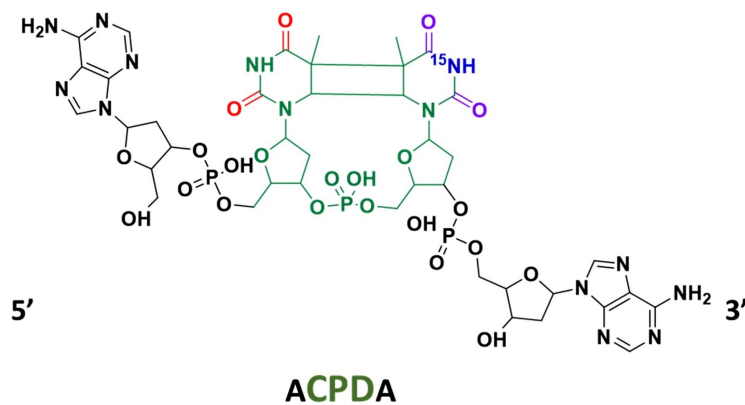
**Figure 3.12.** Schematic representation of the structure of AT̂TA with a selective $^{15}$N label on 3′ side
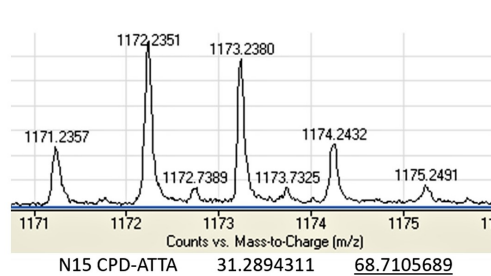
**Figure 3.13.** ESI-MS chromatogram of AT̂TA showing $^{15}$N enrichment in the molecule
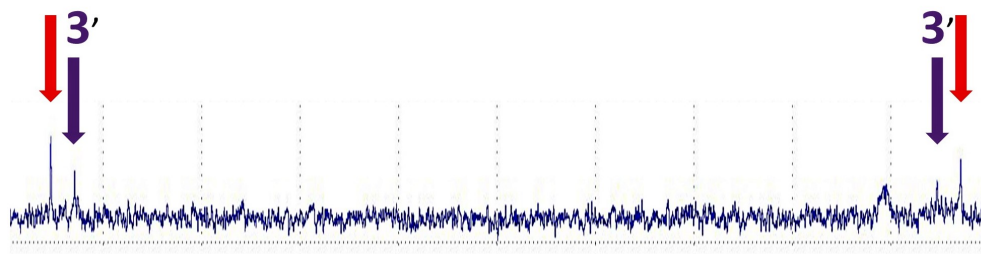


**Figure 3.14.** Section from $^{13}$C NMR spectrum of $^{15}$N labeled AT̂TA showing C2=O and C4=O groups. Please refer to Figure 3.31 for the complete spectrum.
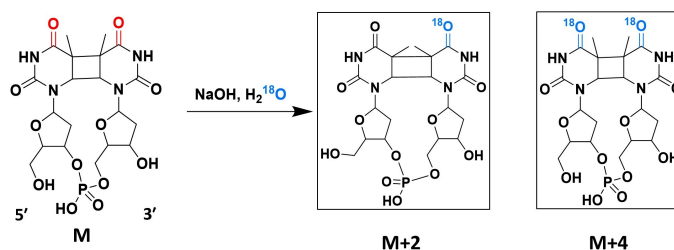


**Figure 3.15.** Products obtained after alkaline hydrolysis of T̂T lesion in presence of $^{18}$O labeled water

## 3.3  Discussion

There are very few studies devoted to understanding the alkaline hydrolysis of cyclobutane pyrimidine dimer (CPD) lesions [5], [92], [93]. Unfortunately, studies have only explored the reactivity of CPD lesions derived from thymine (nucleobase only) or thymidine (nucleosides only) models, none of which reflect the true polymeric state of DNA in living systems.

89

Here we investigated the alkaline reactivity of the most common DNA photolesion encountered in living cells, *i.e.*, cyclobutane pyrimidine dimer (CPD). Photo-irradiation of living cells results primarily in the formation of *cis-syn* isomer of CPD. Earlier work on cyclobutane pyrimidine dimers resulting from thymine (nucleobase) or thymidine (nucleoside) models clearly show that the *cis-syn* CPD is stable in the presence of a high concentration of alkali (1M) at room temperature. Our results with cyclobutane pyrimidine dimers resulting from dinucleotide TpT (described in Chapter 2) parallel these results (Figure 2.1). However, our investigation of the same reaction in $^{18}$O labeled water seemingly proved that, similar to other DNA lesions, CPD indeed undergoes a water addition at the C4 carbonyl group leading to the formation of a hemiaminal intermediate. However, this intermediate does not lead to any hydrolysis products and rapidly reverts to the starting material (Figure 2.2). Moreover, the two possible C4 carbonyl groups present on the 3′ and 5′ thymines of a CPD lesion show different chemical reactivities, with the C4=O group on 3′ sidebeing the initial point of hydrolytic attack. *Following our findings in Chapter 2, this chapter has now described the replication of these results in an oligonucleotide setting (in tetranucleotide, ATTA and hexanucleotide, AATTAA), indicating that the asymmetric alkaline reactivity observed between the C4 carbonyl groups on the 3′ and 5′ thymines in CPD, is an intrinsic property of the CPD residue. Moreover, similar to dinucleotide T̂T, the C4=O group on 3′ side in AT̂TA and AAT̂TAA is more reactive than the one on 5′ side (Figure 3.16)*
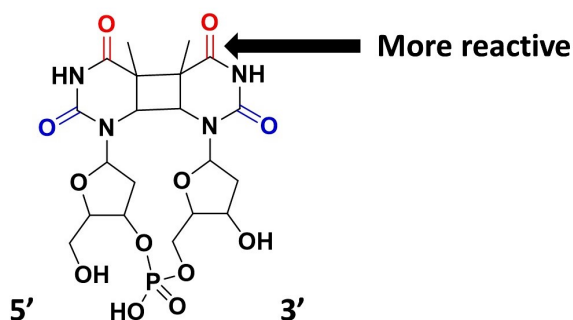


**Figure 3.16.** Schematic representation of the order of alkaline reactivity in CPD-TpT

### 3.3.1 Biological consequences

As noted in Chapter 2, both the direct-photoreversal enzyme photolyase and the excision repair enzyme T4 endonuclease V employ base flipping to access the thymine dimer lesion. ***The mechanistic cycle showing CPD repair by the photolyase enzyme clearly shows the C4=O group on 3′ end as the first site of electron attack in a CPD molecule. However, there is no known evidence to prove that. Our results with dinucleotide ($T\hat{T}$) and now oligonucleotide models ($AA\hat{TT}AA$ and $A\hat{TT}A$), provide a firm and clear evidence to support this observation!*** (Figure 2.22)

### 3.4 Methods

### 3.4.1 Materials and general methods

All solvents and chemicals were of analytical grade and purchased from Sigma, Fisher or VWR and used without further purification. NMR spectra were obtained using a Bruker 400 MHz NMR Fourier transform spectrometer using deuterium oxide as a solvent and with residual water acting as an internal standard. Mass spectrometric (MS) analyses were obtained via electrospray ionization (ESI) employing an ion-trap mass analyzer. HR-MS analyses were performed using a Q-TOF LC/MS spectrometer; data were acquired via "Agilent MassHunter Workstation Data Acquisition (B.03.00)" software and analyzed via "Qualitative Analysis of MassHunter Acquisition Data (B.03.00)" software.

### 3.4.2 HPLC product analyses

HPLC analyses were performed at room temperature using a Waters (Milford, MA) HPLC system coupled to a 2489 UV-Vis detector at 260 nm and 230 nm. A Waters $C^{18}$ RP column (2.5 $\mu$m particle size, 50 $\times$4.6 mm i.d.) was equilibrated in solvent A (10 mM triethylammonium acetate in water, pH 10.0), and compounds were eluted with an ascending gradient (1%-10%) of acetonitrile in 20 min at a flow rate of 1 mL/min. Semi-preparative HPLC analyses were performed at room temperature with the same Waters HPLC setup.

An XBridge OST C$^{18}$ column (2.5 $\mu$m particle size, 50 $\times$10 mm i.d.) was equilibrated in solvent A (10mM ammonium acetate in water, pH 6.8), and compounds were eluted with an ascending gradient (1-10%) of acetonitrile in 20 min at a flow rate of 4.73 mL/min. Products were confirmed by LC/MS spectrometry and NMR spectroscopy.

### 3.4.3   LC/MS product analyses

LC/MS-based assays of $^{18}$O incorporation were conducted via an Agilent 6520 Accurate Mass Q-TOF LC/ MS spectrometer using a Waters C$^{18}$-RP column (2.5 $\mu$m particle size, 50 $\times$4.6 mm i.d.). The column was equilibrated in solvent A (10 mM ammonium acetate in water) and acetonitrile (solvent B) in 20 min at a flow rate of 1 mL/min. The mass signals were monitored using negative ion mode.

### 3.4.4   Formation of CPD-containing oligonucleotides

Oligonucleotides were prepared manually using controlled pore glass (CPG) beads. AA$\hat{TT}$AA and A$\hat{TT}$A were obtained after UV-B (302 nm) irradiation of the aqueous solutions of the corresponding oligonucleotides in ice-cold solution for $\approx$ 4 hours. The UV-B irradiated reaction mixture was subjected to RP-HPLC purification to purify the CPD-containing oligonucleotides. The purified oligonucleotides were desalted using RP-HPLC and their concentrations were determined using UV-visible absorption spectroscopy (Molar extinction coefficient for AATTAA and ATTA was obtained using the *oligoanalyzer tool* from IDT DNA technologies, $\epsilon$=69600 M$^{-1}$ cm$^{-1}$ for AATTAA and $\epsilon$=45600 M$^{-1}$ cm$^{-1}$ for ATTA) [102]. Figures 3.17 and 3.18 show $^{13}$C and $^{31}$P NMR spectra for hexanucleotide AATTAA. Figures 3.19 and 3.20 show $^{13}$C and $^{31}$P NMR spectra for AA$\hat{TT}$AA. Figures 3.21 and 3.22 represent the $^{13}$C NMR specta showing $^{18}$O incorporation in AA$\hat{TT}$AA at T=1 day and T=5 days.

Figures 3.23 and 3.24 represent the $^{13}$C and $^{31}$P NMR spectra for tetranucleotide A$\hat{TT}$A. Figures 3.25 and 3.26 represent the $^{13}$C NMR spectrum showing $^{18}$O incorporation in A$\hat{TT}$A at T=1 day and T=5 days.
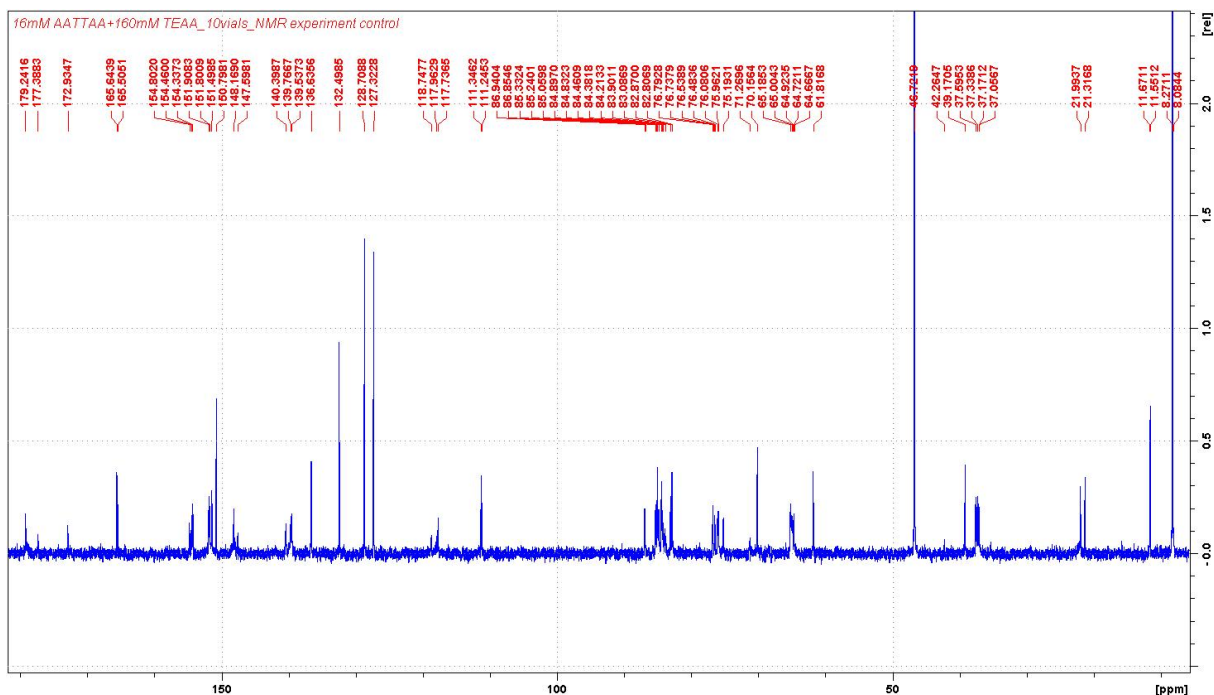
**Figure 3.17.** $^{13}$C NMR spectrum for hexanucleotide AATTAA

### 3.4.5 Synthesis of A$T\hat{T}$A containing a selective $^{15}$N label on 3′ side

$^{15}$N labeled thymidine and thymidine phosphoramidite were synthesized using the protocol developed by Bdour *et al* [99]. The $^{15}$N labeled thymidine phosphoramidite was then used for ATTA synthesis using CPG beads. A$T\hat{T}$A with a $^{15}$N label on 3′ side was obtained after UV-B (302 nm) irradiation of the aqueous solutions of the $^{15}$N labeled ATTA in ice-cold solution for $\approx$ 4 hours. The UV-B irradiated reaction mixture was subjected to RP-HPLC purification to purify the $^{15}$N labeled A$T\hat{T}$A. The purified oligonucleotide was desalted using HPLC and its concentrations was determined using UV-visible absorption spectroscopy ($\epsilon$=45600 M$^{-1}$ cm$^{-1}$). Figures 3.27, 3.28, 3.29 and 3.30 show H$^1$, $^{13}$C, $^{31}$P and $^{15}$N NMR spectra for $^{15}$N-labeled thymidine phosphoramidite that was used to synthesize A$T\hat{T}$A with a selective $^{15}$N label on its 3′ side. Figures 3.31 and 3.32 show $^{13}$C and $^{31}$P NMR spectra for this molecule.

93
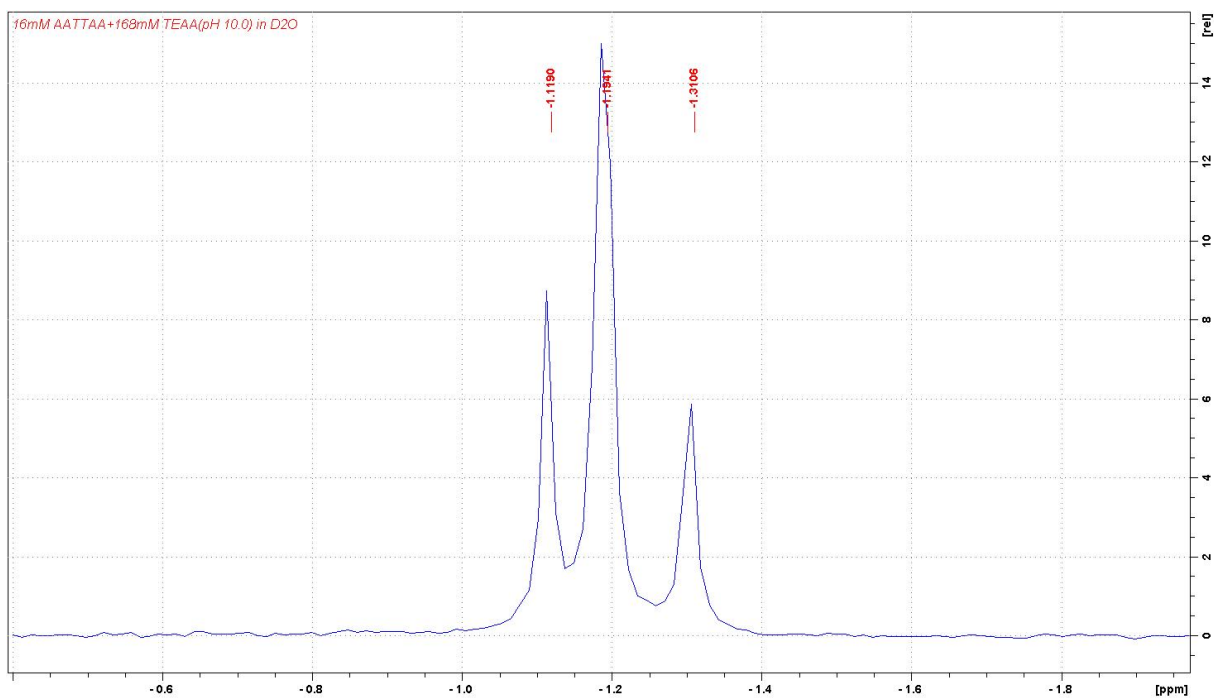
**Figure 3.18.** $^{31}$P NMR spectrum for hexanucleotide AATTAA
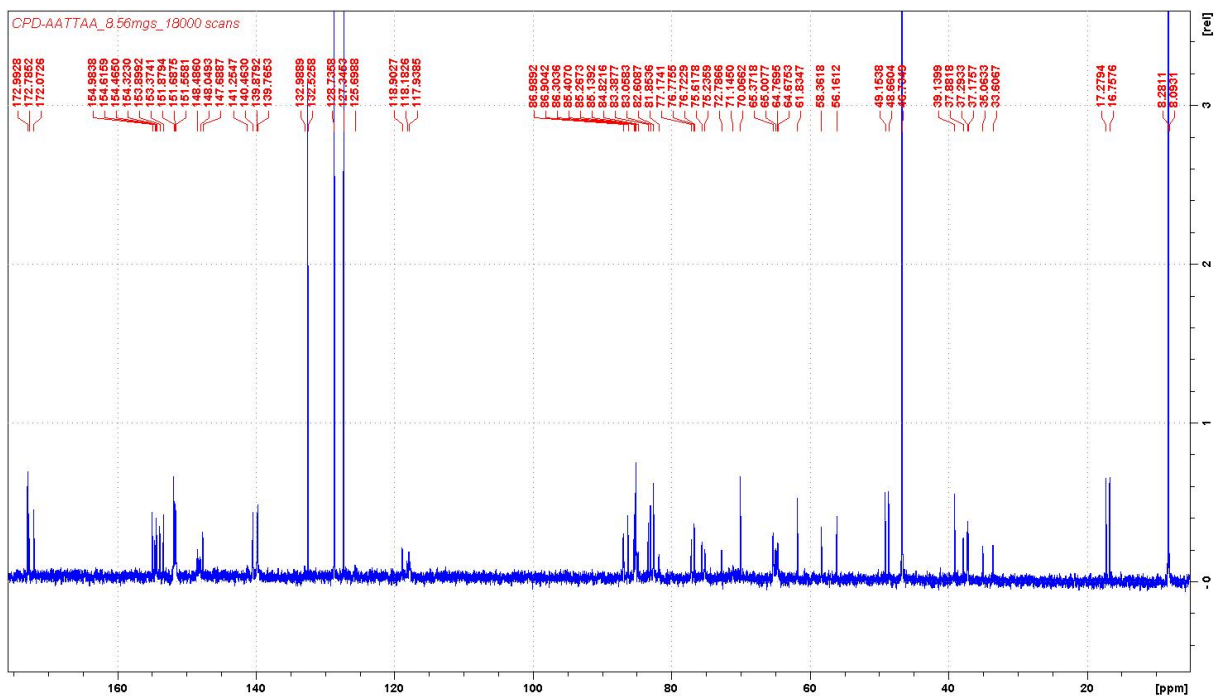


**Figure 3.19.** $^{13}$C NMR spectrum for $AA\hat{TT}AA$
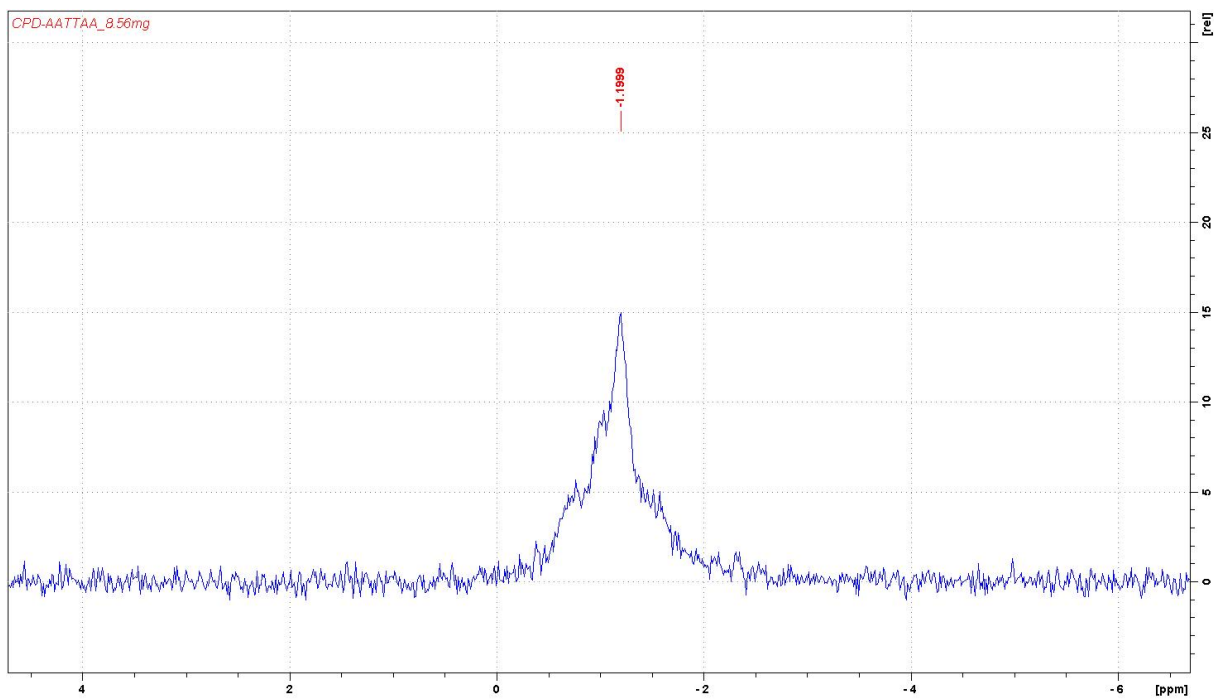
**Figure 3.20.** $^{31}$P NMR spectrum for AA$T\hat{T}$AA
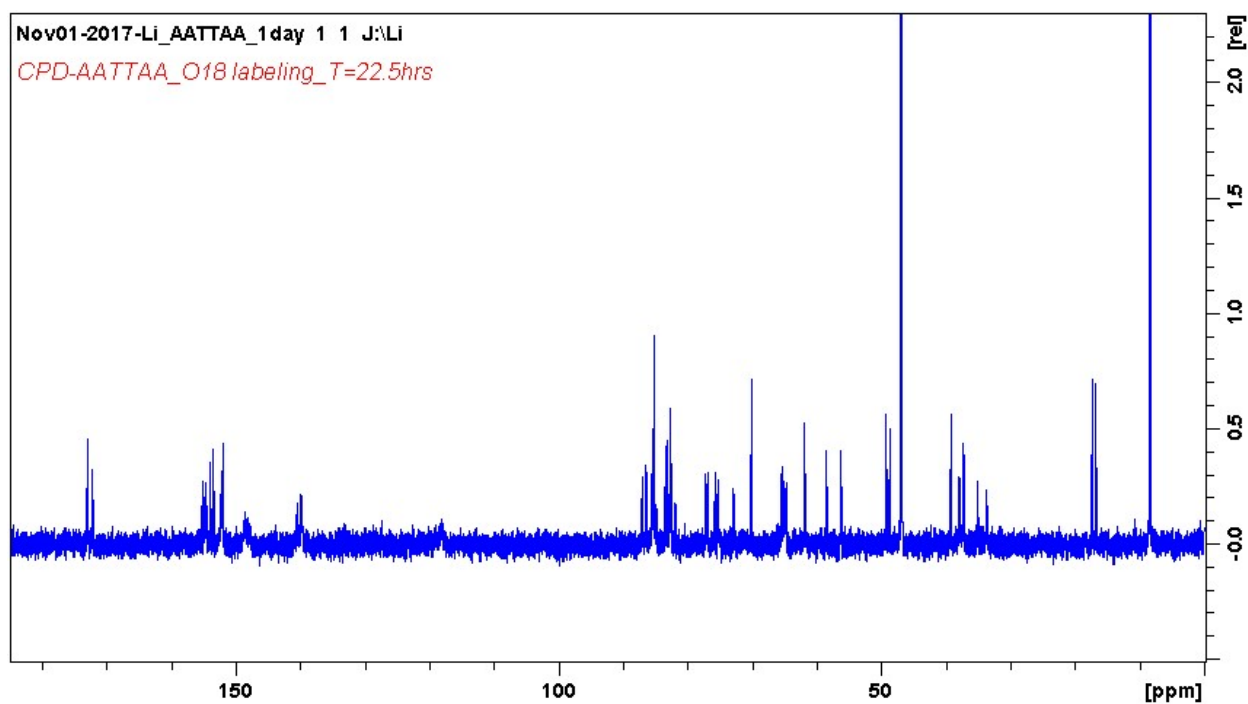


**Figure 3.21.** $^{13}$C NMR spectrum showing $^{18}$O incorporation in AA$T\hat{T}$AA at T= 1 day
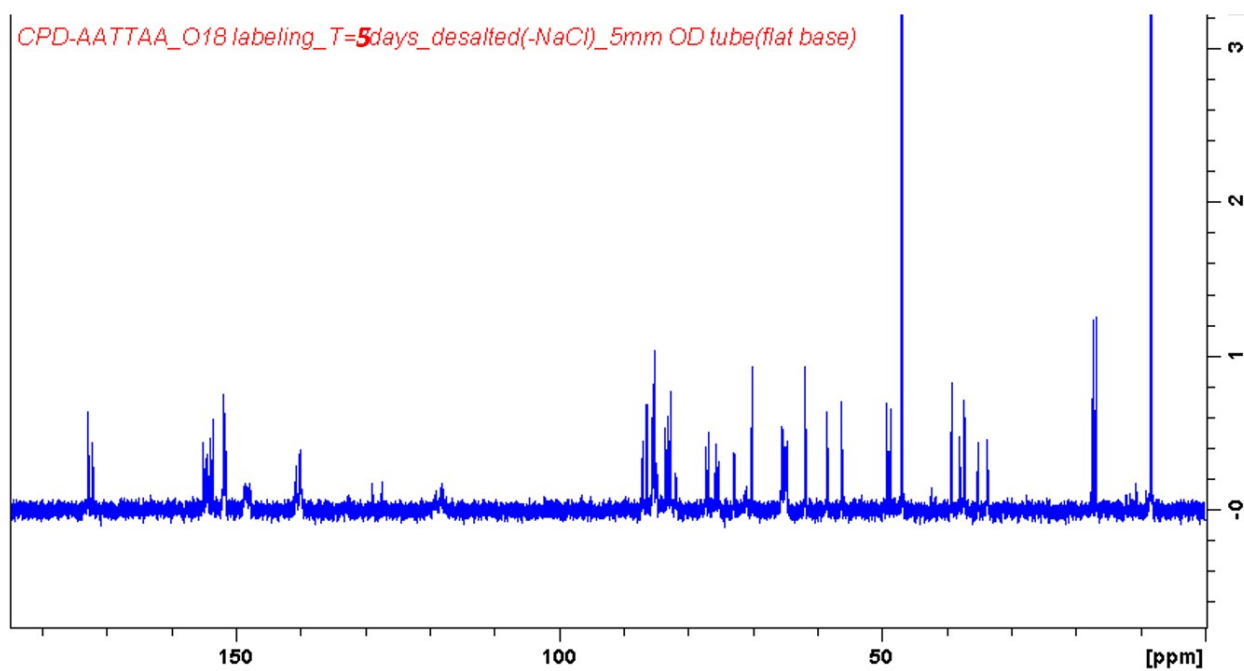
**Figure 3.22.** $^{13}$C NMR spectrum showing $^{18}$O incorporation in AA$T\hat{T}$AA at T= 5 days
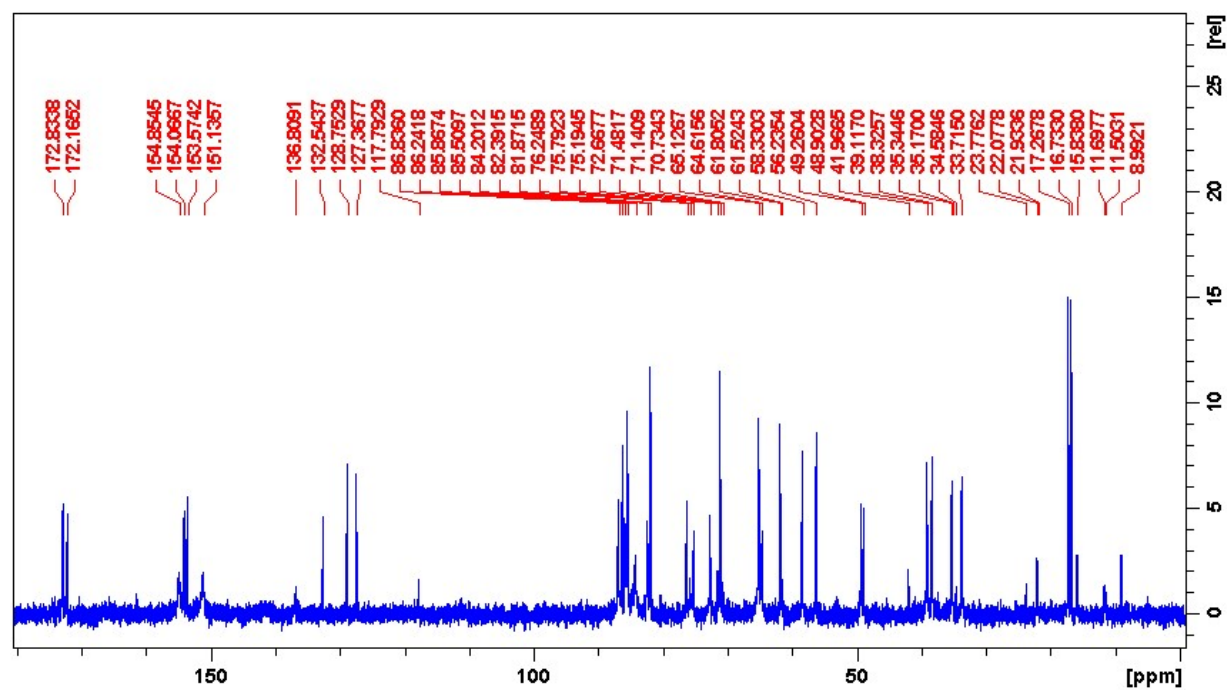


**Figure 3.23.** $^{13}$C NMR spectrum for A$T\hat{T}$A
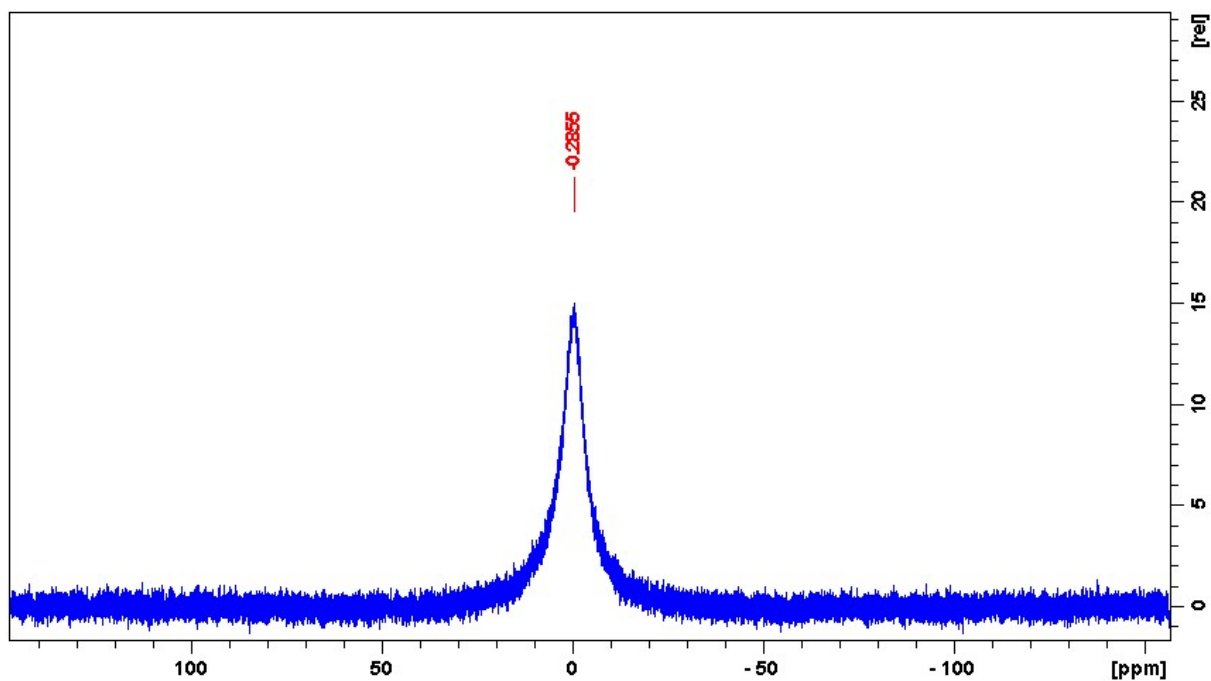
**Figure 3.24.** $^{31}$P NMR spectrum for A$\hat{T}$TA
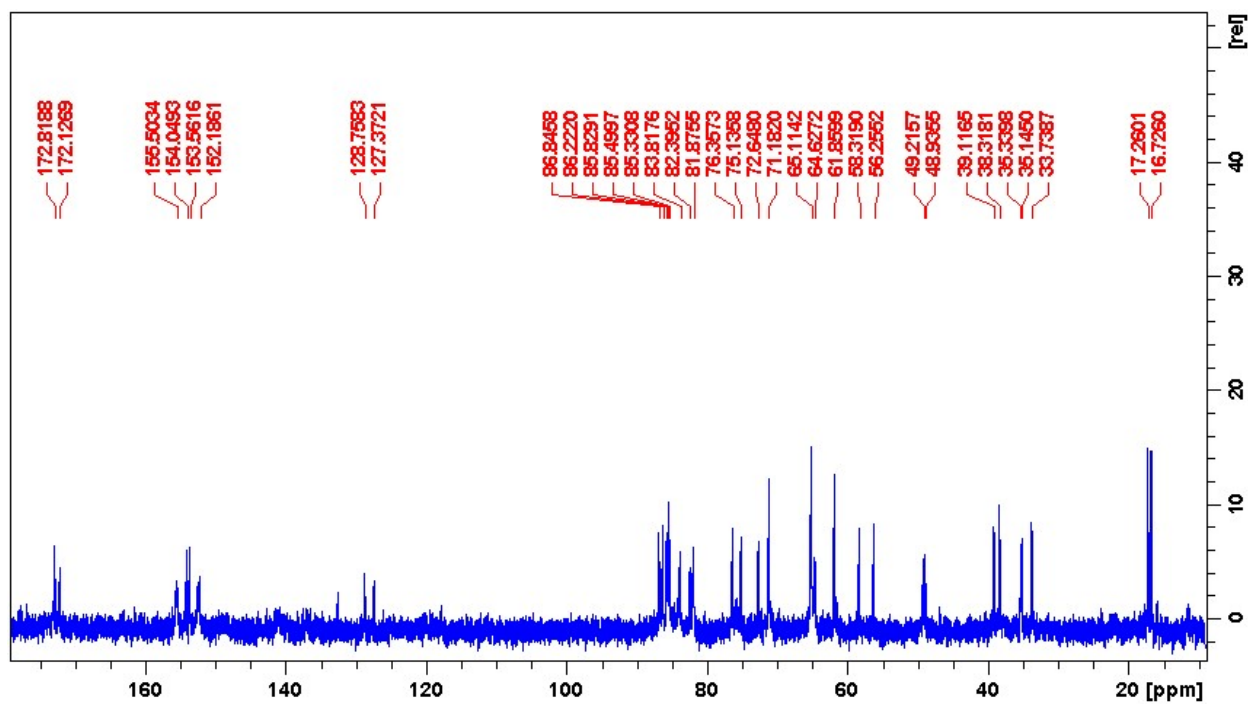


**Figure 3.25.** $^{13}$C NMR spectrum showing $^{18}$O incorporation in A$\hat{T}$TA at T= 1 day
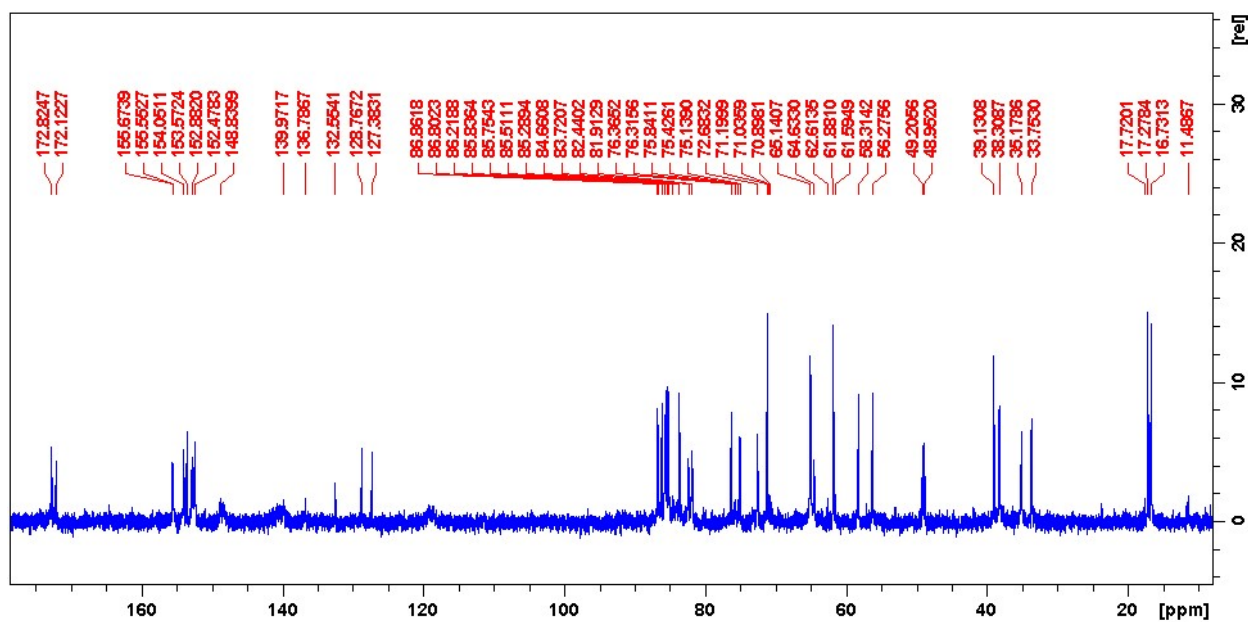
**Figure 3.26.** $^{13}$C NMR spectrum showing $^{18}$O incorporation in A$T\hat{T}$A at T= 5 days
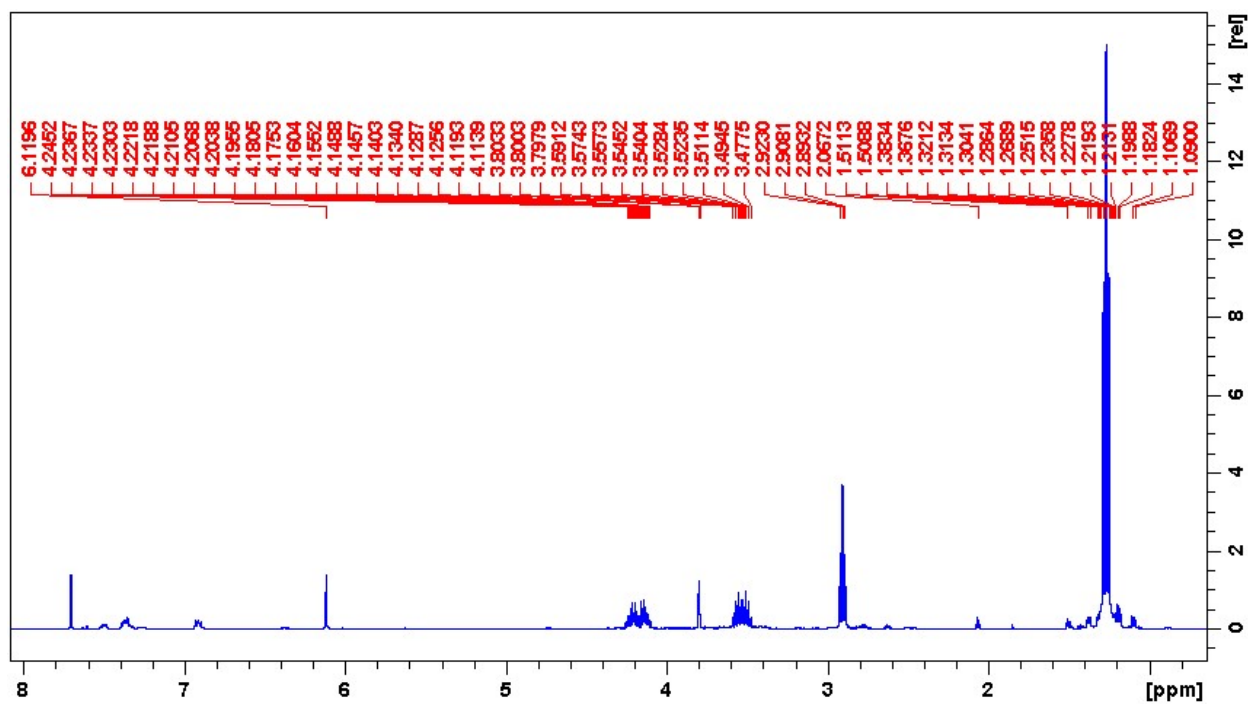


**Figure 3.27.** H$^1$ NMR spectrum for $^{15}$N-labeled thymidine phosphoramidite
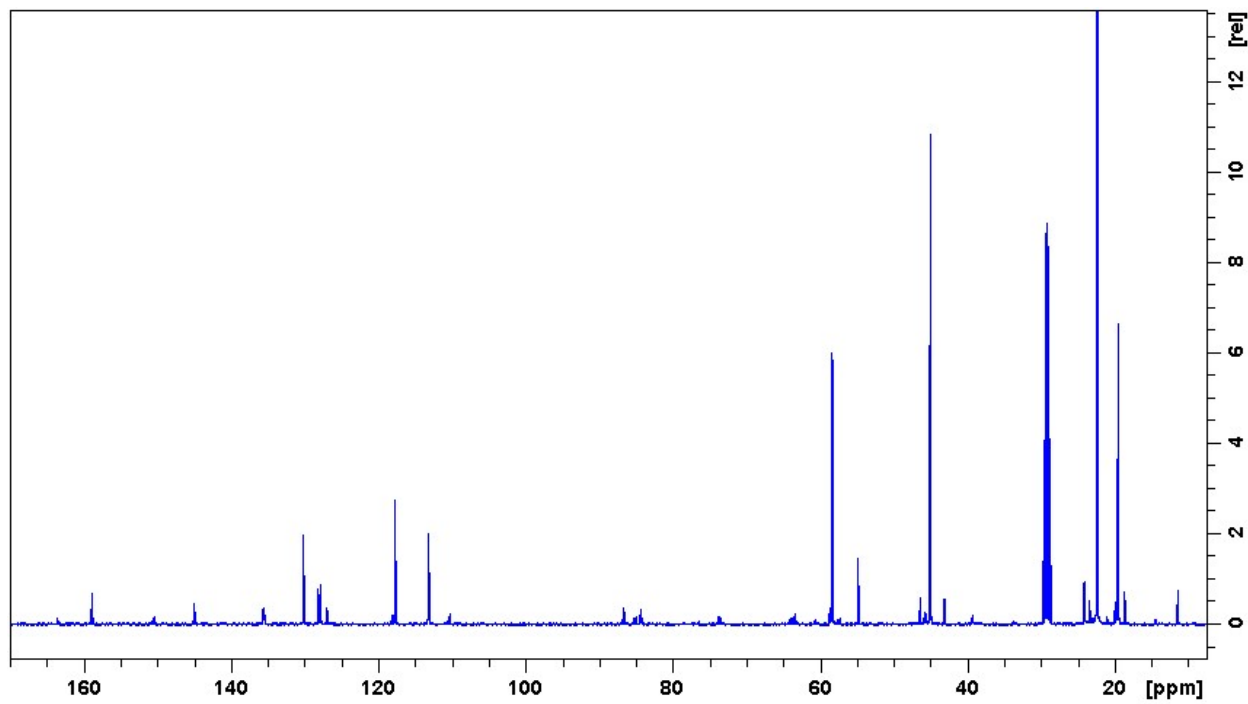
**Figure 3.28.** $^{13}$C NMR spectrum for $^{15}$N-labeled thymidine phosphoramidite
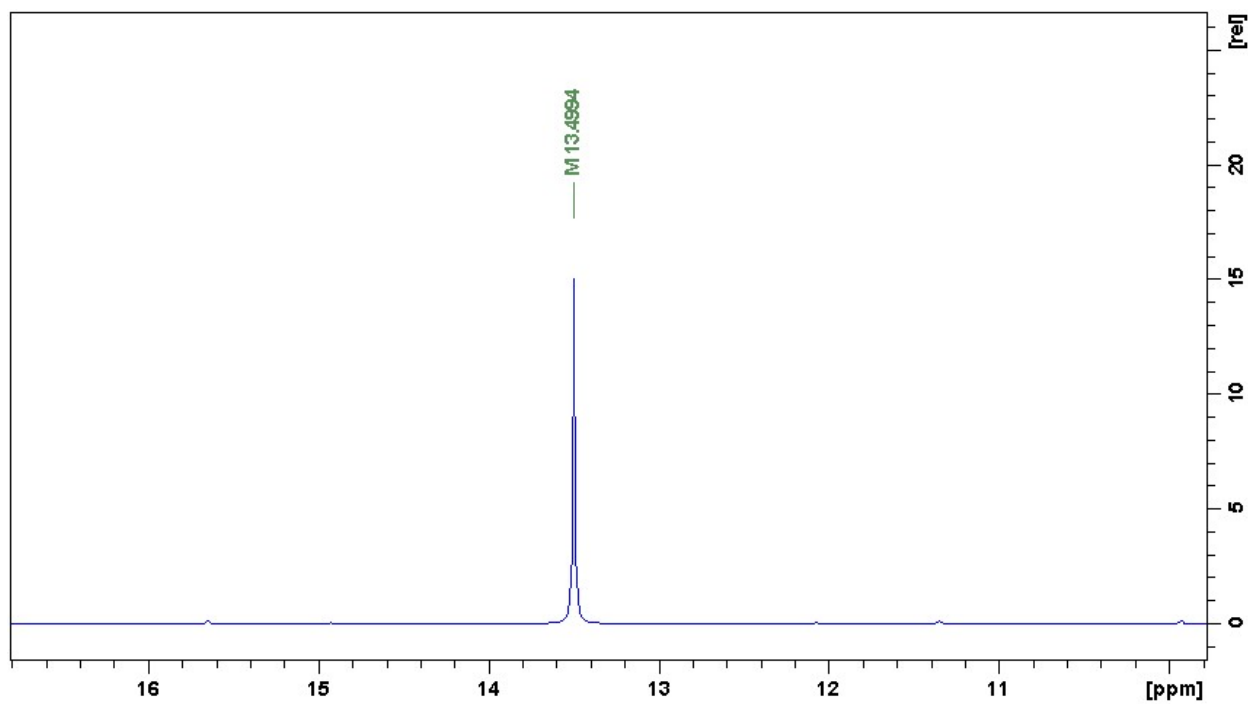


**Figure 3.29.** $^{31}$P NMR spectrum for $^{15}$N-labeled thymidine phosphoramidite
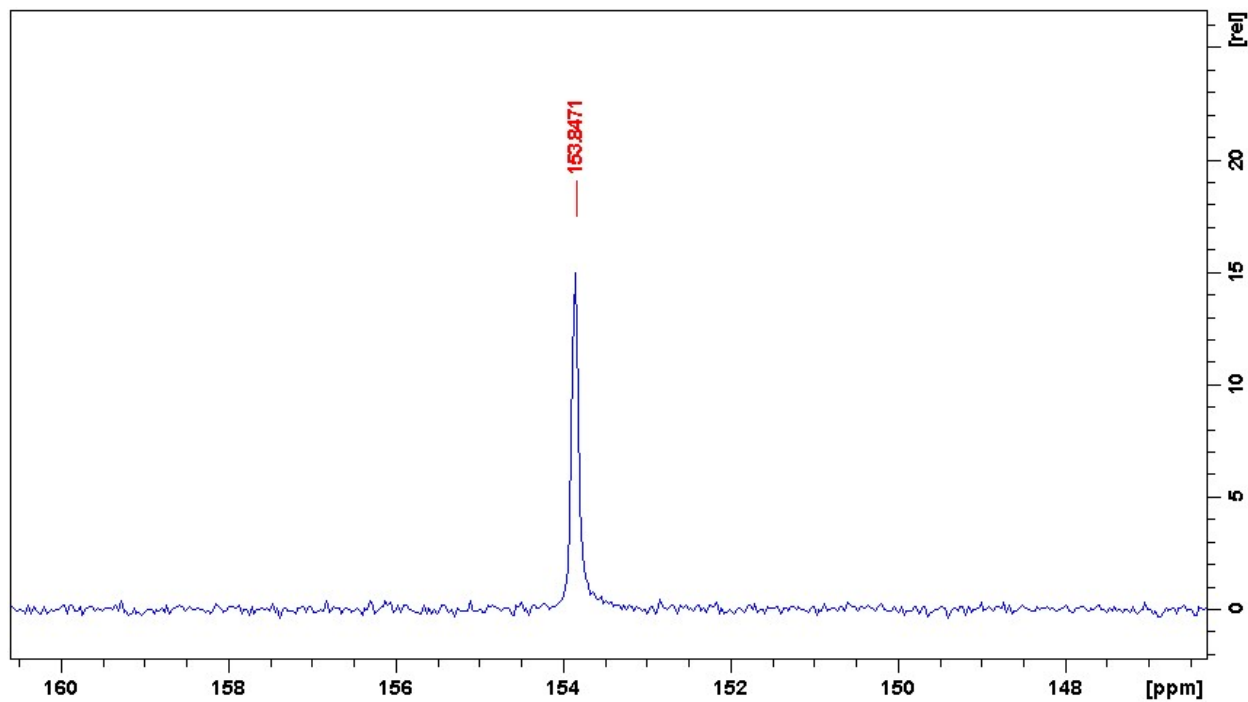
**Figure 3.30.** $^{15}$N NMR spectrum for $^{15}$N-labeled thymidine phosphoramidite
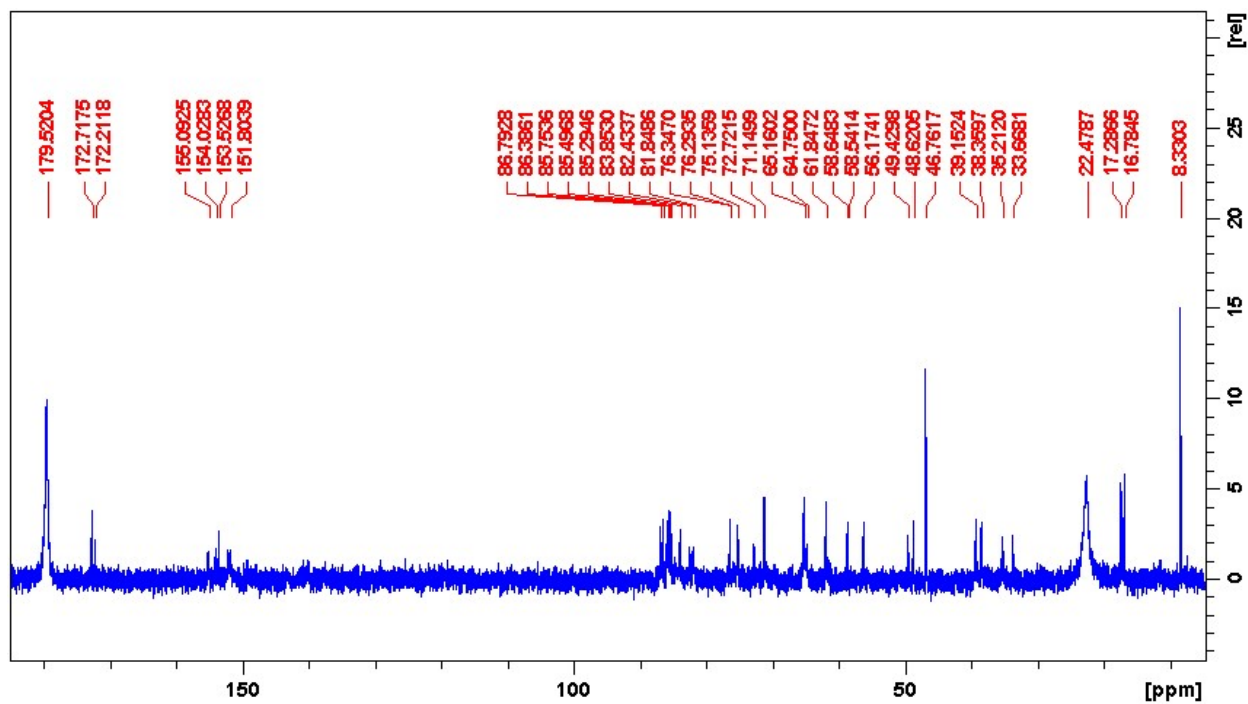


**Figure 3.31.** $^{13}$C NMR spectrum for $A\hat{T}TA$ with a selective $^{15}$N-label on 3′ side
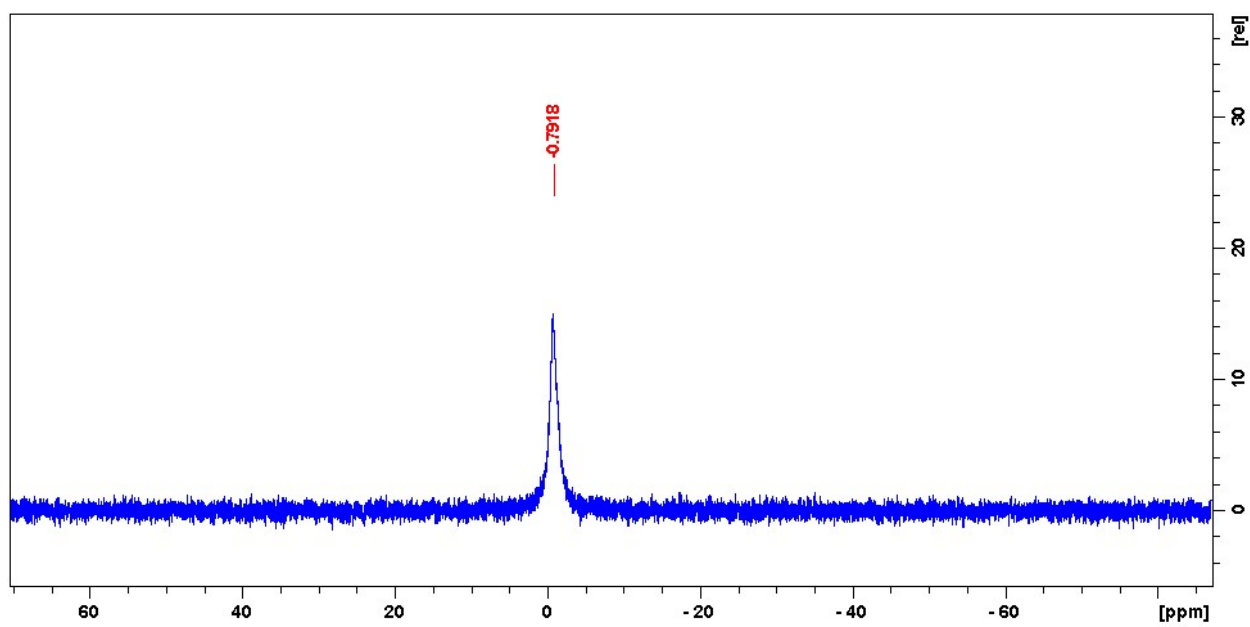
**Figure 3.32.** $^{31}$P NMR spectrum for $A\hat{TT}A$ with a selective $^{15}$N-label on 3′ side

# 4. INVESTIGATION OF THE HYDRAZINE REACTIVITY OF CYCLOBUTANE PYRIMIDINE DIMER (CPD) LESIONS: A POTENTIAL MEANS OF LESION REPAIR?

## 4.1 Introduction

In order to explore the reactivities of the two C4=O groups (and the lability of their respective N3-C4 bonds) in CPD, the alkaline reactivity of CPD nested in dinucleotide and oligonucleotide contexts was investigated in Chapters 2 and 3. Earlier published work on cyclobutane pyrimidine dimers resulting from thymine and thymidine clearly showed that *cis-syn* CPD is stable in presence of high concentration of alkali (1 M) at room temperature (Figure 1.27)[5]. Our results on cyclobutane pyrimidine dimers resulting from dinucleotide TpT confirmed these results (Figure 2.1); and through our investigation of the same reaction in $^{18}$O labelled water we proved that, similar to other DNA lesions, CPD undergoes a water addition at the C4=O group leading to the formation of a hemiaminal intermediate. This intermediate, however, does not lead to any hydrolysis products and completely reverts to the starting lesion (Figure 2.2). Moreover, as revealed in Chapters 2 and 3, the two C4=O groups present on the 3′- and 5′-thymines in a CPD lesion show different chemical reactivities, reflected by different rates of exchange with the incoming nucleophile leading to the hemiaminal intermediate. Further, the results obtained with the dinucleotide model (CPD-TpT or $\hat{TT}$) were replicated in an oligonucleotide setting and in various structural variants of CPD-TpT, to prove that the observed asymmetry in alkaline reactivity, between C4=O groups on the 3′- and 5′-thymines in CPD, is an intrinsic property of the CPD residue.

Since simple alkaline treatment failed to open the pyrimidine ring of CPD even under conditions of high alkalinity and elevated temperatures, stronger nucleophiles were examined in our quest to investigate the lability of the N3-C4 bond (as observed in other DNA lesions with a saturated pyrimidine ring) (Figure 1.23)[6]. Along with various nitrogen and sulfur containing nucleophiles (nitrogen and sulfur being stronger nucleophiles than oxygen) like lysine and 2-mercaptoethanol (both of which yielded some reaction products, further experiments required to explore the nature of these products), we tried hydrazine monohydrate, which is known for its increased nucleophilicity on account of the *'alpha effect'* of the two

neighbouring nitrogen atoms [104]–[106]. We expected a nucleophilic attack by nitrogen on the C4=O group followed by a cleavage of the N3-C4 bond, similar to that observed upon treatment of all other sunlight-induced DNA lesions with an alkali [6].

*As detailed below, a rapid and complete chemical reversal of dimeric CPD to the two canonical bases (TpT) was observed upon lesion treatment with hydrazine (Figure 4.1).* The finding is particularly interesting as it demonstrates a means of chemical DNA repair. In the work described below, the intricacies of the reaction are described and the reaction pathway was probed by characterizing the intermediate(s) involved using various experimental techniques (independently and in tandem).



Chemical Formula: $C_{20}H_{27}N_4O_{12}P$
Molecular Weight: 546.43

Chemical Formula: $C_{20}H_{27}N_4O_{12}P$
Molecular Weight: 546.43
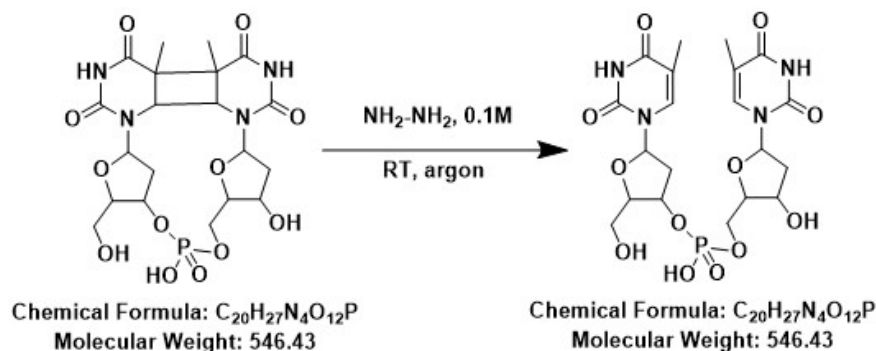
**Figure 4.1.** General scheme for hydrazine mediated CPD repair

## 4.2   Results

### 4.2.1   Investigation of hydrazine-mediated CPD repair using reverse-phase HPLC

Figure 4.2 shows a representative reverse phase HPLC (RP-HPLC) chromatogram of the reaction of 1 mM CPD-TpT with 100 mM hydrazine under argon after 240 minutes of the reaction. The reaction between CPD-TpT and hydrazine monohydrate to yield dinucleotide TpT proceeded with considerable ease at room temperature. However, it did not proceed to completion even after using high concentrations of hydrazine (up to 1 M for 1 mM of CPD-TpT) and utilizing higher temperatures (up to 90°C) under ambient atmosphere. In contrast, the reaction was facile and rapidly proceeded to completion (most of the starting material used up in less than 2 hours) in an inert atmosphere (at room temperature). This

can most likely be attributed to the auto-oxidation of hydrazine reported under aerobic conditions [107]. A striking observation was the continued formation of the product (*i.e.*, TpT) even after rapidly freezing the reaction mixture immediately after mixing the two reactants; indicating the formation of an intermediate species (on reaction of CPD-TpT with hydrazine) that collapsed to TpT by a possible intramolecular rearrangement. Since the intermediate(s) appeared to be unstable at neutral pH (used for HPLC analyses earlier), a basic buffer (10 mM triethylammoniumacetate TEAA, pH 10.0) was used as buffer A during RP-HPLC analyses of this reaction. Buffer B was acetonitrile (as used earlier). TpT was confirmed as the product of the reaction using three independent techniques: UV-visible absorption spectroscopy (Figure 4.3), LC-MS and RP-HPLC co-injection (Figure 4.4), all in the presence of dinucleotide TpT as an internal standard. Please refer to Section 4.4.1, Figures 4.17 and 4.18 for the complete list of spectra at various time points (from T=0 minutes to T=240 minutes) for the reaction between 1 mM CPD-TpT and 100 mM hydrazine under argon atmosphere at room temperature. Figure 4.19 represents the kinetic curve showing the change in concentration of CPD-TpT, TpT and the potential intermediate as determined by RP-HPLC measurements.

In order to determine the effect of change(s) in concentration of CPD-TpT and hydrazine on the rate of the reaction, the same reaction (described above) was conducted by systematically varying the concentration(s) of CPD-TpT and hydrazine keeping other reaction conditions constant. All these experiments were conducted at room temperature under argon atmosphere. The reaction species at various time points were analyzed using RP-HPLC. Figures 4.20 and 4.21 show the spectra recorded at various time points for the reaction between 1 mM CPD-TpT and 200 mM hydrazine. Figure 4.22 shows the change in reaction rate (as a function of the rate of decrease of CPD-TpT) on doubling the concentration of hydrazine, keeping that of CPD-TpT constant. *Since hydrazine is already present in excess (as compared to CPD-TpT) in the reaction mixture, the reaction was expected to proceed via 'pseudo-first order' kinetics, where a change in the concentration of hydrazine should have no effect on the rate of the reaction. The observed change can most likely be attributed to an increase in the pH of the solution, that in turn, had an accelerating effect on the reaction rate.*

Figures 4.23 and 4.24 show the spectra recorded for the reaction between 2 mM CPD-TpT and 100 mM hydrazine. Figure 4.25 shows the change in reaction rate (as a function of the rate of decrease of CPD-TpT), when the concentration of CPD-TpT is doubled keeping that of hydrazine constant. *No change in the reaction rate on doubling the concentration of CPD-TpT was rather surprising; suggesting that the reaction rather proceeded via a 'zero order' kinetics and not the expected 'pseudo-first order' kinetics. It should be pointed out that similar trend was observed while studying the kinetics of $^{18}O$ exchange reaction in cis-syn CPD-TpT* (Appendix A, Figure A.3). **A similarity in the trends of the two reactions ($^{18}O$ labeling and hydrazine-mediated repair) leads to the inference that a CPD-TpT molecule undergoes nucleophilic addition via 'zero order' kinetics, and suggests that the two reactions proceed via a similar mechanism.**
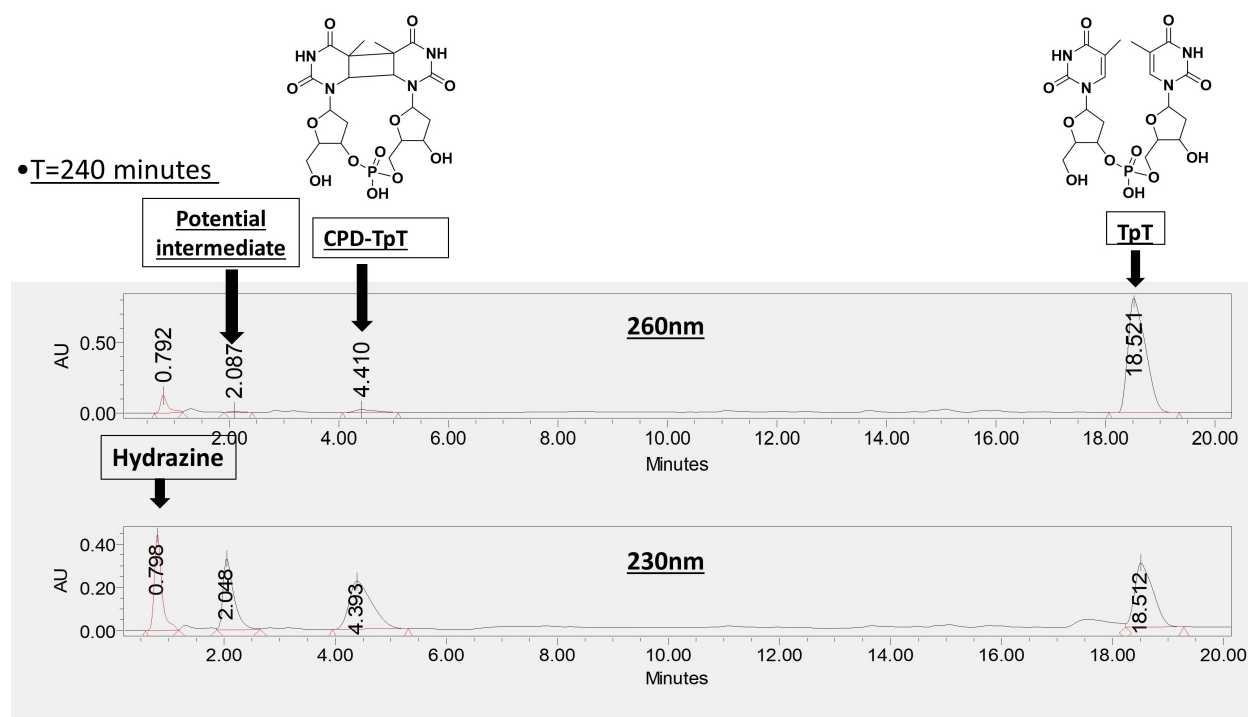


**Figure 4.2.** Reverse-phase HPLC chromatogram of the reaction of CPD-TpT with hydrazine under argon atmosphere

Hydrazine-mediated repair was also tried in various structural variants of CPD-TpT, in an attempt to vary the stacking arrangement of the lesion in aqueous solution, and therefore, obtain a better understanding of the structural intricacies contributing to the speed and

**COMPARISON OF UV-VISIBLE ABSORPTION SPECTRA OF CPD-HYDRAZINE REACTION PRODUCT AND TPT**
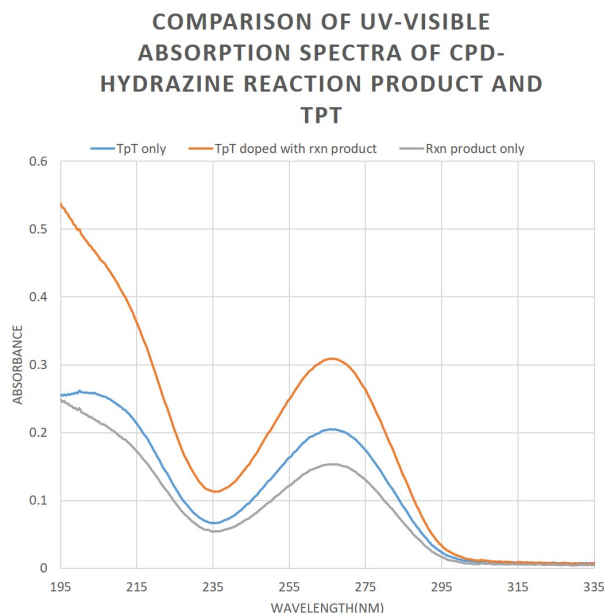
**Figure 4.3.** Comparison of UV-Visible absorption spectra of CPD-Hydrazine reaction product and that of TpT control

efficiency of the reaction. One of these structural variants was a CPD isostere in which the phosphate linker between the thymidine residues was replaced by a methylene linker (CPD-TcT). The goal of the study was to determine the role of phosphate linker and thus, the role of solution conformation of CPD on the outcome of the repair reaction. The reaction between CPD-TcT and hydrazine was found to proceed with similar ease, thereby implying that the phosphate linker (and thus the solution conformation of CPD) has little influence on the outcome of the reaction (Figure 4.5). Please refer to Figure 4.26 for a complete list of spectra recorded at various time points for the reaction between 1 mM CPD-TcT and 100 mM hydrazine under argon atmosphere at room temperature. A comparison between the rate(s) of repair reaction in CPD-TpT and CPD-TcT was made by studying the kinetics of hydrazine-mediated CPD-TcT repair in presence of CPD-TpT as an internal standard (Figure 4.6). The figure clearly illustrates that, even though a change in the nature of the linker does not alter the outcome of the repair reaction, nevertheless, the rate of decay of CPD-TcT (and thus the rate of formation of TcT) is faster than CPD-TpT in presence of the same amount of hydrazine, thereby implying a change in reaction rate with a change in solution conformation of the CPD molecule.

106

**Doped mixture**- 100µl reaction product+40µl TpT
**Control A**- 40µl TpT diluted to 140 µl with DI water
**Control B**- 100 µl of reaction product diluted to 140 µl with DI water
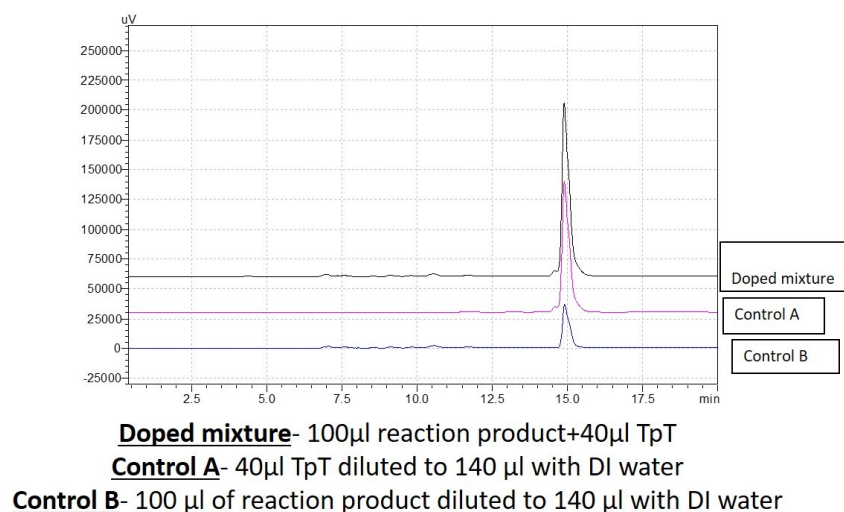
**Figure 4.4.** Reverse-phase HPLC-based doping experiments to identify TpT as CPD + Hydrazine reaction product



Chemical Formula: $C_{21}H_{28}N_4O_{10}$
Molecular Weight: 496.47

Chemical Formula: $C_{21}H_{28}N_4O_{10}$
Molecular Weight: 496.47
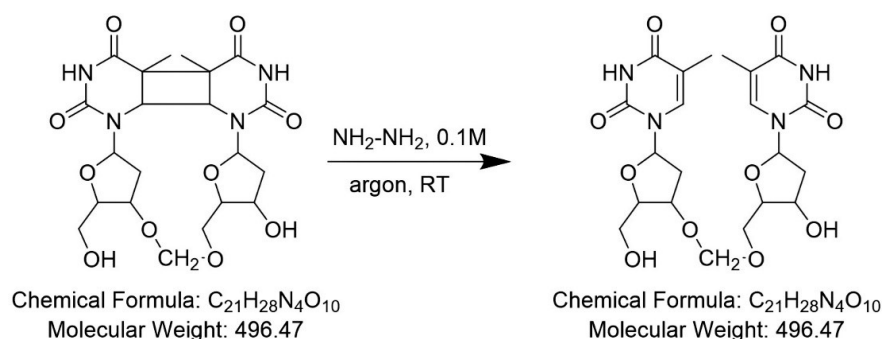
**Figure 4.5.** Reaction scheme involving repair of CPD-TcT lesion to TcT

The CPD-TpT repair reaction was also attempted in the presence of methyl hydrazine instead of hydrazine monohydrate. *Although there was some reaction observed (evidenced by the loss of the CPD-TpT species), no TpT formation was observed during the course of the experiment. This observation, in combination with the results from the reaction of CPD-TpT with lysine, ammonia and mercaptoethanol (during which 'some hydrolysis products' were observed), indicates that the presence of hydrazine monohydrate is crucial for the repair reaction.*

107
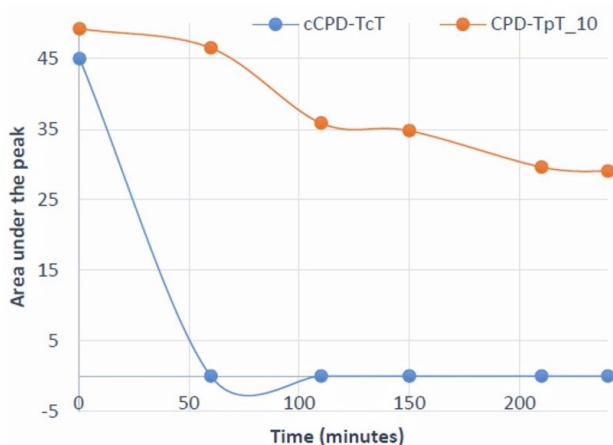
**Figure 4.6.** Rate of decay of CPD-TpT vs CPD-TcT in presence of 100 mM Hydrazine

### 4.2.2 Analyses of the reaction using Q-TOF LC-MS: Investigation of the reaction intermediate(s)

In order to characterize the potential intermediate species observed during the RP-HPLC experiments (Figures 4.17 and 4.18), the reaction between 1 mM CPD-TpT and 100 mM hydrazine was analyzed using a Q-TOF LC-MS. After every 30 minutes, aliquots were drawn out of the reaction mixture (conducted in a flask fitted with an argon balloon) and quickly injected into a LC-MS instrument. The reaction species were monitored under positive ion mode. Figure 4.7 shows the LC-MS profile for the reaction mixture at T=1 minute (immediately after mixing hydrazine with CPD). The chromatogram shows a large CPD peak and a TpT peak. Appearance of the product peak immediately after mixing the two reactants indicates the rapid rate of this reaction. The peak at $m/z$=579 (M+32) most likely corresponds to the adduct formed between CPD/TpT with hydrazine present as a buffer during the LC-MS run, since similar adducts were observed during the control runs as well (Figure 4.8). Figures 4.27, 4.28, 4.29 and 4.30 show the LC-MS and UV-visible profiles for the reaction mixture at various time points (T=30 min to T=120 min). Although the UV-visible profiles show a clear indication of a species with an retention time close to that of CPD-TpT (as observed during the RP-HPLC experiments, Figures 4.17 and 4.18), the elution of these species occurs within the void volume of the $^{18}$C column used for the LC-run. Due to this reason, the mass values of these species cannot be obtained with confidence. It should be noted

here that a CPD-TpT lesion shows very poor affinity towards a [18]C column, and thus has a very low retention time. Retention time for this lesion can be increased by using ion-pairing reagents *e.g.* triethylammonium acetate (TEAA) (or ammonium acetate) that contain a long hydrophobic chain that can bind to the [18]C chains in a column. The positively-charged ammonium groups in these ion-pairing agents bind to the negatively-charged phosphate group in the CPD-TpT lesion, thus resulting in a higher retention time. However, since a mass spectrometer is incompatible with TEAA buffer (and the reaction intermediates were found to be unstable under neutral pH, thereby limiting the use of ammonium acetate), the basic conditions during LC-MS experiment were maintained using 10 mM hydrazine solution as buffer A, that shows no ion-pairing abilities.
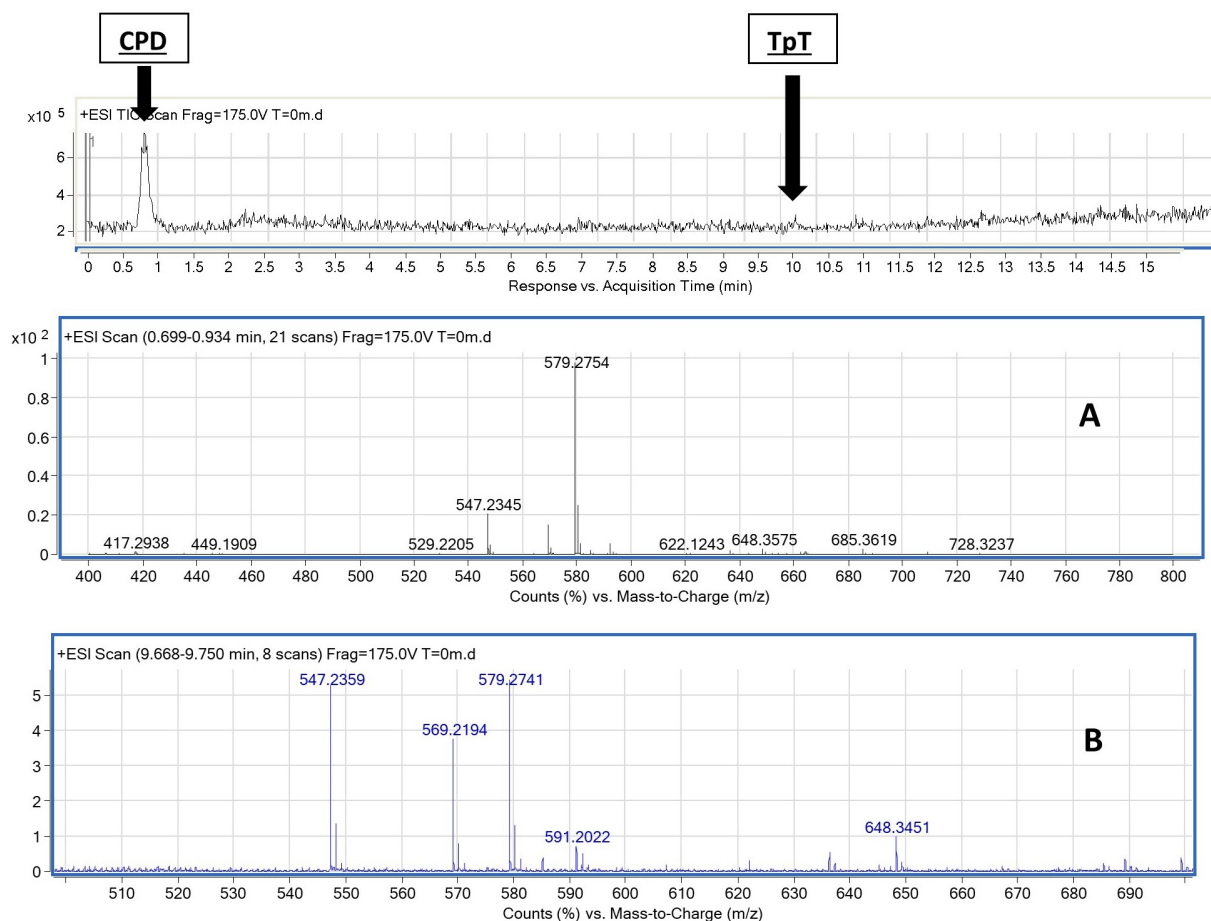


**Figure 4.7.** LC-MS Profile for CPD + hydrazine reaction mixture at T=1 min. Panels A and B show the mass values for the LC-MS peaks corresponding to CPD and TpT respectively.
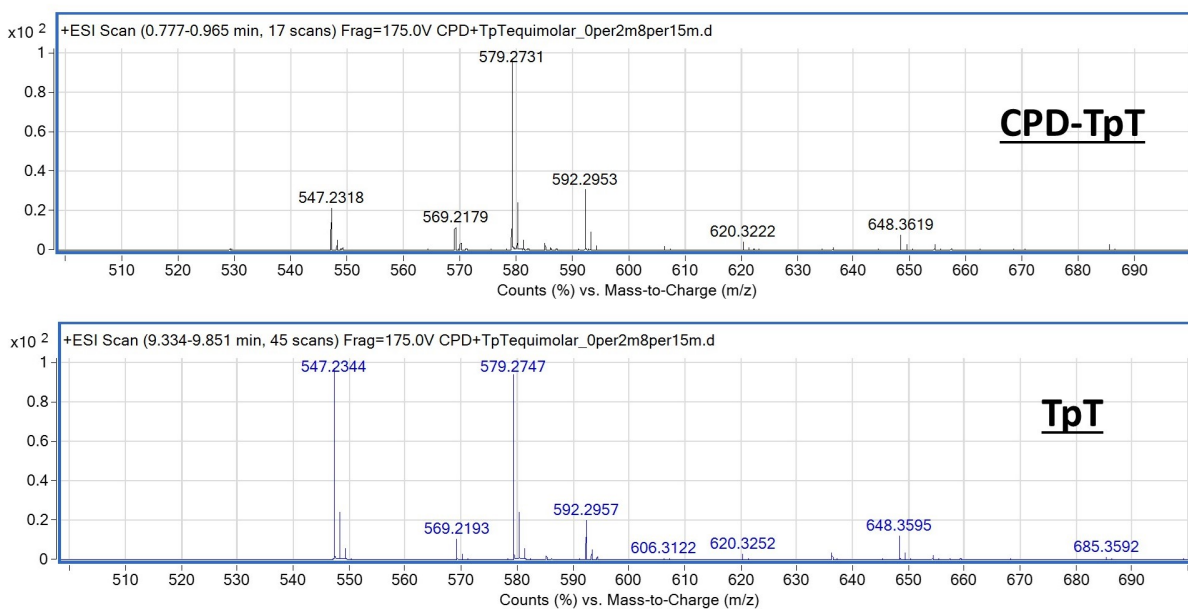
**Figure 4.8.** Mass spectra corresponding to CPD-TpT and TpT controls in presence of 10 mM hydrazine as LC-buffer.

### 4.2.3   Study of CPD + hydrazine reaction kinetics using UV-Visible absorption spectroscopy

In an attempt to shed further light on the reaction mechanism, the reaction kinetics was monitored using UV-visible spectrophotometry. Since it was now known that the reaction was facilitated by an inert atmosphere, the reaction between 1 mM CPD-TpT and 100 mM hydrazine was conducted and monitored under an argon atmosphere. To achieve this, the reaction was conducted in a quartz cuvette that was sealed with an argon balloon. The entire set up was placed in a UV-visible absorption spectrophotometer that recorded the complete absorption profile for the reaction mixture at various time points. An overlay of the UV-visible absorption spectrum of the reaction mixture over a period of 45 minutes showed a marked increase in absorbance at 260 nm with time. This indicates the formation of TpT molecule (Figure 4.9). Figure 4.10 shows the UV-Visible absorption spectra for the controls (CPD-TpT and TpT). *The most striking observation in this experiment was the appearance of an 'isosbestic point' that indicates the presence of an intermediate species during hydrazine-mediated chemical repair of CPD-TpT to dinucleotide TpT, which is consistent with our RP-HPLC and LC-MS results (Figure 4.11).*
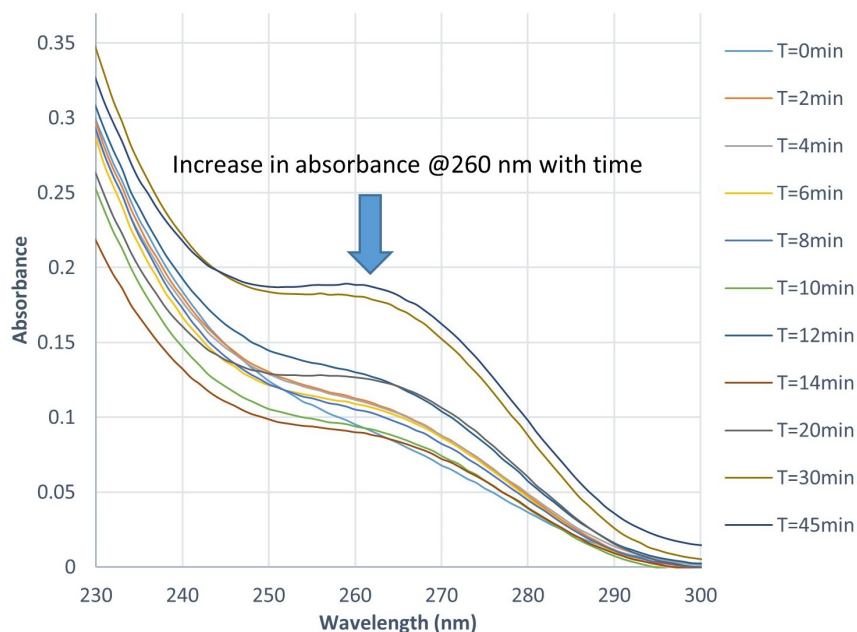
**Figure 4.9.** Overlay of UV-visible chromatograms obtained for the reaction between 1 mM CPD-TpT and 100 mM Hydrazine under argon atmosphere
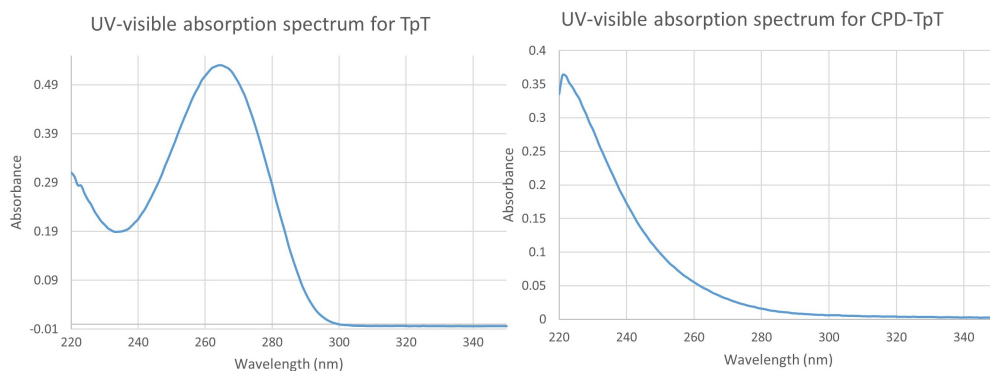


**Figure 4.10.** Control UV-Visible absorption spectrum for CPD-TpT and dinucleotide TpT

### 4.2.4   Analyses using $^1$H, $^{13}$C and $^{31}$P NMR spectroscopies: Identification and characterization of the reaction intermediate(s)

On the basis of our RP-HPLC and LC-MS results, it was determined that the reaction of CPD with hydrazine is favored by an inert atmosphere. These experiments also indicated the presence of an intermediate species that showed a similarity in retention time (and potentially structure) with the CPD-TpT lesion. Analyses of the same reaction (under
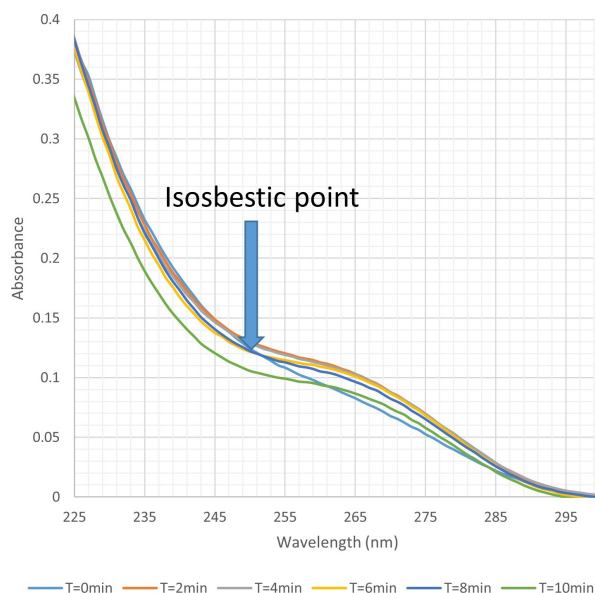
**Figure 4.11.** Overlay of the UV-visible absorption profiles for the reaction mixture (CPD-TpT + hydrazine) to show the isosbestic point

inert conditions) using UV-visible absorption spectroscopy also suggested the presence of an intermediate species (reflected by the presence of an isosbestic point). In an attempt to characterize the potential intermediate(s) and determine the reaction mechanism, the CPD + hydrazine reaction was conducted in an NMR tube (maintained under argon atmosphere) and the reaction progress was followed using $^1$H, $^{13}$C and $^{31}$P NMR.

Based on earlier results describing the alkaline reactivity of DNA lesions (containing a saturated pyrimidine ring), it is known that the C4=O of the pyrimidine ring is the initial site of nucleophilic attack in such molecules [6]. The formation of a tetrahedral intermediate (after the attack of nucleophile on C4=O group) is followed by cleavage of the N3-C4 bond (Figure 1.23). In fact, the *cis-syn* isomer of CPD-thymine was found to react with alkali at elevated temperatures following a similar mechanism [92][93]. The reaction occurred on heating CPD-thymine in presence of 0.1 M NaOH at 75°C and led to the formation of 1,2-*cis*-dimetyl-3,4-*cis*-diureido-1,2-cyclobutane dicarboxylic acid. However, during our investigation of the alkaline hydrolysis of *cis-syn* CPD-TpT (CPD derived from dinucleotide TpT), we failed to obtain any hydrolysis product even under conditions of high alkali concentration (up to 1 M for 1 mM of CPD-TpT) and high temperatures (up to 90°C).

112

On conducting the same reaction in the presence of $^{18}$O labeled water, it was found that even *cis-syn* CPD-TpT undergoes the formation of a similar 'hemiaminal intermediate' as observed in other DNA lesions containing a saturated pyrimidine ring. However, this intermediate reverts to the starting material instead of yielding hydrolysis products (Figure 2.2). Since, hydrazine is a stronger nucleophile than the hydroxide ion (on account of the alpha effect in hydrazine)[104]–[106], it is logical to assume that a nucleophilic attack by hydrazine on *cis-syn* CPD-TpT will result in the cleavage of the N3-C4 bond (Figure 4.12). Thus, if the reaction between *cis-syn* CPD-TpT and hydrazine actually results in the formation of cyclobutane derivative shown in Figure 4.12, and the reaction is monitored using $^{13}$C NMR spectroscopy, the product should differ from the reactant only in terms of the chemical shifts of the C2=O and C4=O groups. In fact, the chemical shifts for both these sets of C=O groups should undergo a downfield shift (based on NMR chemical shift prediction by ChemDraw). This was exactly what we found. Figure 4.13 shows an overlay of the reaction mixture at T=0 hrs and T=4 hrs; with an enlarged image to show the C2=O and C4=O groups at T=0 hrs (blue) and T=4 hrs (red). Figure 4.14 shows a comparison of these groups with the C2=O and C4=O groups of the TpT molecule for reference. It is clearly evident from Figure 4.13 that, out of all the carbon atoms in the CPD molecule, only C2=O and C4=O groups are affected upon interaction with hydrazine (since these are the only carbon atoms in the lesion that undergo a change in chemical shift upon reaction with hydrazine). Even the $^{1}$H NMR spectra for the reaction mixture at T=0 hours and T=4 hours were very similar (since there are no hydrogens on the C4=O groups) that further supports our assignment of the structure of the intermediate. In addition, the $^{31}$P NMR spectrum showed a slight downfield shift in the phosphorus peak at T=4 hours as compared to that at T=0 hours (Figure 4.15). Thus, on the basis of the information from NMR analyses of hydrazine-mediated CPD-TpT repair reaction, the intermediate shown in Figure 4.12 is most likely formed during the reaction.
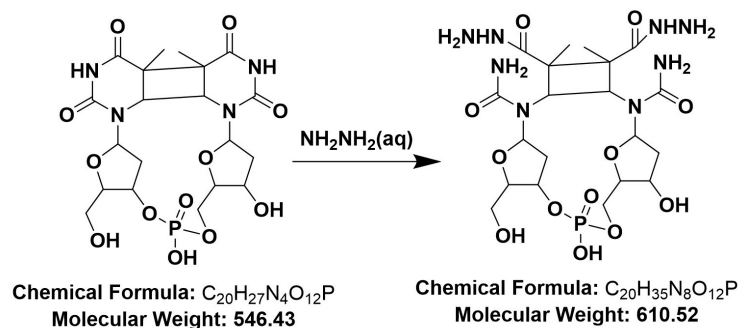
**Figure 4.12.** Potential intermediate formed after the attack of hydrazine on *cis-syn* CPD-TpT
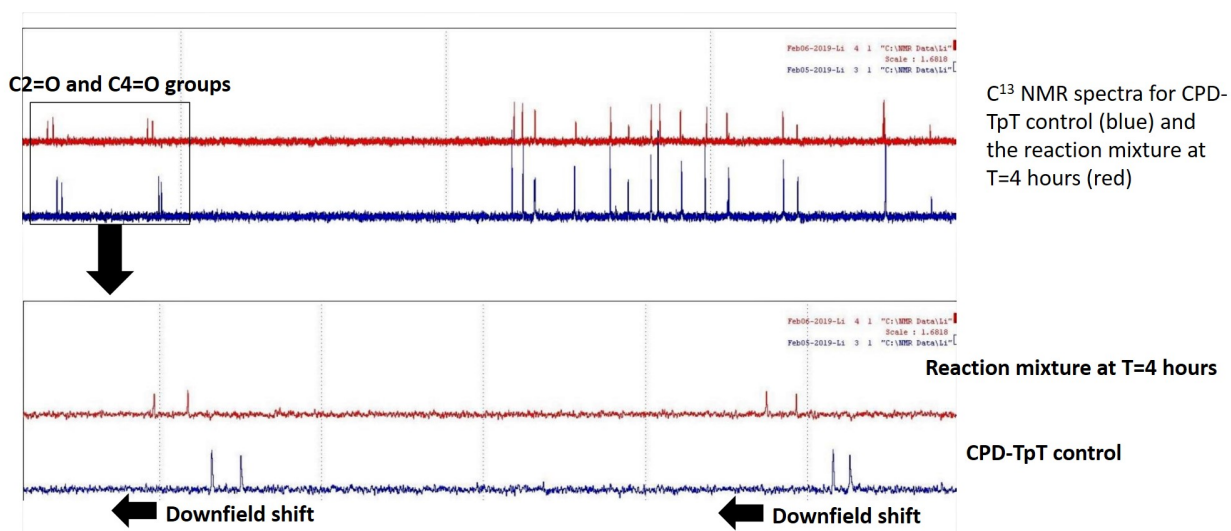


**Figure 4.13.** Top panel: Overlay of the full $^{13}$C NMR spectrum of the reaction mixture at T=0 hrs (blue) and T=4 hrs (red), Bottom panel: Overlay of the $^{13}$C NMR spectrum of the reaction mixture at T=0 hrs (blue) and T=4 hrs (red) showing the C2 and C4 C=O groups. Please refer to Figures 4.31 and 4.32 for the complete spectrum at each of these time points.

## 4.3   Discussion

### 4.3.1   Tentative reaction scheme

Based on our investigation of the CPD + hydrazine reaction using several orthogonal techniques (independently and in tandem with each other) the following information can be drawn about this unique repair reaction.

114
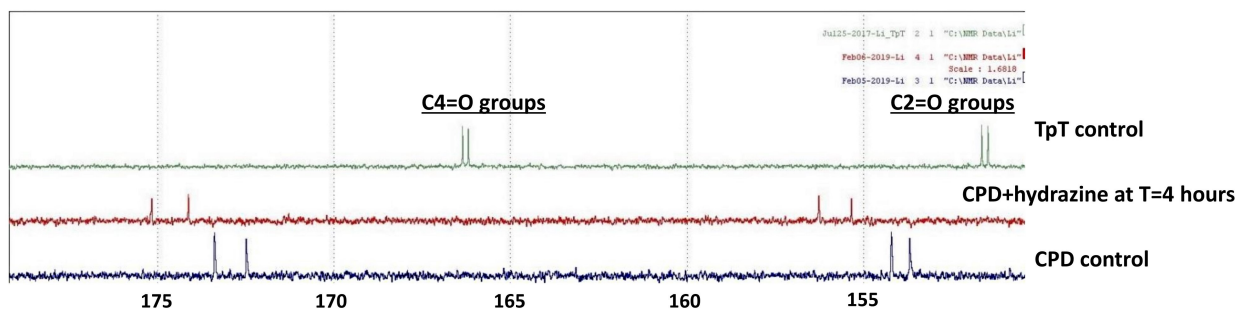
**Figure 4.14.** Overlay of the $^{13}$C NMR spectrum of the reaction mixture at T=0 hrs (blue) and T=4 hrs (red) showing the C2 and C4 C=O groups and the C=O groups of the TpT molecule (control). Please refer to Figure 2.25 for the complete $^{13}$C NMR spectrum for TpT. Figures 4.31 and 4.32 show the complete $^{13}$C NMR spectrum for CPD-TpT + hydrazine reaction mixture at T=0 hours and T=4 hours.
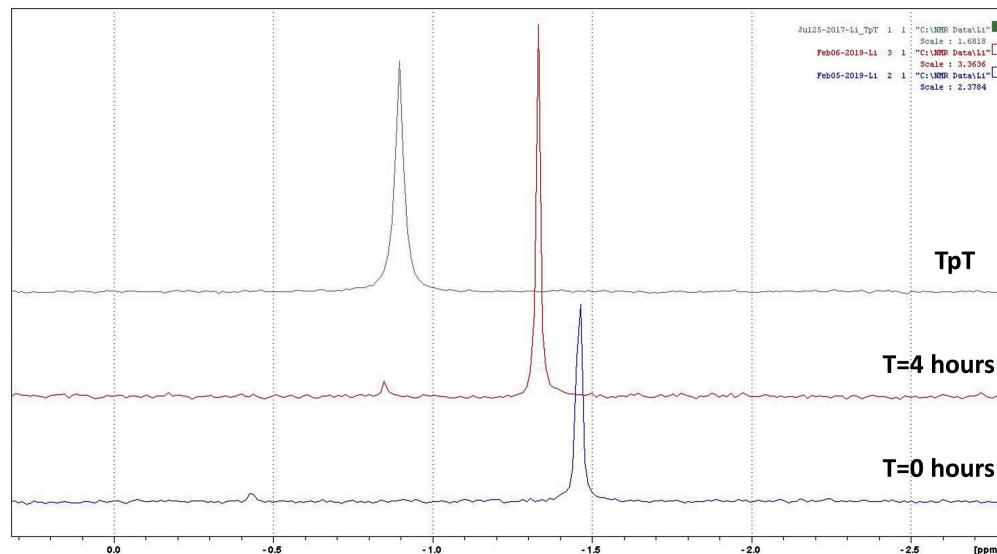


**Figure 4.15.** Overlay of $^{31}$P NMR spectrum of the reaction mixture at T=0 hrs and T=4 hrs

- The reaction between CPD-TpT and hydrazine almost instantly (in less than 1 min after mixing the two reactants) leads to the formation of the ring-opened product shown in Figure 4.12 as reflected by the appearance of the peak due to the potential intermediate in the RP-HPLC spectrum at T=1 min (Figure 4.17).

- The ring-opened product thus formed, favours an inert atmosphere to complete its conversion to dinucleotide TpT. Under these conditions, the conversion to TpT is facile.

115

This was indicated by the enhanced rate of TpT formation under argon atmosphere: <2 hours for reaction completion as compared to several days in presence of air. In fact, the TpT peak appeared in the chromatogram recorded at T=1 minute, immediately upon mixing the two reactants.

- The conversion of the ring-opened intermediate to TpT involves an intramolecular rearrangement as suggested by the continued formation of TpT even after quick freezing the reaction mixture and storing at -20°C.

- The intermediate thus formed is sensitive to changes in pH, under which it collapses back to the starting material, CPD-TpT. This was supported by the complete absence of 'intermediate' peak and a strong CPD-TpT peak on HPLC chromatogram when 10 mM ammonium acetate, pH 6.8 was used as buffer A. In contrast, when 10 mM TEAA, pH 10 was used as buffer A, the peak due to the intermediate appeared consistently across several time points.

Based on these observations, the following reaction scheme is suggested for hydrazine-mediated chemical repair of CPD-TpT to dinucleotide TpT (Figure 4.16).
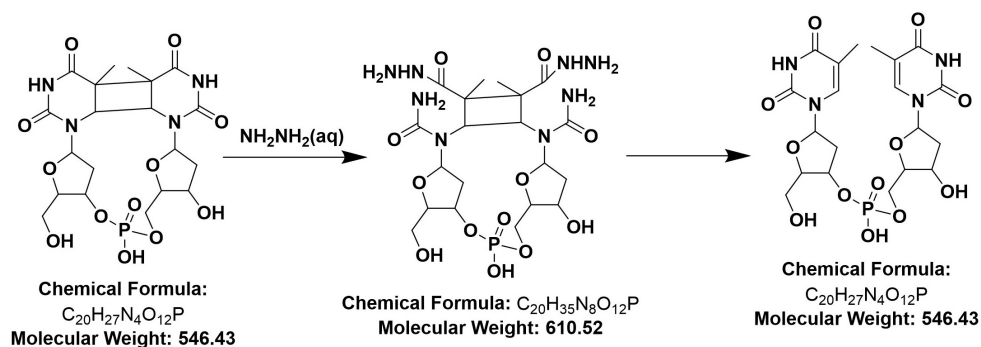


**Figure 4.16.** Reaction scheme for hydrazine-mediated repair of CPD-TpT, including a proposed structure for the intermediate

Interaction of CPD with the hydroxyl group (generated as a nucleophile during the alkaline hydrolysis reaction) provided important information regarding the asymmetric reactivity of the C4=O groups on the $3'$ and $5'$ ends of the lesion. However, these studies failed to provide any information about the lability of the N3-C4 bond in CPD relative to other

sunlight-induced DNA lesions. Also, since the hemiaminal intermediate formed after the attack of hydroxyl group on CPD failed to yield hydrolysis products, the reversibility of the product could not be investigated. Thus, we wondered if the cleavage of N3-C4 bond in CPD could be achieved by employing a stronger nucleophile: hydrazine was chosen for the reaction. However, to our surprise, reaction of CPD-TpT with hydrazine reverted CPD back to the two canonical nucleobases instead of ring opening! (Figure 4.1)

Following the above, detailed investigation of the reaction using several orthogonal experimental techniques led to the observation that the interaction of CPD with hydrazine results in the formation of a tetrahedral intermediate that leads to rupture of the N3-C4 bond as expected. However, the product thus formed is unstable under the reaction conditions and further leads to cleavage of the cyclobutane ring, thereby restoring the thymine nucleobases to their undamaged form (Figure 4.16). We also studied the reaction rate with respect to changes in concentrations of the two reactants. The reaction was carried out at different pH values (in the presence of different concentrations of sodium hydroxide) and at different temperatures with the same outcome. *This reaction was also attempted in the presence of hydrazine and sodium hydroxide in $^{18}O$ labelled water to study the competition between $^{18}O$ labelling reaction of C4=O groups in CPD (described in Chapters 2 and 3) and the repair reaction (described in Chapter 4). It was found that most of the starting material (CPD) was converted to TpT before $^{18}O$ labelling could occur.*

## 4.4   Methods

### 4.4.1   HPLC reaction analyses

The reaction between CPD-TpT and hydrazine was conducted on a Schlenk line at room temperature. At each time point, the reaction mixture was withdrawn out of the reaction flask using a syringe pre-equilibrated with argon. Equal volumes of the reaction mixture (exactly 100 $\mu$L) were injected into the HPLC machine at each time point to enable accurate quantification. Calibration curves for both CPD-TpT and TpT were plotted before the reaction to determine the linear dynamic range of the instrument. HPLC analyses were performed at room temperature using a Waters (Milford, MA) HPLC system coupled to a

2489 UV-Vis detector at 260 nm and 230 nm. A Waters $^{18}$C RP column (2.5 $\mu$m particle size, 50 ×4.6 mm i.d.), that was fitted with an Agilent guard column, was equilibrated in solvent A (10 mM triethylammonium acetate in water, pH 10.0), and compounds were eluted with an ascending gradient (0%-8%) of acetonitrile from 1 min-20 min at a flow rate of 1 mL/min. For RP-HPLC analyses of the reaction between CPD-TcT and hydrazine, 10 mM hydrazine (pH 9-10) was used at buffer A and acetonitrile as buffer B. The compounds were eluted with a gradient of (0%-8%) of acetonitrile from 1 min-24 min, (8%-32%) of acetonitrile from 24 min-34 min and (32%-100%) of acetonitrile from 34 min-35 min: flow rate was maintained at 1 mL/min and exactly 20 $\mu$L of the reaction mixture was injected for each time point.

Figures 4.17 and 4.18 show the complete list of spectra at various time points (from T=0 minutes to T=240 minutes) for the reaction between 1 mM CPD-TpT and 100 mM hydrazine under argon atmosphere at room temperature. Figure 4.19 represents the kinetic curve showing the change in concentration of CPD-TpT, TpT and the potential intermediate as determined by RP-HPLC measurements. Figures 4.20 and 4.21 show the spectra recorded at various time points for the reaction between 1 mM CPD-TpT and 200 mM hydrazine. Figure 4.22 shows the change in reaction rate (as a function of the rate of decrease of CPD-TpT) on doubling the concentration of hydrazine, keeping that of CPD-TpT constant. Figures 4.23 and 4.24 show the spectra recorded for the reaction between 2 mM CPD-TpT and 100 mM hydrazine. Figure 4.25 shows the change in reaction rate (as a function of the rate of decrease of CPD-TpT), when the concentration of CPD-TpT is doubled keeping that of hydrazine constant. Figure 4.26 shows the spectra recorded at various time points for the reaction between 1 mM CPD-TcT (thymidine nucleoside connected by a methylene linker) and 100 mM hydrazine under argon atmosphere at room temperature.

### 4.4.2 LC/MS reaction analyses

CPD-TpT + hydrazine was conducted on a Schlenk line at room temperature. At each time point, the reaction mixture was withdrawn out of the reaction flask using a syringe pre-equilibrated with argon (as described in the previous section). Equal volumes of the reaction mixture (exactly 10 $\mu$L) were rapidly injected into the LC-MS machine (to prevent the degradation of any potential intermediates due to exposure to air) for each time point to
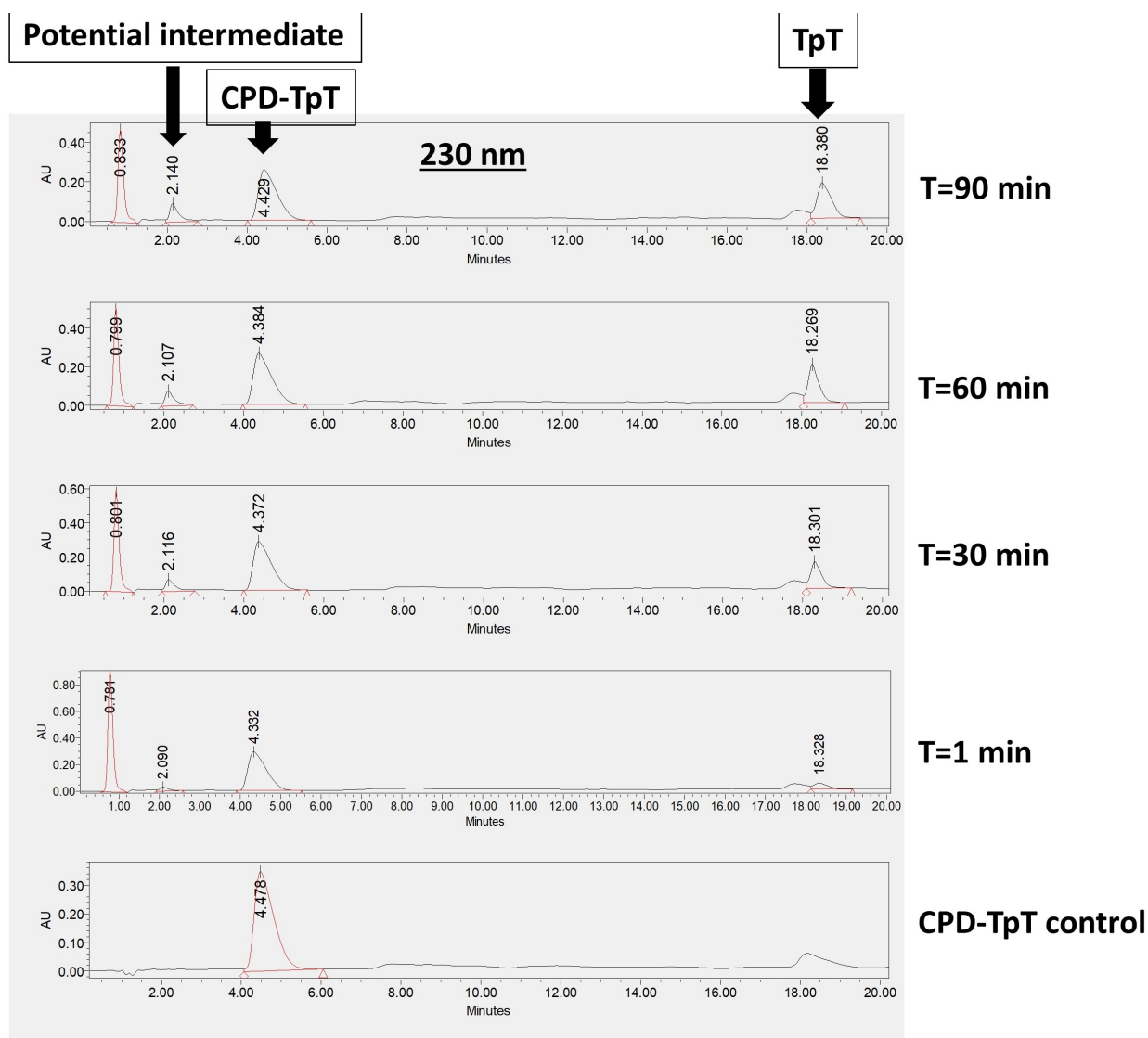
**Figure 4.17.** Reverse-phase HPLC chromatograms showing the change in absorbance at 230 nm of various species in the reaction between 1 mM CPD-TpT and 100 mM hydrazine under argon atmosphere at room temperature from T=0 minutes to T=90 minutes.

maintain consistency among the spectra obtained for various time points. LC/MS-analyses of the CPD + hydrazine reaction was conducted using Agilent 1200-6520 capillary LC-Q-TOF MS spectrometer using a Waters $C^{18}$-RP column (2.5 $\mu$m particle size, 50 ×4.6 mm i.d.) fitted with an Agilent guard column. The column was equilibrated in solvent A (10 mM hydrazine in water, pH 9-10) and compounds were eluted with an ascending gradient (0%-8%) of acetonitrile from 1 min-20 min at a flow rate of 1 mL/min. The mass signals

were monitored using positive ion mode. Figures 4.27, 4.28, 4.29 and 4.30 show the LC-MS and UV-visible profiles for the reaction mixture at various time points (T=30 min to T=120 min).

### 4.4.3   UV-visible spectrophotometry analyses

1 mM CPD-TpT was maintained under argon atmosphere in a quartz cuvette that was sealed with an argon balloon. The path length of the cuvette was chosen as 0.2 cm in order to minimize the overall absorbance of the reaction mixture (Beer-Lambert law, A=$\epsilon$bc) and reduce the noise at lower wavelengths (less than 240 nm), since both CPD-TpT and hydrazine have absorbance maximum in this region. 100 mM hydrazine was aliquoted out in a syringe pre-equilibrated with argon and was rapidly transferred to the cuvette containing CPD-TpT. The spectrophotometer was quickly closed and remained closed for the duration of the experiment. The automated software for the instrument scanned the complete absorption profile for the reaction mixture at various time points.

### 4.4.4   Synthesis and characterization of dinucleotide CPD-TpT

CPD-TpT was synthesized following the protocol developed by Bdour *et al.* [99] (Figure 2.23). CPD-TpT formed after UV-B irradiation of TpT was purified using reverse-phase HPLC (Figure 2.24) and its concentration was determined using UV-Visible absorption spectroscopy (Molar extinction coefficient for CPD-TpT=1500 $M^{-1}$ $cm^{-1}$) [100] [101]. Figures 2.25 and 2.26 show the $^{13}$C and $^{31}$P NMR spectra for TpT. Figures 2.27 and 2.28 show the $^{13}$C and $^{31}$P NMR spectrum for CPD-TpT. Figures 4.31 and 4.32 show the complete $^{13}$C NMR spectrum for CPD-TpT + hydrazine reaction mixture at T=0 hours and T=4 hours respectively.
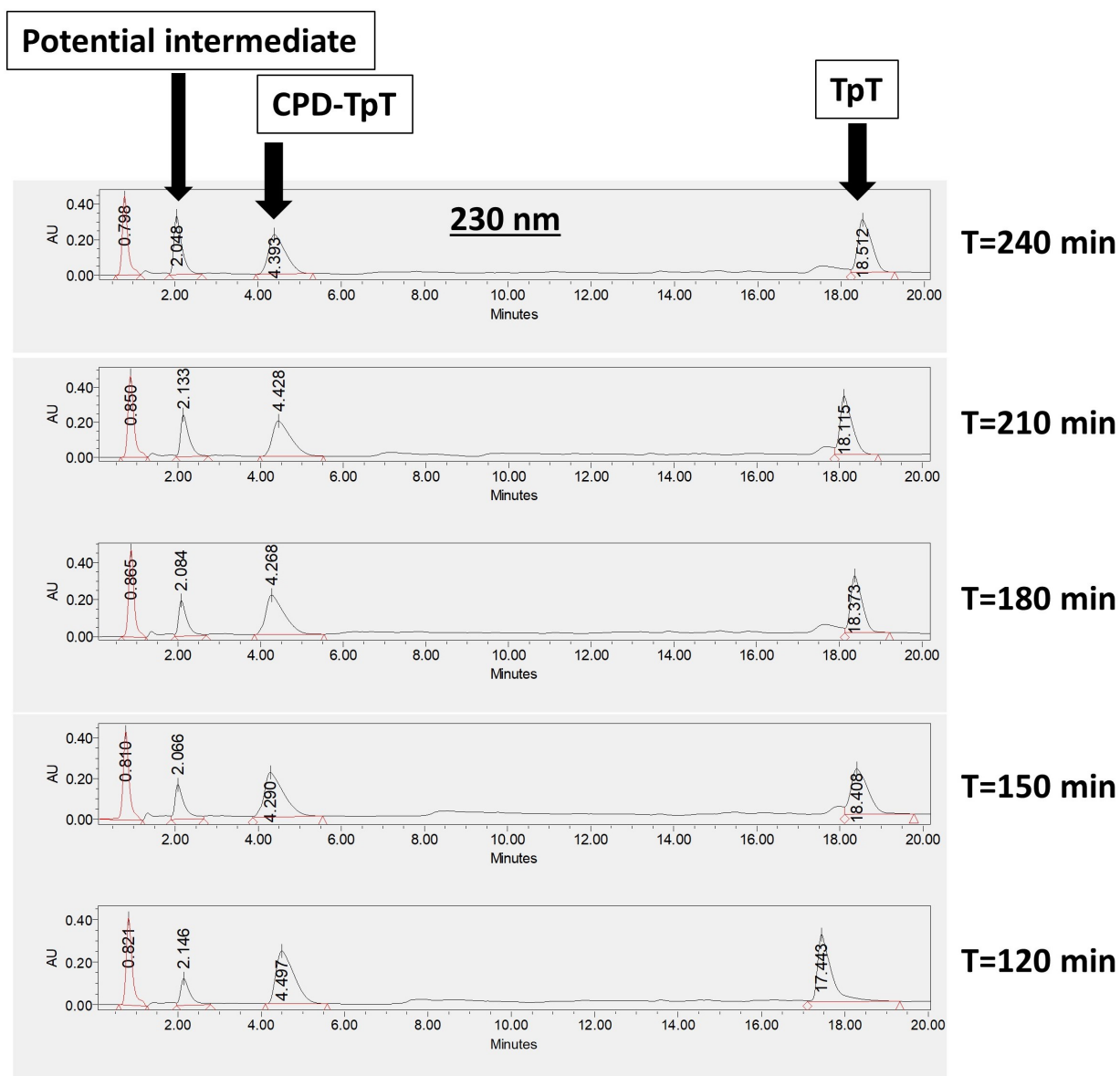
**Figure 4.18.** Reverse-phase HPLC chromatograms showing the change in absorbance at 230 nm of various species in the reaction between 1 mM CPD-TpT and 100 mM hydrazine under argon atmosphere at room temperature from T=120 minutes to T=240 minutes.
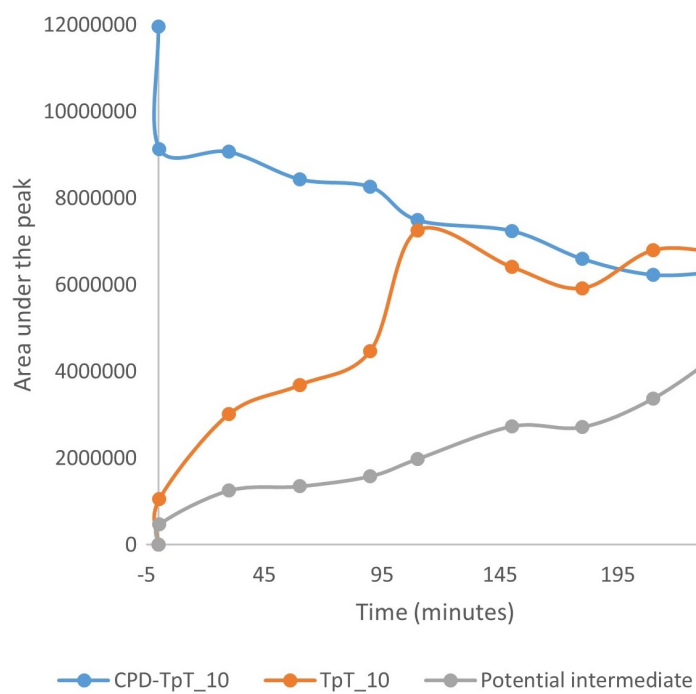
**Figure 4.19.** Kinetic curve showing the change in concentration of CPD-TpT, TpT and the potential intermediate as determined by RP-HPLC measurements.
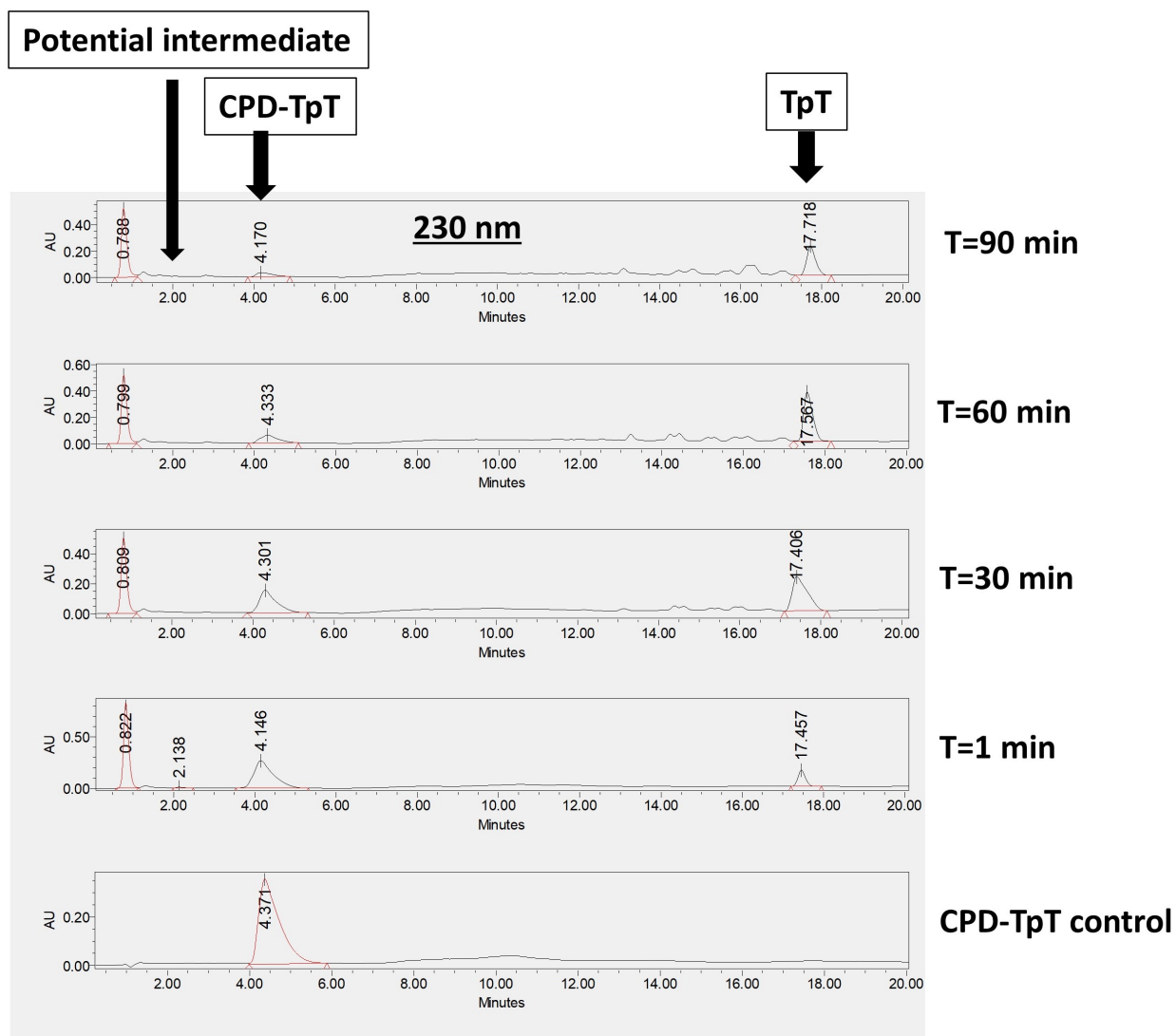
**Figure 4.20.** Reverse-phase HPLC chromatograms showing the change in absorbance at 230 nm of various species in the reaction between 1 mM CPD-TpT and 200 mM hydrazine under argon atmosphere at room temperature from T=0 minutes to T=90 minutes.
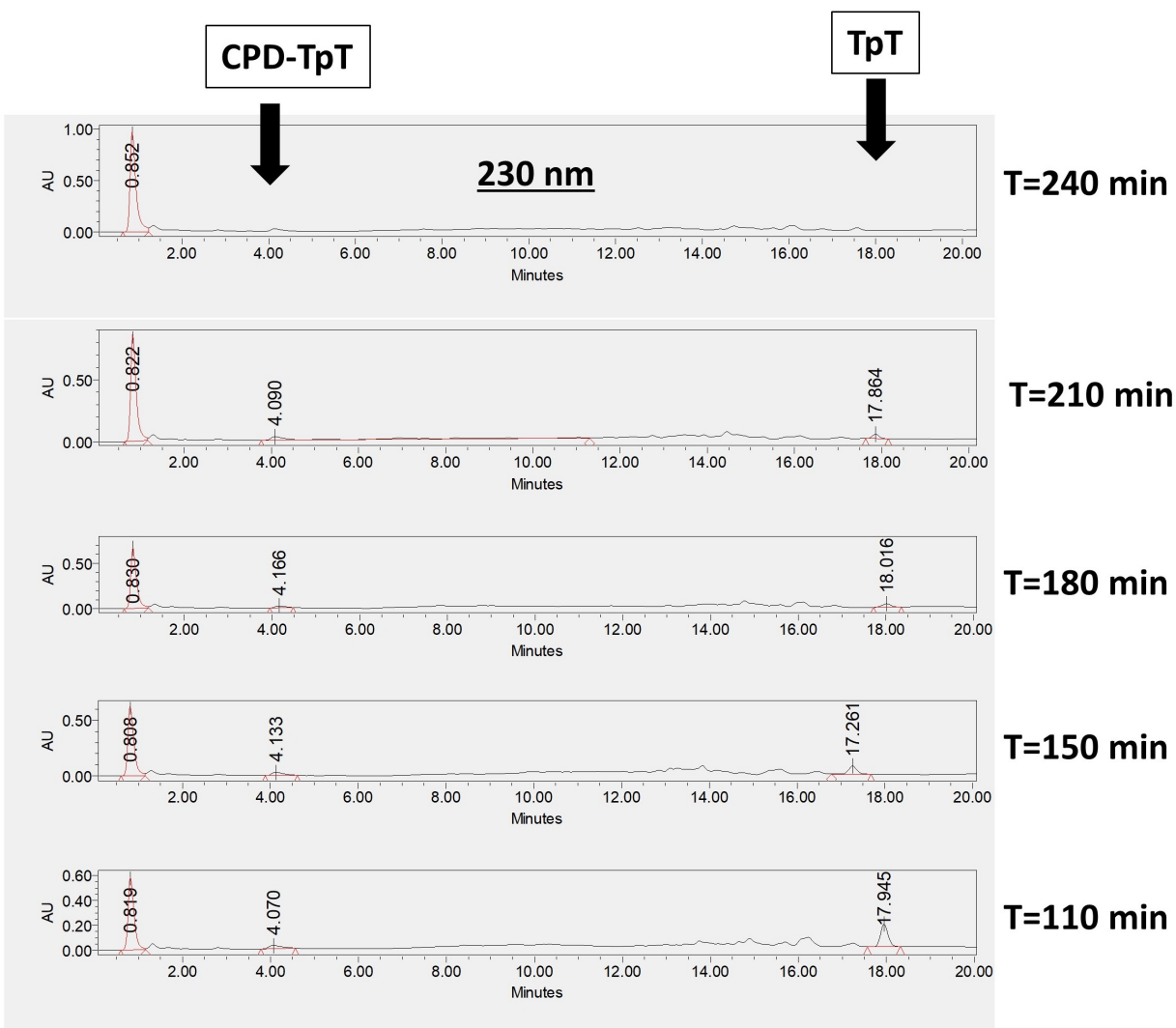
**Figure 4.21.** Reverse-phase HPLC chromatograms showing the change in absorbance at 230 nm of various species in the reaction between 1 mM CPD-TpT and 200 mM hydrazine under argon atmosphere at room temperature from T=120 minutes to T=240 minutes.
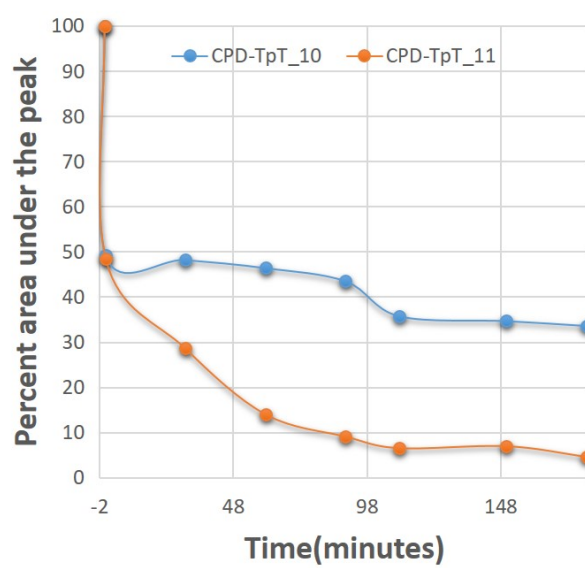
**Figure 4.22.** Variation in the rate of decay of CPD-TpT (reactant) on doubling the concentration of Hydrazine keeping the concentration of CPD-TpT constant
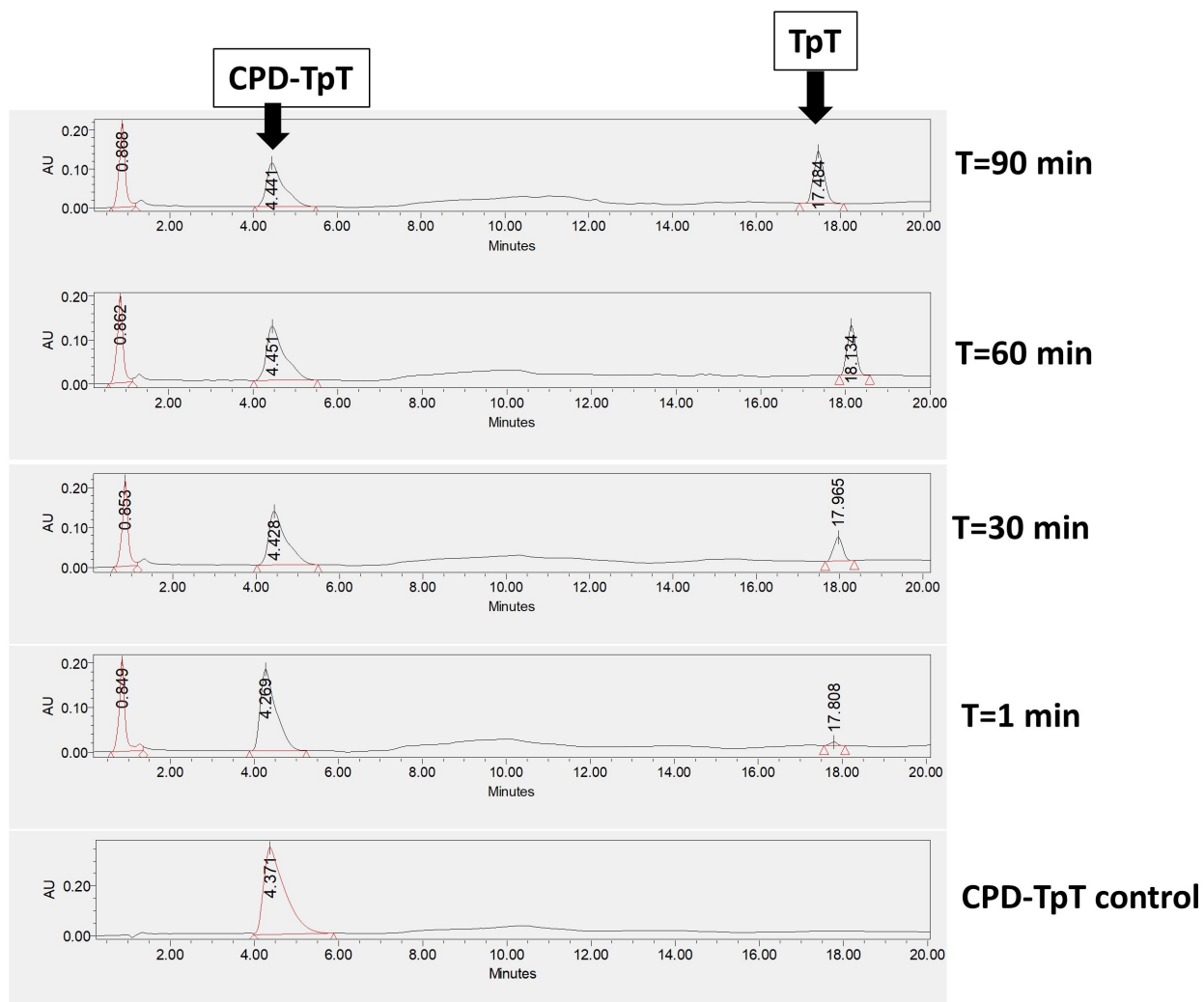
**Figure 4.23.** Reverse-phase HPLC chromatograms showing the change in absorbance at 230 nm of various species in the reaction between 2 mM CPD-TpT and 100 mM hydrazine under argon atmosphere at room temperature from T=0 minutes to T=90 minutes.
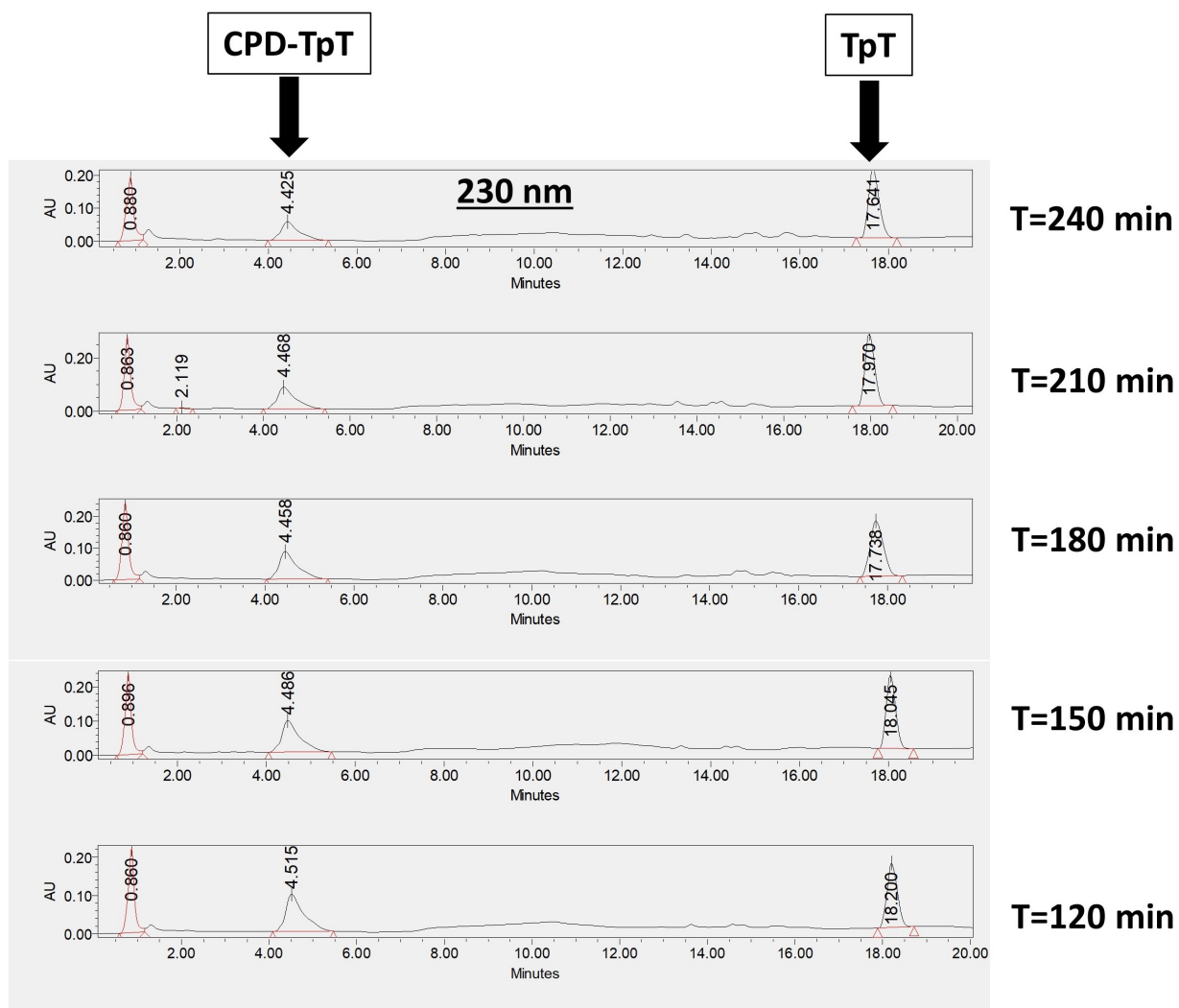
**Figure 4.24.** Reverse-phase HPLC chromatograms showing the change in absorbance at 230 nm of various species in the reaction between 2 mM CPD-TpT and 100 mM hydrazine under argon atmosphere at room temperature from T=120 minutes to T=240 minutes.
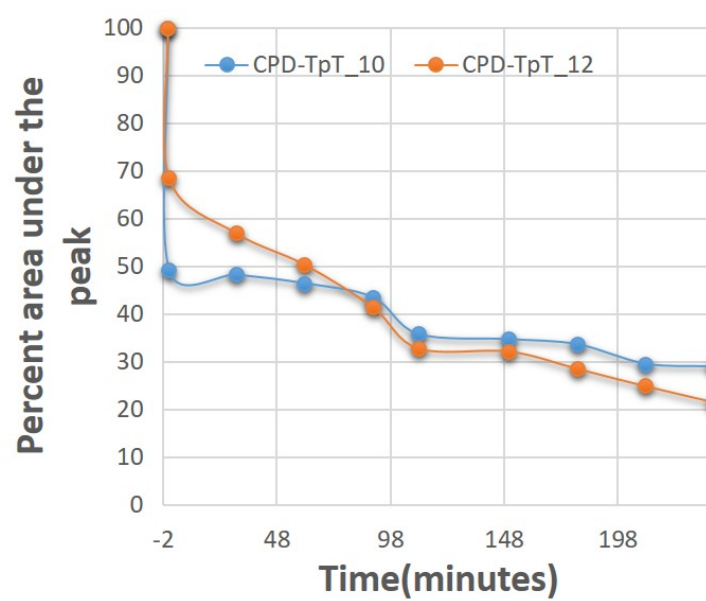
**Figure 4.25.** Variation in the rate of decay of CPD-TpT (reactant) on doubling the concentration of CPD-TpT keeping the concentration of hydrazine constant
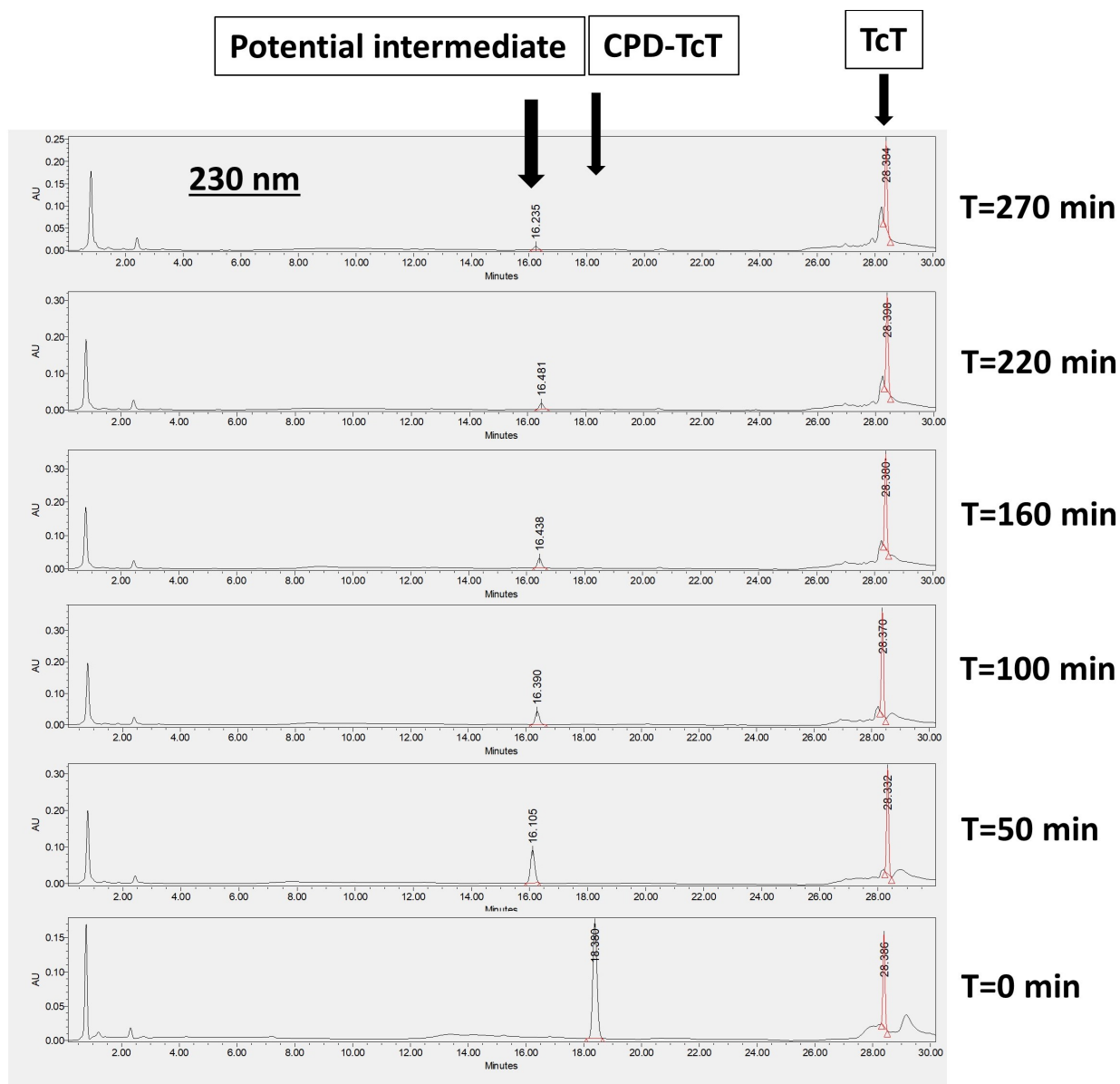
**Figure 4.26.** Reverse-phase HPLC chromatograms showing the change in absorbance at 230 nm of various species in the reaction between 1 mM CPD-TcT and 100 mM hydrazine under argon atmosphere at room temperature from T=0 minutes to T=270 minutes.
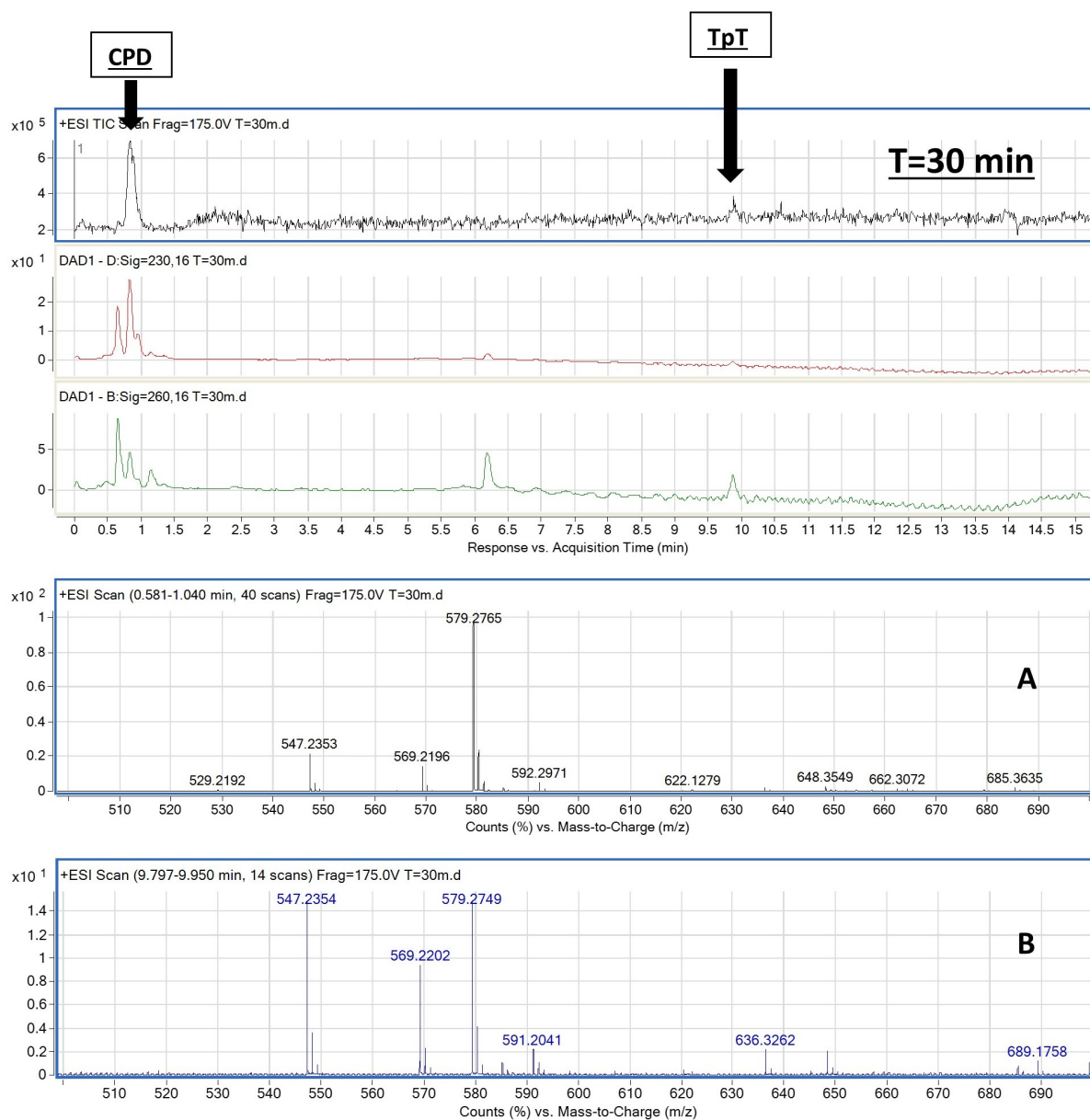
**Figure 4.27.** LC-MS Profile for CPD + hydrazine reaction mixture at T=30 min. Panels A and B show the mass values for the LC-MS peaks corresponding to CPD and TpT respectively.
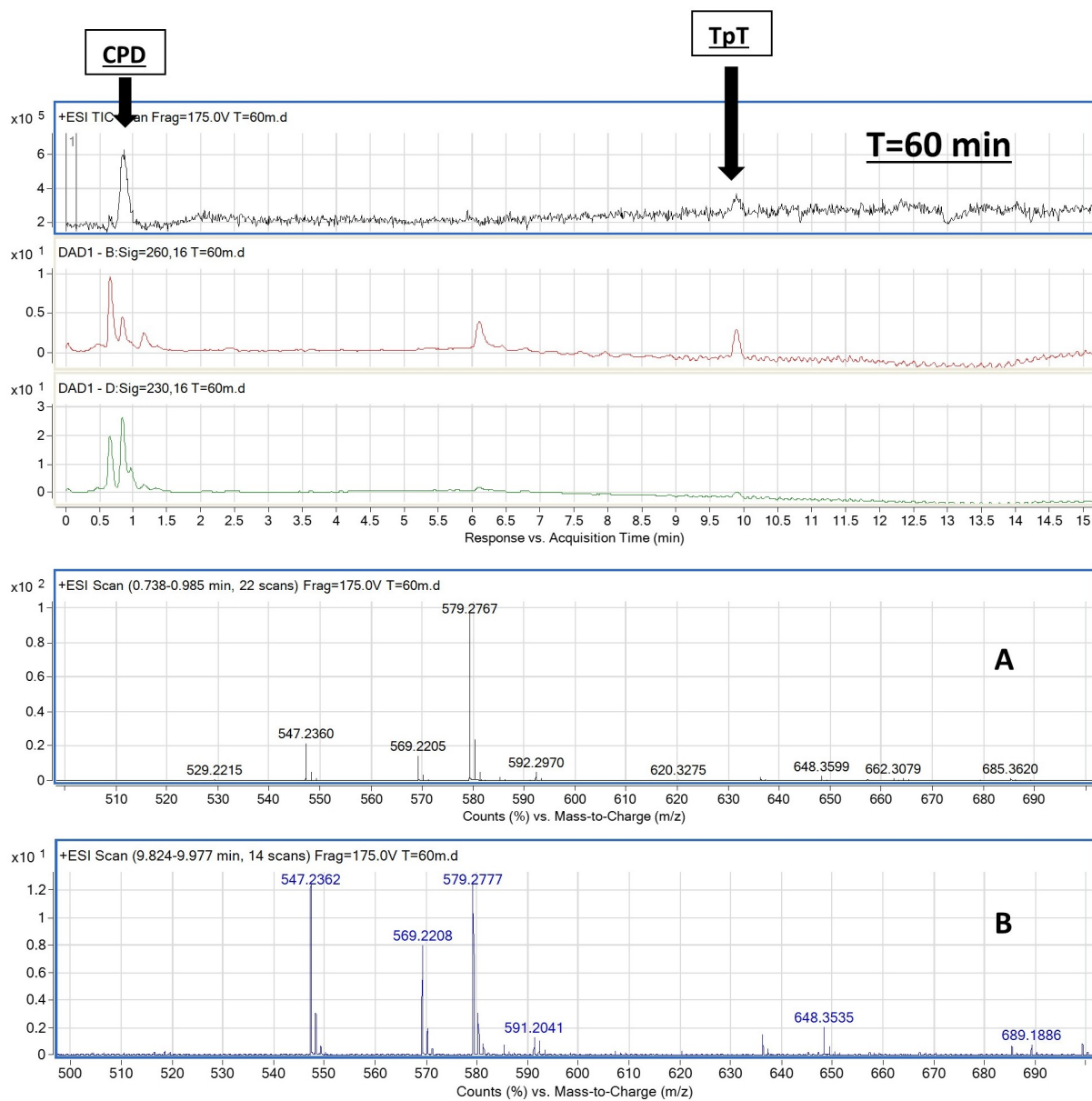
**Figure 4.28.** LC-MS Profile for CPD + hydrazine reaction mixture at T=60 min. Panels A and B show the mass values for the LC-MS peaks corresponding to CPD and TpT respectively.
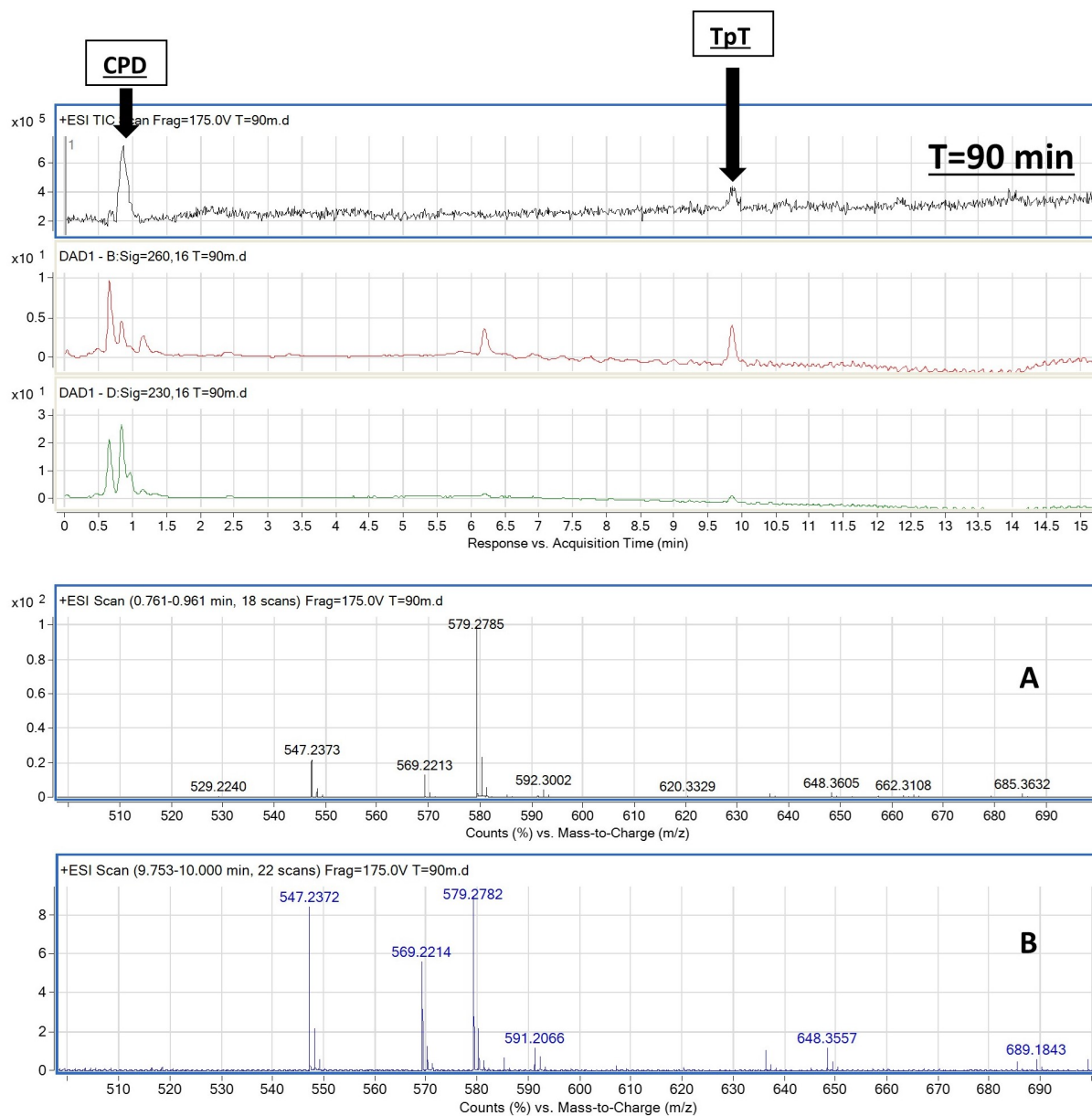
**Figure 4.29.** LC-MS Profile for CPD + hydrazine reaction mixture at T=90 min. Panels A and B show the mass values for the LC-MS peaks corresponding to CPD and TpT respectively.
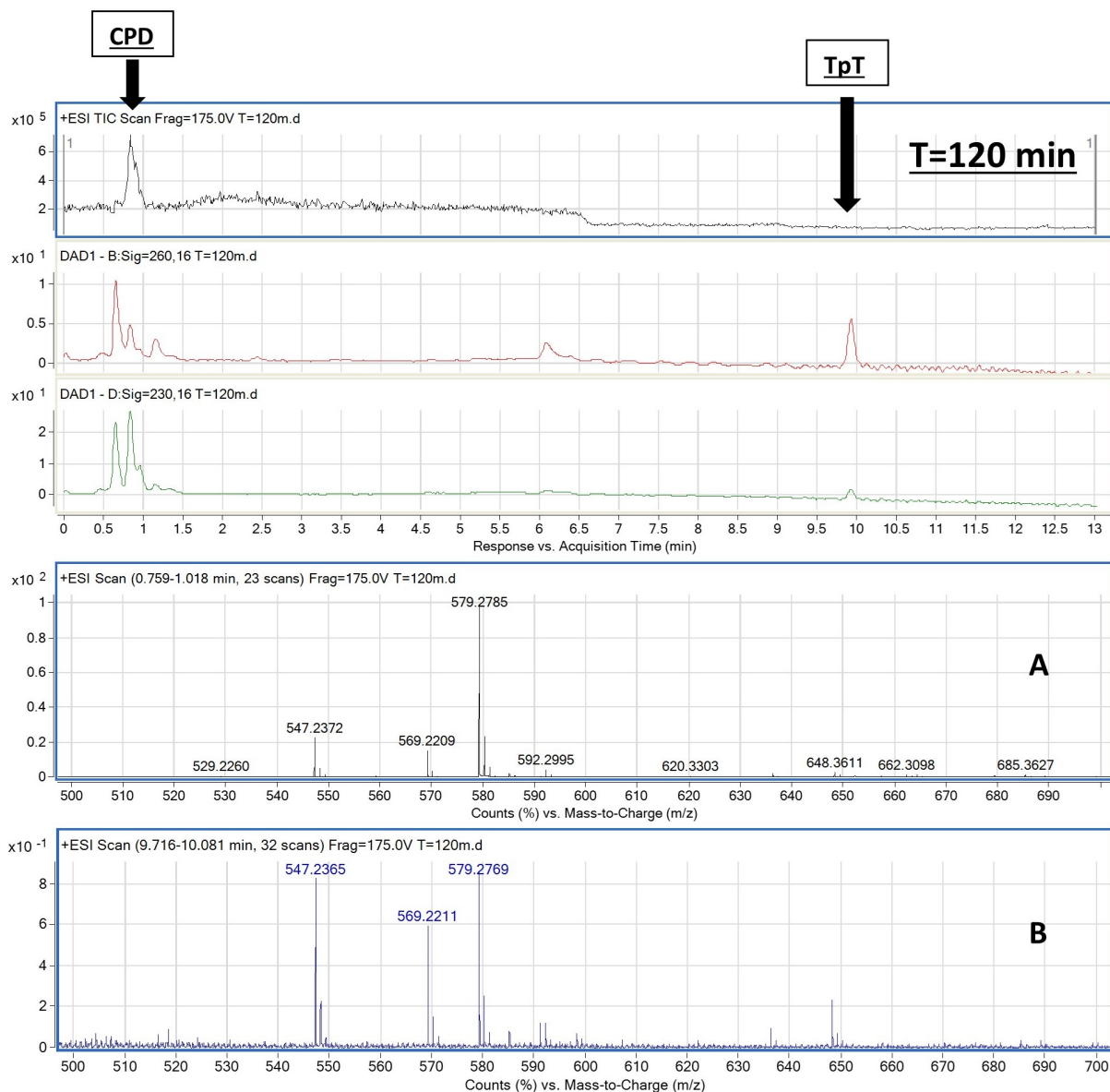
**Figure 4.30.** LC-MS Profile for CPD + hydrazine reaction mixture at T=120 min. Panels A and B show the mass values for the LC-MS peaks corresponding to CPD and TpT respectively.
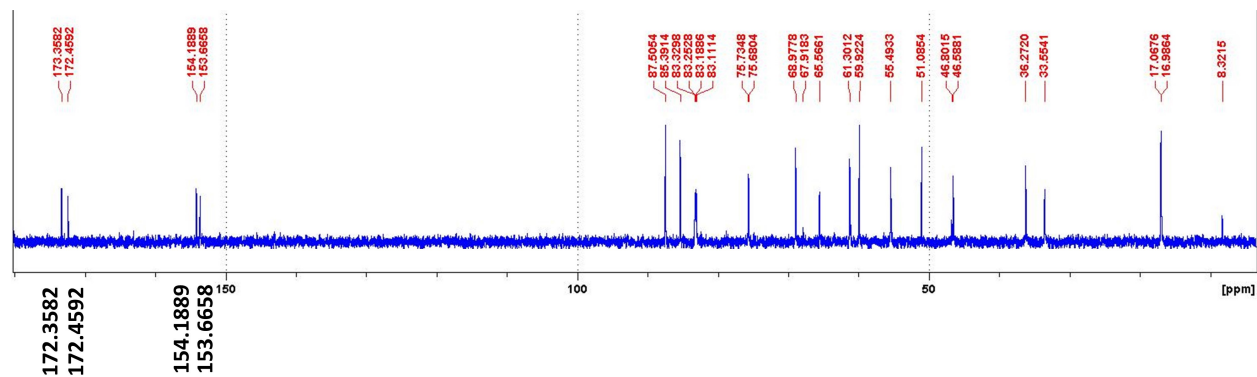
**Figure 4.31.** $^{13}$C NMR spectrum showing CPD-TpT + hydrazine reaction mixture at T=0 hours
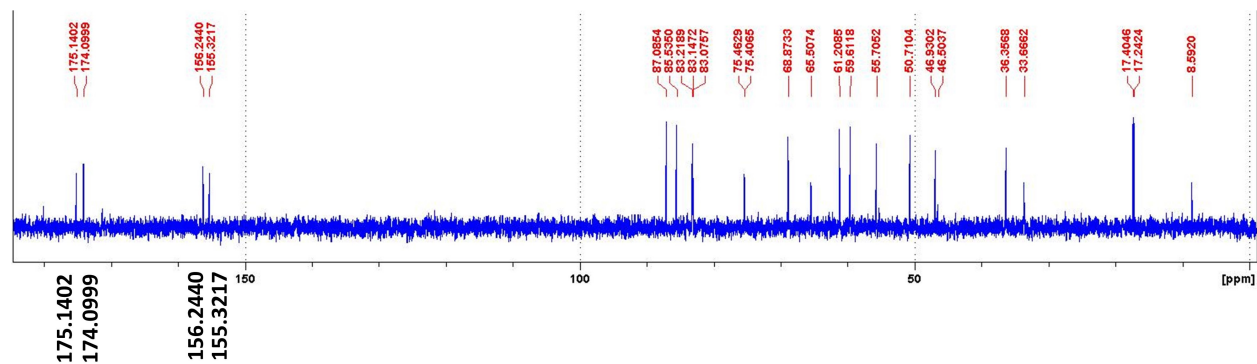


**Figure 4.32.** $^{13}$C NMR spectrum showing CPD-TpT + hydrazine reaction mixture at T=4 hours

134

# 5. SUMMARY

Our research on DNA photodimers, especially cyclobutane pyrimidine dimers (CPDs), demonstrates how chemical techniques can be employed to advance our understanding of the reactivity and repair of these photolesions. The $^{18}$O labeling strategy described in Chapters 2 and 3, for the first time, allowed us to firmly establish the reactivity of CPD, previously viewed as an inert lesion. Use of a dinucleotide CPD model with a selective $^{15}$N label unambiguously established the order of reactivity of the two electrophilic C4=O moieties of the lesion.

In comparison, previous studies on the reactivity of the naturally occurring *cis-syn* isomer of CPD used the isomers derived from simple thymine or thymidine monomers, none of which truly reflects the structural framework of naturally occurring DNA. Our studies of the alkaline lability of *cis-syn* CPD derived from dinucleotide, tetranucleotide and hexanucleotide strands, truly establish the reactivity of *cis-syn* CPD in an alkaline environment, and are more physiologically relevant. The $^{18}$O labeling experiments on tetranucleotide and hexanucleotide CPDs followed the same trend observed in a dinucleotide molecule thereby establishing the inherent reactivity of a CPD lesion. The selectively N$^{15}$-labeled CPD molecule derived from dinucleotide and tetranucletide species further established the C4=O on the 3 side of the lesion as the first site of nucleophilic attack in CPD (Figure 3.16). *Based on our results, the two seemingly identical pyrimidine residues are now established to play distinct roles in the reactivity of cyclobutane pyrimidine dimer (CPD) photolesions.*

Despite the progress made, questions as to the reactivity of CPD photolesions still remain. For instance, what is the role of individual structural moieties (base, sugar, phoshate and methyl group) in the observed reactivity of a CPD lesion? Further, does the reactivity of the individual C4=O groups change with the change in chain length or a change in neighbouring groups? How does a duplex environment affect the observed reactivity pattern? Also, is the CPD lesion inert in an acidic environment? Does the observed asymmetry persists in presence of acids as well?

We have followed through some of these queries and have obtained some preliminary results. For example, our results from $^{18}$O exchange experiments with *cis-syn* and *trans-*

*syn* CPD-TpT isomers show that *trans-syn* CPD-TpT exhibits a similar reaction pattern (asymmetry between the two C4=O groups). However, the reaction rate in case of the *trans-syn* isomer is significantly lower as compared to the *cis-syn* isomer (Figure A.15). *This observation indicates that the stereochemistry of the methyl group (cis vs trans) has a profound effect on the rate of $^{18}O$ exchange in the CPD lesion. This difference probably arises due to the change in accessibility of the C4=O groups with the change in methyl group stereochemistry.* Moreover, $^{18}$O labeling experiments with *cis-syn, trans-syn, cis-anti* and *trans-anti* CPD isomers from thymidine showed that none of these isomers exhibit any detectable $^{18}$O exchange even with high concentrations of base (up to 1nM) or elevated temperatures (up to 75°C) (Figure A.24). On the other hand, similar experiments with CPD lesion containing an unnatural methylene linker ($CH_2$-) instead of the phosphate linker (CPD-TcT) demonstrated a similar asymmetry between the C4=O groups as seen in CPD-TpT. *The results from these two experiments indicate that a linkage between the sugar moieties bearing the CPD lesion is necessary for the formation of a hemiaminal water adduct.* The similarity in reaction pattern between CPD-TpT and CPD-TcT suggests that CPD-TcT adopts a similar stacking arrangement in solution as CPD-TpT, leading to a similar asymmetric reactivity between the two C4=O groups.

The rate of $^{18}$O exchange in CPD has also been shown to vary with an increase in chain length of the strand containing the CPD moiety, as evidenced by our $^{18}$O labeling experiments with CPD generated within dinucleotide, tetranucleotide and hexanucleotide strands. The CPD lesions from dinucleotide and tetranucleotide were observed to exhibit similar $^{18}$O exchange rates (Figure 3.10). In contrast, these rates were significantly reduced in the case of CPD within a hexanucleotide context, most likely due to the increase in steric constraints (Figure 5.1). Also, a change in flanking nucleotides from adenine to guanine was found to affect the reactivity of C4=O groups in a CPD molecule; the rate of $^{18}$O exchange was found to be faster in GG$T\hat{T}$GG as compared to that in AA$T\hat{T}$AA (Figure A.36). Further experiments need to be conducted to explore these phenomena in detail.

*In addition to the elucidation of the reactivity pattern in a cyclobutane pyrimidine dimer, our studies have also discovered a small molecule-mediated total repair of CPD lesion (Figure*

136

*4.1).* We have also achieved the characterization of the intermediate species formed during the reaction leading to a tentative mechanistic route.

The CPD+hydrazine reaction provides the interesting possibility of small molecule-mediated rapid and complete repair of the CPD lesion under ambient conditions (room temperature). In terms of future prospects, it will be interesting to see the outcome of the reaction in an oligonucleotide and duplex environments. In addition, the reaction could be conducted on various structural variants of dinucleotide CPD-TpT, in order to understand the role of base, sugar, phosphate and methyl moieties in its outcome. It will also be interesting to look for similar repair in other DNA lesions, *i.e.*, pyrimidine pyrimidone photoproduct (6-4PP) and 5-pyrimidinyl-5,6-dihydropyrimidine (spore photoproduct, SP).

In order to investigate the role of phosphate linker in the observed repair reaction and to potentially increase the lifetime of reaction intermediates, we carried out the reaction in a CPD variant in which the phosphate linker was replaced by a methylene linker (CPD-TcT). Interestingly, the reaction showed a similar outcome as CPD-TpT (albeit with a slower reaction rate) (Figure 4.6). *These results, along with the $^{18}O$ labeling results discussed above, indicate that the physical presence of the phosphate linker has little effect on the reactivity/repair of a CPD molecule, and the molecule shows similar reactivity as long as the stacking arrangement is maintained.* We also tried the CPD-TpT repair reaction in the presence of methyl hydrazine instead of hydrazine monohydrate. *Although there was some reaction observed (evidenced by the loss of the CPD-TpT species), no TpT formation was observed during the course of the experiment. This observation, in combination with the results from the reaction of CPD-TpT with lysine, ammonia and mercaptoethanol (during which "some hydrolysis products" were observed), indicate that the presence of hydrazine monohydrate is crucial for the repair reaction.*

Our studies on cyclobutane pyrimidine dimer variants described here suggest that organic synthesis and chemical analyses can potentially enable the development of several other useful "tool-sets" that may help in the understanding of the chemistry of DNA lesions in unprecedented detail. In this context, we tentatively bring out the following two directions to demonstrate what may be done in the future.

Firstly, lesion-specific antibodies have played a pivotal role in the development of DNA photobiology. The antibodies for CPD and 6,4-PP were created almost forty years ago. Since then, these antibodies have enabled numerous biological studies involving these photolesions in various organisms including rodents and humans with the use of assays like immunostaining and immunoprecipitation. However, the CPD antibodies that are currently available merely recognize the CPD structure, and can not differentiate between the CPD variants generated from various combinations of di-pyrimidine moieties e.g., CPD lesions generated from TpT, TpC, CpT or CpC steps. Similar problems persist with the 6,4-PP antibodies. More strikingly, no antibodies have been reported for SP photolesion so far. Current advances in immunology have enabled the development of antibodies that are capable of distinguishing minute structural variations in antigens. For instance, monoclonal antibodies that can specifically recognize 5-methylcytosine (5mC) are now commercially available, proving that it is now possible to develop antibodies that can distinguish the subtle structural differences between T/C and 5mC. Therefore, it is possible to generate antibodies that can differentiate between various pyrimidine dimers. In order to make it work, a thorough knowledge of the reactivity pattern of these photolesions is required. This, coupled with careful antibody screening post immunization, should potentially enable the development of antibodies with increased specificity.

Secondly, in comparison with antibody-specific immunoassays that suffer from non-specific antibody binding and/or weak binding as a result of DNA secondary structures, the 'holy grail' for genome-wide DNA photolesion analysis is to exploit the power of lesion-specific chemistry to enable lesion labeling and minimize the structural bias. For instance, during the 8-oxo-7,8-dihydroguanine (OG) sequencing technique recently developed by Burrow's group, the lower redox potential of OG (about 600mV lower than G) was utilized to enable the selective oxidation of OG without affecting the undamaged G in the strand. The electrophilic OG oxidation product that is formed can then be labeled by amine-terminated biotin, allowing the specific identification of modified DNA fragments through biotin-streptavidin interactions for subsequent high-throughput sequencing studies. The basis of the successful development of OG sequencing assay is a good understanding of the redox properties of OG. As a matter of fact, any given DNA lesion may possess some unique chemical properties, the

understanding of which may enable targeted lesion modification, eventually allowing selective enrichment of DNA fragments containing the lesions. As demonstrated in our studies on the alkaline reactivity of SP, 6,4-PP, dHdU and CPD, these lesions show very different chemical reactivities under similar conditions, even though all of them pass through the same *gem-diol* intermediate before ring opening. This difference in alkaline lability may enable us to design assays to specifically target a particular DNA lesion. It is our hope that a thorough understanding of the difference in chemical reactivity among various pyrimidine lesions as well as other DNA lesions is close tied with genome-wide lesion mapping in the near future.
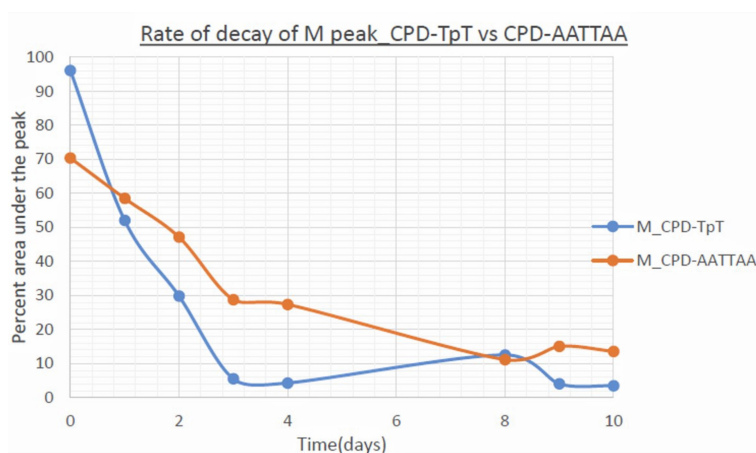


**Figure 5.1.** $^{18}$O labeling of AA$\hat{T}T$AA in presence of $\hat{T}T$ as internal standard

# REFERENCES

[1]  F. E. Hruska, D. J. Wood, K. K. Ogilvie, and J. L. Charlton, "A proton magnetic resonance study of the ultraviolet photoproduct of d (TpT) in aqueous solution," *Canadian Journal of Chemistry*, vol. 53, no. 8, pp. 1193–1203, 1975.

[2]  L. S. Kan, L. Voituriez, and J. Cadet, "Nuclear magnetic resonance studies of cis-syn, trans-syn, and 6-4 photodimers of thymidylyl (3'-5') thymidine monophosphate and cis-syn photodimers of thymidylyl (3'-5') thymidine cyanoethyl phosphotriester," *Biochemistry*, vol. 27, no. 15, pp. 5796–5803, 1988.

[3]  H. Park, K. Zhang, Y. Ren, S. Nadji, N. Sinha, J.-S. Taylor, and C. Kang, "Crystal structure of a DNA decamer containing a cis-syn thymine dimer," *Proceedings of the National Academy of Sciences*, vol. 99, no. 25, pp. 15 965–15 970, 2002.

[4]  M. Higurashi, T. Ohtsuki, A. Inase, R. Kusumoto, C. Masutani, F. Hanaoka, and S. Iwai, "Identification and characterization of an intermediate in the alkali degradation of (6-4) photoproduct-containing DNA," *Journal of Biological Chemistry*, vol. 278, no. 51, pp. 51 968–51 973, 2003.

[5]  B. Witkop and T. Kunieda, "Hydrogenolysis and stereochemistry of photodimers of thymine and thymidine," *Journal of the American Chemical Society*, vol. 93, no. 14, pp. 3493–3499, 1971.

[6]  G. Lin, Y. Jian, K. J. Dria, E. C. Long, and L. Li, "Reactivity of damaged pyrimidines: DNA cleavage via hemiaminal formation at the C4 positions of the saturated thymine of spore photoproduct and dihydrouridine," *Journal of the American Chemical Society*, vol. 136, no. 37, pp. 12 938–12 946, 2014.

[7]  R. E. Dickerson, H. R. Drew, B. N. Conner, R. M. Wing, A. V. Fratini, and M. L. Kopka, "The anatomy of a-, b-, and z-DNA," *Science*, vol. 216, no. 4545, pp. 475–485, 1982.

[8]  R. Wing, H. Drew, T. Takano, C. Broka, S. Tanaka, K. Itakura, and R. E. Dickerson, "Crystal structure analysis of a complete turn of b-DNA," *Nature*, vol. 287, no. 5784, pp. 755–758, 1980.

[9]  W. Saenger, *Principles of nucleic acid structure*. Springer Science & Business Media, 2013.

[10]  X. X. Xia, "Bifacial peptide nucleic acid (bPNA) as a regulator of nucleic acid function," 2015.

[11] A. I. Karsisiotis and M. Webba da Silva, "Structural probes in quadruplex nucleic acid structure determination by NMR," *Molecules*, vol. 17, no. 11, pp. 13 073–13 086, 2012.

[12] N. C. Seeman, J. M. Rosenberg, and A. Rich, "Sequence-specific recognition of double helical nucleic acids by proteins," *Proceedings of the National Academy of Sciences*, vol. 73, no. 3, pp. 804–808, 1976.

[13] T. A. Steitz, "Structural studies of protein–nucleic acid interaction: The sources of sequence-specific binding," *Quarterly Reviews of Biophysics*, vol. 23, no. 3, pp. 205–280, 1990.

[14] T. A. Hamlin, J. Poater, C. F. Guerra, and F. M. Bickelhaupt, "B-DNA model systems in non-terran bio-solvents: Implications for structure, stability and replication," *Physical Chemistry Chemical Physics*, vol. 19, no. 26, pp. 16 969–16 978, 2017.

[15] E. Protozanova, P. Yakovchuk, and M. D. Frank-Kamenetskii, "Stacked–unstacked equilibrium at the nick site of DNA," *Journal of Molecular Biology*, vol. 342, no. 3, pp. 775–785, 2004.

[16] A. K. Aggarwal, D. W. Rodgers, M. Drottar, M. Ptashne, and S. C. Harrison, "Recognition of a DNA operator by the repressor of phage 434: A view at high resolution," *Science*, vol. 242, no. 4880, pp. 899–907, 1988.

[17] R. R. Sinden, C. E. Pearson, V. N. Potaman, and D. W. Ussery, "DNA: Structure and function," in *Advances in Genome Biology*, vol. 5, Elsevier, 1998, pp. 1–141.

[18] T. Ito, "Photodynamic agents as tools for cell biology," in *Photochemical and Photobiological Reviews*, Springer, 1983, pp. 141–186.

[19] T. Lindahl, "Instability and decay of the primary structure of DNA," *Nature*, vol. 362, no. 6422, pp. 709–715, 1993.

[20] A. B. Britt, "DNA damage and repair in plants," *Annual Review of Plant Biology*, vol. 47, no. 1, pp. 75–100, 1996.

[21] K. K. Singh, "The saccharomyces cerevisiae sln1p-ssk1p two-component system mediates response to oxidative stress and in an oxidant-specific fashion," *Free Radical Biology and Medicine*, vol. 29, no. 10, pp. 1043–1050, 2000.

[22] S. Madronich, R. L. McKenzie, L. O. Björn, and M. M. Caldwell, "Changes in biologically active ultraviolet radiation reaching the earth's surface," *Journal of Photochemistry and Photobiology B: Biology*, vol. 46, no. 1-3, pp. 5–19, 1998.

[23] M. Blumthaler and W. Ambach, "Indication of increasing solar ultraviolet-B radiation flux in alpine regions," *Science*, vol. 248, no. 4952, pp. 206–208, 1990.

[24] P. J. Crutzen, "Ultraviolet on the increase," *Nature*, vol. 356, no. 6365, pp. 104–105, 1992.

[25] J. Kerr and C. McElroy, "Evidence for large upward trends of ultraviolet-B radiation linked to ozone depletion," *Science*, vol. 262, no. 5136, pp. 1032–1034, 1993.

[26] D. Lubin and E. H. Jensen, "Effects of clouds and stratospheric ozone depletion on ultraviolet radiation trends," *Nature*, vol. 377, no. 6551, pp. 710–713, 1995.

[27] M. M. Becker and Z. Wang, "Origin of ultraviolet damage in DNA," *Journal of Molecular Biology*, vol. 210, no. 3, pp. 429–438, 1989.

[28] J. Cadet, "Photochemistry and nucleic acids," *Bioorganic Photochemistry*, vol. 1, pp. 1–272, 1990.

[29] J. Cadet and J. R. Wagner, "DNA base damage by reactive oxygen species, oxidizing agents, and UV radiation," *Cold Spring Harbor perspectives in biology*, vol. 5, no. 2, a012559, 2013.

[30] J. Cadet, S. Mouret, J.-L. Ravanat, and T. Douki, "Photoinduced damage to cellular DNA: Direct and photosensitized reactions," *Photochemistry and Photobiology*, vol. 88, no. 5, pp. 1048–1065, 2012.

[31] G. P. Pfeifer and A. Besaratinia, "UV wavelength-dependent DNA damage and human non-melanoma and melanoma skin cancer," *Photochemical & Photobiological Sciences*, vol. 11, no. 1, pp. 90–97, 2012.

[32] V. J. Cannistraro and J.-S. Taylor, "Acceleration of 5-methylcytosine deamination in cyclobutane dimers by g and its implications for UV-induced c-to-t mutation hotspots," *Journal of Molecular Biology*, vol. 392, no. 5, pp. 1145–1157, 2009.

[33] J. S. Taylor, I. R. Brockie, and C. L. O'Day, "A building block for the sequence-specific introduction of cis-syn thymine dimers into oligonucleotides. solid-phase synthesis of tpt [c, s] ptpt," *Journal of the American Chemical Society*, vol. 109, no. 22, pp. 6735–6742, 1987.

[34] T. Mizukoshi, K. Hitomi, T. Todo, and S. Iwai, "Studies on the chemical synthesis of oligonucleotides containing the (6- 4) photoproduct of thymine- cytosine and its repair by (6- 4) photolyase," *Journal of the American Chemical Society*, vol. 120, no. 41, pp. 10 634–10 642, 1998.

[35] S. Iwai, M. Shimizu, H. Kamiya, and E. Ohtsuka, "Synthesis of a phosphoramidite coupling unit of the pyrimidine (6- 4) pyrimidone photoproduct and its incorporation into oligodeoxynucleotides," *Journal of the American Chemical Society*, vol. 118, no. 32, pp. 7642–7643, 1996.

[36] J. Donnellan and R. Setlow, "Thymine photoproducts but not thymine dimers found in ultraviolet-irradiated bacterial spores," *Science*, vol. 149, no. 3681, pp. 308–310, 1965.

[37] C. Desnous, D. Guillaume, and P. Clivio, "Spore photoproduct: A key to bacterial eternal life," *Chemical Reviews*, vol. 110, no. 3, pp. 1213–1232, 2010.

[38] J. M. Villanueva, J. Pohl, P. W. Doetsch, and L. G. Marzilli, "The mutagenic damaged DNA base, 5, 6-dihydrouracil (DHU), incorporated into a 14-mer duplex: NMR evidence that dhu is intrahelical and causes minimal DNA distortion," *Journal of the American Chemical Society*, vol. 121, no. 45, pp. 10 652–10 653, 1999.

[39] A. B. Britt, "Repair of DNA damage induced by ultraviolet radiation.," *Plant Physiology*, vol. 108, no. 3, p. 891, 1995.

[40] B. A. Donahue, S. Yin, J.-S. Taylor, D. Reines, and P. C. Hanawalt, "Transcript cleavage by RNA polymerase ii arrested by a cyclobutane pyrimidine dimer in the DNA template," *Proceedings of the National Academy of Sciences*, vol. 91, no. 18, pp. 8502–8506, 1994.

[41] E. C. Friedberg, G. C. Walker, W. Siede, and R. D. Wood, *DNA repair and mutagenesis*. American Society for Microbiology Press, 2005.

[42] T. Lindahl and R. D. Wood, "Quality control by DNA repair," *Science*, vol. 286, no. 5446, pp. 1897–1905, 1999.

[43] F. Thoma, "Light and dark in chromatin repair: Repair of UV-induced DNA lesions by photolyase and nucleotide excision repair," *The EMBO Journal*, vol. 18, no. 23, pp. 6585–6598, 1999.

[44] A. R. Lehmann, "Nucleotide excision repair and the link with transcription," *Trends in Biochemical Sciences*, vol. 20, no. 10, pp. 402–405, 1995.

[45] T. Carell and R. Epple, "Repair of UV light induced DNA lesions: A comparative study with model compounds," *European Journal of Organic Chemistry*, vol. 1998, no. 7, pp. 1245–1258, 1998.

[46] K. Sugasawa, J. M. Ng, C. Masutani, S. Iwai, P. J. van der Spek, A. P. Eker, F. Hanaoka, D. Bootsma, and J. H. Hoeijmakers, "Xeroderma pigmentosum group C

protein complex is the initiator of global genome nucleotide excision repair," *Molecular Cell*, vol. 2, no. 2, pp. 223–232, 1998.

[47] P. Robins, C. J. Jones, M. Biggerstaff, T. Lindahl, and R. D. Wood, "Complementation of DNA repair in xeroderma pigmentosum group A cell extracts by a protein with affinity for damaged DNA.," *The EMBO Journal*, vol. 10, no. 12, pp. 3913–3921, 1991.

[48] S. N. Guzder, P. Sung, L. Prakash, and S. Prakash, "Yeast DNA-repair gene RAD14 encodes a zinc metalloprotein with affinity for ultraviolet-damaged dna," *Proceedings of the National Academy of Sciences*, vol. 90, no. 12, pp. 5433–5437, 1993.

[49] H. Naegeli, L. Bardwell, and E. C. Friedberg, "The DNA helicase and adenosine triphosphatase activities of yeast Rad3 protein are inhibited by DNA damage. a potential mechanism for damage-specific recognition.," *Journal of Biological Chemistry*, vol. 267, no. 1, pp. 392–398, 1992.

[50] S. Nocentini, "Rejoining kinetics of DNA single-and double-strand breaks in normal and DNA ligase-deficient cells after exposure to ultraviolet C and gamma radiation: An evaluation of ligating activities involved in different DNA repair processes," *Radiation Research*, vol. 151, no. 4, pp. 423–432, 1999.

[51] M. Wakasugi and A. Sancar, "Order of assembly of human DNA repair excision nuclease," *Journal of Biological Chemistry*, vol. 274, no. 26, pp. 18 759–18 768, 1999.

[52] S. N. Guzder, P. Sung, L. Prakash, and S. Prakash, "Yeast Rad7-Rad16 complex, specific for the nucleotide excision repair of the nontranscribed DNA strand, is an ATP-dependent DNA damage sensor," *Journal of Biological Chemistry*, vol. 272, no. 35, pp. 21 665–21 668, 1997.

[53] A. Sancar, "DNA excision repair," *Annual Review of Biochemistry*, vol. 65, no. 1, pp. 43–81, 1996.

[54] O. I. Kovalsky, L. Grossman, and B. Ahn, "The topodynamics of incision of UV-irradiated covalently closed DNA by the escherichia coli Uvr (A) BC endonuclease," *Journal of Biological Chemistry*, vol. 271, no. 52, pp. 33 236–33 241, 1996.

[55] Y. Zou and B. Van Houten, "Strand opening by the UvrA2B complex allows dynamic recognition of DNA damage," *The EMBO Journal*, vol. 18, no. 17, pp. 4889–4901, 1999.

[56] A. Sancar, "Structure and function of DNA photolyase," *Biochemistry*, vol. 33, no. 1, pp. 2–9, 1994.

[57] S.-T. Kim, K. Malhotra, C. A. Smith, J.-S. Taylor, and A. Sancar, "Characterization of (6-4) photoproduct DNA photolyase.," *Journal of Biological Chemistry*, vol. 269, no. 11, pp. 8535–8540, 1994.

[58] A. Sancar, "No" end of history" for photolyases," *Science*, vol. 272, no. 5258, pp. 48–49, 1996.

[59] T. Todo, S.-T. Kim, K. Hitomi, E. Otoshi, T. Inui, H. Morioka, H. Kobayashi, E. Ohtsuka, H. Toh, and M. Ikenaga, "Flavin adenine dinucleotide as a chromophore of the xenopus (6-4) photolyase," *Nucleic Acids Research*, vol. 25, no. 4, pp. 764–768, 1997.

[60] A. Yasui, A. Eker, S. Yasuhira, H. Yajima, T. Kobayashi, M. Takao, and A. Oikawa, "A new class of DNA photolyases present in various organisms including aplacental mammals.," *The EMBO Journal*, vol. 13, no. 24, pp. 6143–6151, 1994.

[61] T. Todo, "Functional diversity of the DNA photolyase/blue light receptor family," *Mutation Research. DNA Repair*, vol. 434, no. 2, pp. 89–97, 1999.

[62] H.-W. Park, S.-T. Kim, A. Sancar, and J. Deisenhofer, "Crystal structure of DNA photolyase from escherichia coli," *Science*, vol. 268, no. 5219, pp. 1866–1872, 1995.

[63] R. P. Rastogi and R. P. Sinha, "Genotoxin-induced DNA damage: Detection, recovery and influence on human health," *Advances in Life Sciences*, pp. 275–310, 2011.

[64] A. Sancar, "Structure and function of DNA photolyase and cryptochrome blue-light photoreceptors," *Chemical Reviews*, vol. 103, no. 6, pp. 2203–2238, 2003.

[65] N. Arichi, A. Inase, S. Eto, T. Mizukoshi, J. Yamamoto, and S. Iwai, "Mechanism of the alkali degradation of (6–4) photoproduct-containing DNA," *Organic & Biomolecular Chemistry*, vol. 10, no. 11, pp. 2318–2325, 2012.

[66] J. A. Lippke, L. K. Gordon, D. E. Brash, and W. A. Haseltine, "Distribution of UV light-induced damage in a defined sequence of human DNA: Detection of alkaline-sensitive lesions at pyrimidine nucleoside-cytidine sequences," *Proceedings of the National Academy of Sciences*, vol. 78, no. 6, pp. 3388–3392, 1981.

[67] M. Lukin and C. de los Santos, "NMR structures of damaged DNA," *Chemical Reviews*, vol. 106, no. 2, pp. 607–686, 2006.

[68] J.-H. Lee, G.-S. Hwang, J.-K. Kim, and B.-S. Choi, "The solution structure of dna decamer duplex containing the dewar product of thymidylyl $(3 \rightarrow 5)$ thymidine by nmr and full relaxation matrix refinement," *FEBS letters*, vol. 428, no. 3, pp. 269–274, 1998.

[69] R. P. Rastogi, A. Kumar, M. B. Tyagi, R. P. Sinha, *et al.*, "Molecular mechanisms of ultraviolet radiation-induced DNA damage and repair," *Journal of Nucleic Acids*, vol. 2010, 2010.

[70] D. A. Pearlman, D. Pirkle, S. Kim, *et al.*, "Molecular models for DNA damaged by photoreaction," *Science*, vol. 227, no. 4692, pp. 1304–1308, 1985.

[71] H. Kamiya, S. Iwai, and H. Kasai, "The (6-4) photoproduct of thymine-thymine induces targeted substitution mutations in mammalian cells," *Nucleic Acids Research*, vol. 26, no. 11, pp. 2611–2617, 1998.

[72] G. Lin, Y. Jian, H. Ouyang, and L. Li, "An unexpected deamination reaction after hydrolysis of the pyrimidine (6-4) pyrimidone photoproduct," *Organic Letters*, vol. 16, no. 19, pp. 5076–5079, 2014.

[73] R. E. Johnson, L. Haracska, S. Prakash, and L. Prakash, "Role of DNA polymerase $\eta$ in the bypass of a (6-4) tt photoproduct," *Molecular and Cellular Biology*, vol. 21, no. 10, pp. 3558–3563, 2001.

[74] J. Yamamoto, D. Loakes, C. Masutani, S. Simmyo, K. Urabe, F. Hanaoka, P. Holliger, and S. Iwai, "Translesion synthesis across the (6–4) photoproduct and its Dewar valence isomer by the Y-family and engineered DNA polymerases," in *Nucleic Acids Symposium Series*, Oxford University Press, vol. 52, 2008, pp. 339–340.

[75] A. R. Young, C. A. Chadwick, G. I. Harrison, J. L. Hawk, O. Nikaido, and C. S. Potten, "The in situ repair kinetics of epidermal thymine dimers and 6-4 photoproducts in human skin types i and ii," *Journal of Investigative Dermatology*, vol. 106, no. 6, pp. 1307–1313, 1996.

[76] K. M. de Lima-Bessa, M. G. Armelini, V. Chiganças, J. F. Jacysyn, G. P. Amarante-Mendes, A. Sarasin, and C. F. M. Menck, "Cpds and 6-4pps play different roles in UV-induced cell death in normal and NER-deficient human cells," *DNA Repair*, vol. 7, no. 2, pp. 303–312, 2008.

[77] H.-L. Lo, S. Nakajima, L. Ma, B. Walter, A. Yasui, D. W. Ethell, and L. B. Owen, "Differential biologic effects of cpd and 6-4pp UV-induced DNA damage on the induction of apoptosis and cell-cycle arrest," *BMC Cancer*, vol. 5, no. 1, pp. 1–9, 2005.

[78] K. McAteer, Y. Jing, J. Kao, J.-S. Taylor, and M. A. Kennedy, "Solution-state structure of a dna dodecamer duplex containing a cis-syn thymine cyclobutane dimer, the major uv photoproduct of DNA," *Journal of Molecular Biology*, vol. 282, no. 5, pp. 1013–1032, 1998.

[79] J.-H. Lee, G.-S. Hwang, and B.-S. Choi, "Solution structure of a DNA decamer duplex containing the stable 3 t g base pair of the pyrimidine (6–4) pyrimidone photoproduct

[(6–4) adduct]: Implications for the highly specific 3 t→ c transition of the (6–4) adduct," *Proceedings of the National Academy of Sciences*, vol. 96, no. 12, pp. 6632–6636, 1999.

[80] G. P. Pfeifer, R. Drouin, A. D. Riggs, and G. P. Holmquist, "In vivo mapping of a DNA adduct at nucleotide resolution: Detection of pyrimidine (6-4) pyrimidone photoproducts by ligation-mediated polymerase chain reaction.," *Proceedings of the National Academy of Sciences*, vol. 88, no. 4, pp. 1374–1378, 1991.

[81] J.-H. Yoon, C.-S. Lee, T. R. O'Connor, A. Yasui, and G. P. Pfeifer, "The DNA damage spectrum produced by simulated sunlight," *Journal of Molecular Biology*, vol. 299, no. 3, pp. 681–693, 2000.

[82] M. Higurashi, T. Ohtsuki, A. Inase, R. Kusumoto, C. Masutani, F. Hanaoka, and S. Iwai, "Identification and characterization of an intermediate in the alkali degradation of (6-4) photoproduct-containing DNA," *Journal of Biological Chemistry*, vol. 278, no. 51, pp. 51 968–51 973, 2003.

[83] N. Arichi, J. Yamamoto, C. Takahata, E. Sano, Y. Masuda, I. Kuraoka, and S. Iwai, "Strand breakage of a (6–4) photoproduct-containing DNA at neutral pH and its repair by the ERCC1–XPF protein complex," *Organic & Biomolecular chemistry*, vol. 11, no. 21, pp. 3526–3534, 2013.

[84] H. Fairhead and P. Setlow, "Binding of DNA to alpha/beta-type small, acid-soluble proteins from spores of bacillus or clostridium species prevents formation of cytosine dimers, cytosine-thymine dimers, and bipyrimidine photoadducts after UV irradiation.," *Journal of Bacteriology*, vol. 174, no. 9, pp. 2874–2880, 1992.

[85] B. Setlow, D. Sun, and P. Setlow, "Interaction between DNA and alpha/beta-type small, acid-soluble spore proteins: A new class of DNA-binding protein.," *Journal of Bacteriology*, vol. 174, no. 7, pp. 2312–2322, 1992.

[86] R. Moeller, T. Douki, J. Cadet, E. Stackebrandt, W. L. Nicholson, P. Rettberg, G. Reitz, and G. Horneck, "UV-radiation-induced formation of DNA bipyrimidine photoproducts in bacillus subtilis endospores and their repair during germination," *International Microbiology*, vol. 10, no. 1, pp. 39–46, 2007.

[87] D. G. Lemaire and B. P. Ruzsicska, "Kinetic analysis of the deamination reactions of cyclobutane dimers of thymidylyl-3', 5'-2'-deoxycytidine and 2'-deoxycytidylyl-3', 5'-thymidine," *Biochemistry*, vol. 32, no. 10, pp. 2525–2533, 1993.

[88] I. Singh, Y. Lian, L. Li, and M. M. Georgiadis, "The structure of an authentic spore photoproduct lesion in DNA suggests a basis for recognition," *Acta Crystallographica Section D: Biological Crystallography*, vol. 70, no. 3, pp. 752–759, 2014.

[89] G. Lin, C.-H. Chen, M. Pink, J. Pu, and L. Li, "Chemical synthesis, crystal structure and enzymatic evaluation of a dinucleotide spore photoproduct analogue containing a formacetal linker," *Chemistry–A European Journal*, vol. 17, no. 35, pp. 9658–9668, 2011.

[90] O. R. Ludek, G. K. Schroeder, C. Liao, P. L. Russ, R. Wolfenden, and V. E. Marquez, "Synthesis and conformational analysis of locked carbocyclic analogues of 1, 3-diazepinone riboside, a high-affinity cytidine deaminase inhibitor," *The Journal of Organic Chemistry*, vol. 74, no. 16, pp. 6212–6223, 2009.

[91] L. Frick, R. Wolfenden, E. Smal, and D. C. Baker, "Transition-state stabilization by adenosine deaminase: Structural studies of its inhibitory complex with deoxycoformycin," *Biochemistry*, vol. 25, no. 7, pp. 1616–1621, 1986.

[92] M. Malone, M. Pellow-Jarman, and L. Salter, "Alkaline hydrolysis of cis-syn thymine dimer at elevated temperature," *South African Journal of Chemistry*, vol. 42, no. 4, pp. 166–168, 1989.

[93] G. Blackburn and R. Davies, "The structure of thymine photo-dimer," *Journal of the Chemical Society C: Organic*, pp. 2239–2244, 1966.

[94] T. L. Mega and R. L. Van Etten, "The oxygen-18 isotope shift in carbon-13 nuclear magnetic resonance spectroscopy. 15. studies of [18o, 1, 4-13c2] succinic acid and [18o] dimethylmaleic anhydride," *Journal of the American Chemical Society*, vol. 115, no. 25, pp. 12 056–12 059, 1993.

[95] J. C. Vederas, "Structural dependence of oxygen-18 isotope shifts in carbon-13 NMR spectra," *Journal of the American Chemical Society*, vol. 102, no. 1, pp. 374–376, 1980.

[96] A. Dessinges, S. Castillon, A. Olesker, T. T. Thang, and G. Lukacs, "Oxygen-17 NMR and oxygen-18-induced isotopic shifts in carbon-13 NMR for the elucidation of a controversial reaction mechanism in carbohydrate chemistry," *Journal of the American Chemical Society*, vol. 106, no. 2, pp. 450–451, 1984.

[97] S. Berger, R. Etten, J. Risley, and N. Sergeyev, *Isotope effects in NMR spectroscopy.* Springer, 1990.

[98] T. M. Koning, J. J. van Soest, and R. Kaptein, "NMR studies of bipyrimidine cyclobutane photodimers," *European journal of biochemistry*, vol. 195, no. 1, pp. 29–40, 1991.

[99] H. M. Bdour, J. L.-F. Kao, and J.-S. Taylor, "Synthesis and characterization of a [3-15n]-labeled cis-syn thymine dimer-containing DNA duplex," *The Journal of Organic Chemistry*, vol. 71, no. 4, pp. 1640–1646, 2006.

[100] G. Whitson, *Concepts in radiation cell biology.* Elsevier, 2012.

[101] M. Herbert, J. LeBlanc, D. Weinblum, and H. Johns, "Properties of thymine dimers," *Photochemistry and Photobiology*, vol. 9, no. 1, pp. 33–43, 1969.

[102] M. J. Cavaluzzi and P. N. Borer, "Revised UV extinction coefficients for nucleoside-5 -monophosphates and unpaired DNA and RNA," *Nucleic Acids Research*, vol. 32, no. 1, e13–e13, 2004.

[103] H. White, "Manual oligonucleotide synthesis using the phosphoramidite method," in *New Nucleic Acid Techniques*, Springer, 1988, pp. 193–213.

[104] J. E. Dixon and T. C. Bruice, ". alpha. effect. V. kinetic and thermodynamic nature of the. alpha. effect for amine nucleophiles," *Journal of the American Chemical Society*, vol. 94, no. 6, pp. 2052–2056, 1972.

[105] J. M. Garver, S. Gronert, and V. M. Bierbaum, "Experimental validation of the $\alpha$-effect in the gas phase," *Journal of the American Chemical Society*, vol. 133, no. 35, pp. 13 894–13 897, 2011.

[106] S. Davey, "Gas-phase kinetics: Analysing the $\alpha$-effect," *Nature Chemistry*, vol. 3, no. 10, p. 753, 2011.

[107] E. Gilbert, "Studies on hydrazine. the auto-oxidation," *Journal of the American Chemical Society*, vol. 51, no. 9, pp. 2744–2751, 1929.

# A. APPENDIX

## A.1 Determination of the kinetics of $^{18}$O labeling experiments of CPD-TpT

CPD-TpT was synthesized following the protocol developed by Bdour *et al* [99] (Figure 2.23). CPD-TpT formed after UV-B irradiation of TpT was purified using reverse-phase HPLC (Figure 2.24) and its concentration was determined using UV-Visible absorption spectroscopy. Before conducting a detailed analysis of the kinetics of $^{18}$O exchange reaction in CPD-TpT, calibration curves were drawn in order to determine the linear range for Q-TOF HR-MS instrument response in response to CPD-TpT concentration, and to obtain reliable quantification data during the experiments. In order for a thorough investigation of the reaction kinetics, the variation in reaction rate was studied in response to change(s) in reaction temperature, concentrations of CPD-TpT and NaOH. *It was found that the change in rate of decrease of CPD-TpT (i.e. the rate of the first exchange) was negligible in response to a significant change in concentration(s) of the two reactants (CPD-TpT and NaOH). Similar trends were observed with the rate of decrease of (M+2) species and the concurrent rate of increase of (M+4) peak, stating no detectable changes in the rate of the second exchange. Since NaOH is already in excess as compared to CPD-TpT, the reaction was expected to proceed via a 'pseudo-first order' kinetics. No change in the reaction rate on changing the NaOH concentration simply states that a further increase in the pH of the reaction medium does not increase the concentration of $^{18}$OH- ions and thus has no effect on the reaction rate. The indifference of the reaction rate to change in CPD-TpT concentration, however, insinuates a 'zero order' kinetics.* The results are summarized in the sections that follow:

### A.1.1 Effect of temperature on the rate of $^{18}$O labeling reaction

In order to determine the dependence of $^{18}$O exchange reaction rate on temperature, variation in M, (M+2) and (M+4) species were recorded over time during the reaction of 1mM CPD-TpT in presence of 100 mM NaOH in $^{18}$O labeled water at room temperature (RT), 40°C and 60°C. It was found that the reaction rates on heating the reaction mixture were substantially higher than the ones at RT, as expected; the first $^{18}$O exchange was completed in less than 3 hours at 60°C whereas it took 40 hours at RT. Figure A.1 shows

the representative equation at the kinetic curve for the reaction at RT. A comparison between the reaction rates at 40°C and 60°C as a function of the rate of change in M, (M+2) and (M+4) peaks is shown in Figure A.2.

**Kinetics of $^{18}$O exchange reaction between 1.3 mM of CPD-TpT+100 mM NaOH at room temperature (RT)**

| Time(hrs) | M_RT | M+2_RT | M+4_RT |
|---|---|---|---|
| 0 | 4233291 | 179498 | 0 |
| 16 | 1559689 | 1456583 | 127027 |
| 40 | 761087 | 2310221 | 364583 |
| 48 | 700823 | 2349920 | 426131 |
| 144 | 529151 | 2277164 | 828371 |



O18 labeling reaction kinetics at RT
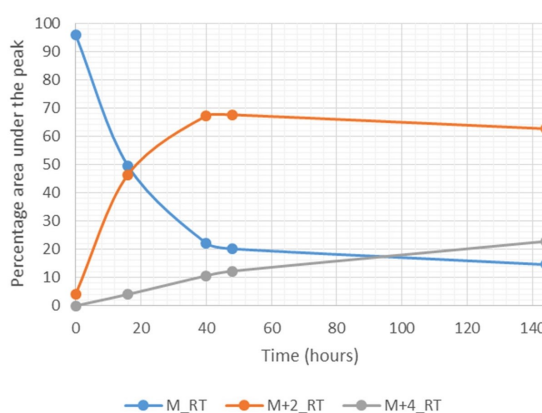
**Figure A.1.** Variation of M, (M+2) and (M+4) species with time during the $^{18}$O exchange reaction of 1.3 mM of CPD-TpT in presence of 100 mM NaOH at room temperature (RT)

**Kinetics of $^{18}$O exchange reaction between 1.3 mM of CPD-TpT+100 mM NaOH at 40°C and 60°C**

## A.1.2   Effect of the concentration(s) of CPD-TpT and NaOH on the rate of $^{18}$O labeling reaction

Figures A.3 and A.4 show the change in reaction rate with changes in the concentration(s) of CPD-TpT and NaOH respectively. Figure A.5 summarizes these results.

| Time(hours) | M_40 deg | M+2_40 deg | M+4_40 deg | M_60 deg | M+2_60 deg | M+4_60 deg |
|---|---|---|---|---|---|---|
| 0 | 95.02818 | 4.97182 | 0 | 95.0281792 | 4.971820804 | 0 |
| 2 | 63.92564 | 34.34276 | 1.7316 | 15.25367728 | 70.91638873 | 13.82993399 |
| 4 | 46.27453 | 49.96043 | 3.76504 | 7.076808835 | 66.50872323 | 26.41446793 |
| 6 | 32.26254 | 62.07491 | 5.66255 | 7.918581087 | 38.68259719 | 53.39882172 |



**Figure A.2.** Comparison of the reaction rates as a function of the rate(s) of change of M, (M+2) and (M+4) species at 40°C and 60°C

| Time(hours) | M_1.3mM CPD | M+2_1.3mM CPD | M+4_1.3mM CPD | M_2.6mM CPD | M+2_2.6mM CPD | M+4_2.6mM CPD |
|---|---|---|---|---|---|---|
| 0 | 95.028179 | 4.9718208 | 0 | 92.76382 | 7.236176 | 0 |
| 2 | 15.253677 | 70.916389 | 13.829934 | 18.90547 | 71.28833 | 9.806194 |
| 4 | 7.0768088 | 66.508723 | 26.414468 | 10.0319 | 73.15426 | 16.81384 |
| 6 | 7.9185811 | 38.682597 | 53.398822 | 8.332871 | 64.36415 | 27.30298 |



**Figure A.3.** Comparison of the reaction rates as a function of the rate(s) of change of M, (M+2) and (M+4) species during the $^{18}$O exchange reaction of 1.3 mM and 2.6 mM of CPD-TpT in presence of 100 mM NaOH at 60°C

## A.2  Effect of the relative Stereo-chemistry of C6-methyl groups (*cis vs trans*) on the electron transfer potential of cyclobutane pyrimidine dimer (CPD) lesions

In living organisms, CPD mostly occurs in two conformations: *cis-syn* and *trans-syn*; with the *cis-syn* isomer formed in major amounts ( 98%). Once we found the differential reactivity of the two C4=O groups in *cis-syn*CPD-TpT, we wondered if a change in the relative stereo-chemistry of the two C6 methyl groups (and thus, a change in the packing arrangement in

152

| Time(hours) | M_100mM NaOH | M+2_100mM NaOH | M+4_100mM NaOH | M_200mM NaOH | M+2_200mM NaOH | M+4_200mM NaOH |
|---|---|---|---|---|---|---|
| 0 | 95.028179 | 4.9718208 | 0 | 86.44857 | 13.03887 | 0.512561 |
| 120 | 15.253677 | 70.916389 | 13.829934 | 23.92562 | 68.06039 | 8.013993 |
| 240 | 7.0768088 | 66.508723 | 26.414468 | 9.831744 | 72.86791 | 17.30034 |
| 360 | 7.9185811 | 38.682597 | 53.398822 | 3.72458 | 42.13722 | 54.13819 |



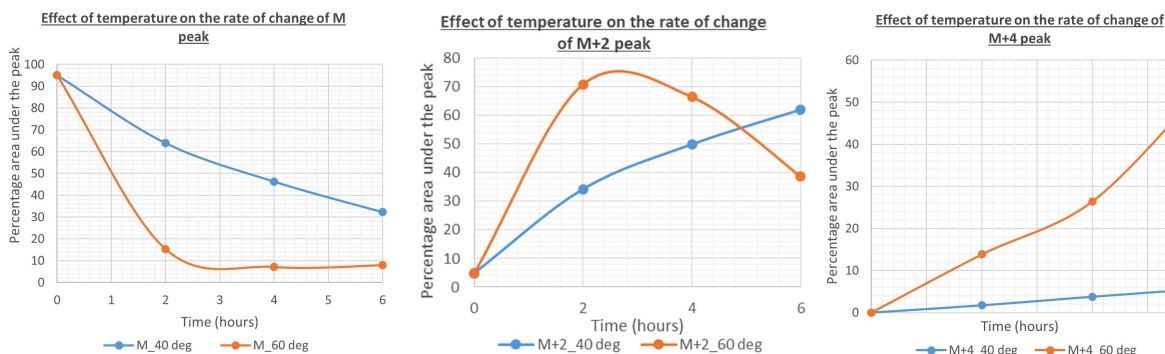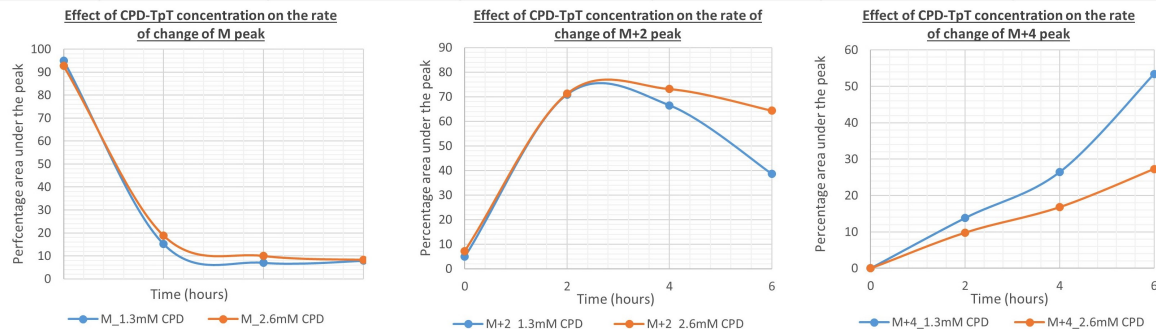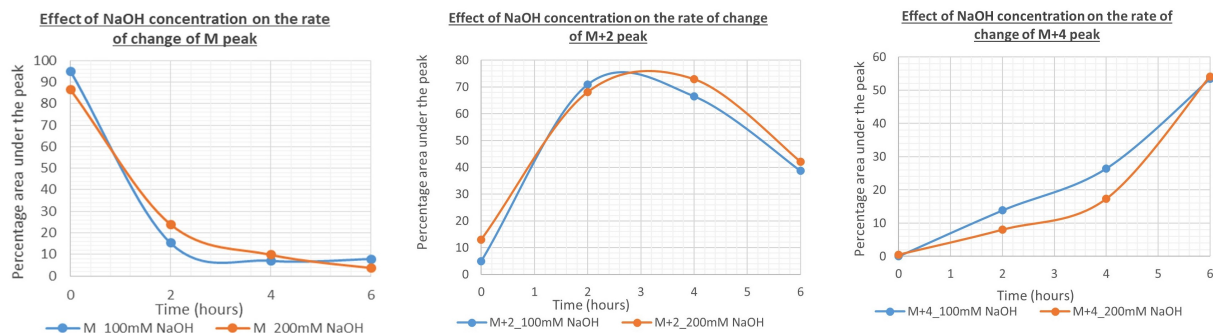**Figure A.4.** Comparison of the reaction rates as a function of the rate(s) of change of M, (M+2) and (M+4) species during the $^{18}$O exchange reaction of 1.3 mM of CPD-TpT in presence of 100 mM and 200 mM NaOH at 60°C

**Effect of the concentrations of CPD-TpT and NaOH on the rate of the reaction**
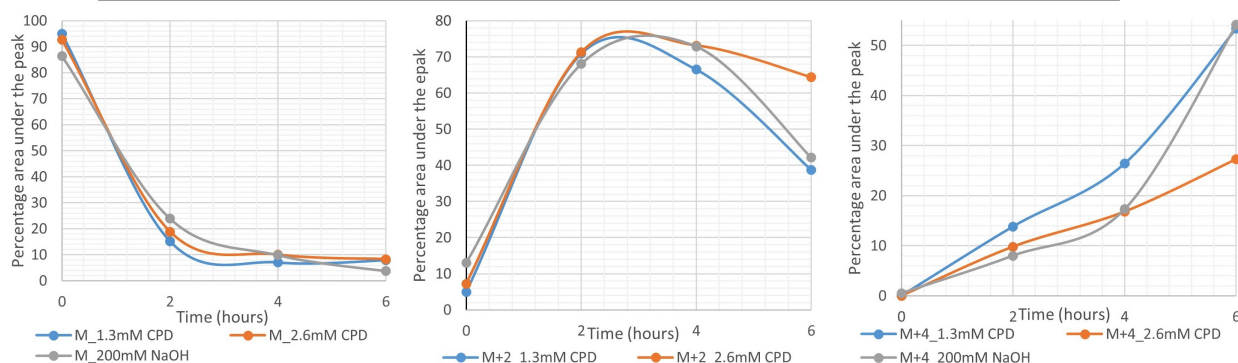


**Figure A.5.** Comparison of the reaction rates as a function of the rate(s) of change of M, (M+2) and (M+4) species with change(s) in concentrations of CPD-TpT and NaOH at 60°C

solution) will affect the outcome of the $^{18}$O exchange reaction. To address that, we conducted the $^{18}$O labeling reaction in *cis-syn*CPD-TpT in presence of equal amount of the *trans-syn* isomer as an internal standard. TpT was synthesized following the protocol developed by Bdour *et al* [99]. UV-B photo-irradiation of TpT in ice for 4 hours yielded a mixture of *cis-syn* and *trans-syn* isomers in the ratio 98:2 (Figure A.6). The two isomers were purified using reverse-phase HPLC using 10mM ammonium acetate (pH 6.8) and acetonitrile as the buffers

(Figure A.7). Their respective concentrations were determined using UV-Visible absorption spectroscopy (Figure A.8).

Calibration curves for both *cis-syn* and *trans-syn* CPD-TpT were drawn to determine the linear range for Q-TOF HR-MS instrument response as a function of concentration of the two compounds (Figures A.9 and A.10). $^{18}$O exchange reaction was conducted in a single pot containing a mixture of 3mM of *cis-syn* and *trans-syn* CPD-TpT isomers in presence of 250 mM of NaOH at 75°C. We chose to heat the reaction mixture because when the same reaction was carried out at room temperature, *trans-syn* CPD-TpT showed no detectable $^{18}$O exchange for a period of 8 days (Figures A.11 and A.12). The reaction rate(s) for the two isomers (at 75°C) are individually described as a function of variation in M, (M+2) and (M+4) peaks in Figures A.13 and A.14. Figure A.15 shows a comparison of the rate(s) in the two isomers.

*From the kinetic curves, it can be clearly seen that although a change in the relative stereo-chemistry of the C6 methyl groups does not change the outcome of the reaction, it brings about a significant change in the rate of the reaction. The trans-syn isomer was found to react a lot more slowly as compared to the trans-syn isomer. This can most likely be attributed to the reduced accessibility of the C4=O groups to the $^{18}$OH- ions, when the C6 methyl groups are trans with respect to each other.*

## A.3 Effect of phosphate linker on the chemical reactivities of carbonyl groups in cyclobutane pyrimidine dimer (CPD) lesions

In order to study the effect of phosphate linker on the chemical reactivities of the carbonyl groups in a CPD molecule, we studied the $^{18}$O exchange reaction in CPD-thymidine in presence of CPD-TpT as an internal standard. It should be noted that CPD-thymidine lacks the 'phosphate linker' that connects the two thymidine residues in a CPD-TpT molecule. *Any change observed between the chemical reactivities in the two molecules can most likely be attributed to the change in stacking arrangement of the molecules in solution.* UV-B photo-irradiation of thymidine at 4°C in 35% acetone-water mixture led to four stereo-isomers of CPD-thymidine namely *cis syn*, *cis anti*, *trans syn* and *trans anti* (Figure A.16).
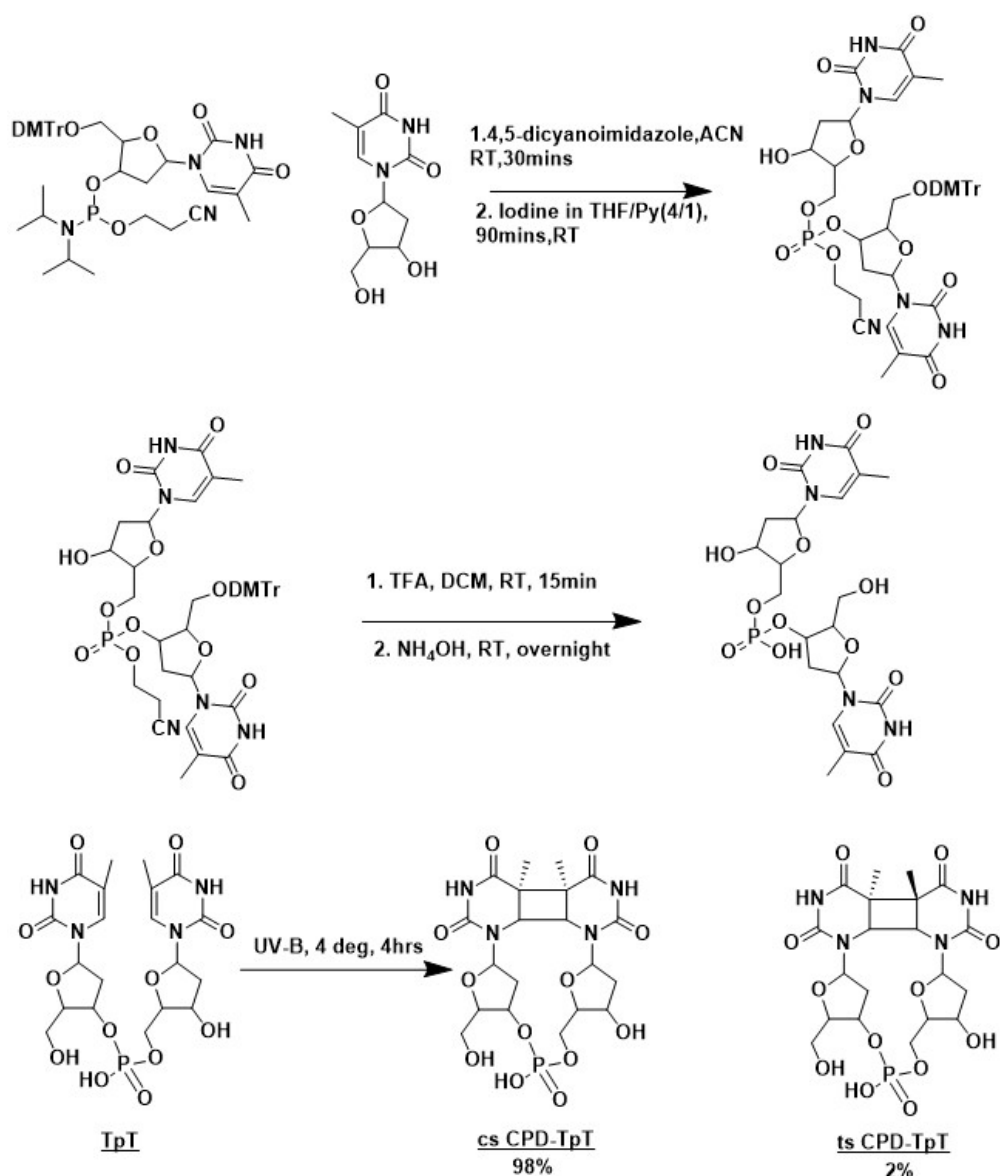
**Figure A.6.** Reaction scheme for the synthesis of cis-syn and trans-syn CPD-TpT

*It should be pointed out here that photo-irradiation of TpT under similar conditions yields only two out of these four stereo-isomers i.e.cis syn and trans syn CPD-TpT. This is because, the presence of the phosphate linker between the two thymidine moieties in TpT, reduces the degrees of freedom of the molecule and prevents the thymidine rings to adopt an 'anti' conformation with respect to each other. The absence of this kind of structural constraint also leads to a slower rate of photo-reaction in thymidine.* The reaction peaks after approximately 19 hours in contrast to 4 hours for CPD-TpT formation in > 90% yield.

| | Name | Retention Time | Area | % Area | Height | Int Type | Peak Type |
|---|------|----------------|------|--------|--------|----------|-----------|
| 1 | | 2.251 | 1002563 | 97.74 | 69018 | bb | Unknown |
| 2 | | 10.823 | 23177 | 2.26 | 2289 | bb | Unknown |

**Figure A.7.** Reverse-phase HPLC chromatograms showing the relative amounts of cis-syn and trans-syn isomers of CPD-TpT formed after UV-B photo-irradiation of TpT
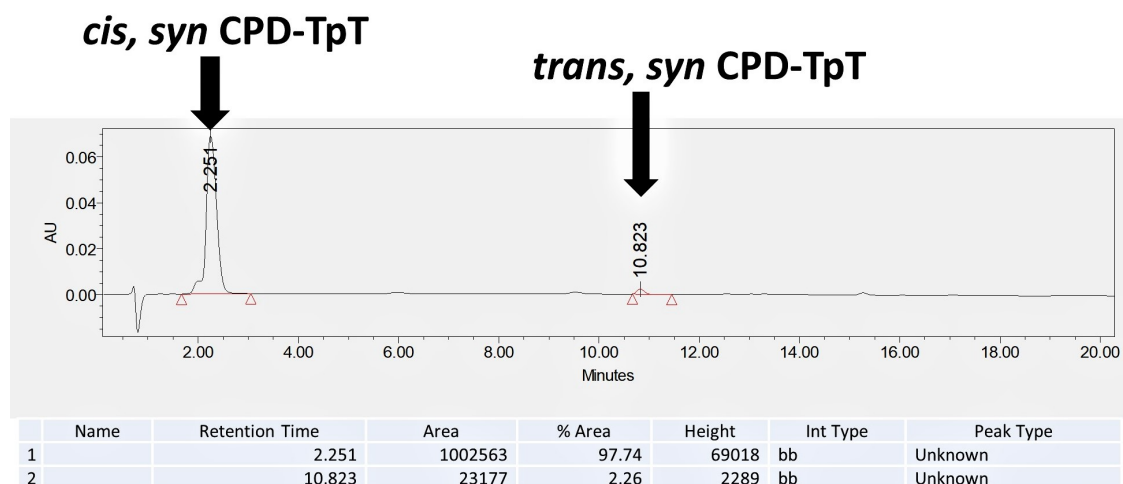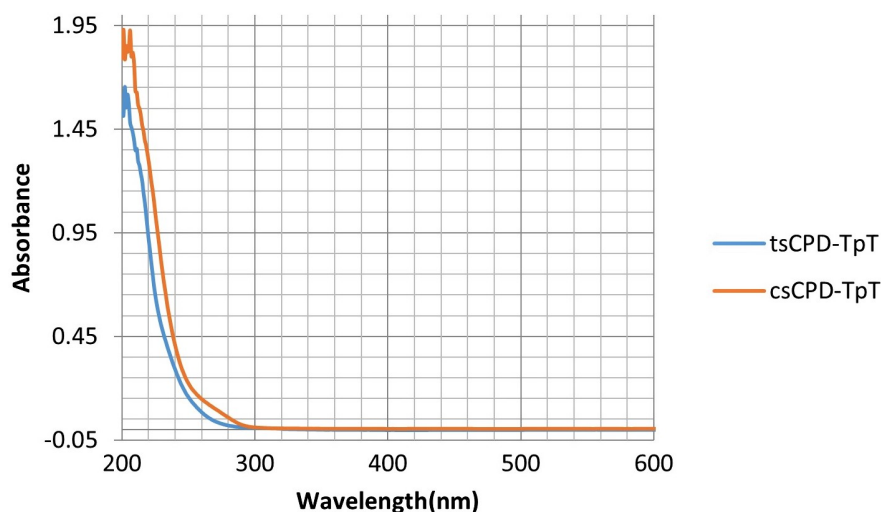


**Figure A.8.** UV-Visible absorption spectra for cis-syn and trans-syn isomers of CPD-TpT

Figure A.17 shows the HPLC chromatogram for the reaction mixture after 18.5 hours of photo-irradiation. Concentration of the CPD-thymidine isomers was determined using their absorbance (Figure A.18) and the molar extinction coefficient (available online). Figures A.19, A.20, A.21 and A.22 show $C^{13}$ NMR spectra for the four CPD-thymidine isomers.

In order to compare the rate(s) of $^{18}O$ exchange between CPD-thymidine and CPD-TpT, the exchange reaction was conducted for each isomer in presence of CPD-TpT as an internal standard. The reaction was done at room temperature to prevent any degradation
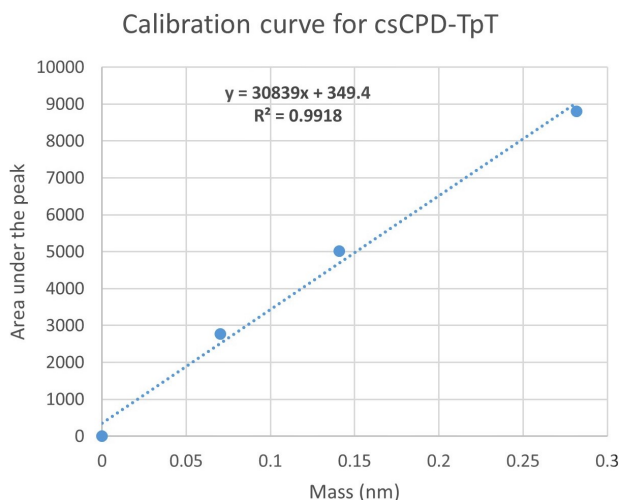
**Figure A.9.** Calibration curve for cis-syn CPD-TpT
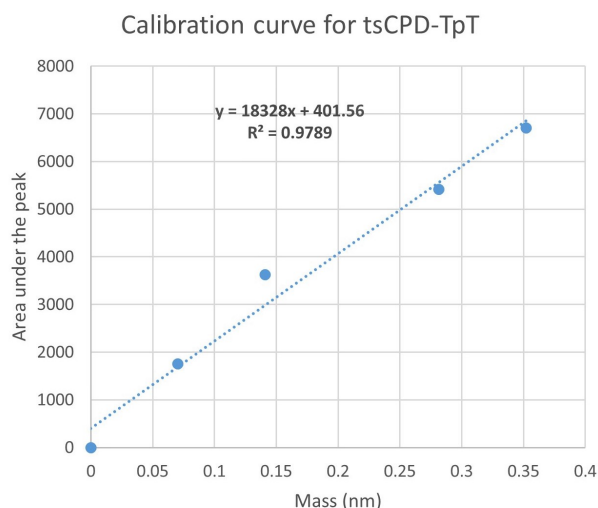


**Figure A.10.** Calibration curve for trans-syn CPD-TpT

of the more reactive isomers (*trans anti*) in presence of high concentration of NaOH. *As expected, CPD-TpT showed rapid exchange with the first exchange (C4=O on 3' side) almost complete in less than 24 hours, after which the second exchange (C4=O on 5' side) started showing up (Figure A.23). In contrast, none of the four stereo-isomers of CPD-thymidine showed any significant signs of $^{18}O$ exchange over the 11 days for which the reaction was monitored (figure A.24).* The reaction was first conducted in presence of 100 mM NaOH to avoid

**Figure A.11.** $^{18}$O exchange reaction of cis-syn CPD-TpT in presence of 250 mM NaOH at room temperature

any degradation/hydrolysis of *trans anti* CPD-thymidine. However, the NaOH concentration was increased to 250 mM when no change was observed any of the CPD-thymidine isomers in presence of 100 mM NaOH. The reaction was stopped at 11 days, since most of the *trans anti* isomer was hydrolyzed by that time (Figure A.25).

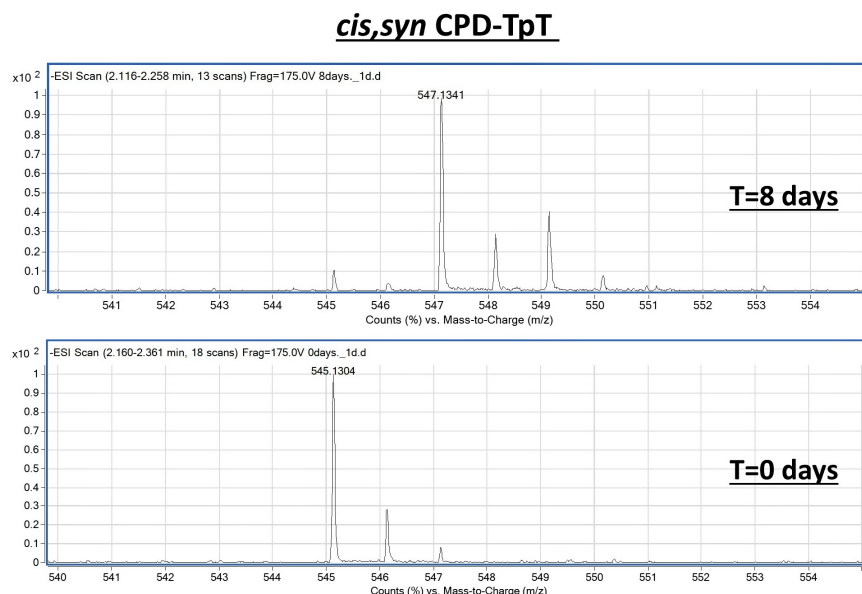Figure A.26 shows that none of the CPD-thymidine isomers underwent a nucleophilic exchange during the course of the reaction, which in turns underscores the importance of the phosphate linker and thus, the stacked conformation in solution to the chemical reactivity of the carbonyl groups in a CPD molecule. In the absence of this three-dimensional packing arrangement, the carbonyl groups remain chemically inert towards a nucleophile. These results also explain the 'chemical inertness' of the *cis-syn* isomer of CPD known so far (Figure A.27).

## A.4   Effect of neighboring bases on the electron transfer potential of cyclobutane pyrimidine dimer (CPD) lesions

*So far, we have studied various aspects of the intricacies of the chemical reactivities of carbonyl groups in a CPD molecule. We studied the effect of increase in chain length on*
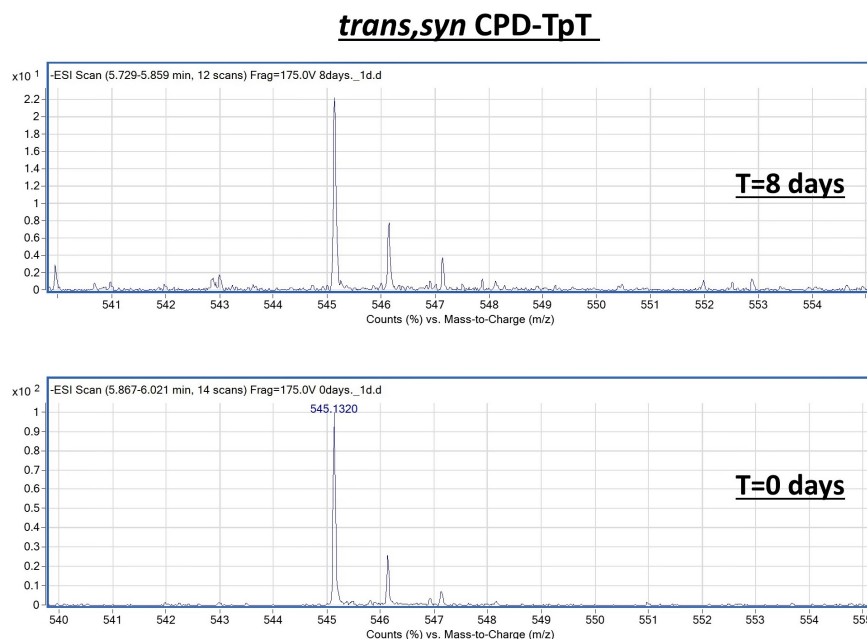
**_trans,syn_ CPD-TpT**



**Figure A.12.** $^{18}$O exchange reaction of trans-syn CPD-TpT in presence of 250 mM NaOH at room temperature

*the electron transfer potential of carbonyl groups. We also studied the effect of changes in concentration(s) of the two reactants. This was followed by a study of the effect of changes in stereo-chemistry of the C6 methyl groups and the effect of the presence/absence of phosphate linker on the reactivity pattern. We also studied the chemical reactivities under different reaction conditions i.e. at various values of pH and temperature.* The next question we ask ourselves is the effect of neighboring groups (A vs G) surrounding the CPD molecule on the outcome and rate of the nucleophilic exchange reaction. To this effect, we decided to compare the rate(s) of $^{18}$O exchange in CPD-AATTAA and CPD-GGTTGG.

CPD-GGTTGG was prepared after UV-B irradiation of GGTTGG (commercially available). The reaction was particularly challenging because the guanosine moiety is known to undergo oxidation rapidly even under conditions of slight increase in the reaction temperature. As a result, GGTTGG underwent rapid degradation by the heat produced by the UV-B lamp long before any cycloaddition could occur; thereby reducing the yield of the reaction drastically. We tried to circumvent around this problem by conducting the photo-reaction in ice, and by reducing the exposure time to minimise the oxidation reaction, but that led to
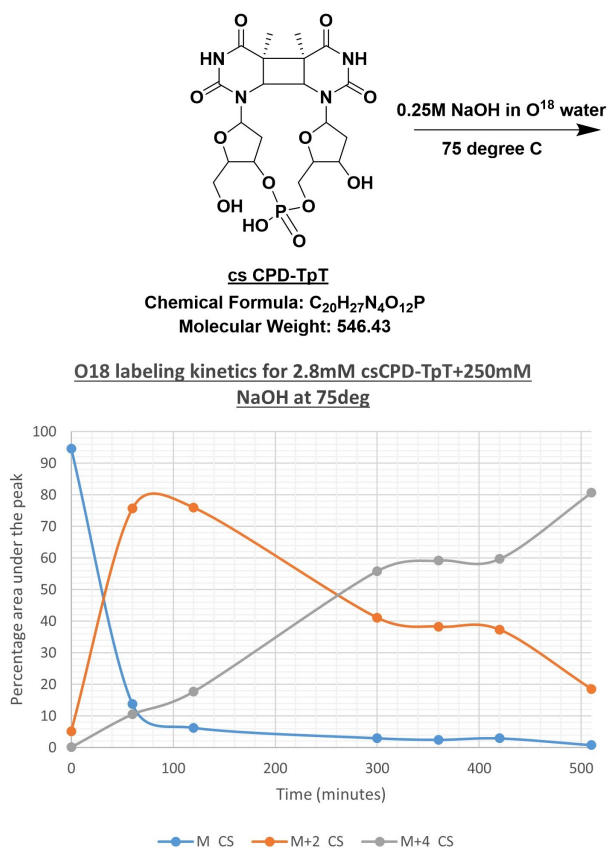
**Figure A.13.** Rate(s) of change of M, (M+2) and (M+4) species during the $^{18}$O exchange reaction of cis-syn CPD-TpT in presence of NaOH

only minor improvements in the yield. We tried to compensate this by collecting unreacted starting material (GGTTGG) after HPLC purification of CPD-GGTTGG and subjecting it to another round of UV irradiation. Figure A.28 shows the RP-HPLC chromatogram for the reaction mixture after UV-B photo-irradiation. As can be seen from the figure, the yield of the product is only 15% after the first round of photo-irradiation. It is even lower after the second round, probably due to partial degradation/oxidation of the starting material after the first round.

Concentration of the product i.e. CPD-GGTTGG was determined by recording its UV-Visible absorption spectrum and using the extinction coefficient value available online (Figure A.29). $^{18}$O exchange reaction was done by suspending 1mM of CPD-GGTTGG in $^{18}$O labeled water in presence of 100 mM NaOH at room temperature. The reaction was also tried in presence of 250 mM and 500 mM concentrations of NaOH. Figure A.30 shows the
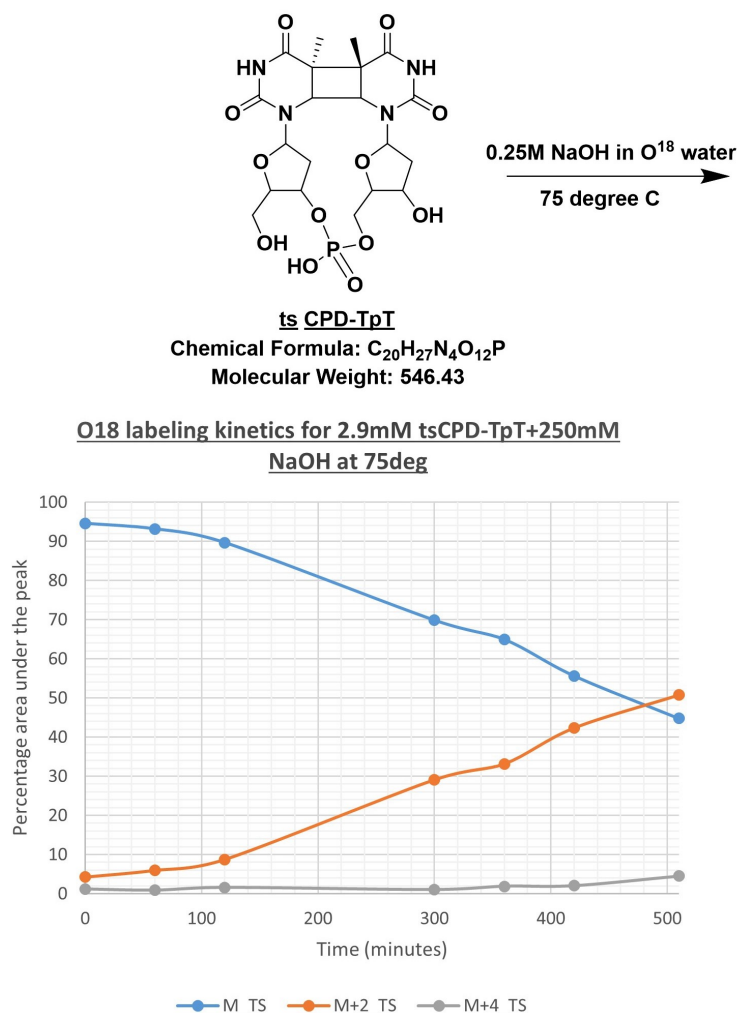
**Figure A.14.** Rate(s) of change of M, (M+2) and (M+4) species during the $^{18}$O exchange reaction of trans-syn CPD-TpT in presence of NaOH

calibration curve for CPD-GGTTGG, plotted to determine the linear range of Q-TOF HR-MS instrument response as a function of amount of compound injected. Figures A.31, A.32 and A.33 summarize the results. Figure A.34 compiles the results from the three reactions. It can be seen that the reaction rate shows only minor changes with variation in NaOH concentration. This is in agreement to the results obtained in CPD-TpT under similar conditions (Figure A.4), and can most likely be attributed to changes in the solution pH.
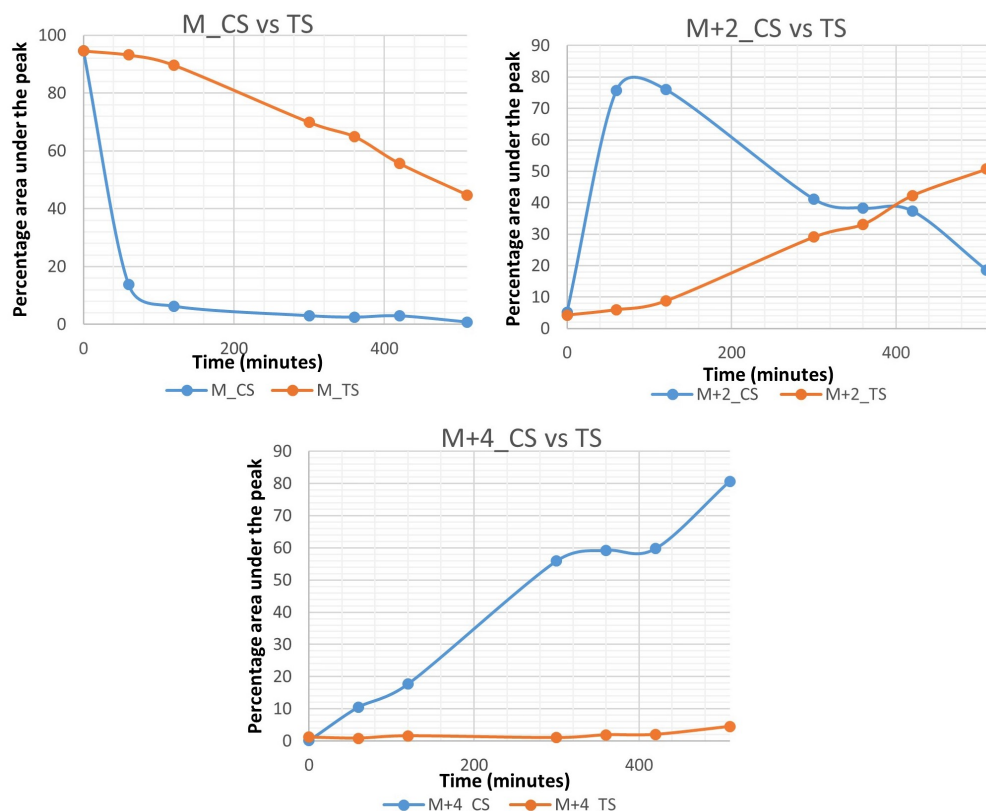
**Figure A.15.** Comparison of the reaction rates as a function of the rate(s) of change of M, (M+2) and (M+4) species during the $^{18}$O exchange reaction of cis-syn and trans-syn isomers of CPD-TpT in presence of NaOH

In order to compare the rate(s) of $^{18}$O exchange in CPD-GGTTGG and CPD-AATTAA, CPD-AATTAA was obtained by a UV-B irradiation of an aqueous solution of AATTAA for around 4 hours. The *cis-syn* isomer required for our experiments was purified out of the UV-irradiated mixture using reverse-phase HPLC followed by desalting and lyophilisation (Figure 3.3). The concentration of CPD-AATTAA was determined using UV-Visible absorption spectroscopy (Figure 3.4). The resulting powder (after lyophilisation) was suspended in $^{18}$O labelled water and adjusted for the required NaOH concentration. Figure A.35 shows the calibration curves for CPD-AATTAA. Figures A.36, A.37 and A.38 show a comparison of the reaction rates.i.e. effect of changes in neighboring groups on the rate of $^{18}$O exchange reaction in a CPD molecule. It can be clearly seen that the reaction in CPD-GGTTGG is slightly higher than that in CPD-AATTAA. *The variation in reaction rate can be attributed*
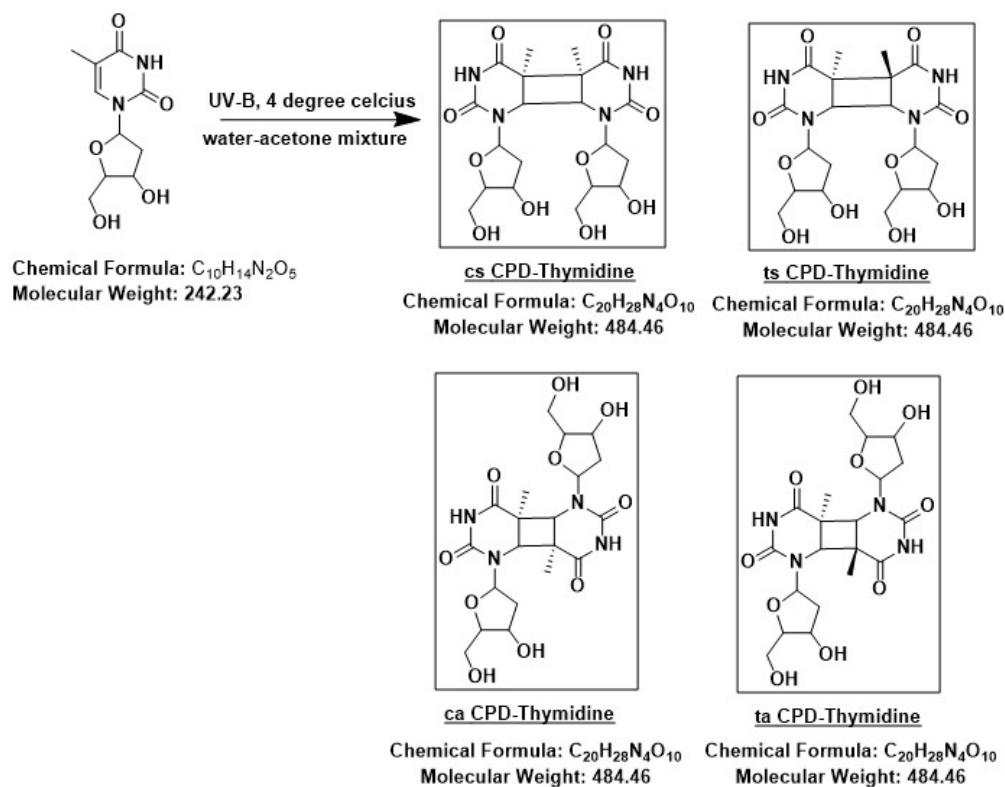
**Figure A.16.** Reaction scheme for UV-B photo-irradiation of thymidine leading to CPD-thymidine

to the small differences in steric constraints imposed by the groups surrounding the CPD moiety (A vs G) or the chemical/electronic nature of the group itself. **In general, it can be concluded with confidence that the neighboring groups surrounding the CPD moiety do have an effect on the rate at which it reacts; with the CPD moiety surrounded by more guanosines undergoing exchange at a faster pace that the one surrounded by more adenosines.**

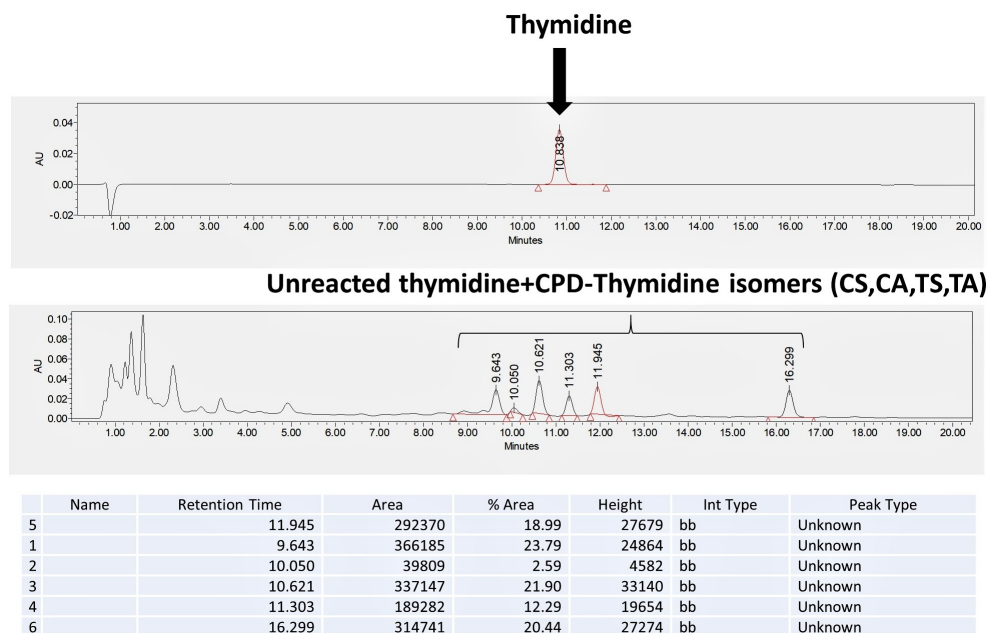**Figure A.17.** RP-HPLC chromatogram showing thymidine after 18.5 hours of UV-B photo-irradiation

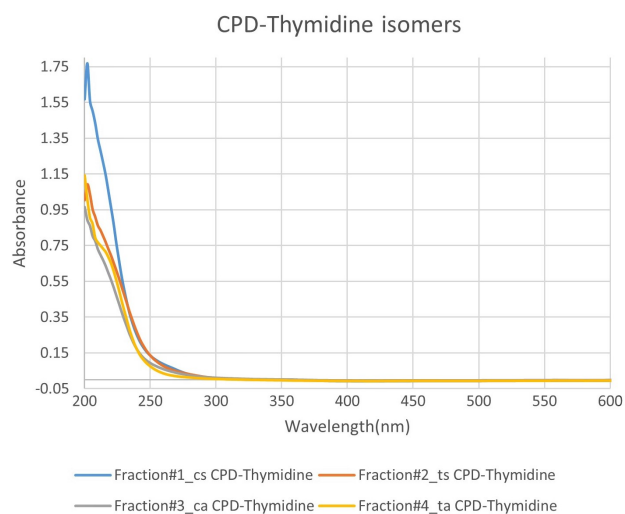| | Name | Retention Time | Area | % Area | Height | Int Type | Peak Type |
|---|---|---|---|---|---|---|---|
| 5 | | 11.945 | 292370 | 18.99 | 27679 | bb | Unknown |
| 1 | | 9.643 | 366185 | 23.79 | 24864 | bb | Unknown |
| 2 | | 10.050 | 39809 | 2.59 | 4582 | bb | Unknown |
| 3 | | 10.621 | 337147 | 21.90 | 33140 | bb | Unknown |
| 4 | | 11.303 | 189282 | 12.29 | 19654 | bb | Unknown |
| 6 | | 16.299 | 314741 | 20.44 | 27274 | bb | Unknown |



**Figure A.18.** UV-Visible absorption spectrum for various isomers of CPD-thymidine
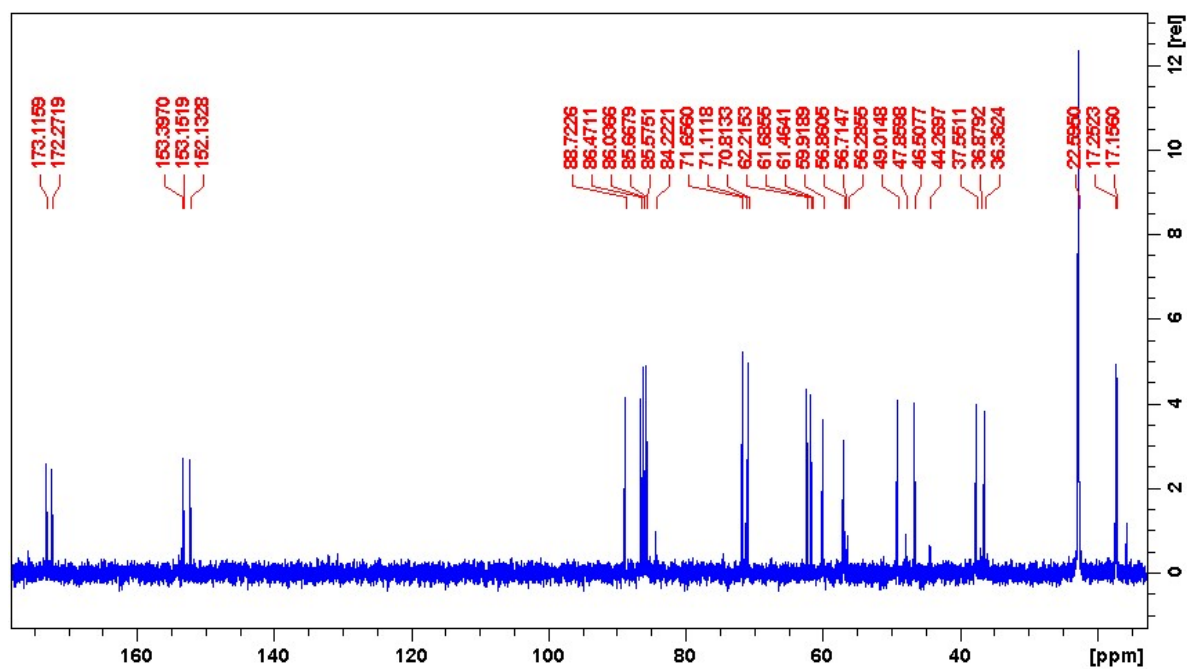
164

**Figure A.19.** C$^{13}$ NMR spectrum for *cis-syn* CPD-thymidine



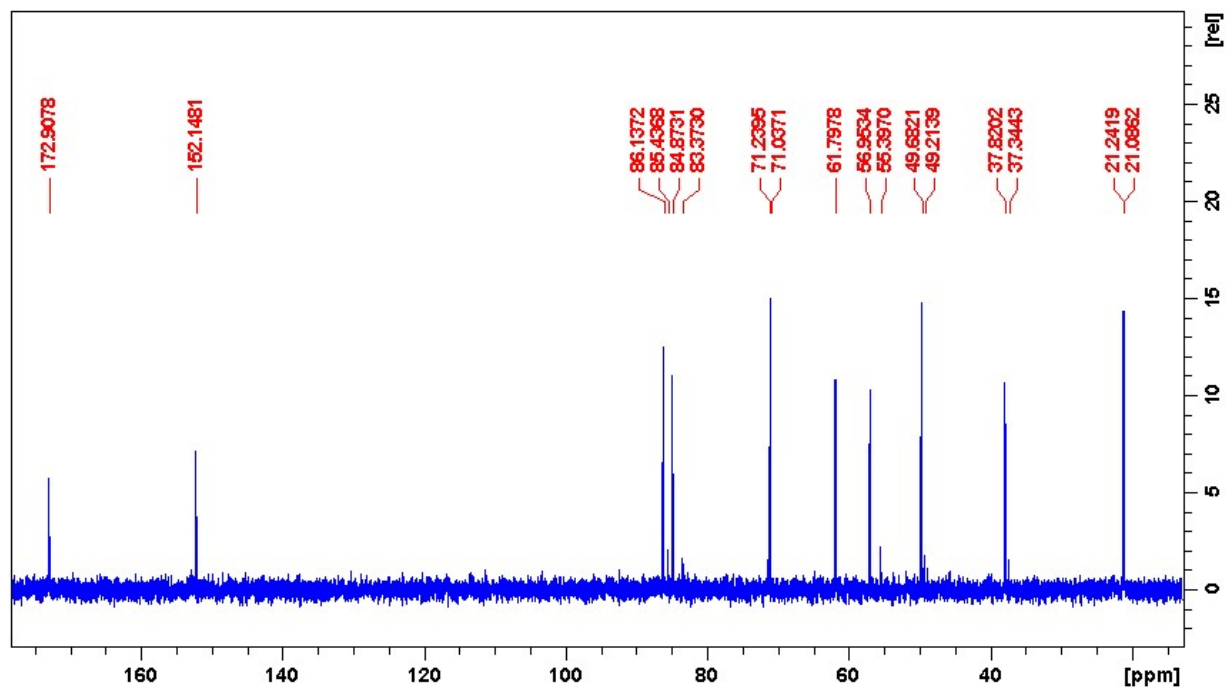**Figure A.20.** C$^{13}$ NMR spectrum for *cis-anti* CPD-thymidine
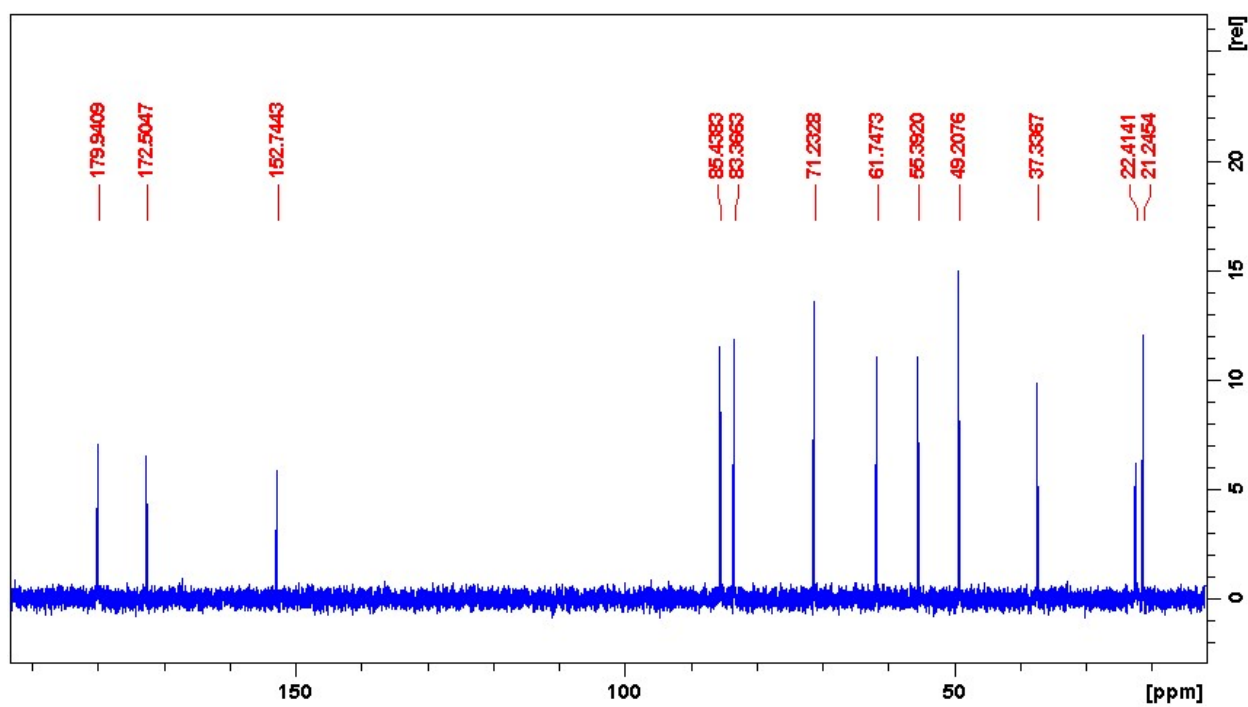
**Figure A.21.** C$^{13}$ NMR spectrum for *trans-syn* CPD-thymidine
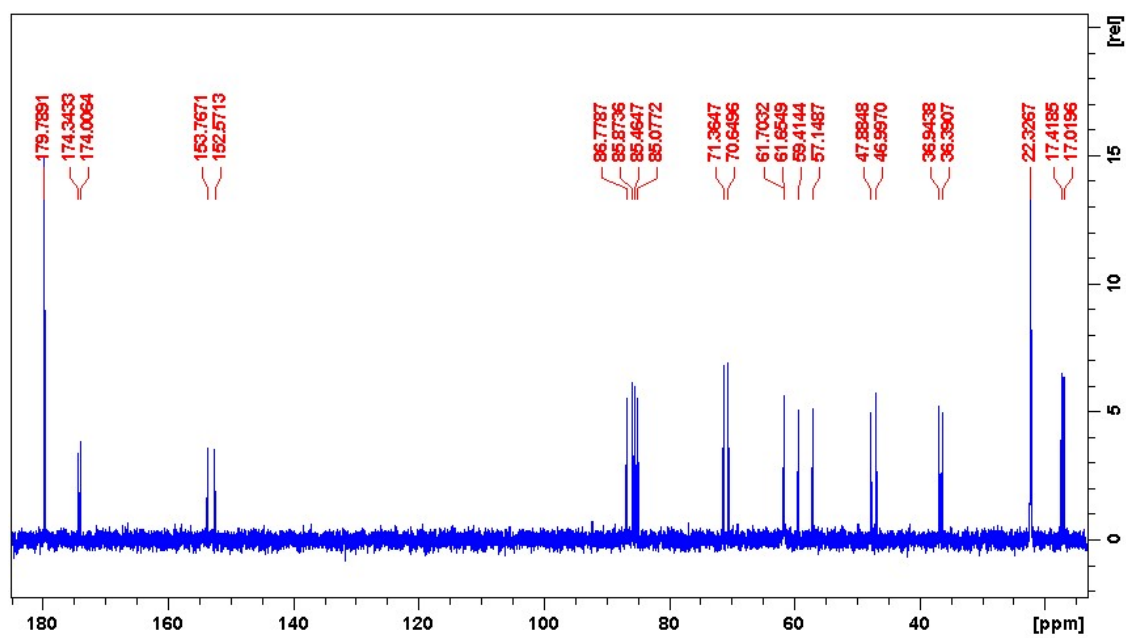


**Figure A.22.** C$^{13}$ NMR spectrum for *trans-anti* CPD-thymidine

166
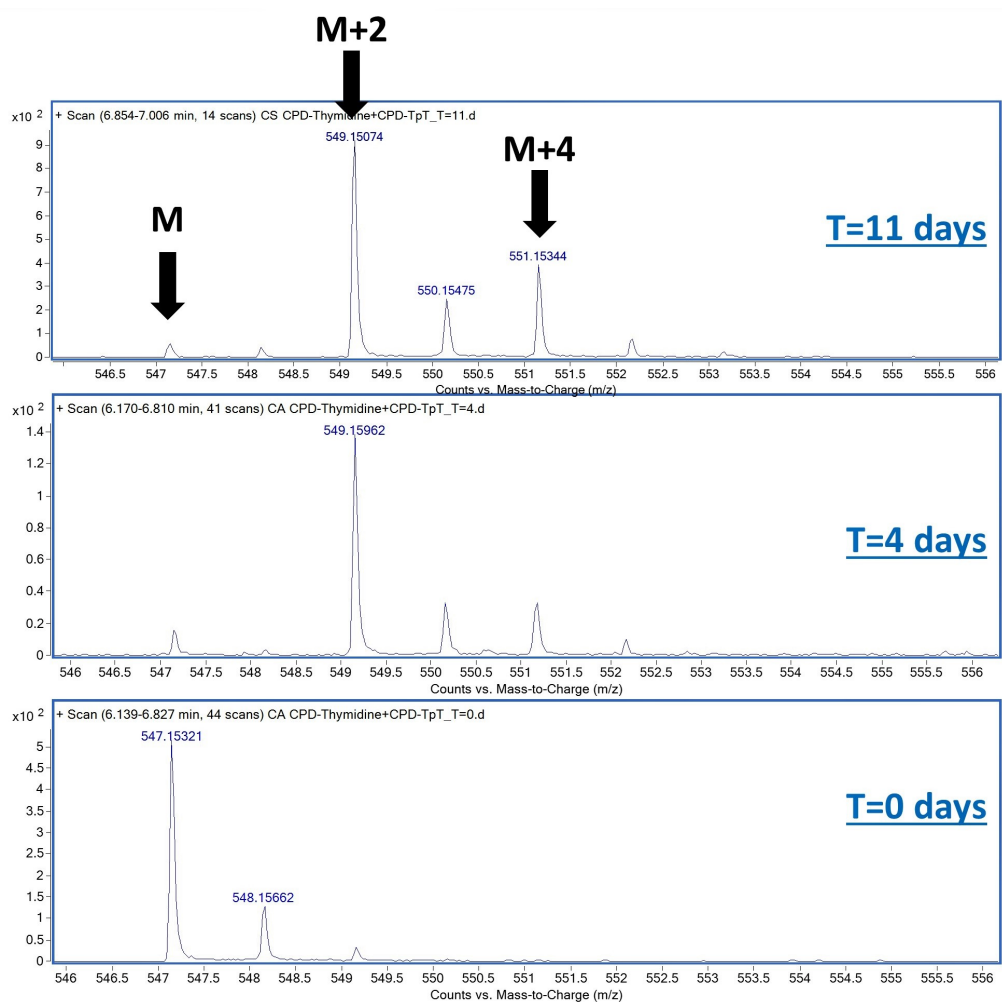
**Figure A.23.** ESI-MS spectra overlaid to show $^{18}$O exchange in CPD-TpT over 11 days
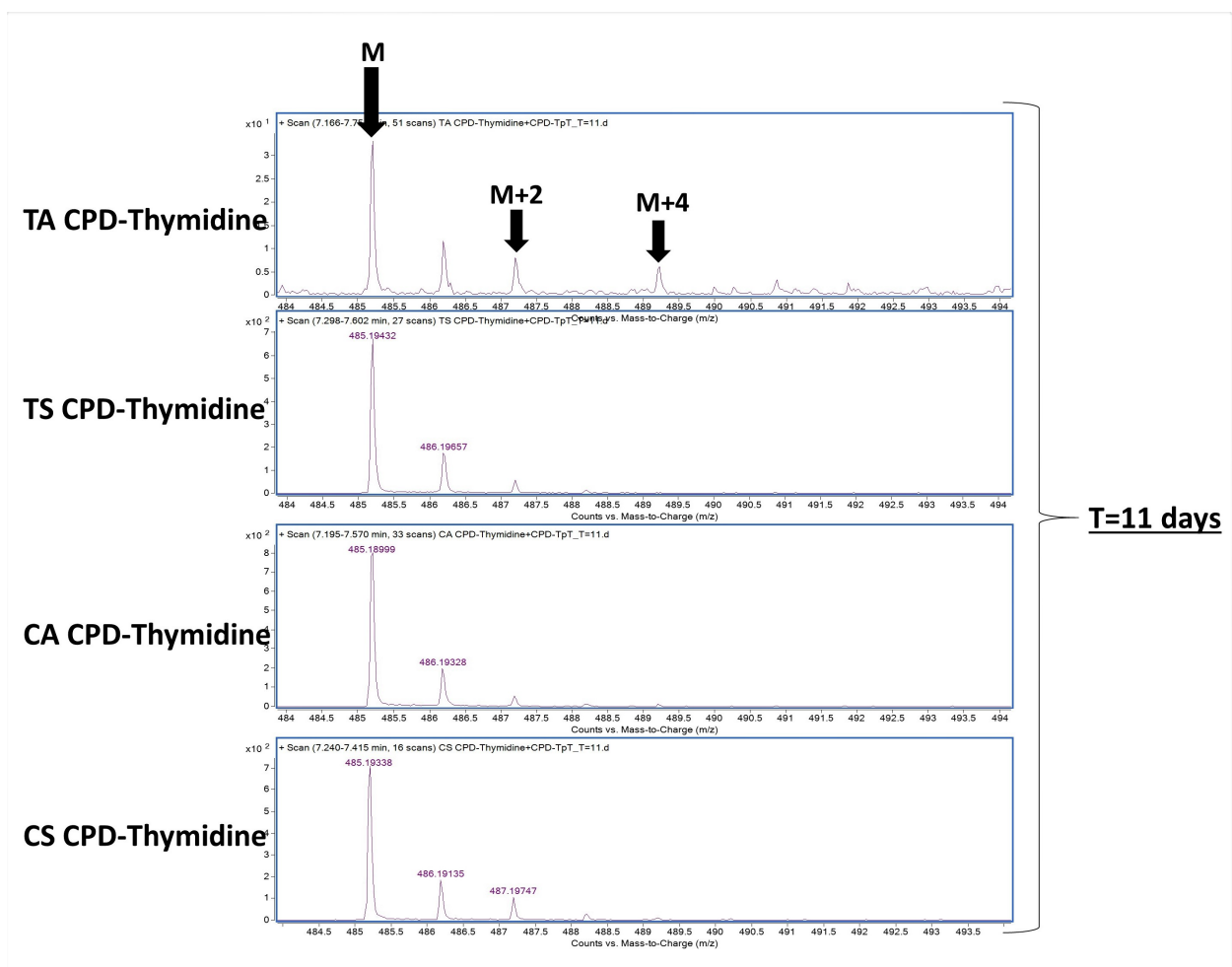
**Figure A.24.** ESI-MS spectra overlaid to show $^{18}O$ exchange in various isomers of CPD-thymidine over 11 days
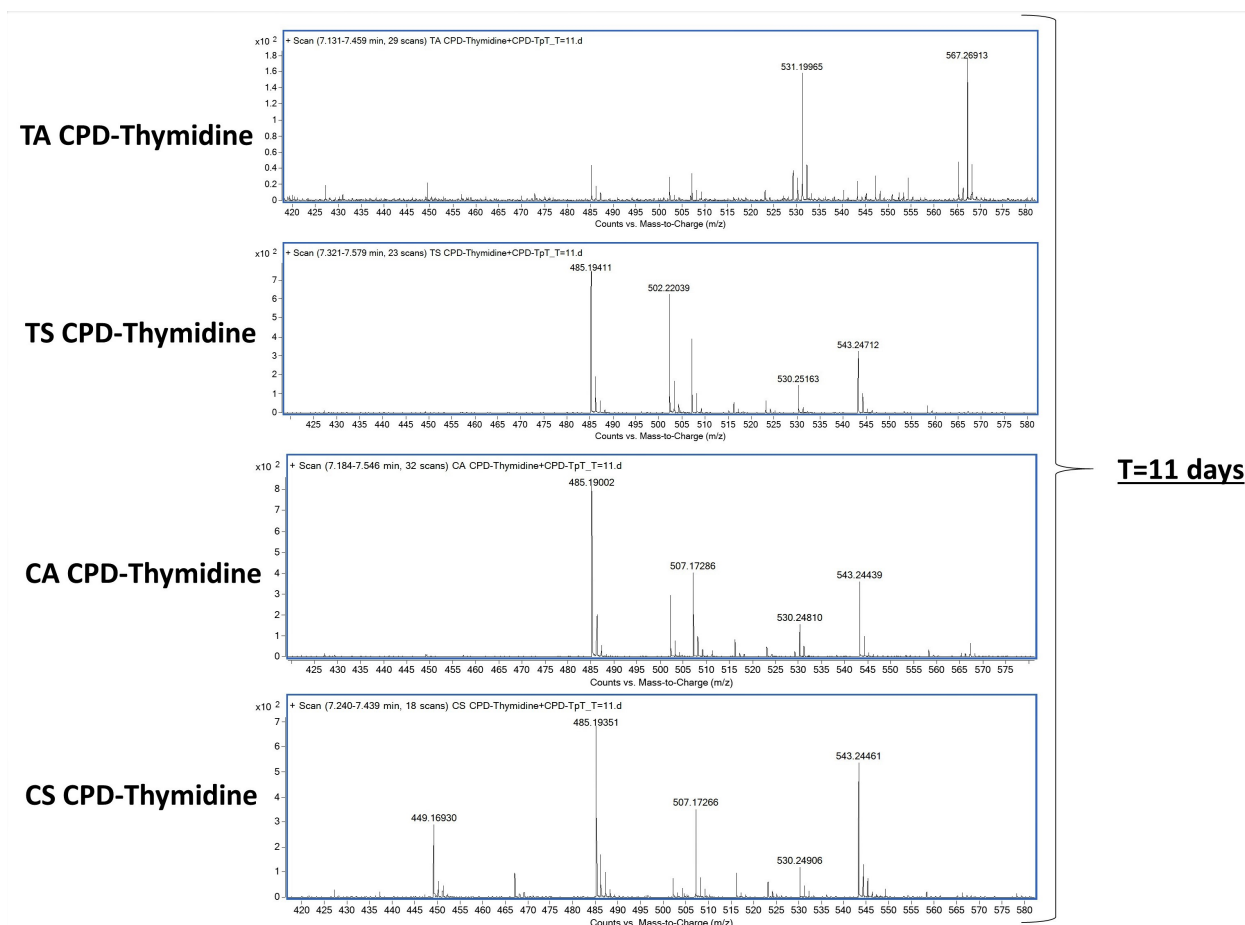
**Figure A.25.** Reaction scheme showing the degradation of trans,anti isomer of CPD-thymidine after 11 days of alkali exposure
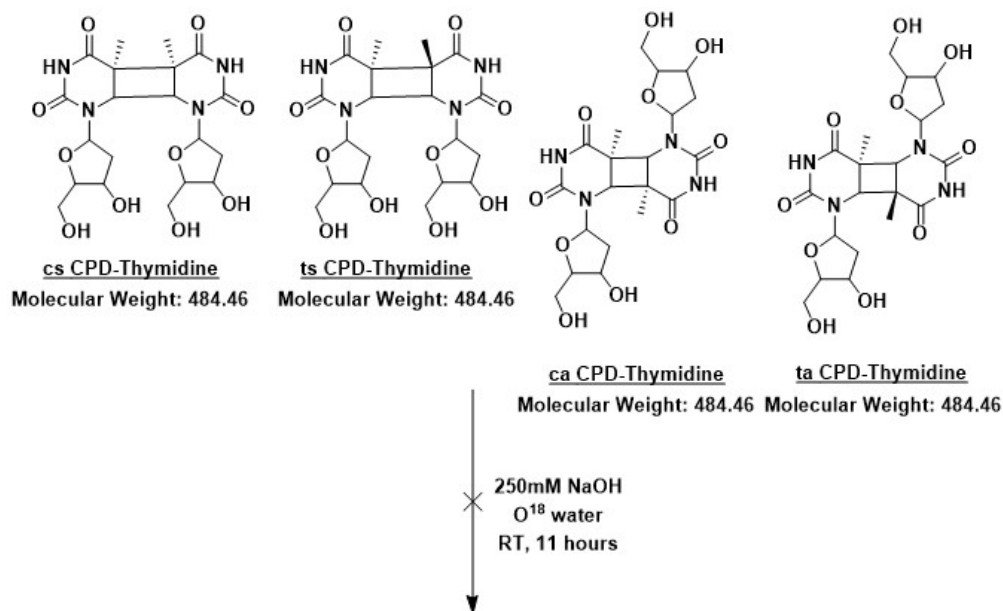
**Figure A.26.** Reaction scheme summarizing the alkaline reactivities of CPD-thymidine isomers
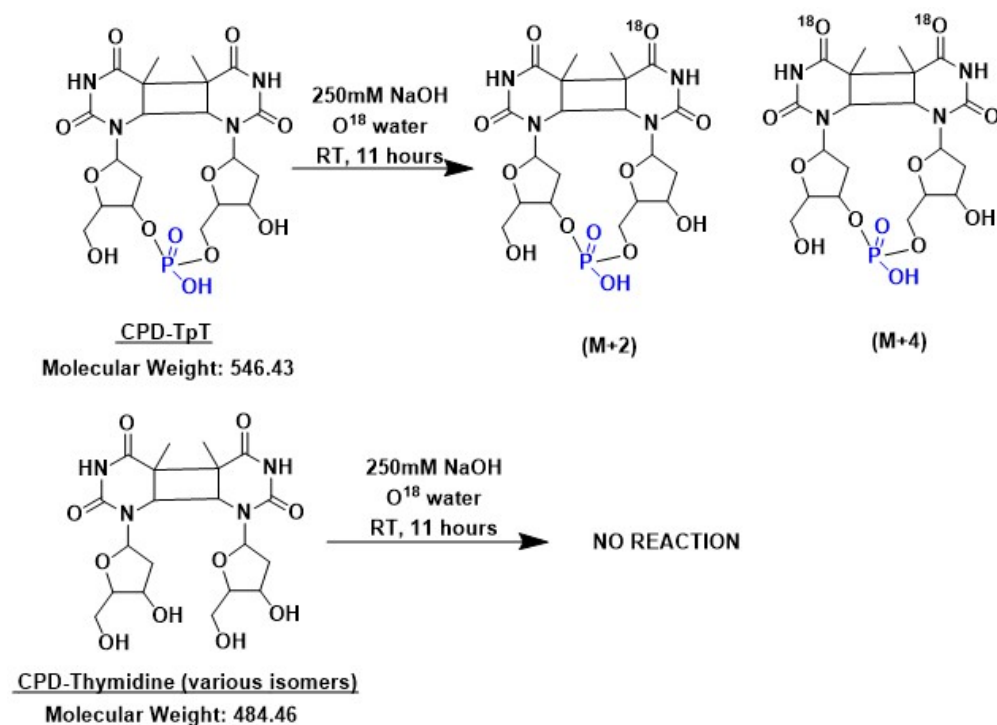


**Figure A.27.** Reaction scheme comparing the alkaline reactivities of CPD-TpT and various isomers of CPD-thymidine
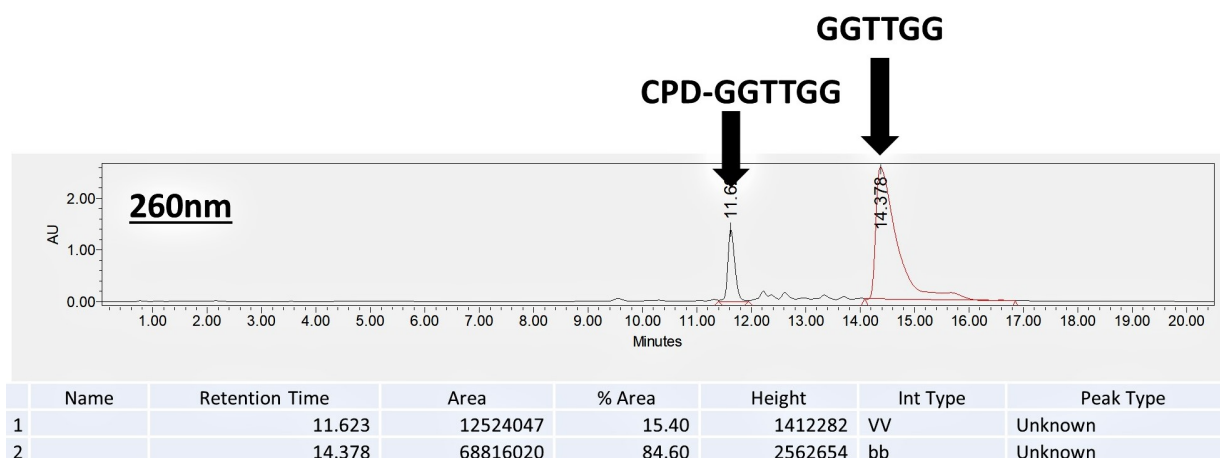
**Figure A.28.** RP HPLC chromatogram showing CPD-GGTTGG and unreacted GGTTGG after UV-B irradiation in ice
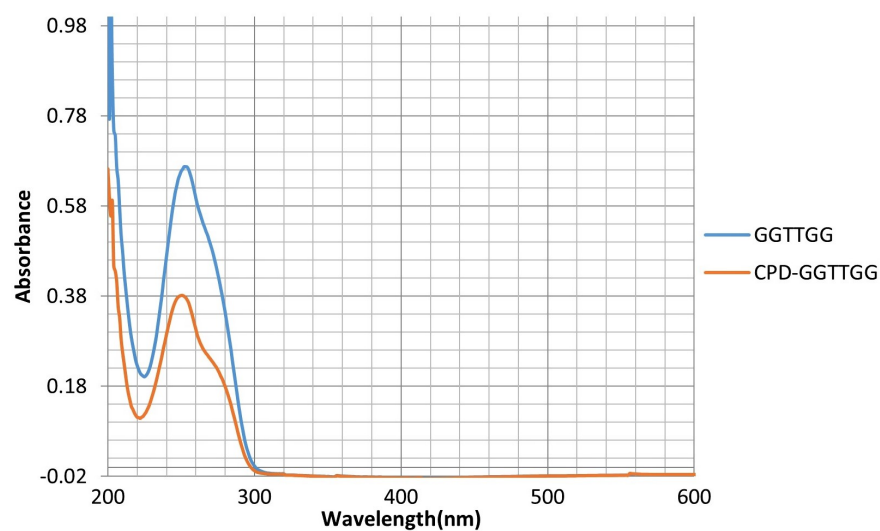


**Figure A.29.** UV-Visible absorption spectrum for CPD-GGTTGG and GGTTGG
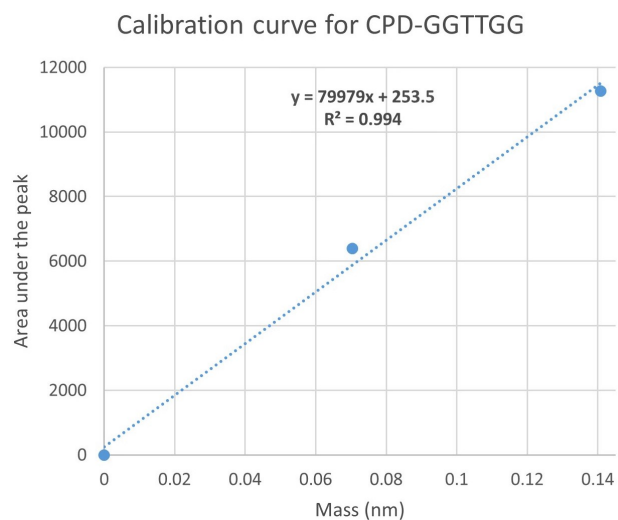
**Figure A.30.** Calibration curve for CPD-GGTTGG
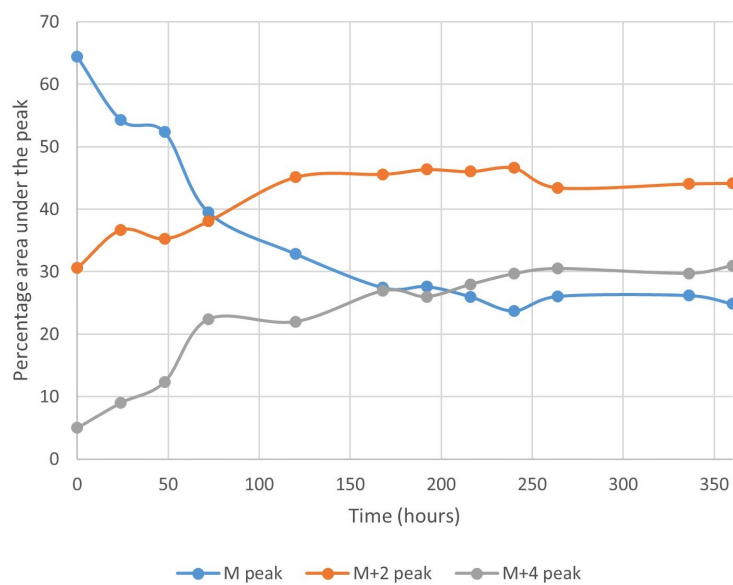


**Figure A.31.** $^{18}$O exchange for CPD-GGTTGG in presence of 100 mM of NaOH at room temperature
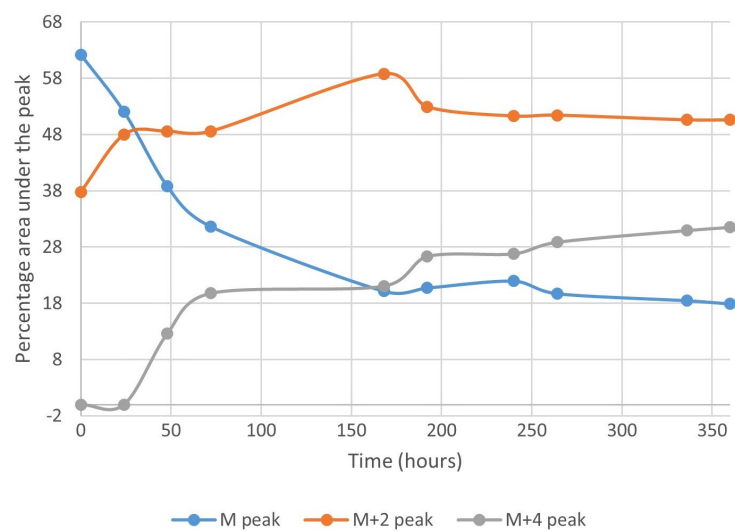
**Figure A.32.** $^{18}$O exchange for CPD-GGTTGG in presence of 250 mM of NaOH at room temperature
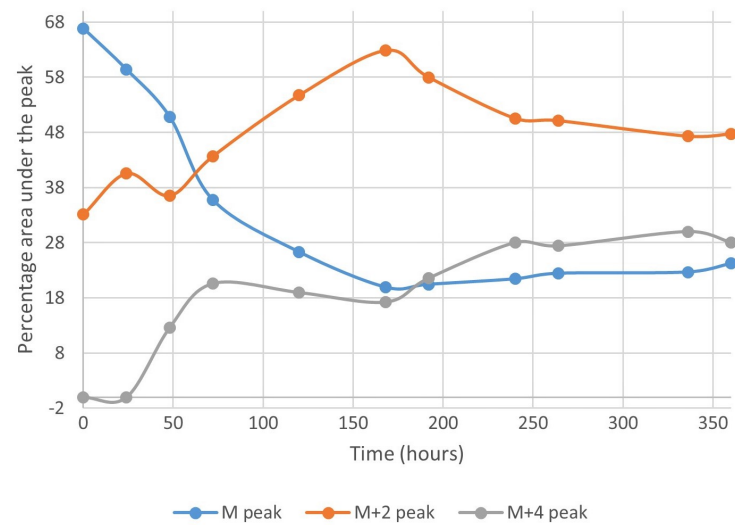


**Figure A.33.** $^{18}$O exchange for CPD-GGTTGG in presence of 500 mM of NaOH at room temperature
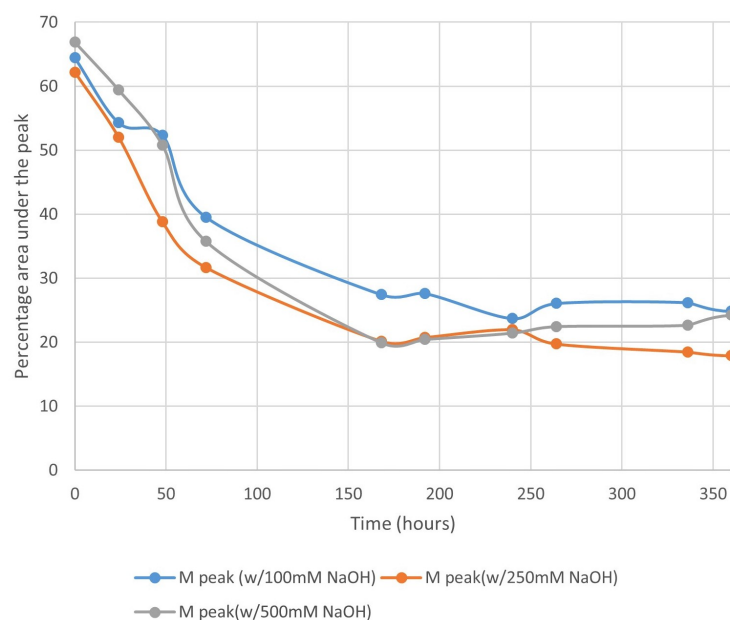
**Figure A.34.** Comparison of the rates of $^{18}O$ exchange in CPD-GGTTGG in presence of various amounts of NaOH
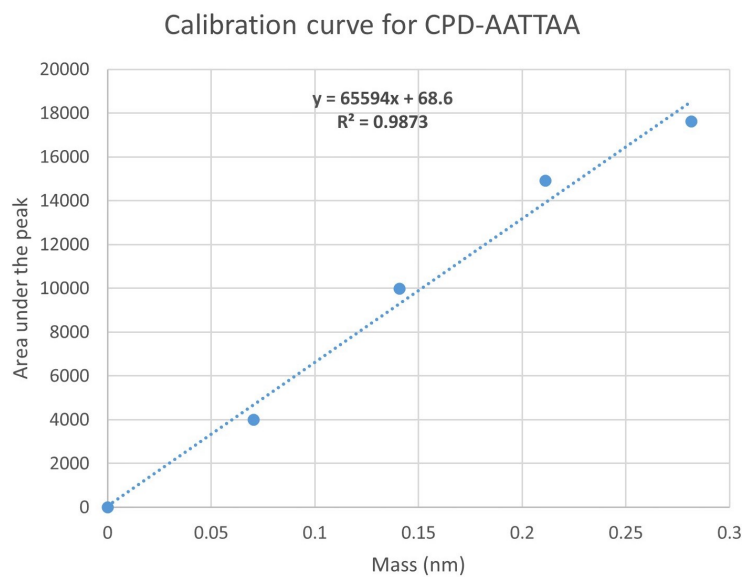


**Figure A.35.** Calibration curve for CPD-AATTAA
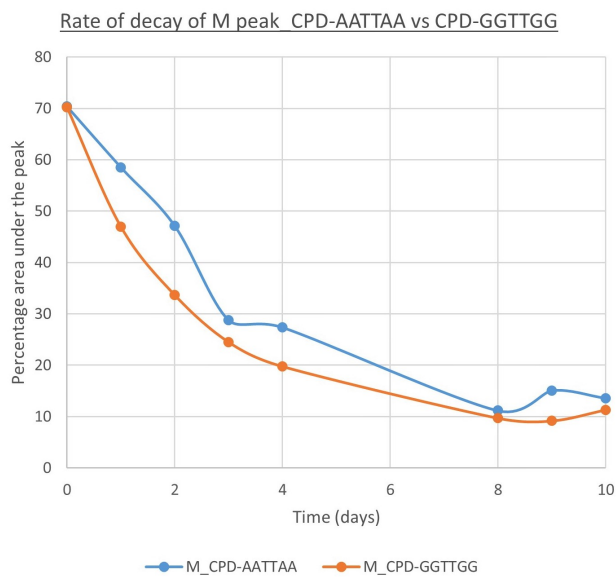
**Figure A.36.** Comparison of the rates of change in M peak during $^{18}$O exchange reaction in CPD-GGTTGG and CPD-AATTAA
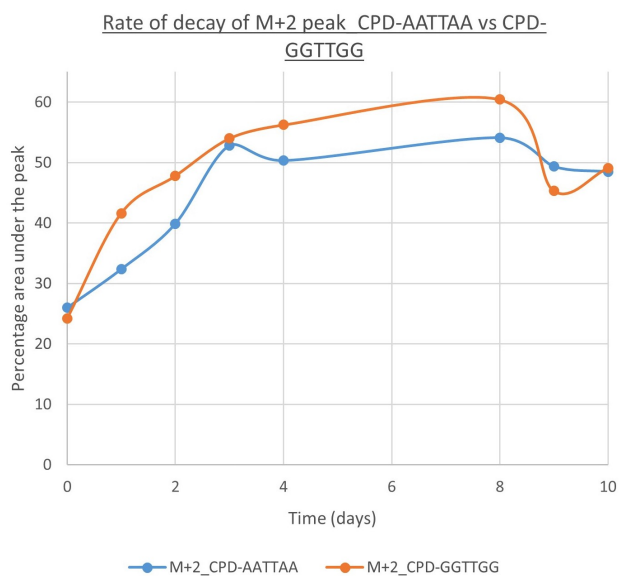


**Figure A.37.** Comparison of the rates of change in M+2 peak during $^{18}$O exchange reaction in CPD-GGTTGG and CPD-AATTAA
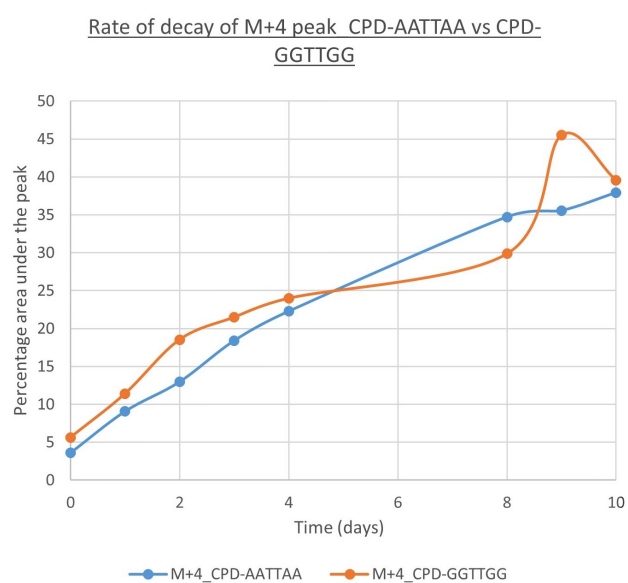
**Figure A.38.** Comparison of the rates of change in M+4 peak during $^{18}$O exchange reaction in CPD-GGTTGG and CPD-AATTAA

# VITA

## RITU CHATURVEDI

**EDUCATION**

*Ph.D.*, Department of Chemistry and Chemical Biology

Indiana University-Purdue University Indianapolis (IUPUI), Indianapolis     December 2019

Thesis - Reactivities Leading To Potential Chemical Repair of Sunlight-Induced DNA Damage: A Mechanistic Study Of Cyclobutane Pyrimidine Dimer (CPD) Lesions Under Alkaline Conditions; GPA 3.955/4.0

*M.S.*, Chemistry

University of Delhi, Delhi, INDIA; First Class                                        May 2010

**PROFESSIONAL EXPERIENCE**

*Indiana University-Purdue University Indianapolis (IUPUI)*       January 2020 – present

Post-Doctoral Researcher, Department of Chemistry and Chemical Biology, Indianapolis, IN

Use of gas-phase ion/ion reactions to increase Ion Mobility (IM) resolution for various compound classes

*Indiana University-Purdue University Indianapolis (IUPUI)*     August 2015 – December 2019

Graduate Researcher, Department of Chemistry and Chemical Biology, Indianapolis, IN

- Multi-step organic synthesis of dinucleotide UV lesions

- Study of alkaline reactivity of UV-induced DNA lesions (at dinucleotide and oligonucleotide level) using three independent techniques- Reverse-phase HPLC, UV-Visible spectroscopy and mass spectrometry.

- First-ever synthesis of dinucleotide CPD-TpT lesion with a selective $N^{15}$ label on $3'$ side.

- Solid phase synthesis of tetra-nucleotide ATTA and its UV-B photoproduct CPD-ATTA using Controlled Pore Glass (CPG) beads

- First-ever synthesis of tetra-nucleotide CPD-ATTA lesion with a selective $N^{15}$ label on $3'$ side using CPG beads.

- First discovery of small molecule-mediated total repair of CPD lesion

*Indiana University-Purdue University Indianapolis (IUPUI)*    August 2015 – December 2019

Teaching Assistant (TA), Department of Chemistry and Chemical Biology, Indianapolis, IN

- Teaching Assistant (TA) for undergraduate General Chemistry laboratory courses for 10 semesters

*Indian Institute of Technology (IIT) Kanpur, Kanpur, INDIA*

Research Assistant (RA), Department of Chemistry                January 2011 – July 2015

- First-ever preparation of non-fluorescent variants of Green Fluorescent Protein (GFP) by single-point mutations in the amino-acid sequence of the protein chromophore
- Reconstitution of Green Fluorescent Protein (GFP) by encapsulation of synthetic imidazolinone derivatives in the non-fluorescent variants, and exploration of their applications in photo-voltaic systems

*University of Lucknow, Lucknow, INDIA*                August 2010 – December 2010

Department of Chemistry, National Post Graduate College, Lucknow, INDIA

- Lecturer (Physical Chemistry)

**PROFESSIONAL COURSES**

- Native Mass Spectrometry; Instructors: Vicki Wysocki (The Ohio State University), Sophie Harvey (The Ohio State University), David Russell (Texas A&M University), Arthur Laganowski (Texas A&M University), Jim Prell (University of Oregon), Michael Marty (University of Arizona)
- Peptides and Proteins in Mass Spectrometry; Instructors: Matthew Foster (Duke University), Arthur Moseley (Duke University), Douglas Sheeley (NIH), Eric Soderblom (Duke University)
- Protein Structural Analysis by Mass Spectrometry: Hydrogen Exchange and Covalent Labeling; Instructors: Mark Chance (Case Western Reserve), John Engen (Northeastern University), Janna Kiselar (Case Western Reserve), Thomas W. Wales (Northeastern University)

- Highly Successful Strategies for LC/MS Quantitation: Current Applications and Emerging Technologies, Pittcon 2017, Chicago, USA

**INSTRUMENTATION SKILLS**

- Proficient in the use of UV-Visible absorption spectroscopy, high performance liquid chromatography (HPLC) (analytical and preparative scale), NMR spectroscopy and ESI-MS for the characterization and quantification of small molecules and oligonucleotides

- Handling and analysis of plasmids using standard techniques

- Chromatographic techniques for the purification and desalting of proteins, study and characterization of proteins using electrophoresis and Circular Dichroism (CD) spectroscopy

**PUBLICATIONS (manuscripts in preparation)**

- Determination of electron transfer potential of carbonyl groups of cyclobutane pyrimidine dimer (CPD) lesions (FULL PAPER)

- Investigation of small molecule-mediated cyclobutane pyrimidine dimer (CPD) repair (FULL PAPER)

**GRANT PROPOSAL WRITING EXPERIENCE**

OVCR COVID-19 Rapid Response Grant, IUPUI Office of the Vice Chancellor for Research; *Title of Project: Development of Ion Mobility-Mass Spectrometry (IM-MS) based methods for rapid screening of drug candidates for the COVID-19 protease drug target*

**INVITED TALKS**

Understanding the electron transfer potential of the ketone groups in cyclobutane pyrimidine dimers; 2017 Ohio Inorganic Weekend, The Ohio State University

**AWARDS AND HONORS**

- Lead panelist for 'Being a TA: What's in it for you and your students?' session at the 2019 IUPUI TA Orientation

- IUPUI Dean's Award- 2019, Think Like a Molecule poster session, American Chemical Society (ACS) Indiana section

- Grand Poster Award- 2018, Think Like a Molecule poster session, American Chemical Society (ACS) Indiana section

- Teaching Assistant (TA) of the month (Feb 2017), Department of Chemistry, Indiana University-Purdue University Indianapolis (IUPUI)

- Research Fellowship (JRF and SRF) (January 2011-July 2015), Council for Scientific and Industrial Research (CSIR), Government of India, INDIA

**PERSONAL ACTIVITIES**
Travelling, swimming and painting.